



Project funded by the European Commission under the 6th (EC) RTD Framework Programme (2002- 2006) within the framework of the specific research and technological development programme "Integrating and strengthening the European Research Area"



Project UpWind

Contract No.:
019945 (SES6)

"Integrated Wind Turbine Design"

Final report for WP4.3: Enhancement of design methods and standards

Deliverable D4.3.6 (WP4: Offshore Foundations and Support Structures)

AUTHORS:	Andrew Cordle
AFFILIATION:	Garrad Hassan and Partners Ltd
ADDRESS:	St Vincents Works, Silverthorne Lane, Bristol BS2 0QD
TEL.:	+44 117 972 9900
EMAIL:	andrew.cordle@garradhassan.com
FURTHER AUTHORS:	Daniel Kaufer, Fabian Vorpahl, Tim Fischer, John Dalsgaard Sørensen, Björn Schmidt, Denis Matha, Jorge Lucas, Douglas McCowen, Ricardo Pereira and Kimon Argyriadis
REVIEWER:	John Dalsgaard Sørensen, Fabian Vorpahl and Tim Fischer
APPROVER:	Tim Camp

Document Information

DOCUMENT TYPE	Deliverable report
DOCUMENT NAME:	UpWind_WP4_D4.3.6_Final_Report
REVISION:	-
REV.DATE:	-
CLASSIFICATION:	General Public (R0)
STATUS:	Approved/Released (S0)

Acknowledgement

The presented work was funded by the Commission of the European Communities, Research Directorate-General within the scope of the Integrated Project “UpWind – Integrated Wind Turbine Design” (Project No. 019945 (SES6)).

This report is the result of work jointly carried out by several participants in Task 4.3 “Enhancement of design methods and standards”. Contributions from the University of Stuttgart (M. Kühn, T. Fischer), DTU/Risø (J.D. Sørensen), Delft University of Technology (W. de Vries), DONG A/S (N.J. Tarp-Johansen), GEGR-E (P.W. Cheng), GL Wind (K. Argyriadis, B. Schmidt), RAMBOLL A/S (H. Carstens, P. Passon, N. Kumar), Shell (A. Ploeg), CWMT (F. Vorpahl) and NREL (J. Jonkman) are gratefully acknowledged.

Disclaimer

All rights reserved. No part of this publication may be reproduced or transmitted by any means without written permission of the author(s).

Any use or application of data, methods and/or results etc. occurring in this report will be at the user’s own risk. The institutions of the (co)author(s) accept no liability for damage suffered from the use or application thereof.

STATUS, CONFIDENTIALITY AND ACCESSIBILITY							
Status			Confidentiality			Accessibility	
S0	Approved/Released	X	R0	General public	X	Private web site	
S1	Reviewed		R1	Restricted to project members		Public web site	X
S2	Pending for review		R2	Restricted to European. Commission		Paper copy	X
S3	Draft for comments		R3	Restricted to WP members + PL			
S4	Under preparation		R4	Restricted to Task members +WPL+PL			

PL: Project leader **WPL:** Work package leader **TL:** Task leader

Summary

The overall aim of the UpWind project is to facilitate the large-scale implementation of offshore wind farms across the EU. To achieve this aim, offshore wind farm sites must be bigger and also located in deeper water. The increase in water depth at these sites means that more complex support structures are required to resist the increased overturning moments; either braced support structures such as tripods or jackets, or floating platforms. The increase in number of turbines and greater variability in ground conditions at these sites means that the rapid processing of many design load calculations and design iterations is required, for detailed and efficient wind farm design and optimisation. Advances are needed in terms of cost reduction, upscaling of current technology and increases in reliability.

The objectives of Task 4.3 within UpWind Work Package 4 are to enhance the currently available design tools and methods for the efficient design of large numbers of structures at deep-water sites, and to actively support the development of dedicated international standards which specify best practice for the design of offshore wind farms (e.g. site-specific design, aerodynamic and hydrodynamic impact, low-risk structures, floating concepts). Therefore this report focuses on the development of integrated design tools, the benchmarking activities performed for these tools, advanced modelling approaches and techniques for numerical simulation and the development of design requirements and standards.

In terms of cost, enhancing design tools and methods for the modelling of deep-water support structures is important because it will enable a more accurate and detailed prediction of loads and dynamic response. Improved accuracy in prediction will lead to more optimised structures and cost savings. In this report the development of integrated design tools for both bottom-mounted and floating structures is presented. Benchmarking activities are also presented for these design tools. These are important for verifying the accuracy of the codes available to the industry. An advanced technique for modelling joints in braced support structures, the super-element technique, is presented. The way in which joints are modelled in space-frame support structures such as jackets and tripods can make a significant difference to frequencies and loads so accurate modeling of these joints is essential. The development of advanced modelling techniques for the numerical simulation of aerodynamic, hydrodynamic and mooring line effects for floating wind turbines are also presented.

In terms of upscaling, a greater efficiency in the design process for complex support structures such as tripods or jackets will assist with the large-scale implementation of wind farms in deep water at large offshore sites. In this report recommendations are presented for the implementation of a reduced set of design load cases for the preliminary design of jacket support structures. A design load case parameter analysis for jacket support structures is also performed, to test the relative influence of a number of key design load case parameters affecting offshore wind turbine jacket support structure design.

In terms of reliability, it is important that the international design standards are constantly reviewed and updated to ensure they are in line with industry best practice. In this report a review of the IEC 61400-3 standard is presented, including recommendations for future editions. A reliability-based calibration of safety factors for the fatigue design of offshore wind turbine support structures is also performed. Finally, recommendations are presented for possible extensions to the IEC 61400-3 standard to enable applicability to floating wind turbines, including the implementation of additional/different design load cases.

Table of Contents

Acknowledgement.....	3
Summary.....	5
1. Introduction.....	9
1.1 The Upwind project.....	9
1.2 Work Package 4: Offshore Support Structures and Foundations	9
1.3 Task 4.3: Enhancement of design methods and standards	10
1.4 Report structure and context	10
PART I: Design Methods for Braced Bottom-Mounted Support Structures.....	11
2. Integrated design tools	11
2.1 Coupled aero-elastic and FE approach	11
2.2 Combined multi-body / modal approach	13
2.3 Full Finite Element approach	15
3. Benchmarking of design tools	16
3.1 Comparison of masses and frequencies.....	17
3.2 Comparison of deterministic load cases	18
4. Advanced modelling approaches	21
4.1 Super-element modelling in ADCoS-Offshore	21
4.2 Results of using super-element technique.....	24
5. Development of design requirements.....	32
5.1 Input to development of IEC 61400-3 standard	32
5.2 Reliability-based calibration of safety factors for offshore support structures	39
5.3 Recommendations for offshore design load case implementation	52
5.4 Design load case parameter analysis for jacket structure.....	58
PART II: Design Methods for Floating Support Structures	70
6. Integrated design tools	70
6.1 Modelling methods for floating offshore wind turbines	70
6.2 Overview of available floating design tools	77
7. Benchmarking of design tools	82
7.1 Code-to-measurement comparisons.....	82
7.2 Code-to-code comparisons.....	83
7.3 Case study: testing and validation of GH Bladed v4.0	85
8. Advanced modelling approaches	89
8.1 Aerodynamic theories.....	90
8.2 Hydrodynamic theories	93
8.3 Mooring line dynamics	119
9. Development of design requirements.....	131
9.1 Literature review of floating offshore standards	131
9.2 Extensions to IEC 61400-3 standard for floating structures	133
10. Conclusions	140
References.....	142

1. Introduction

1.1 The Upwind project

The offshore wind energy industry is turning out ever larger numbers of offshore wind turbines every year. Although significant progress has been made in making offshore wind energy more cost-effective, further cost reductions must be achieved to compete on equal terms with other sources of energy, such as gas and coal powered energy and land based wind energy. One way to achieve this is to turn to economies of scale, both in numbers and in terms of power output of turbines. To facilitate this development the EU funded research project UpWind was initiated in 2006. UpWind looks towards wind power of tomorrow; specifically the design of very large turbines (8 to 10MW) standing in wind farms of several hundred MW, both on- and offshore.

The project brings together participants from universities, knowledge institutes and the industry from across Europe. Topics of research are gathered in work packages, for example focussing on aerodynamics & aeroelastics, rotor structure & materials, control systems and electrical grids. One topic specifically geared towards offshore development is the development of offshore support structures, to enable the offshore application of large turbines in deep water sites.

1.2 Work Package 4: Offshore Support Structures and Foundations

The primary objective of the offshore support structure work package (WP4) is to develop innovative, cost-efficient wind turbine support structures to enable the large-scale implementation of offshore wind farms, for sites across the EU. To achieve this objective, the work package focuses on the development of support structure concepts suitable for large turbines and for deep water which are insensitive to site conditions. Further focus lies on the assessment and enhancement of the design methods and the application of integrated design approaches, to benefit from the integrated design of turbines and monopile support structures. The work package is divided into three tasks to execute the research:

- Task 4.1: Integration of support structure and turbine design for monopile structures
- Task 4.2: Support structure concepts for deep-water sites
- Task 4.3: Enhancements of design methods and standards for floating support structures

To this end, three main types of support structure concept are addressed: monopile structures, braced structures and very soft and floating structures. The level of detail in the research reflects the state of current knowledge. The work package aims at making the “next step” in the development of these main concepts:

- For monopile structures the focus is on structural optimisation and pushing the boundaries of the range of application by integrated design.
- For braced support structures the focus is on structural development and making such structures suitable for large scale application.
- For very soft and floating structures the focus is on concept development and on the development of tools to assess these structure types

This report is one of a set of reports which together make up the final reporting of Work Package 4. The work done in Tasks 4.1 and 4.2 are documented in separate final reports [1], [2]. One encompassing report summarises the findings of the WP in an executive summary [3]. The interrelation of the four reports is shown in Figure 1.1.

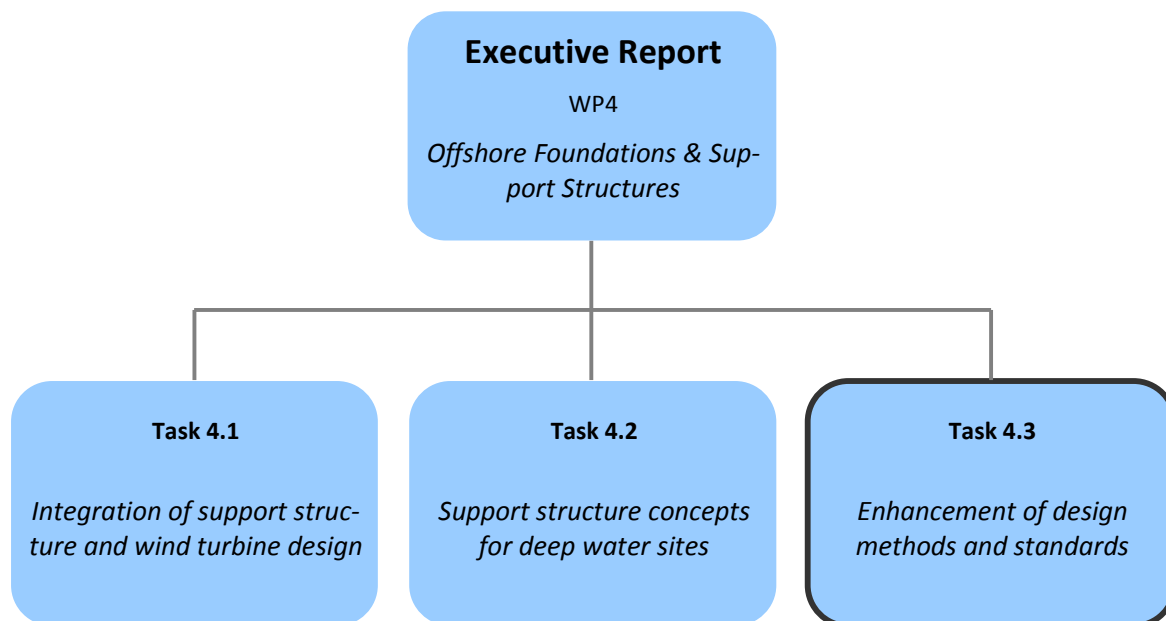


Figure 1.1: Context of reports in WP4

1.3 Task 4.3: Enhancement of design methods and standards

In order to achieve the large-scale implementation of offshore wind farms across the EU, offshore wind farm sites must be bigger, and also located in deeper water. The increase in water depth at these sites means that more complex support structures are required to resist the increased overturning moments; either braced support structures such as tripods or jackets, or floating platforms. The increase in the number of turbines and variability in ground conditions at these sites means that the rapid processing of many design load calculations and design iterations is even more important, for detailed and efficient wind farm design and optimisation. These additional demands require:

- i) A corresponding enhancement of the capabilities of existing design tools and methods to enable detailed modelling of wind turbines mounted on complex support structures;
- ii) Further development of international design standards and best practices for offshore wind turbine design.

In view of this, the objectives of Task 4.3 are twofold: to enhance the available integrated design tools and methods for the automated design of large numbers of structures at deep-water sites, and to actively support the development of dedicated international standards which specify best practice for the design of offshore wind farms (e.g. site-specific design, aerodynamic and hydrodynamic impact, low-risk structures, floating concepts).

1.4 Report structure and context

This report is broadly divided into two parts. Part I deals with the development of design methods for braced bottom-mounted support structures and Part II deals with the development of design methods for floating support structures. Both parts follow the same general structure. First, the development of integrated design tools is presented (Chapters 2 and 6). Next, a summary is given of benchmarking activities performed for these tools (Chapters 3 and 7). Third, advanced modelling approaches currently used or under development are presented (Chapters 4 and 8). Finally, the development of design requirements and standards is described and recommendations given for further optimisation of the design process (Chapters 5 and 9).

PART I: Design Methods for Braced Bottom-Mounted Support Structures

Historically aeroelastic simulation tools have been developed for onshore wind turbine simulations. It is possible to adapt these tools for offshore applications, but often with limitations in the possible support structures. Monopile structures can be modelled relatively simply as they are effectively longer towers, which is unproblematic as long as the offshore sites remain in shallow waters. However in deeper water it is often necessary to move to more complex sub-structures such as jackets or tripods. Performing integrated analysis of such structures presents new challenges.

Chapter 2 presents three different approaches to performing integrated design load calculations for fixed-bottom offshore wind turbines with complex support structures. The coupled approach, the combined multibody/modal approach and the full finite element approach are described, and examples given of codes which use these approaches.

Chapter 3 presents a summary of benchmark studies performed with the above three design tools. The simulations and comparisons presented are an important step in verifying the accuracy of such tools.

Chapter 4 presents advanced approaches to enable a more detailed modelling of joints in braced support structures. The way in which joints are modelled in space-frame support structures such as jackets and tripods can make a significant difference to frequencies and loads.

Chapter 5 presents recommendations for the development of the IEC 61400-3 standard, together with guidance on the implementation of design load cases for preliminary design and a design load case parameter analysis for jacket support structures. A reliability-based review of safety factors for offshore support structures is also performed.

2. Integrated design tools

2.1 Coupled aero-elastic and FE approach

This section describes the first workarounds in simulating offshore wind turbines with bottom-mounted space frame sub-structures and the step towards full integrated simulations using software couplings on the level of equations of motions, also known as sub-structuring methods. The development is explained using the example of the aeroelastic tool Flex5 coupled with finite element codes. It means that two specialised software packages are coupled rather than extending the foundation methods in the wind turbine code Flex5. The latter one is described in [4]. Two strategies have been found: the sequential coupling approach [5] and the full integrated coupling approach [6], [7]. They differ in accuracy and coupling effort. The coupling methods explained here can be assigned to other tools as well.

Limitations in Flex5

Flex5 is a modal based simulation tool with a maximum of 28 degrees of freedom, which is enough for representing the important mode shapes of a wind turbine. The motion of slender components like the tower, the monopile or the rotor blades are dominated by their lower natural frequencies. Only six degrees of freedom are reserved in Flex5 for the motion of the foundation. For modelling more complex sub-structures than a monopile, more degrees of freedom are necessary.

Flex5 is a well-fitted tool for simulating onshore wind turbines and offshore wind turbines mounted on a monopile. Many wind turbines have been designed using Flex5. The aim of the couplings is to combine specialised offshore tools with Flex5 to extend the usability of both.

Sequential coupling

The sequential coupling approach consists of a series of separated simulations. The simulation tools are kept separate and are applied one after the other. This coupling approach has been realised with Flex5 and ASAS(NL) [5]. ASAS(NL) is a finite element tool specifically developed for offshore applications. The overall time integration of Flex5 is used to solve the equations of motion. A reduced generalised foundation model with six degrees of freedom is needed for representing the complex sub-structure. This reduced model is created in the finite element tool out of the detailed finite element model. Besides the model the hydrodynamic loading history is treated analogously. Parts of the results (internal forces or displacements) from Flex5 are transferred back as boundary conditions to the finite element tool, which allows a retrieval simulation in the finite element tool to obtain member forces in the complex foundation model. The flow chart of the sequential approach is shown in Figure 2.1.

Advantages and disadvantages

The two simulation tools do not interact directly, which makes the modifications in the codes simple. The computational effort is higher than a stand-alone simulation in Flex5 because of the additional retrieval run. The coupling is missing dynamic interactions between the sub-structure and specific phenomena of the wind turbine due to the strong reduced foundation model. An outcome of this missing link is that the internal forces calculated in the retrieval run are different compared to an integrated solution. This coupling approach can only represent linear problems of the foundation, as any non-linear problem is linearised during the reduction process. The calculation of hydrodynamic loading is based on a fixed structure, as the motion of the overall wind turbine is unknown to this point.

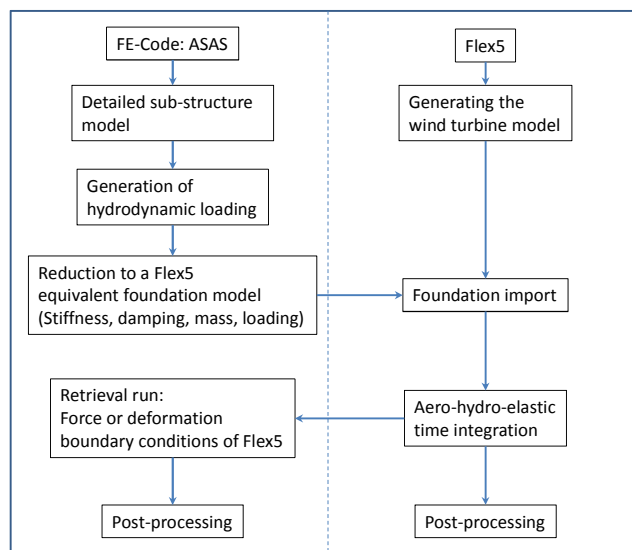


Figure 2.1: Flow chart of the sequential coupling approach

Full integrated coupling

The most accurate simulation of offshore wind turbines (OWT) with complex sub-structures is achieved if the complete set of equations of motion of the entire offshore model is solved in one numerical solver. To do so, the equations of Flex5 need to be combined with the equations of the finite element code. The interface point is the connection between the tower and the sub-structure. Similar to the sequential approach Flex5 is used to model the wind turbine and to compute the aerodynamic loading. The finite element code is used to model the sub-structure and to compute the hydrodynamic loading. An interface, accessible by both tools, is employed to exchange parts of the equations of motion of the tools during runtime. The wind turbine model of Flex5 is considered as a super-element in the finite element code with a maximum number of 28 degrees of freedom. The other way round would end up in an enormous amount of work because it is difficult to introduce further degrees of freedom in Flex5.

In every time step the system matrices of Flex5, i.e. mass M , stiffness S , damping D , and the current loading F is transferred to the finite element code. There the models are combined on the level of equations of motion and the hydrodynamic loads are added. The equations are solved in the finite element code. The results, i.e. displacements, velocities and accelerations (x, \dot{x}, \ddot{x}) are used in Flex5 to update the geometry, the loading and the controls. Figure 2.2 shows the coupling process and data exchange.

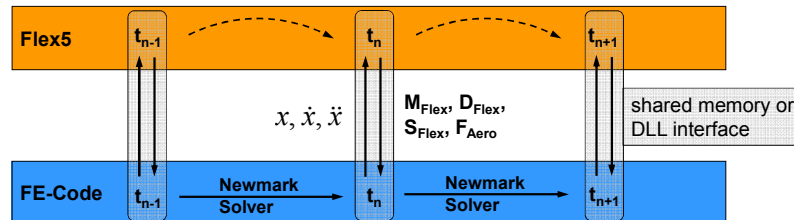


Figure 2.2: Process of the full integrated coupling between Flex5 and a finite element code [7]

Three full integrated couplings have been realized: Flex5-FECOS [6], Flex5-Poseidon and Flex5-ASAS [7]. The first one was created within UpWind, the two other couplings have been created in the Project OWEA - Verification of offshore wind turbines [8]. The interface and the modelling capabilities are different between the tools, but the coupling method is the same. FECOS is a finite element code compiled as a dynamic link library (DLL) and is included in Flex5 directly. Therefore no special interface is necessary to handle the data exchange. Flex5-Poseidon uses a shared memory interface where both tools access the same memory. Flex5-ASAS uses a separate DLL for the data exchange.

Advantages and disadvantages

An important advantage of the full integrated coupling is that specific simulation codes are combined without losing their potential. The application possibility of the coupled tools has been extended. The method considers dynamic effects between the wind turbine and the support structure. The load calculation takes relative velocities of the entire structure into account. Non-linear problems can also be simulated using Flex5-ASAS.

The main disadvantage is the computational time. The simulation speed is lower than the sequential approach and much lower than a Flex5 stand-alone simulation. The reasons for this can be found in the large number of freedoms and the data exchange between the tools in every time step. The simulation speed can be increased if a reduction method is implemented in the finite element code, but this restricts the simulations to linear problems.

2.2 Combined multi-body / modal approach

This section describes the GH Bladed software code as an example of an integrated design tool for calculating wind turbine performance and dynamic response [9]. Bladed was originally developed for the modelling of onshore fixed-bottom wind turbines, but has been extended to include hydrodynamic loading for the modelling of offshore wind turbines. In the last year the core structural dynamic calculation in the code has been extended to incorporate multibody dynamics.

The Bladed code uses a modal representation to model the structural dynamics of a wind turbine. This approach has the major advantage of giving an accurate and reliable representation of the dynamics of a wind turbine with relatively few degrees of freedom, making it a fast and efficient means of computation. In the previous version of the Bladed code, the modal properties of the rotating and non-rotating components of the system (i.e. the rotor and tower) were computed independently using a finite element representation of the structure, then coupled together using the appropriate equations of motion in the dynamic response

analysis. In the new multibody code, flexible components such as the blades and tower are modelled with a modal representation. However, instead of modelling the whole turbine as a single dynamic structure consisting of one rotor and tower with coupling between rotor modes and tower modes hard-wired into the code, the structure can now be modelled with any number of separate bodies, each with individual modal properties, which are coupled together using the equations of motion.

Each mode is defined in terms of the following parameters:

- Modal frequency
- Modal damping coefficient
- Mode shape represented by a vector of displacements

The mode shapes and frequencies of the blade and tower (the main flexible components in a standard wind turbine model) are calculated based on the position of the neutral axis, mass distribution along the body and bending stiffness along the body, as well as other parameters specific to the body in question. The modal damping for each mode is a user input to the model.

The use of multibody dynamics enables a completely self-consistent, rigorous formulation of the structural dynamics of a wind turbine. The blade modes are modelled individually with fully coupled flapwise, edge-wise and torsional degrees of freedom, and are valid for any pitch angle. Advanced definition options are available for the blade geometry and structure, and additional degrees of freedom in the drive train and gearbox can be easily modelled.

For modelling the support structure a multi-member model may be used, consisting of an arbitrary space-frame structure with any number of straight interconnecting beam elements with given mass and stiffness properties. Craig-Bampton style modes are used for the support structure, with a torsional degree of freedom included for all support structure types, not just multiple-member support structures. The support structure is not necessarily axisymmetric, so the resulting mode shapes will be three-dimensional with all six degrees of freedom at each node. Figure 2.3 shows an example of a mode shape for a braced support structure, in this case a three-legged tripod.

Soil springs can be modelled in Bladed via a user-defined force-displacement relationship at multiple foundation stations on the sub-structure. This includes the possibility to define non-linear relationships between force and displacement.

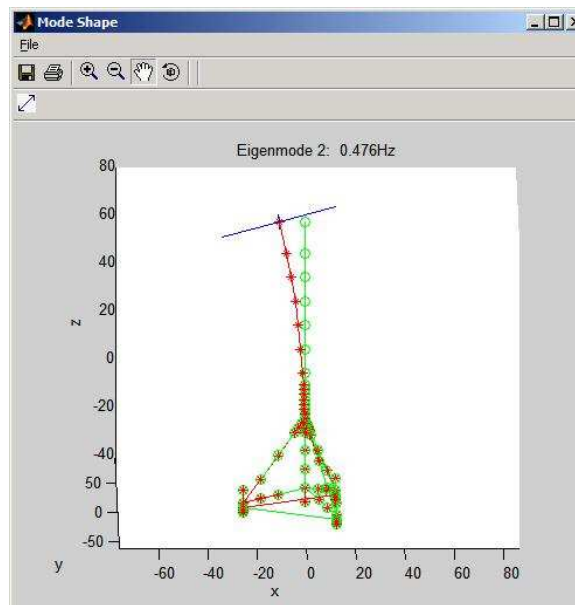


Figure 2.3: Example of multi-member support structure mode in Bladed

2.3 Full Finite Element approach

The offshore wind turbine simulation approach presented in this section is based on ADCoS, a nonlinear finite element (FE) system for aero-servo-elastic simulation of onshore wind turbines.

ADCoS uses a direct time integration method to resolve the equations of motion that describe the dynamic system as a whole. Therefore no modal transformation is performed and no modal analysis is needed for simulation. Furthermore each time step is iterated until a convergence criterion is reached and for that reason nonlinear effects, like 2nd order pitch moments resulting from large blade deflections or torsional stiffening of the blades due to different rotational speeds, are directly included in the time domain simulations. Torsional flutter, a highly nonlinear instability that can occur due to a disadvantageous combination of aerodynamic loads of a rotor blade, may be reproduced in detail as described in [11].

Support structures are defined as FE beam models using a two noded beam element with 12 DOF, based on an Euler-Bernoulli-Formulation, in ADCoS. With this approach, local effects concerning single members of branched structures are described as well. Local natural frequencies for example can be found in load spectra of member loads. ADCoS is described in [11] in more detail.

To allow for simulation of offshore wind turbines, ADCoS is combined with ASAS, a FE tool widely used in the offshore Oil & Gas industries to simulate offshore structures. Furthermore a macro allows for input of structural models from the general purpose FE tool ANSYS for convenient structural modeling and optimization. In ASAS, hydrodynamic loads based on all common wave theories and Morison's equation as well as hydrostatic loads can be calculated. Buoyancy may be included in relation to the time dependent water surface based on displaced water mass or based on integration of hydrostatic pressures around the submerged members. The loads calculated in ASAS are transferred into ADCoS-Offshore as nodal loads. The calculation of wave loads and the overall time domain simulation are separated in the current simulation procedure. Therefore effects resulting from relative kinematics due to superimposed wave and structural motion cannot be described. Although those effects are negligible for many structures, a new version of ADCoS-Offshore that includes relative structural motions in wave load calculations is currently tested. The ADCoS-Offshore approach allows consideration of soil characteristics in the overall turbine model. The easiest way to connect the support structure model to the soil is to clamp it at mudline. It is obvious that this approach is not very realistic. Therefore, user defined stiffness matrices can be included at mudline in ADCoS-Offshore to account for the flexibility of the embedded pile. For detailed simulation, those stiffness matrices can be derived using ASAS based on a nonlinear P-y approach as described in [12] that is recommended by the American Petroleum Institute [13]. In this case pile group effects resulting from loads transferred from one pile to another via the soil medium are included as well.

Even though a modal analysis is not part of the transient time domain simulation a modal analysis is a helpful supplementary tool to understand dynamic behavior of a structure. Figure 2.4 shows the 2nd global bending mode of the offshore jacket structure of a 5-MW turbine 30 m of water in ADCoS-Offshore (left) and ANSYS (right) as an example.

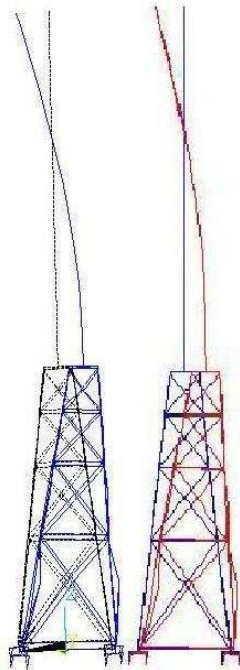


Figure 2.4: 2nd global bending mode of a jacket structure including local portion in ANSYS (left) and ADCoS-Offshore (right)

The description of the global eigenmode, including a clearly visible local displacement in the lowest jacket field, is perfectly the same in both tools. In this figure the turbine itself is represented with a lumped mass in ANSYS whereas the ADCoS-Offshore model includes the fully flexible turbine. ADCoS-Offshore is described in more detail in [14]. A validation of the simulation results obtained with this tool has been realized via code to code comparison and is described in [16] and [19].

3. Benchmarking of design tools

Benchmarking exercises are important for the purpose of validating design tools against each other. A number of WP4 members were involved in the OC3 code comparison project under IEA Wind Task 23 [18], in which a monopile and a tripod support structure were modelled and compared using the coupled tools partly developed in Upwind WP4. This included basic comparisons of frequencies and masses, together with time histories and auto spectra derived from simplified load cases.

For the following IEA Wind Task 30, the Work Package has provided a reference jacket model for the continuation of the comparison work with a more complex structure. Again, several WP members are involved in the new IEA Wind Task and gave support on the jacket structure modeling. The goal will be, as for the monopile and tripod in the IEA Wind Task 23, to reduce uncertainties between different design tools in the wind energy community and therefore enable more accurate designs in the future. For jacket structures in particular such a code to code comparison is important, as it seems to be the preferred support structure type of the coming years in medium to deep waters.

In addition to the above interface with the IEA Wind Task code comparison projects, benchmarking exercises have been performed for the tools presented in Chapter 2. Three fully integrated tools are applied in the analysis - namely Flex5-Poseidon, GH Bladed and ADCoS-Offshore, all of which can be used for simulating arbitrary bottom mounted offshore wind turbines. The benchmarking exercises carried out in this chapter are performed with the NREL 5MW baseline wind turbine [52] mounted on the UpWind refer-

ence jacket support structure designed by Rambøll [54]. The reference comparison is based on masses, natural frequencies and time series of deterministic load cases.

3.1 Comparison of masses and frequencies

The first step in the benchmarking exercise is the comparison of the global model data and the dynamics of the reference wind turbine. This ensures that there is no mistake in the reference model before different modelling aspects are analysed. For the calculation of masses and natural frequencies the turbine was idling while blade one initially is pointing upwards. As shown in Table 3.1, all codes show almost identical masses, only the mass of the tower differs slightly due to different interpolations of cross-sectional properties in the codes, but this difference is negligible.

Table 3.1: Mass comparison of the reference model

		Flex-Poseidon	GH Bladed	IWES AdCoS	standard deviation
Rotor-Nacelle-Assembly	[t]	349.6	349.6	349.6	0.00
Tower (68m)	[t]	216.7	215.4	216.6	0.58
Transiton piece (TP)	[t]	666.0	666.0	666.0	0.00
Jacket	[t]	609.1	609.1	609.1	0.00
Jacket + TP	[t]	1275.1	1275.1	1275.1	0.00
Jacket + TP + Tower	[t]	1491.8	1490.5	1491.7	0.58

Good agreements can be found in the comparison of natural frequencies too. Only natural frequencies up to the second eigenmode of a component are included. Flex5 represents the motion of the blades and the tower only by its first two eigenmodes per direction. Therefore the assessment of a third blade or support structure mode is not reasonable here. Figure 3.1 illustrates the results of the three simulation codes.

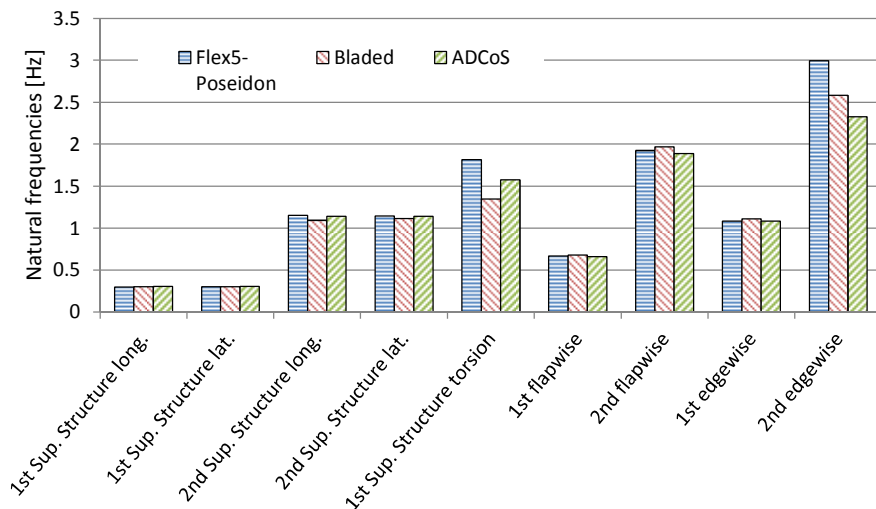


Figure 3.1: Natural frequencies of the reference model

3.2 Comparison of deterministic load cases

Deterministic load cases have been defined to compare the results on the level of time series. The load cases have increasing complexity. Aerodynamic loading and hydrodynamic loading have been simulated separately, followed by combined loading. The course of oscillation and amplitudes of the time series is very equal in all analysed cases. Simulations have been carried out with a constant wind speed of 8m/s and an aligned extreme stream function wave of 8m wave height and a wave period of 10s. Table 3.2 gives an overview of the three simulated cases.

Table 3.2: Simulated load cases for code-to-code comparison

Load case	Description	Wind conditions	Wave conditions	Directionality
1.1	Just wind, still water	Constant, 8m/s	Still water	Wind from North (0°)
1.2	Just waves, no wind	No wind	Stream function with H=8m and T=10s	Waves from North (0°)
2.1	OWT operating with wind and waves	Constant, 8m/s	Stream function with H=8m and T=10s	Wind and waves co-linear from North (0°)

Overall seven sensors (load effects) have been selected for the reference validation. Four of them are located in the jacket. Figure 3.2 shows the position of the jacket sensors. The remaining three sensors are the rotor speed, electrical power output and the out-of-plane bending moments of blade number one. The wind turbine is pointing in the negative direction of the global x-axis in the picture.

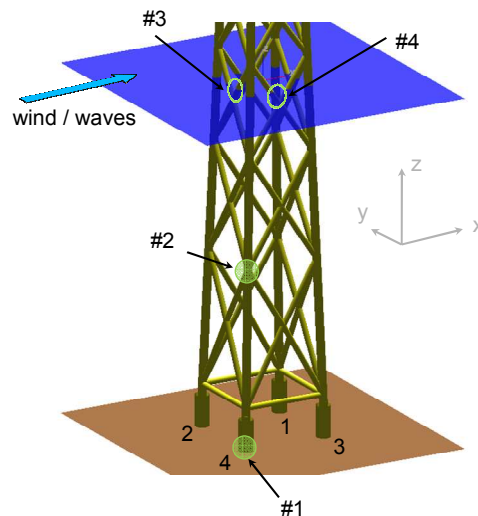


Figure 3.2: Position of sensors at the reference jacket

Exemplarily the time series of the combined wind and wave case (case 2.1) for the turbine sensors is shown in Figure 3.3. The curves show good agreement, even if some small differences in rotor speed and power output are visible. This is due to differences in the power loss definition and power controller implementations. Still, the differences are marginal and the resulting out-of-plane bending moment of blade one gives a good agreement.

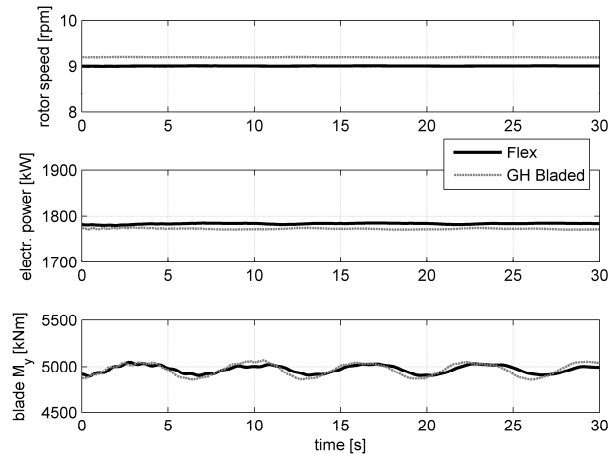


Figure 3.3: Time series of rotor speed, power output and blade out-of-plane bending moment blade 1 (from top) for load case 2.1

In presenting the results from the comparison of the jacket loads just sensor #1 is shown in Figure 3.4, for the purpose of brevity. As for turbine sensors, each time series is shown for a time period of 30s. This already includes a cut-off of the first 10s of simulations to eliminate initial transients.

As for the turbine sensors, the overall trends of the time series of Bladed and Flex5-Poseidon are matching well. A small shift in magnitude for the axial force (F_x) can be seen. This is because the controllers could not be modelled in such a way that they gave exactly the same operating conditions. This resulted in a difference in rotor speed between Bladed and Flex, which can be seen in the top graph in Figure 3.3. The resulting difference feeds into the blade loads and also further down into the support structure loads. This can be validated by comparing Figure 3.5 (just wind) and Figure 3.6 (just waves), as the shift is only visible for the pure wind case. Another visible difference is seen in the phase shift. This seems to come from differences in wave modelling and loading, as the phase shift is only recognizable for the pure wave case (compare Figure 3.6) and not for wind and calm sea (compare Figure 3.5).

In conclusion, this short chapter on benchmarking of simulation tools shows good agreements for all stated codes in terms of masses and frequencies as well as for loads. Observed discrepancies can be explained in terms of differences in modelling.

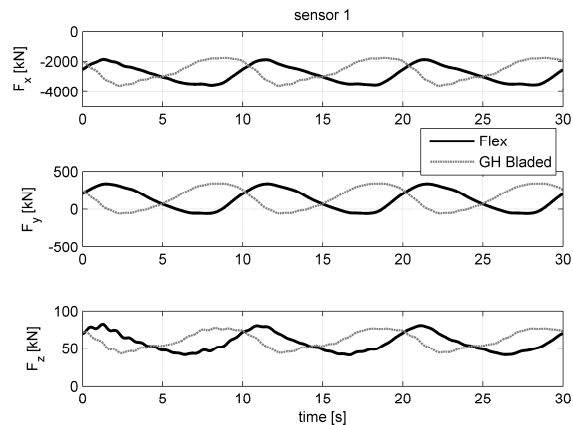


Figure 3.4: Time series of axial force F_x , shear force F_y and F_z of jacket sensor #1 (from top) for load case 2.1

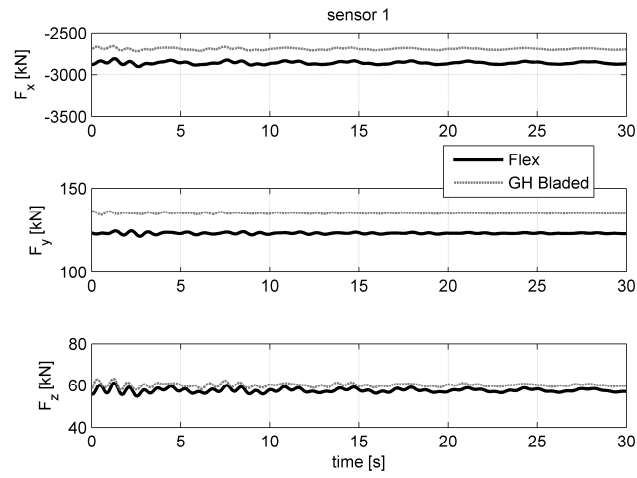


Figure 3.5: Time series of axial force F_x , shear force F_y and F_z of jacket sensor #1 (from top) for load case 1.1 (wind only)

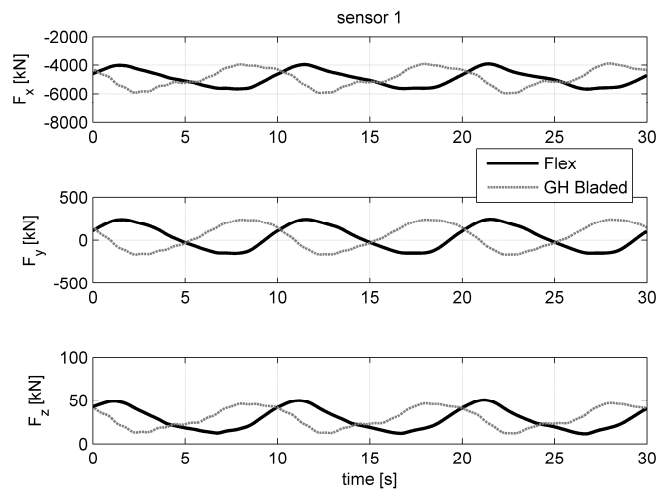


Figure 3.6: Time series of axial force F_x , shear force F_y and F_z of jacket sensor #1 (from top) for load case 1.2 (waves only)

4. Advanced modelling approaches

There are a number of features unique to multi-member support structures which require enhancement of the current design tool capabilities and techniques. In particular the presence of complex joints needs to be taken into account.

The most basic approach to modelling joints in a braced support structure is to include joint cans. Joint can properties differ from basic tube properties in terms of increased wall thicknesses. A preliminary study was performed using the UpWind reference jacket support structure with and without joint cans [54], to determine the influence of joint can modelling on the dynamic simulation of the structure. The mass difference due to joint can modeling was found to be approximately 1.7% with respect to the offshore wind turbine structure as a whole, and the differences concerning the first 18 natural frequencies were under 0.8%. These differences are relatively minor, and therefore it is concluded that the modelling of joint cans is not expected to lead to significant changes in the loads resulting from dynamic simulations.

In the remainder of this chapter, an advanced approach to enable a more detailed modelling of joints in multi-member space-frame support structures is analysed, namely the super-element technique.

4.1 Super-element modelling in ADCoS-Offshore

As mentioned in Section 2.3, branched support structures for offshore wind turbines (OWT) are basically modelled in ADCoS-Offshore as FE beam elements. These elements are clamped at the nodes, where the centerlines of the members intersect. This leads to a fairly good representation of the single tubular members of the structures, but to a less accurate representation of the joints themselves. Usually, the joint stiffness is overestimated with this approach. This is due to the fact that local joint flexibilities, resulting for example from local chord indentation next to the connection between chord and brace due to a bending moment on the brace, are not taken into account.

This is a crucial issue as for numerous OWT structures, fatigue life is a design driver and the greatest calculated fatigue damage is found at the joints of the structures [56]. Furthermore, fatigue life prediction is heavily influenced by local joint flexibilities for comparable structures as described for example in [57]. Thus, further development of OWT design tools towards more detailed joint representation for simulation of turbines with braced support structures is an important development.

In the offshore oil and gas industries, simplified beam models of complex support structures are used for load simulation as well. In those simulations, joints may be modeled with beam elements including local joint flexibilities using parametric formulae as developed in [58] for example. A more accurate approach is the so-called super-element or sub-structuring approach. Sub-structuring methods are applicable independent of joint type and dimensions and lead to a stiffness representation of the substructure that is as close to reality as detailed FE simulations with the shell or volume type elements that are used in more detailed models. Furthermore, these methods are implemented in commercially available general purpose FE tools such as ANSYS or MSC.NASTRAN as a standard advanced modeling feature. Sub-structuring methods are described in detail in the corresponding software documentation [59] and [60].

In the course of the UpWind project, a sub-structuring or super-element approach has been implemented in the ADCoS-Offshore code [14] to enhance joint modelling. An analysis using sub-structuring in ADCoS-Offshore is generally performed as described in the following. To facilitate comprehension, different examples are shown:

- Detailed joint modeling in a general purpose FE tool like ANSYS or MSC NASTRAN.
- Condensation of detailed joint using a reduction procedure such as Guyan reduction [61] or the Craig-Bampton method [62].
- Super-element inclusion in ADCoS-Offshore.
- Inclusion of wave loads on the super-element.

- Time domain simulation in ADCoS-Offshore.

As an example, the central joint of a tripod [16] is modelled with shell elements in ANSYS as shown in Figure 4.1. The figure shows the tripod as a whole as well (small figure on the left). The model consists of the shell structure (blue), the master nodes which are connecting points to the rest of the tripod structure (black dots) and the stiff connections which are implemented between the masters and the detailed joint (pink lines between master nodes and shell structure). The real deformation of a loaded joint includes an ovalization of the tubular members near the connection. This must be taken into account when deciding on the position of the master nodes, which means that the distance between master node and the welding should not be too short.

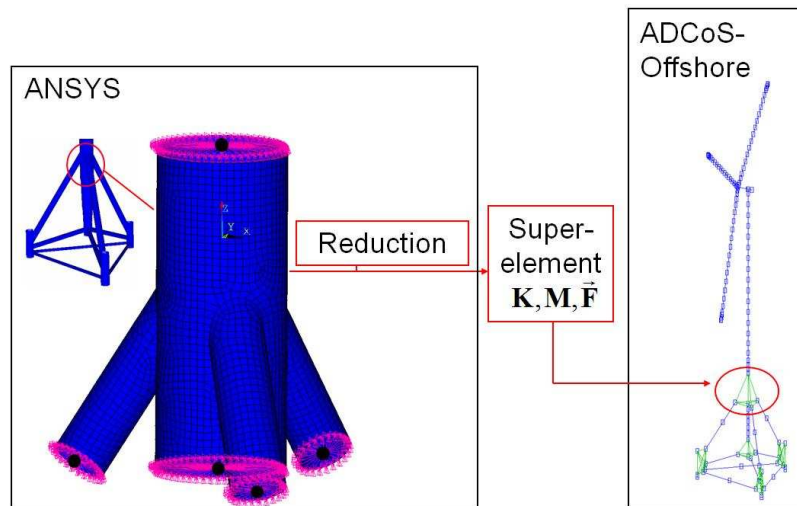


Figure 4.1: Super-element approach in ADCoS-Offshore. The central joint of a tripod is condensed and the super-element is included in the overall turbine model for time domain simulation.

In the next step, a Guyan reduction procedure is used and the model is reduced to the number of DOF of the five master nodes. Six DOFs at each of the five master nodes lead to a super-element with 30 DOFs. The super-element, in detail a linear stiffness matrix, a mass matrix and a load vector for the master DOF, is included in ADCoS-Offshore in the next step. As already mentioned, the stiffness matrix has 30 DOF. In the reduction procedure, the transformation of the stiffness matrix is not an approximation: the stiffness representation is exact and therefore the stiffness properties between the master nodes in the super-element model are defined with the same accuracy as in the detailed shell model.

The mass matrix has the same number of DOF as the stiffness matrix and contains the mass of the joint that is distributed to the master's DOF. Those mass properties are included in the overall system later on to describe the dynamic behavior of the system forming the inertia term of the equation of motion. Obviously, the reduction of the mass matrix is an approximation, as it is not possible to reduce the number of DOF of a dynamic system and to conserve the level of accuracy at the same time. But this is not considered to be of vital importance for time domain simulation of OWT with branched support structures as the internal mass distribution in the super-element (here the tripod central joint) has no significant influence on the overall dynamic behavior of the OWT. It is expected that in the described case even a lumped mass for the whole joint would not lead to significant errors. The accuracy of the described mass representation is comparable to the mass representation of the basic beam model that has been used before the implementation of the super-element feature.

The static load vector, that is part of the super-element, comprises the forces and moments on the master nodes resulting from dead weight of the joint. The super-element load vector is added to the system load

vector. The loads resulting from dead weight at the master nodes are obviously the same as for the detailed model.

The inclusion of hydrodynamic loads on the super-elements in ADCoS-Offshore is not trivial. As mentioned in Section 2.3, wave loads on the members of OWT support structures are calculated in ASAS quasi statically with given geometry and Morison's equation so far. Those distributed loads were transformed to equivalent nodal loads and included to the dynamic model afterwards.

This general approach is used with the newly developed super-element feature as well, but some modifications must be realized. In ASAS, the outer diameter and/or the hydrodynamic coefficients of the beam models representing the joints may be adapted to account for the real joint geometry, which is more complicated in the case of a cast joint for example. The result of this calculation step is a file containing the wave loads on each node for each time step to be included in the dynamic simulation. The problem with this approach combined with the newly developed super-element feature is that the file contains loads on nodes that have been condensed and that are therefore no longer available in the dynamic model in ADCoS-Offshore. The described problem is shown in Figure 4.2. Compared to the former model in ADCoS-Offshore, the slave nodes of the super-element, which should be loaded with forces and moments resulting from waves, are no longer available (shown in red).

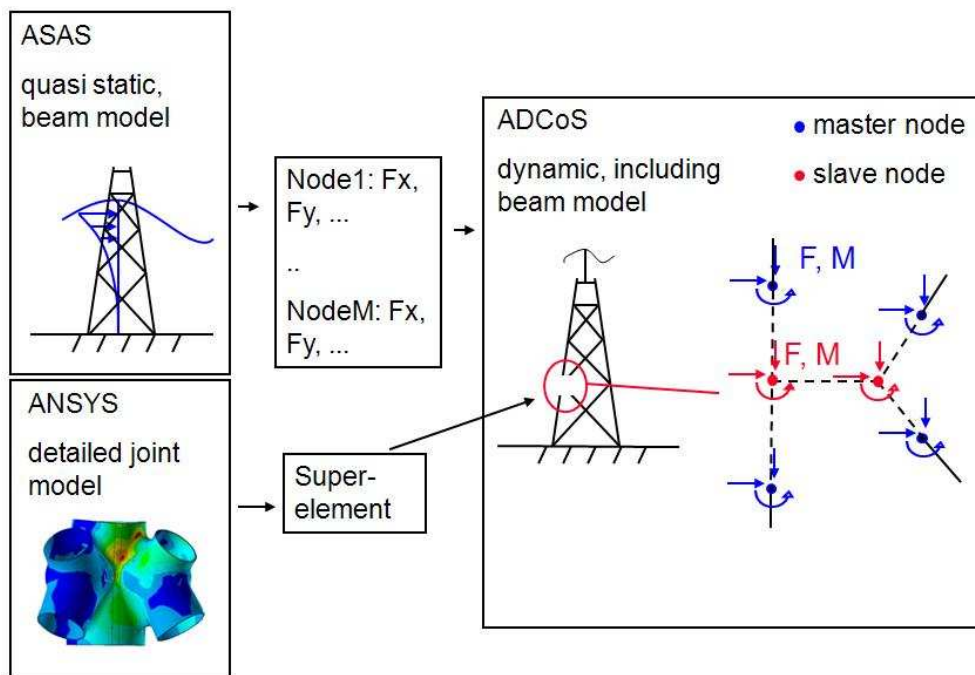


Figure 4.2: Problem of wave loading on condensed nodes in ADCoS-Offshore.

It is solved via distribution of the loads on the slave nodes on the neighboring masters as follows:

- The loads on the slave nodes are read from the nodal load file that has been described above, written to a slave load vector F_s and deleted in the file.
- In the model in ASAS, all nodes at master node positions are clamped and all slave nodes are loaded statically with unit loads consecutively. This results in a total number of supplementary virtual static load cases of $n \times 6$ each with a unit load in one direction at one slave node. For each of those load cases the reaction forces - that are not equal to zero only at the neighboring masters that are clamped - are written to an output file.
- The reactions are read from the output file from step 2 and written to a reaction force matrix R .

- A supplementary load vector for the master nodes F_m is calculated with the reaction force matrix \mathbf{R} from step 3 and the slave load vector F_s that was defined in step 1. This vector F_m is written to the nodal load file. With this approach, all wave loads on the slaves are distributed to the neighboring masters by means of the reaction force matrix as a load distribution key.
- Steps 1 and 4 are repeated for each time step. This results in a modified nodal load file for the dynamic time domain simulation.

With this approach, the global values of the wave loads remain the same as for an unmodified model. Only a distribution to other nodes has been performed. The modifications described herein are verified as shown in [64].

Verification of super-element implementation

The correct implementation of the super-element in ADCoS-Offshore is verified via code-to-code comparison against the general purpose FE tool ANSYS using component models and static load cases. The stiffness matrix, the mass matrix and the static load vector of the super-element in ADCoS are compared to their ANSYS counterparts. A realistic model of a tripod central node is used. The stiffness matrix is checked via displacement comparisons along all six degrees of freedom, and for the mass matrix verification the first ten natural frequencies are compared. The static load vector (or the dead weight) of the model is verified comparing vertical force and two moment components for an asymmetrically clamped structure loaded only by gravity. The wave load input is verified by means of a comparison of the wave loads on the basic beam structure and the wave loads modified as described above. Here as well, the resulting differences are negligible. The results show that the implementation of the super-element and the wave load input are realized correctly as only very minor deviations are found in general. This is described in more detail in the respective UpWind report [63] and published in [64].

4.2 Results of using super-element technique

The impact on simulation results of using super-elements to model joints was studied using the NREL 5MW baseline turbine [53] on the tripod support structure in 45m of water that was defined in the course of the Offshore Code Comparison Collaboration project which operated under IEA Wind Task XXIII [16].

In the aeroelastic code ADCoS-Offshore, the tripod was modelled

- as a basic beam model (beam model) and
- in terms of a model including beam- and super-elements (super-element model)

The tripod standard beam model for the use in ADCoS-Offshore is defined with FE Euler-Bernoulli beam elements. The conical parts of the structure are set up as stepped members in the model. The modeling is mainly based on the findings from the third phase of the OC3 project as described in [16], [18] and [19] but some further modifications were realized. Firstly, the overlapping parts of the tripod members at the joints are excluded from the wave load and buoyancy calculation using small supplementary elements. Doubling of masses is avoided because the mass of the small supplementary is set close to zero. This is a simplified approach as the real "doubled" volume (buoyancy), surface (wave load calculation) and steel mass (gravity and dynamics) is still roughly estimated, however, the model is significantly improved by using the supplementary members. Furthermore, the tapered main column of the tripod is finely discretized because this was found to have a significant influence on wave load calculation in the OC3 project. To conclude, this model is as realistic as achievable with standard beam elements and reasonable effort. Therefore, it is suitable to investigate the differences between beam models and the newly developed and more sophisticated structural model.

The super-element model is based on the beam model, whereas the beam elements representing all joints are replaced by super-elements as described above. Master nodes are defined to connect the detailed sub-models to the residual structure. Being located in the centerlines of the tubular chord and brace members those nodes are rigidly connected to the outgoing beam element and rigidly connected to the detailed model via radially arranged rigid link connections. Figure 4.3 shows the tripod model with shell

joints and the central joint in detail. Both models are described in more detail in the respective Upwind report [63] and published in [64].

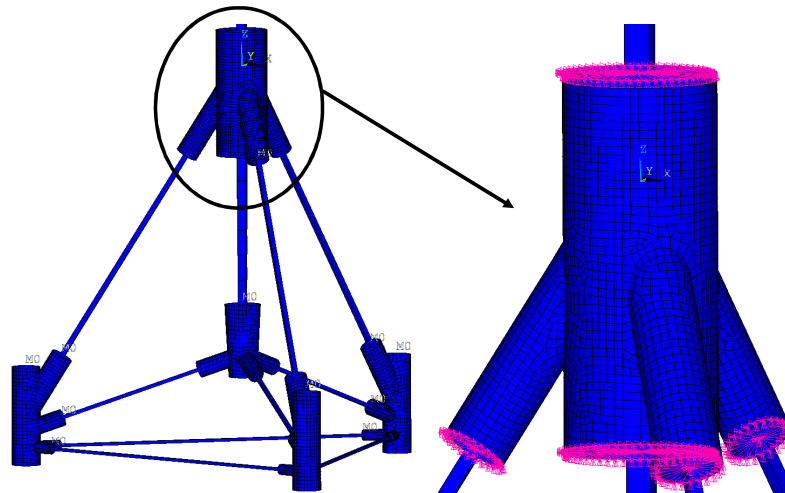


Figure 4.3: Tripod (left) and shell central joint (right).

Natural frequency comparison

After extensive plausibility tests with the support structure models, natural frequency analyses of the total OWT system were performed. To allow for a general view, the most important excitations resulting from the operating turbine (1P, 3P and harmonics) are taken into account. Figure 4.4 shows the 1P range, the 3P range and the first harmonic of the 3P range (6P) for the NREL turbine (light grey boxes). The boxes have different heights relative to one another, to indicate the importance of the excitations; the 3P excitations are expected to be most important. Furthermore, the lowest nine natural frequencies for the beam model (light green lines) and the super-element model (darker green lines) are indicated.

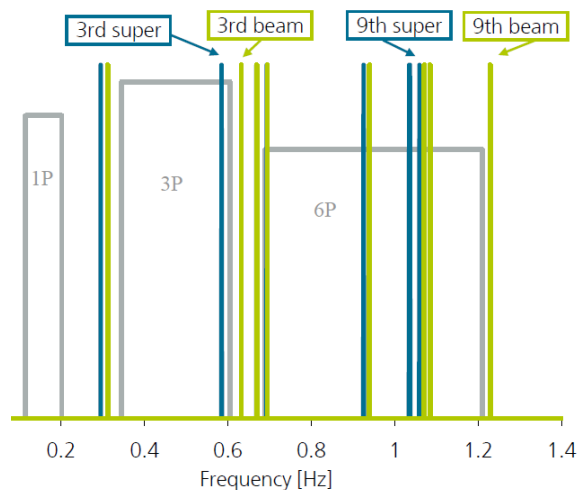


Figure 4.4: Excitation frequency ranges and full system natural frequencies for beam model and super-element model

The following results are found: Firstly, the frequencies associated with the first global bending modes of the support structure are shifted by approximately 5% towards lower frequencies as mentioned before. Those frequencies are among the most important design parameters for OWT support structures as it is common practice to design structures with a first natural frequency between the 1P and the 3P range (soft-stiff design) of the turbine. The allowable frequency gap is relatively small, especially as a distance of about 10% between natural frequency and excitation range has usually to be provided for safety reasons (not shown in Figure 4.4). For the NREL turbine, the more detailed modeling would lead to higher theoretical safety margins, as the frequencies are shifted towards the dead center between the 1P and the 3P range.

Secondly, the third full system natural frequency is shifted into the upper 3P frequency range due to the more realistic support structure modeling. The difference between the third natural frequency calculated with the beam model and the super-element model is about 7%. The excitations mainly due to disturbed wind flow around the tower in the 3P range are considered to bring more energy into the system than its harmonics and even more than the excitations in the 1P range (e.g. see [65]). Furthermore, the natural frequency is found near the upper bound of the 3P range which is associated with rated rotor speed. It is obvious that the turbine operates much more often at rated rotor speed than at lower speeds, as this is the operational speed at all wind speeds above rated wind speed. The maximum rotor thrust occurring at rated wind speed makes a strong dynamic excitation at this speed even more probable.

Thirdly, the ninth natural frequency is shifted to the upper 6P range. This is not too critical, other natural frequencies are found in the 6P range as well.

All in all, the support structure modeling with super-elements leads to changes in comparison to the basic beam model concerning the full system eigenstates that are not negligible.

Load case definition for load comparison

The next step is the study of the impact of super-element modeling of joints on the results of aero-elastic time domain simulations of realistic load cases as described in the respective standards. A heavily reduced set of sub-cases is to be used to get a reasonable balance between simulation effort and proximity to loads simulation as done in OWT certification.

The IEC 61400-3 standard [69] is used to define the load cases, since it is commonly used internationally. All assumptions for external conditions are based on the UpWind design basis [55]. Only DLC 1.2 (normal operation) is taken into account, which is a major fatigue load case covering a significant part of the whole turbine lifetime. This is done for the following reason: the mean wind speeds over the turbine lifetime are well described with a Weibull distribution with the highest probability at approximately 10 m/s for the described offshore site. Very high and very low wind speeds are therefore relatively rare. This means that a turbine with a realistic availability passes a large fraction of the total life time operating under conditions covered by this load case. Furthermore, the summed occurrence of all average wind speeds (10 min average) over $V_{ave} = 24\text{m/s}$ is only 73 hrs/yr, therefore these speeds are not taken into account. With the bin size of 2 m/s, this leads to 11 wind bins as shown in Table 4.1. The average wind speed V_{ave} , turbulence intensity TI, significant wave height H_s and peak period T_p of the Pierson-Moskowitz spectrum and summed occurrence of this wind and wave combination are also shown.

Table 4.1: Lumped scatter diagram used in super-element study (modified from [55])

V_{ave}	TI	H_s	T_p	Hrs/yr
4	0.2042	1.1	5.88	780.6
6	0.175	1.18	5.76	1230.6
8	0.1604	1.31	5.67	1219.7
10	0.1517	1.48	5.74	1264.9
12	0.1458	1.7	5.88	1121.8

14	0.1417	1.91	6.07	881.3
16	0.1385	2.19	6.37	661.7
18	0.1361	2.47	6.71	427.3
20	0.1342	2.76	6.99	276.1
22	0.1326	3.09	7.4	168.6
24	0.1313	3.42	7.8	85.6

In this study, only one wave direction - with one tripod leg pointing perfectly towards the waves, mentioned as 0 deg in the following - is taken into account, which leads to a further reduction of the number of sub-cases. Yaw errors and three seeds are accounted for, to get stochastically significant outputs. Wind and wave misalignment is not accounted for as required in the standard, only three different wind directions are combined with the constant wave direction as for yaw error simulation, the wind direction is modified (+8, 0 and -8 deg) and not the nacelle position (which is kept constant in all sub-cases). All in all, this ends up in only 33 sub-cases.

Loads comparison

The basic results investigated in this section are the load and deflection time series at nodes and members of the OWT. A given position (e.g. tower base) and type of output (e.g. vertical deflection) is called "output sensor" or "sensor" in the following. The results for the sensors are analyzed in processed formats such as extremes or damage equivalent loads (DEL). All DEL presented in this section are calculated with a reference number of cycles of $N = 2E8$ and a Wöhler Material Exponent of $m=3$ (which is common for welded steel parts) and extrapolated to one year of operation using the occurrences given in Table 4.1.

The global coordinate system used here is defined as follows: the x-axis points downwind along the mean wind direction and the wave direction; the z-axis points vertically upwards; and the y-axis forms a right handed coordinate system.

The simulations performed in this study provide a vast number of results, therefore, only a small subset of these results is presented. The sensors in the tripod mentioned in the following sections are visualized in Figure 4.5 using a picture of the super-element model.

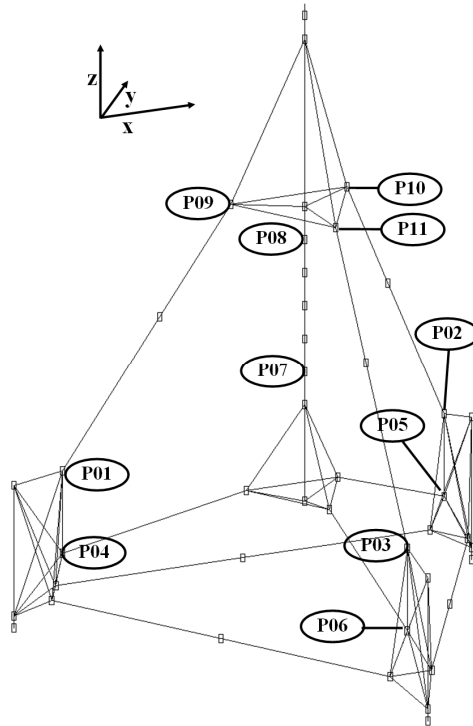


Figure 4.5: Output positions in the tripod.

At each of the output positions, forces and moments are investigated in terms of member loads, whereas the outputs at nodes where more than two members intersect are the member loads of legs and braces acting upon the joints. Loads at positions P07 and P08 are expressed in global coordinates, all other outputs are given in local coordinates defined as follows: the local x-axis is aligned with the member axis; the local z-axis is perpendicular to a plane formed by the global x-axis and the local x-axis; and the y-axis forms a right handed coordinate system. In case of a local x-axis and the global x-axis being parallel, the local y-axis is parallel to the global y-axis. For all outputs in local axes, the x-axis points away from the closest joint. This leads to sensors named such as P03Mx describing the member moment around the local x-axis (the torsional moment) at position P3 (in the downwind leg with negative global y-coordinates as shown in Figure 2).

Table 4.2 shows the absolute extreme values of the tower top deflection in the global coordinate system for all the load cases simulated. Values for the beam model and the super-element model are given together with the differences between both, with the differences related to the super-element results. The values for UX-MIN and RY-MIN are close to zero and not shown.

Table 4.2: Extreme values of tower top axial deflections and rotations for the beam- and the super-element model.

Value	Beam	Super	Diff [%]
UX-MAX	0.503	0.56	10.2
UY-MIN	-0.262	-0.323	18.9
UY-MAX	0.121	0.166	27.1
UZ-MIN	-0.015	-0.022	31.8
UZ-MAX	-0.011	-0.02	45
RX-MIN	-0.094	-0.129	27.1
RX-MAX	0.256	0.298	14.1

RY-MAX	0.474	0.502	5.6
RZ-MIN	-0.228	-0.458	50.2
RZ-MAX	0.228	0.469	51.4

The super-element model leads to increased deflection extremes that are significant and lie between 5.6% and 51.4% comparing the beam and the super-element model. The largest differences occur for the rotation about the global z-axis (vertical) RZ_{min} and RZ_{max} . In Table 4.3, the extremes of the tower base loads in global coordinates are shown. Values are not shown if they are very small compared to the other results, especially compared to their direct counterpart. This is the case for Fx_{min} and Mx_{min} as Fx_{max} and Mx_{max} have significantly higher absolute values. Again, the differences between the super-element and the beam element results given on a percentage basis are related to the super-element results.

Table 4.3: Extreme values of tower base loads for the beam- and the super-element model.

Force / moment component	Beam [kN] / [kNm]	Super [kN] / [kNm]	Difference [%]
Fx_{max}	866	876	1.14
Fy_{min}	-417	-484	13.84
Fy_{max}	315	351	10.26
Fz_{min}	-7078	-7081	0.04
Fz_{max}	-6741	-6719	-0.33
$Mx1_{min}$	-19893	-23274	14.53
$Mx1_{max}$	36867	41132	10.37
$My1_{max}$	72506	71988	-0.72
$Mz1_{min}$	-8341	-8026	-3.92
$Mz1_{max}$	8541	7774	-9.87

The differences for Fx_{max} , Fz_{min} , Fz_{max} and My_{max} are relatively small and not further considered. The forces in y-direction and the associated bending moment around the x-axis are higher for the super-element model. The torsional moments in the tower are reduced applying the super-element model.

Figure 4.6 gives the DEL at the tower base for both the beam and the super-element model.

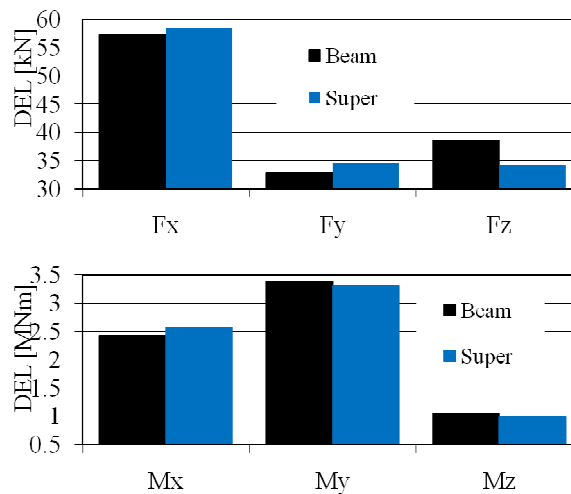


Figure 4.6: DEL at tower base

It is directly visible that there is no clear tendency. For F_x and M_x , the super-element model leads to slightly increased DEL, whereas for M_y and M_z the opposite is the case. F_y increases and F_z clearly decreases due to the super-element modeling.

To sum up, the tower top deflection displacement results confirm the conclusions drawn in [20]. The globally more compliant structure leads to larger deflections. In [20] it is stated that the support structure becomes more compliant especially in torsion, which is confirmed here with significantly increased deflections around the global z-axis. The influence of these changes on the loads is reviewed by means of the load maxima at the tower bottom firstly. Several load components remain almost unchanged. Apart from that, the side-to-side shear forces and bending moments are increased. This may result from the increased dynamic loading – visible through the increased deflections shown in Table 4.2 – which overcompensates the load reduction due to the more compliant central tripod joint in the super-element model. However, this is only meant as part of a stepwise plausibility check as in this study a fatigue load case set is investigated and therefore extreme loads are not in the focus. Nevertheless, these increased loads should be analyzed in more detail. The significantly higher tower torsional deflections do not lead to higher loads for the super-element model; in contrast, the torsional moments are significantly decreased. This is an important result as the increase of torsional deflection is quite significant. A shift of the tower torsional natural frequency into the upper 3P dynamic excitation range of the turbine and the corresponding risk of increased dynamic excitations is stated in [20]. Based on the tower base DEL presented herein this is not confirmed as the DEL around the tower torsional axis (M_z) is even decreased.

Figure 4.7, Figure 4.8 and Figure 4.9 show the DEL for the output positions P1, P2 and P3.

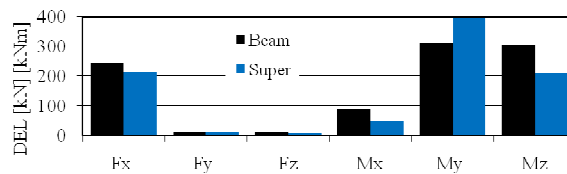


Figure 4.7: DEL in the upwind leg close to the joint connecting the pile sleeve (position P1).

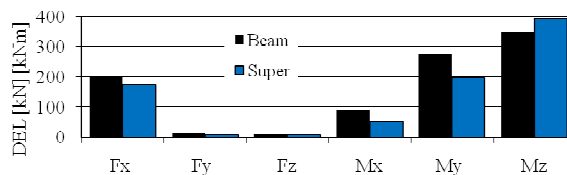


Figure 4.8: DEL in the first downwind leg close to the joint connecting the pile sleeve (position P2).

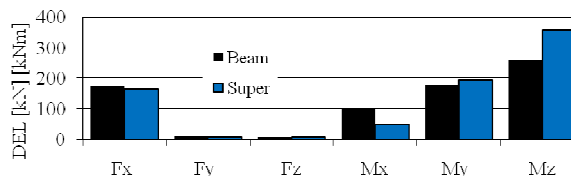


Figure 4.9: DEL in the second downwind leg close to the joint connecting the pile sleeve (position P3).

The differences between the beam- and super-element results are obviously significant for some of the values shown (e.g. the moments at position P1) and not for others (e.g. the axial load Fx at position P3). Furthermore, most of the DELs decrease using super-elements, but some increase such as the DEL of the bending moment My at position P1. This general situation is confirmed with the DEL at positions P4 to P11 (results not shown).

Table 4.4 provides condensed results from investigating DELs at all sensors from position P1 to P11. It gives the largest differences calculated for all sensors, whereas DELs with very small absolute values compared to the other DELs at the same positions are not taken into account. For example a DEL for the bending moment My at a given position is not taken into account if My has a smaller order of magnitude than Mz, even if the difference between the beam- and super-element results are huge. In this case the larger bending moment will dominate all further processing steps leading to a component design. In the below table the percentage differences refer to the super-element results, with negative values describing lower DELs for the super-element model than for the beam model.

Table 4.4: Largest differences in calculated DEL at positions P1 to P11.

Sensor	Beam [KNm]	Super [kNm]	Diff [%]
P01Mx	89	49	-81.9
P01Mz	307.4	210.99	-45.7
P02Mx	91.846	51.948	-76.8
P02My	274.61	196.16	-40
P03My	103.21	51.175	-101.7
P04Mx	191.6	86.494	-121.5
P05Mz	210.03	63.495	-230.8
P06My	96.974	54.178	-79
P09My	189.97	137.9	-37.8
P10Mz	91.339	54.914	-66.3
P11Mx	102.75	53.675	-91.4

Three results are evident. The differences are very large for these sensors - the maximum difference for P05Mz is close to a factor of four - and the super-element model leads to smaller DELs for each of those "large difference outputs". Furthermore, there are no forces in the list which means that the largest differences of significant outputs occur for bending and torsional moments. The results shown in Figure 4.7, Figure 4.8 and Figure 4.9 imply that due to the super-element modeling, DELs near joints may be reduced e.g. because of higher joint flexibilities. But on the other hand, the model is changed to such an extent that other effects such as a modified global load distribution scheme in the tripod – which is a statically over-determined structure – may have an opposite effect governing the shift of DEL toward larger values for the super-element model. This implies that the global load distribution scheme in the tripod is sensitive to relatively small stiffness changes in single members (or joints), a conclusion that matches with the results described in [18], where it is described that the loads in the tripod are significantly differing dependent on the beam formulation used. However, the results presented in Table 4.4 show that in the cases of large differences between beam- and super-element results for relevant absolute values, the use of super-elements leads to massively reduced DEL for the member moments.

In summary, the effects of a super-element modeling approach in the aero-elastic tool ADCoS-Offshore on simulation results for a 5MW OWT on a tripod substructure is investigated. A massively reduced but realistic power production fatigue load case set and the UpWind deep water reference site data are used. The global stiffness of the structure is decreased and the corresponding deflections are therefore increased in the simulations including super-elements. Especially the rotations around the vertical axis are significantly higher. Both points were already described in [20] for a special load case and confirmed herein using the more extensive load case set. The possibility of increased global loads due to the larger deflections and due to the natural frequency shifts - especially for the global torsion mode as the associ-

ated eigenfrequency is shifted into the upper 3P range - was formulated in [20]. This is not confirmed for the torsion, as the extreme values of the torsional moment as well as the corresponding DEL in the tower base are even reduced with the super-elements. The side-to-side loads are increased in terms of extremes, but the more important corresponding DELs do not show results that are that clear.

For the DELs in the tripod itself, investigated at 11 different output positions, the results are not straightforward to interpret at a first glance. Some loads increase, others decrease and some remain unchanged. The step from a beam to a super-element model activates effects increasing or decreasing local loads and - dependent on the position and load situation - one or the other effect may dominate. However the changes that do occur are significant, and the load paths in the statically over-determined structure seem to change globally. However, the largest changes of DEL with significant values show the clear tendency of decreased moments using the super-element model and these results show again the large differences in the DEL calculated with the two models.

To conclude, more detailed studies are essential to fully understand the influence of the super-element approach for the loads simulation of OWT with tripod structures under realistic conditions. But it is obvious that the more detailed joint modeling with super-elements in the fully-coupled simulation leads to remarkable differences in the results and should therefore be applied for this type of structure.

5. Development of design requirements

As offshore wind farm sites become larger and there is greater site variability, the optimization of support structure design and efficiency of the design process becomes increasingly important. In terms of the IEC 61400-3 international design standard both normative requirements and informative methodologies need to be updated and improved in accordance with the advancement of the industry.

Section 5.1 presents a summary of recommendations for the development of the international IEC 61400-3 design standard for bottom-mounted offshore wind turbines. As part of WP4 an interim review of the first edition of the standard was performed [22], including recommendations for the development of future editions. A review of various models for irregular, non-linear waves suitable for design purposes was also performed, in order to judge their relevance for future offshore wind farms (see [21]).

Section 5.2 presents the results of reliability-based investigations into the required safety factor / Fatigue Design Factor (FDF) values to be used for fatigue design of steel sub-structures for offshore wind turbines. Design and limit state equations are formulated and stochastic models for the uncertain strength and load parameters are described.

Section 5.3 presents recommendations for the implementation of a reduced set of offshore wind turbine design load cases according to the IEC 61400-3 standard for the preliminary design of jacket support structures. The number of design load cases required for full offshore support structure design is potentially very large, and this can become even more impractical when complex multiple-member support structures are considered.

Section 5.4 presents results from a design load case parameter analysis performed for a jacket support structure, in order to investigate the driving fatigue and extreme load cases for this support structure type.

5.1 Input to development of IEC 61400-3 standard

The IEC 61400-3 standard [69] provides a set of international guidelines for the design of bottom-mounted offshore wind turbines. The standard, which was developed by a working group of international experts, provides design requirements for offshore wind turbines and their support structures, and provides much needed international consistency in a rapidly growing industry.

Following the publication of the IEC 61400-3 standard in January 2009, a Maintenance Team is expected to be formed in order to begin work on a second edition of the standard. This section presents a summary of recommendations for this and future revisions of the standard, based on [22]. The proposals include contributions from researchers, consultants, manufacturers and developers involved in the offshore wind industry, as well as a summary of comments made by the IEC national committees.

5.1.1 Marine conditions

The marine conditions at an offshore wind turbine site include waves, sea currents, water level, sea ice, marine growth, scour and seabed movement. The design of the support structure must be based on marine conditions which are representative of the offshore wind turbine site. The structural integrity of the rotor-nacelle assembly must also be demonstrated taking proper account of the marine conditions at the specific site at which the offshore wind turbine will be installed.

Severe sea state

The severe sea state model, defined in Sections 6.4.1.3 and 6.4.1.4 of the standard, is used for the calculation of ultimate loads acting on an offshore wind turbine during power production. It is considered in combination with normal wind conditions and is used in design load case DLC 1.6. This load case models the situation after an extreme storm event which may have caused the offshore wind turbine to shut down, in which the wind speed has reduced to a level which has enabled the turbine to start up again. Because the wind speed usually dies down more quickly than the wave height, a situation can occur in which the turbine is operating and the waves are still at an extreme level. This is the situation modelled by DLC 1.6. It is proposed that a general review of the DLC 1.6 load case should be undertaken, in order to determine whether or not the above design situation is the most realistic one that should be modelled by this load case. This review should also examine the best way for this load case to model the required design situation, and whether or not the severe sea state model meets the requirements of this load case.

Extreme and reduced wave height

The extreme wave height (EWH) and reduced wave height (RWH), defined in Sections 6.4.1.6 and 6.4.1.7 of the standard, are used for the extreme deterministic design wave and reduced deterministic design wave with recurrence periods of 50 years (H_{50} , H_{red50}) and 1 year (H_1 , H_{red1}). The standard states that if the values of the above wave heights cannot be determined from site-specific measurements, then it may be assumed that:

$$H_{50} = 1,86 H_{s50} \quad \text{and} \quad H_1 = 1,86 H_{s1}$$

and

$$H_{red50} = 1,3 H_{s50} \quad \text{and} \quad H_{red1} = 1,3 H_{s1}$$

These factors assume a Rayleigh distribution of wave heights.

It is proposed that the analysis of the EWH and RWH should be improved. There is an argument that the factors used are too simplistic and non-conservative and should be changed. For instance, the factor of 1.86 applied to H_{s50} gives the most likely largest wave height in a 3-hour sea state with 50-year return period, but this does not necessarily correspond to the 50-year wave height H_{50} . The assumption of the Rayleigh distribution does provide some conservatism given the shallow water location of most of the present and planned offshore wind farms. It is also recognised that changing this factor of 1.86 would necessitate reconsideration of other safety factors. However given that in the future an increasing number of deep water locations will be used for offshore wind farms it is recommended that the analysis of these wave heights is reconsidered.

Water levels

For the calculation of hydrodynamic loading on an offshore wind turbine, the variation in water level at the site should be taken into account. This water level variation is defined in the IEC 61400-3 standard with five levels: Lowest Still Water Level (LSWL), Lowest Astronomical Tide (LAT), Mean Sea Level (MSL), Highest Astronomical Tide (HAT), Highest Still Water Level (HSWL).

From the experience gained by the offshore wind industry, in particular for support structure design in locations where the tidal variation is not significant (for example in the Baltic Sea), it has been found that the number of water levels considered becomes computationally very expensive for comparatively little change in design. It is proposed that the analysis of the number of water levels to be considered is improved, to give more flexibility to reduce computation where the tidal variation does not have a significant impact on support structure design. It is also recommended that expected long-term water level changes over the lifetime of the turbine should be considered in this discussion.

5.1.2 Design situations and load cases

For design purposes, the lifetime of an offshore wind turbine can be represented by a set of design situations covering the normal and extreme conditions that an offshore wind turbine may experience. Within each design situation several design load cases must be considered. The minimum set of design load cases to be considered is specified in Table 1 in Section 7.4 of the IEC 61400-3 standard.

The external conditions experienced by an offshore wind turbine include marine conditions as well as the wind conditions experienced by onshore machines. This introduces a number of additional parameters into the design load calculations such as waves, currents, tides and wind/wave directionality. The result is that the number of simulations required to ensure that all design situations in an offshore wind turbine's lifetime are covered is dramatically increased. The large number of combination possibilities leads to a potentially overwhelming amount of computation for the design engineer.

It is proposed that the design load case table should be reviewed. This review should have the following aims:

1. An analysis of whether the specified load cases model the design situations experienced by an offshore wind turbine in a satisfactory way.
2. A reduction in the number of simulations required to fulfil the specified load case combinations, including a methodology for how to reduce this number.
3. An analysis, using experience of offshore wind turbine design, of which parameters typically result in unnecessary conservatism in rotor-nacelle assembly and support structure design.

It is recommended that the Maintenance Team for the second edition of the IEC 61400-3 standard considers these aims in the context of a complete review of the design load case table

Normal external conditions

Design load case DLC 1.2 specifies that a Normal Sea State must be considered for fatigue load calculations, taking into account the joint probability distribution of H_s , T_p and V_{hub} . It is proposed that a more detailed methodology be given for the number of wave heights and wave periods to consider for each wind speed bin, and the process by which these values can be obtained from the metocean data. Recommendations could also be given for how to reduce the number of simulations required in order to meet the design load case requirements. The methodology used for this process is not normative, and therefore should be included in an informative Annex.

For the calculation of loads acting on the support structure, the standard specifies that in general (with the exception of load cases involving a transient change in mean wind direction and those involving the wind turbine in a parked situation) the wind and waves may be assumed to be co-directional. The standard also states that the multi-directionality of the wind and waves should be taken into account, as this can have an

important influence on support structure loads, depending on the extent to which the support structure is non-axisymmetric. The experience of the offshore wind turbine industry to date has showed that the misalignment of wind and waves can be very important in calculating support structure loads, especially for fatigue loading. In some cases the wind-wave misalignment can drive the design of the structure, in particular for monopile support structures. In order to improve the standard it is proposed that an improved definition of wind-wave misalignment should be considered. One option is to include a simple but realistic set of situations to be considered during design, for instance to give typical values for wind-wave misalignment as a function of wind speed. However it is recognised that the wind-wave misalignment may vary significantly between offshore wind turbine sites. It is recommended that this issue be discussed for future revisions of the standard

Extreme external conditions

The design load cases that relate to storm or extreme wave conditions (DLC 1.6, 6.1, 6.2, 7.1 and 8.2) are defined in Table 1 in Section 7.4 of the standard with two or three different combinations of wind and wave conditions, labelled a, b and c. These combinations include turbulent inflow with stochastic sea states and/or deterministic design waves, and steady wind models with deterministic design waves. This is to ensure that the load cases take proper account of the dynamic response of the offshore wind turbine to wind, wave and current loads as well as non-linear wave kinematics. It is proposed that the presentation of these load cases in the load case table be discussed by the maintenance team for future revisions of the standard. The load case table could be clarified by condensing options a, b and c into one load case, and updating the associated text in Sections 7.4.1, 7.4.6, 7.4.7, 7.4.8 and 7.5.4 [23]. This may allow more flexibility in the method of calculating extreme loads whilst still providing guidance on achieving the load case requirements.

The design load case table also allows for design situations involving power production with the occurrence of a fault. The faults experienced by offshore wind turbines may be more severe than for onshore wind turbines, and the time lapse between a fault occurring and maintenance taking place may also be much longer. For this reason remote control of offshore wind turbines is increasingly being adopted by offshore wind turbine manufacturers and offshore wind farm operators. It is proposed that requirements regarding the safety system and remote control of offshore wind turbines be described in more detail for future editions of the IEC 61400-3 standard. It is also proposed that a further study be undertaken into safety factors for fault load cases, in particular to establish a probabilistic model where realistic failure rates, downtimes and environmental conditions are used to assess the reliability of the turbine and to compare it to other load cases.

Other requirements

The design condition for evaluating cracks in concrete and soil settling is defined in Section 7.5.5 of the IEC 61400-3 standard with two alternatives, based on power production load cases:

1. the load from the bending moment that is exceeded 1% of the time
2. the load from the bending moment associated with maximum mean thrust plus 1.28 times the standard deviation (the 90% fractile).

It is questionable whether or not the first alternative for crack width evaluation is appropriate, as it indicates a time dependency for the crack width which is not necessarily correct [24]. It is recommended that these two alternatives be discussed and evaluated for future reviews of the standard.

The required air gap for offshore wind turbine support structures is not addressed in detail in the current edition of the IEC 61400-3 standard. It is proposed that forthcoming editions of the standard include an improved analysis of run up and required air gap, as a function of support structure type and wave conditions.

The IEC 61400-3 standard does not currently contain any guidelines regarding the conversion of land based turbines to offshore. It is proposed that for future revisions of the standard the maintenance team consider the possibility of including these requirements in the standard. This could involve for example

guidelines for the inclusion of climate control in the rotor-nacelle assembly. This would take the form of an informative Annex.

The IEC 61400-3 standard uses the partial safety factor format to account for the uncertainties and variability in loads and material properties, the uncertainties in the analysis methods and the importance of structural components with respect to the consequences of failure. A partial safety factor of 0.9 is specified for favourable loads, including pretension and gravity loads that significantly relieve the total load response. However there has been some discussion over whether this value is adequate: for concrete structures it may be too conservative, whereas for structures with backfill it may be non-conservative. It is recommended that this issue be discussed within the context of offshore load calculations by the IEC 61400-3 Maintenance Team as part of the next edition of the standard. It is acknowledged that the Maintenance Team for the IEC 61400-1 design standard are already considering this issue. This will hopefully provide useful additional insight to the discussion.

5.1.3 Assessment of external conditions

Because of the variability in external conditions between sites, a site investigation must always be carried out for the design of an offshore wind turbine support structure. There is therefore an argument for saying that the whole of Section 12, "Assessment of the external conditions at an offshore wind turbine site" should be moved forward and replace Section 6 "External conditions". It is recommended that this issue be discussed by the Maintenance Team for the IEC 61400-3 standard.

Assessment of wind conditions

The following parameters are required to be estimated for the assessment of the wind conditions at an offshore wind turbine site:

- extreme 10-min average wind speed with a 50-year recurrence period;
- wind speed probability density function;
- ambient turbulence standard deviation;
- wind shear;
- air density.

Where site-specific data are not available for turbulence standard deviation, the standard specifies that the value may be estimated using the below equation:

$$\sigma_1 = \frac{V_{\text{hub}}}{\ln(z_{\text{hub}}/z_0)} + 1,28 \cdot (1,44\text{m/s}) \cdot I_{15}$$

It is possible that the value of $1.44 \cdot I_{15}$ used to represent σ_σ is not conservative, and should be increased to reflect the higher value of σ_σ at some offshore locations. It is proposed that the formula used for turbulence standard deviation where site data are not available should be re-considered in future revisions of the standard.

Assessment of seabed movement and scour

The stability of the seabed is extremely important in the design of offshore wind turbine foundations. Sea floor variations are defined in the standard as a combination of the following:

- Local scour characterised by steep sided scour pits around structural elements
- Global scour characterised by shallow scoured basins of large extent around a structure
- Overall seabed movement of sand waves, ridges and shoals etc.

The local and global scour around an offshore wind turbine foundation is a function of the support structure type and the local soil conditions, as well as the hydrodynamic climate of the offshore wind turbine site. The IEC 61400-3 standard states that the extent of scour and the required scour protection must be

determined on the basis of previous records from nearby sites, from model tests, or from calculations calibrated by prototype or model tests.

It is proposed that for future revisions of the standard the section on seabed movement and scour be extended to include rough assumptions and conservative estimates for scour to be considered. The section should also describe in more detail typical methodologies for determining scour, with additional references. Given the site-specific nature of scour and the difficulty of providing normative guidance on values to assume, these extensions could take the form of an additional informative Annex.

Assessment of soil conditions

The soil properties at a proposed offshore wind turbine site must be assessed by a professionally qualified geotechnical engineer, providing sufficient information to characterise soil properties throughout the region that will affect the foundation. The standard currently states that site-specific soil data shall in principle be established for each foundation within the wind farm. From the experience gained in the offshore wind industry, in particular regarding the variability of site conditions and the impact of soil properties on foundation design, it is confirmed that a thorough investigation of soil conditions across the whole site is crucial for the design of offshore wind turbine foundations and support structures.

Section 12.15 of the IEC 61400-3 standard contains a list of general soil investigations to be made at a proposed offshore wind turbine site, and a list of the data that must be provided from these investigations to be used as the basis of the foundation design. Given the importance of the soil conditions to the foundation and support structure design, it is proposed that the standard should also include an analysis of the different methods for modelling soil conditions (e.g. P-Y springs, FEM etc). This could take the form of an additional informative Annex. For an example of an existing guideline which includes more detail on this subject, see [25]. It is recommended that the maintenance team consider for future revisions of the standard the level of detail that should be specified regarding site-specific soil investigation.

5.1.4 Informative Annexes

Annex D: Calculation of hydrodynamic loads: Morison's equation

The viscous drag and inertia loading on an offshore wind turbine support structure is commonly calculated using Morison's equation. The equation for a static member is:

$$F = \frac{1}{2} C_d \rho D |U| U + C_m \rho A \dot{U}$$

When there is significant movement in the structure, the relative velocity and acceleration of the structure to the waves modify the drag and inertia forces respectively. The force resulting from the relative acceleration can be analysed most conveniently using the concept of an added mass of water which is constrained to move with the structure. In order to model the effect of the relative acceleration an added mass coefficient C_a is included in Morison's equation, which then becomes:

$$F = \frac{1}{2} C_d \rho D |U_r| U_r + C_m \rho A \dot{U}_w - C_a \rho A \dot{U}_s$$

The standard currently states that $C_a = C_m - 1$ for slender, cylindrical members of fixed structures. However there may be more constraint required on the use of this relation, as the added mass also depends on the frequency of the oscillation and the deflection of the tower curve. It is recommended that for future revisions of the standard the value of C_a and the conditions under which this relation is valid are addressed in more detail.

Annex D: Calculation of hydrodynamic loads: Vortex induced vibrations

When steady flow passes a solid body such as a cylindrical pile, there may be vortices formed which shed into the flow beyond the body. These vortices cause a dynamic loading on the body, which can be highly

damaging if the frequency of the excitation coincides with a natural frequency of the structure. In order to avoid the range of conditions at which resonance can occur, it is important to predict the frequencies at which large amplitudes of oscillation may be expected.

Section D.4 addresses the issue of vortex induced vibrations, giving a methodology for calculating the critical velocities at which resonances will occur for a given structure. However this theory is only valid for steady currents and cannot be used for waves unless the period is very long, i.e. if the KC number is high. In the light of this it is recommended that this whole section should be revised in any future revisions of the standard.

Annex D: Calculation of hydrodynamic loads: Appurtenances

For relatively small appurtenances it is sufficient to account for the additional hydrodynamic forces in the dimensions and/or force coefficients assumed for the modelled elements. Section D.5 describes a method for calculating equivalent hydrodynamic coefficients C_{deq} and C_{meq} taking into account appurtenances and marine growth on a monopile support structure. The appurtenances are approximated by vertical circular cylinders, characterized by an equivalent diameter d_i . Using this method the equivalent hydrodynamic coefficients are calculated by:

$$C_{deq} = \left\{ \frac{D'}{D} C_{ds}(R, e) \cdot WAF_d(K) + \sum_{i=1}^N \left[\frac{d_i'}{D} \cdot C_{dsi}(R_i, e) \cdot WAF_{di}(K_i) \cdot IF_{di}(\phi_i, K_i) \right] \right\}$$

and

$$C_{meq} = \left\{ \frac{(D')^2}{D^2} C_m(K, C_{ds}) + \sum_{i=1}^N \left[\left(\frac{d_i'}{D} \right)^2 \cdot (1 + (C_{mi}(K_i, C_{dsi}) - 1) \cdot IF_{mi}(\phi_i, K_i)) \right] \right\}$$

In the above equations IF_{di} and IF_{mi} are interference factors expressing the variation in hydrodynamic coefficient for the appurtenance due to the presence of the monopile. In order to calculate these factors the designer is referred to the reference documents [25] and [26].

An improvement to the method currently stated in the standard has been proposed [27], using C_d and C_m values from [28] and ignoring the wake amplification factor WAF_d . The method for calculating IF_{di} and IF_{mi} is also expressed in more detail in the proposed method, including separate calculations for blocking and shielding regimes for both factors. It is recommended that the maintenance team consider this proposed method in future revisions of the standard.

It has also been proposed that in future revisions of the standard indicative values should be given for secondary loads and loads on secondary structures. In some instances these may be higher than loads on primary structures, so it is important they are well defined. It is recommended that this proposal be discussed by the Maintenance Team.

Annex E: Ice loading

Annex E of the standard provides guidance with regard to ice load calculations. The standard states that the following ice loads should be assessed:

- horizontal load due to temperature fluctuation in a fast ice cover (thermal ice pressure);
- horizontal load from a fast ice cover subject to water level fluctuations and in terms of arch effect;
- horizontal load from moving ice floes;
- pressure from hummocked ice and ice ridges due to both subduction and ridging processes;
- vertical force from fast ice covers subject to water level fluctuations.

Further description of the sea ice design load cases is given in Section 7.4.9 of the standard. These descriptions include methods for calculating horizontal loads from moving ice for both cylindrical and sloping structure shapes. Simplified equations are also given for calculating dynamic ice loads, which can be used if statistical data or measurements are not available. It is proposed that Annex E be reviewed for any future revisions of the IEC 61400-3 standard, with particular reference to simplifying the ice design load cases. It may also be necessary to extend the treatment of dynamic ice loading. It is recommended that these issues be discussed by the Maintenance Team.

5.1.5 Summary

The publication of the IEC 61400-3 international design standard is a valuable step forward for the offshore wind industry, and addresses an important need. The standard specifies the essential design requirements to ensure the engineering integrity of offshore wind turbines, and provides a unified approach to codifying offshore wind turbine requirements. However the industry has matured and advanced since the standard was first written and consequently there are a number of shortfalls in the document. This section identifies some areas in which the standard may be improved, in particular by suggesting specific areas for further discussion when the IEC 61400-3 Maintenance Team is formed.

Amongst the proposals made in this report, some are considered to be of higher priority than others. The following are agreed to be the most important:

- Review of the design load case table, with the aim of simplifying the parameters considered and reducing the number of simulations required to meet the design load case requirements (where possible).
- More detailed guidance to be included regarding site-specific requirements to allow for site variability, such as the assessment of soil conditions.

5.2 Reliability-based calibration of safety factors for offshore support structures

This section describes reliability-based investigations on the required safety factor / Fatigue Design Factor (FDF) values to be used for fatigue design of steel substructures for offshore wind turbines. The Fatigue Design Factors (FDF) are for linear SN-curves with slope m related to the partial safety factors for fatigue load, γ_f and strength, γ_m by: $FDF = (\gamma_f \gamma_m)^m$. Design and limit state equations are formulated and stochastic models for the uncertain strength and load parameters are described. Further, the effect of possible inspections during the design lifetime is investigated. The results indicate that for fatigue critical details where the fatigue load is dominated by wind load FDF values equal to 2.5 are required. If wave load is dominating slightly larger FDF values are required. For a full description of the derived models and equations see [29].

The support structure for offshore wind turbines contributes with a substantial part of the total cost of an offshore wind farm. In order to increase the competitiveness of offshore wind energy it is therefore important to minimize the cost of energy considering the whole life cycle. In this section reliability based calibration of safety factors to be used for fatigue design of steel support structures is considered. Safety factors used for the design of oil & gas support structures are generally calibrated to a reliability level which is larger than the one required for offshore wind turbines. In this section safety factors are calibrated to a minimum reliability level both without and with inspections during the life time.

Design equations to be used for deterministic, code-based design and corresponding limit state equations to be used for reliability assessment are formulated. In the limit state equations uncertain parameters are modelled as stochastic variables. In the design equations safety factors for fatigue strength and load or equivalently Fatigue Design Factors (FDF) are used to secure the required reliability level.

Since design and limit state equations are equivalent a detailed model of the fatigue damage is generally not needed for a reliability-based assessment of fatigue safety factors. It is 'only' important to model the

uncertain parameters carefully. Three fatigue load cases are considered: 1) wave load dominating; 2) wind load dominating for a single wind turbine; 3) wind load dominating for a wind turbine in a wind farm. Stochastic models for assessment of the fatigue reliability are formulated for these three cases. SN-curves and Miner's rule with linear damage accumulation are used as recommended in most relevant standards, for example [28], [30] and [69].

Table 5.1: Fatigue Design Factors required.

Failure critical detail	Inspections	ISO 19902	GL / DNV	EN 1993-1-9
Yes	No	10	2.0 (3.0)	2.5 (4.5)
Yes	Yes	5	1.5 (2.0)	1.5 (2.0)
No	No	5	1.5 (2.0)	1.5 (2.0)
No	Yes	2	1.0 (1.0)	1.0 (1.0)

Table 5.1 shows required FDF values for fatigue design in various standards: ISO 19902 2007 for fixed offshore steel structures for oil & gas platforms [28], GL Guideline for the certification of offshore wind turbines [31], DNV Design of offshore wind turbine structures, OS-J101 [32] and Eurocode 3: Design of steel structures - Part 1-9: Fatigue [33]. The FDF values shown for GL / DNV and EN 1993-1-9 are determined using a linear SN-curve with slope equal to 3 and 5 in brackets. The FDF values are specified for critical and non-critical details and for details that can or cannot be inspected.

For manned offshore steel jacket structures for oil & gas production typically a maximum annual probability of failure in the range $10^{-5} - 5 \cdot 10^{-5}$ is accepted. For unmanned structures a maximum annual probability of failure in the range $10^{-4} - 2 \cdot 10^{-4}$ is accepted.

First, reliability models are formulated for the cases with wind load only. Probabilistic models are described for reliability assessment of wind turbines where wind load is dominating (over wave loads). The models are mainly based on [34]. Design by linear SN-curves is considered for a single wind turbine. A representative design parameter z is introduced, e.g. cross-sectional area or section modules. z is determined from the design equation for a wind turbine in free flow. This corresponds to designing to the 'limit' for fatigue according to the deterministic requirements in the standard using partial safety factors. z is used in the limit state equation with model uncertainties for Miner's rule, wind load effects and local stress analysis to estimate the reliability index and probability of failure with the given reference time interval, see details in [29].

Next, wind turbines in a wind farm wake and non-wake conditions also have to be accounted for. The Frandsen model for effective turbulence in [30] is used. The design equation and limit state equation can then be re-written and the reliability index or probability of failure estimated. Bi-linear SN-curves are also considered.

Third, reliability models are formulated for the case with wave load only. The design parameter z is again determined from the design equation for a structural detail, and used in the limit state equation with model uncertainties for Miner's rule, wave load effects and local stress analysis to estimate the reliability index or probability of failure with the given reference time interval, see details in [29].

Finally fatigue design factors and corresponding partial safety factors are calibrated to reliability levels appropriate for offshore wind turbines. Linear and bi-linear SN-curves and the consequences of fatigue failure of a fatigue critical detail are considered. Initially, safety factors are calibrated assuming no inspections of the critical details. Next, reliability-based methods are presented as basis for assessing the influence of inspections on the required FDF values. In order to model the influence of inspections a fracture mechanics model is calibrated to the same reliability level as the SN-curve approach. Finally, the resulting reduced FDF values in case of inspections are presented for different inspection qualities.

5.2.1 Results – reliability level and FDF values

If one fatigue critical detail is considered then the annual probability of failure is obtained from:

$$\Delta P_{F,t} = P_{\text{COL|FAT}} P(\text{Fatigue failure in year } t)$$

Where $P(\text{Fatigue failure in year } t)$ is the probability of failure in year t and $P_{\text{COL|FAT}}$ is the probability of collapse of the structure given fatigue failure – modelling the importance of the detail. The probability of failure in year t is estimated using the limit state equations described above, see [29] for details.

Given a maximum acceptable probability of failure (collapse), $\Delta P_{F,\text{max}}$ the maximum acceptable annual probability of fatigue failure (with one year reference time) and corresponding minimum reliability index become:

$$\Delta P_{F,\text{max},\text{FAT}} = \Delta P_{F,\text{max}} / P_{\text{COL|FAT}}$$

$$\Delta \beta_{\text{min},\text{FAT}} = -\Phi^{-1}(\Delta P_{F,\text{max},\text{FAT}})$$

where $\Phi(\)^{-1}$ is the inverse standard Normal distribution function.

The probabilistic modelling used for offshore wind turbine support structures in the following is based on the probabilistic models used for offshore oil & gas jacket structures. Therefore, results for this case are included to demonstrate that the probabilistic modelling used in this section is consistent with the reliability level required for this type of structure. Next, results of reliability analyses and calibrated FDF values for offshore wind turbines are considered using the probabilistic models modified to correspond to offshore wind conditions.

Steel jacket substructure for oil & gas – wave load

The stochastic model shown in Table 5.2 is considered as representative for a fatigue sensitive detail in an offshore steel jacket structure for oil & gas where consequences of failure are large, see [35], [36] and [37]. It is assumed that the design lifetime is $T_L = 30$ year and the number of stress ranges per year is $\nu = 5.10^6$.

Table 5.2: Stochastic model – welded steel detail. N: Normal; LN: LogNormal.

Variable	Distribution	Expected value	Standard deviation / Coefficient Of Variation	Comment
Δ	N	1	$COV_{\Delta} = 0.30$	Model uncertainty Miners rule
X_{Wave}	LN	1	$COV_{\text{Wave}} = 0.10$	Model uncertainty wave load
X_{SCF}	LN	1	$COV_{\text{SCF}} = 0.10$	Model uncertainty stress concentration
m_1	D	3		Slope SN-curve
$\log K_1$	N	from $\Delta\sigma_D$	$\sigma_{\log K_1} = 0.20$	Uncertainty SN-curve
m_2	D	5		Slope SN-curve
$\log K_2$	N	from $\Delta\sigma_D$	$\sigma_{\log K_2} = 0.25$	Uncertainty SN-curve
$\Delta\sigma_F$	D	71 MPa		Fatigue strength
log K_1 and log K_2 are fully correlated				

Table 5.3 shows annual reliability indices for different FDF values. FDF = 10 is used for fatigue critical details which cannot be inspected. The annual reliability index is seen to be 4.3 corresponding to an annual probability of failure equal to 10^{-5} . This reliability level corresponds to that generally required for fatigue critical details with large consequences of failure.

Table 5.3: Annual reliability index for different FDF values.

FDF	1	2	3	5	10
$\Delta\beta$	2.39	2.84	3.16	3.63	4.32

Steel substructure for offshore wind turbines – wave load

In Table 5.4 is shown examples of how to model the uncertainty related to estimation of stress concentration factors, X_{SCF} (partly based on [38]). Five values of COV_{SCF} are used to model different levels of analysis and complexity.

Table 5.4: Examples of COV_{SCF} .

COV_{SCF}	Fatigue critical detail
0.00	Statically determinate systems with simple fatigue critical details (e.g. girth welds) where FEM analyses are performed
0.05	Statically determinate systems with complex fatigue critical details (e.g. multi-planar joints) where FEM analyses are performed
0.10	Statically in-determinate systems with complex fatigue critical details (e.g. doubler plates) where FEM analyses are performed
0.15	2 dimensional tubular joints using SCF parametric equations
0.20	Tubular joints in structures where tubular stiffness is modeled by Local Joint Flexibility (LJF) models and SCF parametric equations are used

Basically it is assumed that $COV_{SCF} = 0.10$ and $COV_{Wave} = 0.10$. If the response is quasi-static then the number of stress cycles is typically $\nu = 5 \cdot 10^6$. It is assumed that the design lifetime is $T_L = 20$ year.

For offshore wind turbines where the consequences of failure is typically less serious compared to offshore oil & gas structures the maximum acceptable annual probability of failure is in the range $\Delta P_{F,max} = 10^{-4} - 10^{-3}$, corresponding to the reliability level for an unmanned fixed offshore structure, see above.

If a linear SN-curve with $m = 3$ is used then Table 5.5 shows the required FDF values for $\Delta P_{F,max} = 10^{-4}$, $2 \cdot 10^{-4}$, 10^{-3} and for $P(COL|FAT) = 1.0, 0.5, 0.1$ and 0.01 . In brackets is shown the corresponding values of the product of the load and material partial safety factors $\gamma_f \gamma_m$. The importance of using $m = 5$ is shown below.

Table 5.5: Required FDF and corresponding partial safety factors $\gamma_f \gamma_m$ in () for given $\Delta\beta_{min,FAT}$ ($\Delta P_{F,max,FAT}$). (–) indicates that $FDF \leq 1$.

$P(COL FAT)$	3,1 (10^{-3})	3,5 ($2 \cdot 10^{-4}$)	3,8 (10^{-4})
1.0	2.40 (1.34)	3.38 (1.50)	4.32 (1.63)
0.5	1.98 (1.26)	2.88 (1.42)	3.73 (1.55)
0.1	1.11 (1.03)	1.87 (1.23)	2.60 (1.37)
0.01	(–)	(–)	1.26 (1.08)

It is noted that for a linear SN-curve the same FDF values are obtained if $\nu = 5.10^7$ is used. For a minimum annual reliability index equal to 3.5, FDF = 3.4 is obtained if the consequence of the fatigue failure is large. Table 5.6 shows the required FDF values for different values of COV_{SCF} . It is seen that if $COV_{SCF} = 0.00$ (very good assessment of fatigue stresses) is used then the required FDF is 2.8 and the corresponding partial safety factor is 1.4. Table 5.7 shows the required FDF values for different values of COV_{Wave} .

Table 5.6: Required FDF and corresponding partial safety factors $\gamma_f \gamma_m$ in () for different values of COV_{SCF} .

COV_{SCF}	0.00	0.05	0.10	0.15
FDF ($\gamma_f \gamma_m$)	2.83 (1.42)	2.97 (1.44)	3.38 (1.50)	4.10 (1.60)

Table 5.7: Required FDF and corresponding partial safety factors $\gamma_f \gamma_m$ in () for different values of COV_{Wave} .

COV_{Wave}	0.05	0.10	0.15
FDF ($\gamma_f \gamma_m$)	2.97 (1.44)	3.38 (1.50)	4.10 (1.60)

If a bi-linear SN curve is used then the required FDF values shown in Table 5.8 and Table 5.9 are obtained. Also shown are the decreases in design values using a bi-linear SN-curve instead of a linear SN-curve. It is seen that compared to a linear SN-curve larger FDF values are required, but at the same time smaller design values (less material needed) are obtained.

Table 5.8: FDF and corresponding partial safety factors in () for $\nu = 5.10^6$. Bi-linear SN-curve.

$\Delta\beta_{min,FAT} (\Delta P_{F,max,FAT})$	3,1 (10-3)	3,5 (2 10-4)	3,8 (10-4)
FDF	3.42	5.46	7.73
z_{Bilin} / z_{lin}	0.93	0.94	0.94

Table 5.9: FDF and corresponding partial safety factors $\gamma_f \gamma_m$ in () for $\nu = 5.10^7$ and given $\Delta\beta_{min,FAT} (\Delta P_{F,max,FAT})$. Bi-linear SN-curve.

$\Delta\beta_{min,FAT} (\Delta P_{F,max,FAT})$	3,1 (10-3)	3,5 (2 10-4)	3,8 (10-4)
FDF	4.74	7.94	> 10
z_{Bilin} / z_{lin}	0.79	0.79	

Table 5.10 shows required FDF values if the lower linear SN-curve with slope $m_2 = 5$ is used and $\Delta\sigma_F = 71$ MPa for $N_D = 2.10^6$. Also shown are the corresponding partial safety factors calculated using the slope m_2 . It is seen that the required FDF values are much higher than using the upper linear SN-curve with slope $m_1 = 3$, but the partial safety factors are slightly lower. A decrease in design values is also seen. It is noted that the change in standard deviation of the SN-curve for the two branches influences both the reliability and the mean value of the SN-curve.

Table 5.10: FDF and corresponding partial safety factors $\gamma_f \gamma_m$ in () given $\Delta\beta_{min,FAT} (\Delta P_{F,max,FAT})$

$\Delta\beta_{min,FAT} (\Delta P_{F,max,FAT})$	3,1 (10-3)	3,5 (2 10-4)	3,8 (10-4)
FDF ($m_1 = 3$)	2.40 (1.34)	3.38 (1.50)	4.32 (1.63)
FDF ($m_2 = 5$)	3.31 (1.27)	5.44 (1.40)	7.73 (1.51)
z_{m_2} / z_{m_1}	0.90	0.89	0.87

Steel substructure for offshore wind turbines – wind load

In this section reliability analysis and Fatigue Design Factors are performed for fatigue sensitive details in a steel substructure for a single wind turbine and for a wind turbine in a wind farm.

The mean wind speed is assumed to be Weibull distributed with scale parameter = 10.0 m/s and shape coefficient = 2.3. It is assumed that the reference turbulence intensity is $I_{ref}=0.14$.

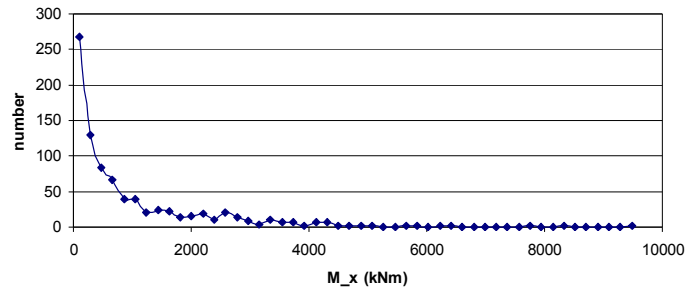


Figure 5.1: Number of load cycles in a 10 minutes period for mudline bending moment. Mean wind speed equal to 14 m/s.

Figure 5.1 shows a typical distribution of stress ranges for a pitch controlled wind turbine for mudline bending moments, see [34]. Generally, the stress ranges can be modelled by a Weibull distribution. The Weibull shape coefficient k is typically in the range 0.8 – 1.0. These results are for cases where the response is dominated by the “background” turbulence in the wind load. The corresponding number of load cycles per year is typically $v = 5 \cdot 10^7$.

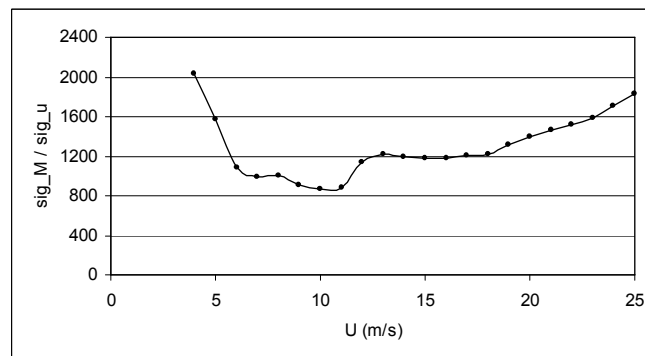


Figure 5.2: $\sigma_{\Delta\sigma}(U)/\sigma_u(U)$ for mudline bending moment – pitch controlled wind turbine.

In Figure 5.2 is shown a typical example for a pitch controlled wind turbine of $\alpha_{\Delta\sigma}(U)/z = \sigma_{\Delta\sigma}(U)/\sigma_u(U)$, i.e. the ratio between the standard deviations of stress ranges and turbulence at a given mean wind speed U . The ratio is seen to be non-linear due to the effect of the control system.

Single wind turbine

The stochastic model shown in Table 5.2 is used with X_{Wind} LogNormal distributed with expected value = 1 and coefficient of variation, $COV_{Wind} = 0.10$. If a linear SN-curve with $m = 3$ is used then Table 5.11 shows the required FDF values for $\Delta P_{F,max} = 10^{-4}$, $2 \cdot 10^{-4}$, 10^{-3} and for $P(COL|FAT) = 1.0, 0.5, 0.1$ and 0.01 . In brackets is shown the corresponding values of the product of the load and material partial safety factors $\gamma_f \gamma_m$. For a minimum annual reliability index equal to 3.5, FDF = 2.3 (and partial safety factor 1.31) is obtained if the consequence of the fatigue failure is large.

Table 5.11: Required FDF and corresponding partial safety factors $\gamma_f \gamma_m$ in () for given $\Delta\beta_{min,FAT}$ ($\Delta P_{F,max,FAT}$). (-) indicates that $FDF \leq 1$.

$P_{COLIFAT}$	3,1 (10^{-3})	3,5 ($2 \cdot 10^{-4}$)	3,8 (10^{-4})
1.0	1.61 (1.17)	2.27 (1.31)	2.90 (1.43)
0.5	1.33 (1.10)	1.93 (1.25)	2.51 (1.36)
0.1	1.0 (1.0)	1.25 (1.08)	1.74 (1.20)
0.01	1.0 (1.0)	1.0 (1.0)	1.0 (1.0)

Table 5.12 shows the required FDF values for different values of COV_{SCF} . It is seen that if $COV_{SCF} = 0.00$ (very good assessment of fatigue stresses) is used then the required FDF is 1.9 and the corresponding partial safety factor is 1.24. Table 5.13 shows the required FDF values for different values of COV_{Wind} .

Table 5.12: Required FDF and corresponding partial safety factors $\gamma_f \gamma_m$ in () for different values of COV_{SCF} . $\Delta\beta_{min,FAT} = 3.5$.

COV_{SCF}	0.00	0.05	0.10	0.15
FDF ($\gamma_f \gamma_m$)	1.90 (1.24)	1.99 (1.26)	2.27 (1.31)	2.75 (1.40)

Table 5.13: Required FDF and corresponding partial safety factors $\gamma_f \gamma_m$ in () for different values of COV_{Wind} . $\Delta\beta_{min,FAT} = 3.5$.

COV_{Wind}	0.05	0.10	0.15
FDF ($\gamma_f \gamma_m$)	1.99 (1.26)	2.27 (1.31)	2.75 (1.40)

Table 5.14 shows the required FDF values for different values of $\sigma_{\log K_1}$ for the SN-curve. It is seen that smaller values of $\sigma_{\log K_1}$ implies higher required FDF values. This is because with fixed value of the characteristic SN-curve the mean value of $\log K_1$ decreases with an effect on the reliability which is relatively larger than the decrease in uncertainty of the SN-curve.

Table 5.14: Required FDF and corresponding partial safety factors $\gamma_f \gamma_m$ in () for different values of $\sigma_{\log K_1}$. $\Delta\beta_{min,FAT} = 3.5$.

$\sigma_{\log K_1}$	0.15	0.20	0.20
FDF ($\gamma_f \gamma_m$)	2.34 (1.33)	2.27 (1.31)	2.26 (1.31)

Table 5.15 shows the required FDF values for different values of the model uncertainty of Miner's rule, COV_{Δ} . It is seen that if $COV_{\Delta} = 0.00$ is used then the required FDF is 1.8 and the corresponding partial safety factor is 1.2.

Table 5.15: Required FDF and corresponding partial safety factors $\gamma_f \gamma_m$ in () for different values of COV_{Δ} . $\Delta\beta_{min,FAT} = 3.5$.

COV_{Δ}	0.00	0.20	0.30
FDF ($\gamma_f \gamma_m$)	1.81 (1.22)	2.01 (1.26)	2.27 (1.31)

Table 5.16 shows the required FDF values for different values of the $\alpha_{\Delta\sigma}(U)$ function, namely the function in Figure 5.2 and one where $\alpha_{\Delta\sigma}(U)$ is constant. It is seen that almost the same FDF values are obtained.

Table 5.16: Required FDF and corresponding partial safety factors $\gamma_f \gamma_m$ in () for different values of COV_{Δ} . $\Delta\beta_{min,FAT} = 3.5$.

$\alpha_{\Delta\sigma}(U)$	Mudline moment, Figure 2	Constant
FDF ($\gamma_f \gamma_m$)	2.27 (1.31)	2.24 (1.31)

If a bi-linear SN curve is used then the required FDF values are shown in Table 5.17. Also shown are the decreases in design values using a bi-linear SN-curve instead of a linear SN-curve. It is seen that compared to a linear SN-curve larger FDF values are required, but at the same time smaller design values are obtained.

Table 5.17: FDF and corresponding partial safety factors $\gamma_f \gamma_m$ in () and given $\Delta\beta_{min,FAT}$ ($\Delta P_{F,max,FAT}$). Bi-linear SN-curve.

$\Delta\beta_{min,FAT}$ ($\Delta P_{F,max,FAT}$)	3,1 (10^{-3})	3,5 ($2 \cdot 10^{-4}$)	3,8 (10^{-4})
FDF	2.45	3.96	5.62
z_{Bilin} / z_{lin}	0.84	0.84	0.84

Wind turbine in wind farm

The stochastic model shown in Table 5.2 is used with model uncertainty on wind load, X_{Wind} and model uncertainty on wake effect model, X_{Wake} LogNormal distributed with expected values = 1 and coefficient of variations $COV_{Wind} = 0.10$ and $COV_{Wake} = 0.10$. This stochastic model is considered as representative for a fatigue sensitive detail where consequences of failure are large, partly on [39], [40] and [41] and partly based on engineering judgment. It is assumed that 5 wind turbines are close to the wind turbine considered with distance between wind turbines $d_i = 4$ rotor diameters.

Table 5.18: Required FDF and corresponding partial safety factors $\gamma_f \gamma_m$ in () for given $\Delta\beta_{min,FAT}$ ($\Delta P_{F,max,FAT}$). (-) indicates that $FDF \leq 1$.

$P_{(COL FAT)}$	3,1 (10^{-3})	3,5 ($2 \cdot 10^{-4}$)	3,8 (10^{-4})
1.0	1.80 (1.22)	2.54 (1.37)	3.26 (1.48)
0.5	1.49 (1.14)	2.17 (1.29)	2.81 (1.41)
0.1	1.0 (1.0)	1.40 (1.12)	1.95 (1.25)
0.01	1.0 (1.0)	1.0 (1.0)	1.0 (1.0)

If a linear SN-curve with $m = 3$ is used then Table 5.18 shows the required FDF values for $P_{F,max} = 10^{-4}$, $2 \cdot 10^{-4}$, 10^{-3} and for $P_{(COL|FAT)} = 1.0, 0.5, 0.1$ and 0.01 . In brackets is shown the corresponding values of the product of the load and material partial safety factors $\gamma_f \gamma_m$. For a minimum annual reliability index equal to 3.5 $FDF = 2.3$ (and partial safety factor 1.31) is obtained if the consequence of the fatigue failure is large.

Table 5.19 shows the required FDF values for different values of COV_{Wake} . It is seen that the required FDF is not sensitive with respect to COV_{Wake} .

Table 5.19: Required FDF and corresponding partial safety factors $\gamma_f \gamma_m$ in () for different values of COV_{Wake} .

COV_{Wake}	0.05	0.10	0.15
FDF ($\gamma_f \gamma_m$)	2.54 (1.36)	2.54 (1.37)	2.55 (1.37)

5.2.2 FDF values with inspections

The theoretical basis for reliability-based planning of inspection and maintenance for fatigue critical details in offshore steel substructures is described for example in [35], [37], [42], [43], [44] and [45]. Risk- and reliability-based inspection planning is widely used for inspection planning for oil & gas steel jacket structures. Fatigue reliability analysis of jacket-type offshore wind turbine considering inspection and repair is also considered in [46] and [47]. In this section examples are presented describing how much FDF values can be reduced if inspections are performed.

For the fatigue sensitive details / joints to be considered in an inspection plan, the acceptance criteria for the annual probability of fatigue failure may be assessed using a measure for the decrease in ultimate load bearing capacity given failure of each of the individual joints to be considered together with the annual probability of joint fatigue failure. For offshore structures the RSR (Reserve Strength Ratio) is often used as a measure of the ultimate load bearing capacity.

If the RSR given joint fatigue failure is known (can be obtained from a non-linear FEM analysis), it is possible to establish the corresponding annual collapse failure probability $P_{(COL|FAT)}$ if information is available on applied characteristic values for the capacity, live load, wave height, ratio of the environmental load to the total load and coefficient of variation of the capacity.

For fatigue failures the requirements to safety are typically given in terms of a required Fatigue Design Factor (FDF). As an example [28] and [48] specify FDF values from 1 to 10. For each joint j the conditional probabilities of structural collapse given failure of the considered joint $P_{(COL|FAT)_j}$ are determined and the individual joint acceptance criteria for the annual probability of joint fatigue failure are found.

Inspection planning as described above requires information on costs of failure, inspections and repairs. Often these are not available, and the inspection planning is based on the requirement that the annual probability of failure in all years has to satisfy the reliability constraint

$$\Delta P_{F,t} \leq \Delta P_{F,max,FAT}$$

for all years during the life cycle of the structure. Further, in risk-based inspection planning the planning is often made with the assumption that no cracks are found at the inspections. If a crack is found, then a new inspection plan has to be made based on the observation.

If all inspections are made with the same time intervals, then the annual probability of fatigue failure could be as illustrated in Figure 5.3. The inspection planning is based on the no-find assumption. This way of inspection planning is the one which is most often used. Often this approach results in increasing time intervals between inspections.

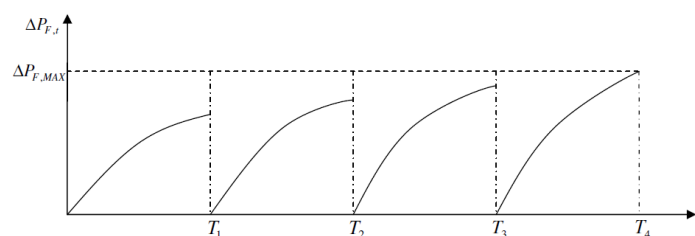


Figure 5.3: Illustration of inspection plan with equidistant inspections.

A Fracture Mechanical (FM) modelling of the crack growth is applied assuming that the crack can be modelled by a 2-dimensional semi-elliptical crack. It is assumed that the fatigue life may be represented by a fatigue initiation life and a fatigue propagation life. It is therefore:

$$N = N_I + N_P$$

Where N is the number of stress cycles to failure, N_I is the number of stress cycles to crack propagation and N_P is the number of stress cycles from initiation to crack through.

The number of stress cycles from initiation to crack through is determined on the basis of a two-dimensional crack growth model. The crack is assumed to be semi-elliptical with length $2c$ and depth a .

The crack growth can be described by the following two coupled differential equations.

$$\begin{aligned} \frac{da}{dN} &= C_A (\Delta K_A)^m & a(N_0) &= a_0 \\ \frac{dc}{dN} &= C_C (\Delta K_C)^m & c(N_0) &= c_0 \end{aligned}$$

Where C_A , C_C and m are material parameters, a_0 and c_0 describe the crack depth a and crack length c , respectively, after N_I cycles and where the stress intensity ranges are $\Delta K_A(\Delta\sigma)$ and $\Delta K_C(\Delta\sigma)$. ΔK_A and ΔK_C are obtained based on the models in [49] and [50].

The stress range $\Delta\sigma$ is obtained from

$$\Delta\sigma = X_{Wave} X_{SCF} \cdot Y \cdot \Delta\sigma^e$$

where X_{Wave} , X_{SCF} are model uncertainties, Y is the model uncertainty related to geometry function and $\Delta\sigma^e$ is the equivalent stress range:

$$\Delta\sigma^e = \left[\frac{1}{n} \sum_{i=1}^{n_\sigma} n_i \Delta\sigma_i^m \right]^{1/m}$$

The total number of stress ranges per year is $n = \sum_{i=1}^{n_\sigma} n_i$.

In the assessment of the equivalent constant stress range the effect of a possible lower threshold value ΔK_{TH} on the crack growth inducing stress intensity factor ΔK has not been taken into account explicitly. This effect is assumed implicitly accounted for by evaluation of the equivalent stress range using the appropriate SN-curve exponent m .

The crack initiation time N_I is modelled as Weibull distributed with expected value μ_0 and coefficient of variation equal to 0.35, see e.g. [51].

The limit state function is written

$$g(\mathbf{X}) = N - n t$$

where t is time in the interval from 0 to the service life T_L .

To model the effect of different weld qualities, different values of the crack depth at initiation a_0 can be used. The corresponding assumed length is 5 times the crack depth. The critical crack depth a_c is taken as the thickness of the tubular member.

The parameters $\mu_{\ln C}$ and μ_0 are now fitted such that difference between the probability distribution functions for the fatigue live determined using the SN-approach and the fracture mechanical approach is minimized as illustrated in the example below.

Alternatively, or in addition to the above modelling the initial crack length can be modelled as a stochastic variable, for example by an exponential distribution function, and the crack initiation time N_I can be neglected.

Probabilistic modelling of inspections

The reliability of inspections can be modelled in many different ways. Often POD (Probability Of Detection) curves are used to model the reliability of the inspections. A POD curve using an exponential model can be written:

$$POD(x) = 1 - \exp\left(-\frac{x}{\lambda}\right)$$

where λ is the expected value of the smallest detectable crack size. Also the Probability of False Indication (PFI) can be introduced and modelled probabilistically.

Results – FDF values with inspections

A steel jacket structure subjected to a loading environment corresponding to the southern part of the North Sea is considered. Table 5.20 shows the stochastic model used for reliability analysis, based on information in [35].

Table 5.20: Uncertainty modelling used for fracture mechanical reliability analysis. D: Deterministic, N: Normal, LN: LogNormal, W: Weibull.

Variable	Dist.	Expected value	Standard deviation
N_I	W	μ_0 (reliability based fit to SN approach)	$0.35 \mu_0$
a_0	D	0.4 mm	
$\ln C_C$	N	$\mu_{\ln C_C}$ (reliability based fit to SN approach)	0.77
m	D	m -value corresponding to the low cycle part of the bi-linear SN-curve	
X_{SCF}	LN	1	0.10
X_{Wave}	LN	1	0.10
X_{Wind}	LN	1	0.10
n	D	Total number of stress ranges per year	
a_c	D	T (thickness)	
Y	LN	1	0.1
T	D	30 mm	
$\ln C_C$ and N_I are correlated with correlation coefficient = -0.5			

Figure 5.4 shows an example of the annual reliability indices obtained when a fracture mechanics model is calibrated to the reliability indices obtained using an SN-approach.

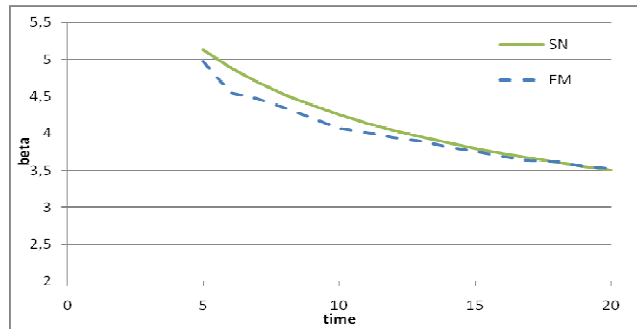


Figure 5.4: Annual reliability indices obtained by the SN-approach and a fracture mechanics model (calibrated).

Further, it is assumed that inspections are performed with three different levels of reliability modelled by exponential POD curves with $\lambda = 2, 5$ and 10 mm (surface cracks lengths). The inspections are assumed to be performed with equidistant times, see Figure 5.3.

Table 5.21 to Table 5.25 show required FDF values for cases with wind / wave loads only, single wind turbine / wind farm and linear / bi-linear SN-curves. It is assumed that $\Delta\beta_{min,FAT} = 3.5$ and $P_{COLIFAT} = 1$. It is seen that significant reductions in required FDF values can be obtained if a good inspection quality is used and e.g. 3 inspections are performed during the design lifetime.

The costs of inspections and possible repairs should be compared to the cost reductions in the initial material costs due to lower FDF values. It is noted that due to correlations between similar fatigue critical details in substructures in wind farms information from inspection of one substructure can be used to update the reliability assessment of nearby substructures.

The results in this section can be considered as representative, but more examples should be considered before implementation in standards. Especially examples where both wind and wave loads are important should be investigated.

Table 5.21: Required FDF and corresponding partial safety factors $\gamma_f \gamma_m$ in (). Single wind turbine and linear SN-curve ($m = 3$). Wind load only.

POD: λ^1	2 mm	5 mm	10 mm	
No inspections				2.27 (1.31)
1 inspection	1.92 (1.24)	2.15 (1.29)	2.20 (1.30)	
2 inspections	1.65 (1.18)	1.94 (1.25)	2.11 (1.28)	
3 inspections	1.46 (1.13)	1.82 (1.22)	2.05 (1.27)	

Table 5.22: Required FDF and corresponding partial safety factors $\gamma_f \gamma_m$ in (). Wind farm and linear SN-curve ($m = 3$). Wind load only.

POD: λ^1	2 mm	5 mm	10 mm	
No inspections				2.54 (1.37)
1 inspection	2.15 (1.29)	2.40 (1.34)	2.49 (1.36)	
2 inspections	1.83	2.17	2.35	

	(1.22)	(1.29)	(1.33)	
3 inspections	1.64 (1.18)	2.05 (1.27)	2.28 (1.32)	

Table 5.23: Required FDF and corresponding partial safety factors $\gamma_f \gamma_m$ in (). Single wind turbine and linear SN-curve (m = 3). Wave load only.

POD: λ^A	2 mm	5 mm	10 mm	
No inspections				3.38 (1.50)
1 inspection	2.85 (1.42)	3.18 (1.47)	3.27 (1.48)	
2 inspections	2.44 (1.35)	2.90 (1.43)	3.15 (1.46)	
3 inspections	2.18 (1.30)	2.66 (1.39)	3.05 (1.45)	

Table 5.24: Required FDF and corresponding partial safety factors $\gamma_f \gamma_m$ in (). Single wind turbine and bi-linear SN-curve. Wind load only.

POD: λ^A	2 mm	5 mm	10 mm	
No inspections				3.96
1 inspection	3.51	3.67	3.80	
2 inspections	2.50	3.18	3.56	
3 inspections	2.15	2.90	3.40	

Table 5.25: Required FDF and corresponding partial safety factors $\gamma_f \gamma_m$ in (). Single wind turbine and bi-linear SN-curve. Wave load only.

POD: λ^A	2 mm	5 mm	10 mm	
No inspections				5.64
1 inspection	4.33	5.03	5.22	
2 inspections	3.50	4.38	4.97	
3 inspections	3.00	3.96	4.69	

5.2.3 Summary

This section describes reliability-based investigations on the required safety factors / FDF values to be used for fatigue design of steel substructures for offshore wind turbines. Design and limit state equations are formulated and stochastic models for the uncertain strength and load parameters are described. In the design equations partial safety factors for fatigue strength and load or equivalently Fatigue Design Factors (FDF) are determined by calibration to a required reliability level. Since design and limit state equations are equivalent a detailed model of the fatigue damage is generally not needed. For the three fatigue load cases considered the fatigue models only have to reflect the effect of using a 90% quantile as characteristic turbulence intensity when wind load is dominating and the uncertainty related to the wake model used for dominating wind load for wind farms.

A reliability level corresponding to a maximum annual probability of failure equal to $2 \cdot 10^{-4}$ is basically assumed. This reliability level corresponds to that typically required for unmanned fixed offshore structures for oil & gas production. The results indicate that for fatigue critical details where the fatigue load is dominated by wind load a FDF value equal to approximately 2.5 is required – slightly smaller FDF values can be used for single wind turbines. If wave load is dominating a larger FDF value is required, approximately 3.5. The differences are mainly due to additional uncertainty due to wakes in wind farms and implicit safety included in the wind load model by using a 90% quantile for the turbulence in deterministic design.

Further, the effect of possible inspections during the design lifetime is investigated. It is assumed that inspections are performed with three different levels of reliability modelled by exponential POD curves with mean length of detectable cracks equal to 2, 5 and 10 mm. The results show that significant reductions in required FDF values can be obtained if a good inspection quality is used and for example 3 inspections are performed during the design lifetime. The costs of inspections and possible repairs should be compared to the cost reductions in the initial material costs due to lower FDF values. It is noted that due to correlations between similar fatigue critical details in substructures in wind farms information from inspection of one substructure can be used to update the reliability assessment of nearby substructures.

The results shown in this section can be considered as representative, but more examples should be considered before implementation in standards. Especially examples where both wind and wave loads are important should be investigated.

5.3 Recommendations for offshore design load case implementation

The following section gives guidance for the implementation of offshore wind turbine design load cases according to the IEC 61400-3 standard for the preliminary design of jacket support structures. To achieve cost-effective support structure design it is important to make the design process as efficient as possible. This is particularly true for the more complex braced support structures used in deeper water, as multiple wind and wave directionality has also to be taken into account. Therefore a reduction in the number of simulations required for the preliminary design stages can result in big savings in time, and also in cost.

The set of design load cases (DLC) listed in this section is intended for predesign with focus on a jacket sub-structure. It is assumed that due to the space frame structure of the jacket, loads and thus wind and wave orientation influence the overall design.

5.3.1 Fatigue Load Analysis

For fatigue predesign two methodologies may be applied:

1. Simplified method considering reduced directionality but two support structure orientations
2. Consideration of site environmental conditions for directional wind and wave distribution and directional load analysis.

As described, the fatigue load analysis is divided into two steps, resulting in two load case sets for two independent fatigue analyses. The first step represents a simplified, fast but conservative first approach assuming wind and waves are aligned. The second approach assumes wind-wave misalignment. Thus, it more precisely represents the site conditions while it reduces the amount of conservativeness by increasing the computational effort.

Neither of the two approaches considers transient DLCs (start, stop, fault events) as they may be left out for a preliminary load analysis that focuses on jacket predesign.

Step 1: Wind and waves in line

Two support structure orientations (0° and 45°) shall be analysed. The support structure orientation is defined with regard to the rotor axis, while the rotor axis is assumed collinear with the wind direction (excluding 8 deg wind misalignment). For conservative simplicity it is assumed that the rotor axis points north. The support is oriented accordingly to N (0°) or NE (45°). The following figures illustrate the 0° and 45° orientation by giving top views on the jacket.



DLC 1.2: Power production

- $V_{in} < V < V_{out}$; $H_s(V)$; $T_p(V)$
- NTM model for turbulent wind
- Wind bin width 2m/s
- One H_s , T_p -combination per wind bin
- Wind misalignment +8 deg or -8 deg
- 6 to 10 seeds per wind bin
- Two support structure orientations (0°; 45°)

Per wind bin a minimum of 6 seeds for 10 minute turbulent wind time series shall be combined with different wind misalignments of +8 deg or -8 deg and different seeds for the random sea state. Generating the sea state by using one H_s , T_p -combination per wind bin is assumed statistically sufficient if combined with 6 different seeds for the random sea state.

DLC 6.4: Idling

- $V < V_{in}$; $V > V_{out}$; $H_s(V)$; $T_p(V)$
- NTM model for turbulent wind
- One H_s , T_p -combination per wind speed
- Wind misalignment +8 deg or -8 deg
- 6 to 10 seeds per wind speed
- Two support structure orientations (0°; 45°)

For one wind speed below V_{in} and one wind speed above V_{out} , a minimum of 6 wind seeds shall be computed in combination with wind misalignment and seeds for sea states as described for DLC 1.2.

DLC 7.2: Idling after fault

- $0 < V < 0.7 V_{ref}$; $H_s(V)$; $T_p(V)$
- NTM model for turbulent wind
- Yaw error 60 deg
- One H_s , T_p -combination per wind speed
- 6 to 10 seeds per wind speed
- Two support structure orientations (0°; 45°)

DLC 7.2 assumes a turbine idling after occurrence of a fault. All wind speed bins used in DLC 1.2, DLC 6.4 and additionally a wind speed of $0.7 V_{ref}$ shall be analysed under the assumption of yaw misalignment in turbulent wind. It is proposed and acceptable for jacket predesign to use one wind direction in combination with a conservative yaw misalignment of 60 deg. A minimum of 6 wind seeds shall be computed in combination with different seeds for sea states.

This would result in 168 simulations for DLC 1.2 and DLC 6.4 (2 support structure orientations · 14 bins · 1 wind sector · 6 seeds = 168). Additionally, 180 simulations for DLC 7.2 (2 support structure orientations · 15 bins · 6 wind seeds = 180) have to be analysed if a yaw error of 60 deg is assumed and if wave seeds are varied with wind seeds. This results in a total of 348 simulations.

Rainflow evaluation

The load cases shall be evaluated in rainflow counts according to two different assumptions for the availability of the turbine (100% and 85% or equivalent conservative value based on failure statistics). Combined with the two support orientations, that means four rainflow counts and weighting analyses have to be performed. The setups are as follows:

1. 100 % availability: rainflow count assuming DLC 1.2 and DLC 6.4 for the complete lifetime, Jacket orientation 0°
2. 100 % availability: rainflow count assuming DLC 1.2 and DLC 6.4 for the complete lifetime, Jacket orientation 45°
3. 85% availability: rainflow count assuming 85 % of lifetime DLC 1.2 and DLC 6.4, 15 % of lifetime DLC 7.2, Jacket orientation 0°
4. 85% availability: rainflow count assuming 85 % of lifetime DLC 1.2 and DLC 6.4, 15 % of lifetime DLC 7.2, Jacket orientation 45°

The highest resulting loads shall be used for jacket predesign.

Step 2: Wind and waves misaligned

The load case definitions of step two are, but for the wind-wave misalignment, equal to the load case definitions given in step one. As step two considers site specific directional distribution with a defined orientation of the support structure regarding north, the support structure orientation must not be varied. For DLC 7.2 no further load cases have to be set up, as assuming wind aligned with waves is conservative with regards to missing aerodynamic damping. Besides that, the IEC standard does not request consideration of wind-wave misalignment for DLC 7.2.

The rainflow evaluation of step 2 includes both the dimensioning step 1 rainflow extended by the directional distributions of step 2 simulations.

Wind-wave misalignment can be considered via several approaches of different complexity, the wind bin based wind-wave rose combination (exact method) or methods of reduced complexity. The exact method assumes that a wind direction – wave direction scatter diagram exists.

This section additionally addresses an approach based on the assumption that wind-wave misalignment is independent of wind speed and wind direction (wind independent method). As wind and wave data for the present site are sufficient to include wind-wave misalignment via the exact method, a comparison to the results of the less complex wind independent method may be useful.

Exact method

The exact method assumes wind-wave misalignment to vary with three parameters: wind speed bin, wind direction and wave direction. Thus, one misalignment has to be computed for each wind bin, wind direction and wave direction combination, resulting in 4032 simulations (2 support structure orientations · 14 bins · 12 wind sectors · 12 wave sectors = 4032) for DLC 1.2 and DLC 6.4 if wind and wave seeds and wind misalignment are varied within. It is assumed that one seed for every single case is statistically sufficient due to the high number of load cases.

Wind independent method

To reduce the sheer amount of simulations and the effort of simulation setup, the wind independent method is based on the assumption that wind-wave misalignment is independent of wind speed and wind direction. First, wind and wave roses are tabulated as probability distributions and the misalignments with according probabilities of misalignments are derived. This is illustrated in the following table:

Table 5.26: Wind/wave misalignment, wind independent method

Wind dir.	Wind direction probability [% wind rose]	Wave dir.	Wave direction probability [% wave rose winddir.]	Misalignment	Probability of misalignment $P(\varphi_{miss})$
0°	P(0° wind)	0°	P(0° wave 0° wind)	0°	P(0° wind) · P(0° wave)
0°	P(0° wind)	30°	P(30° wave 0° wind)	30°	P(0° wind) · P(30° wave)
...	P(0° wind)	
0°	P(0° wind)	330°	P(330° wave 0° wind)	330°	P(0° wind) · P(330° wave)
30°	P(30° wind)
...					
330°	P(330° wind)				

Next, the probabilities are summed up for each misalignment:

$$P(\varphi_{miss=i}) = \sum P(\varphi_{miss=i}) \quad i = 0^\circ; 30^\circ \dots 330^\circ$$

As the structural orientation is axi-symmetric to the wind direction (assuming active yaw and representation of wind misalignment via 8 deg rotor misalignment), the probabilities of misalignment can be taken as average of the sum of misalignments axi-symmetric to the wind direction, for instance:

$$P(\varphi_{miss=30^\circ}) = P(\varphi_{miss=330^\circ}) = 0.5 \cdot (P(\varphi_{miss=30^\circ}) + P(\varphi_{miss=330^\circ}))$$

This would result in half of the simulations of the exact method (2 support structure orientations · 14 bins · 12 wind sectors · 6 misalignments = 2016 simulations) for DLC 1.2 and DLC 6.4 if wind and wave seeds and wind misalignment are varied within. Furthermore, the setup of load cases would be significantly less time consuming compared to the exact method. Following example is used to illustrate the further load case setup:

- P($\varphi_{miss=0^\circ}$) = 30 %
- P($\varphi_{miss=30^\circ}$) = 25 %
- P($\varphi_{miss=-30^\circ}$) = 25 %
- P($\varphi_{miss=60^\circ}$) = 10 %
- P($\varphi_{miss=90^\circ}$) = 10 %

The exemplary misalignments would result in the following load case setup regarding wind and wave directions:

Table 5.27: Example load case setup with wind/wave misalignment

Global wind direction	Global wave direction
0°	0°; 30°; -30°; 60°; 90°
30°	30°; 60°; 0°; 90°; 120°
...	
330°	330°; 0°; 300°; 30°; 60°

For DLC 7.2 it has to be considered that the turbine is not yawing. Thus, the wind direction equals the yaw misalignment.

Proposal for further misalignment studies

For a study in between both approaches (exact and wind independent approach), the assumption that misalignment is independent of the wind bin but not the wind direction or that the misalignment is independent of the wind direction but not the wind bin would be conceivable. The advantage of such in between studies would be that the directional distributions for the wind and sea state setup would be at hand as already derived (in between) for the wind independent method. Thus, the study would mainly be a matter of computation and evaluation.

5.3.2 Extreme Load Analysis

The extreme load analysis considers a reduced set of load cases for preliminary jacket design. Nevertheless, DLCs 6.1 and 6.2 are of high computational effort. Unfortunately, the effort is mandatory as DLC's 6.1 and 6.2 are assumed to be the main design drivers for the jacket sub-structure.

For all other DLCs proposed for preliminary jacket design (DLC 2.2; DLC 1.6; DLC 2.3) the IEC standard [69] states wind aligned with waves if both approach from the worst case direction regarding loads. Thus, no wind wave misalignment but two support structure orientations shall be analysed for those load cases.

Statistical load extrapolation according to [30] is not considered in this section as it mainly affects RNA loads so is not considered necessary within the scope of preliminary jacket design.

DLC 6.1a: Idling in storm

- $V = V_{ref}$
- Turbulent 50-year-wind
- 50 year sea state with embedded $H_{max,50}$ wave
- Wind misalignment +8 deg or -8 deg
- 6 to 10 seeds per wind speed
- Wind-wave misalignment
- Two support structure orientations (0° ; 45°)

DLC 6.1a considers a turbine idling in 50-year storm conditions. Turbulent wind with a minimum longitudinal turbulence intensity of 11 % shall be considered in combination with at least 6 seeds for wind and sea states, according to the IEC standard. Wind-wave misalignment shall include site-specific values derived during fatigue analysis.

During load case computation the influence of the aerodynamic wake model shall be investigated. Practically, using GH Bladed, this includes variation of the wake model in Bladed's 'Aerodynamic Control' Panel between 'Frozen Wake' and 'Dynamic Inflow' and checks of the time series for occurrence of resonance generated by numerical uncertainties.

DLC 6.2a: Idling in storm during grid loss

- $V = V_{ref}$
- Grid loss (yaw inactive -> yaw misalignment)
- Turbulent 50-year-wind
- 50-year sea state with embedded $H_{max,50}$ wave
- Wind misalignment +8 deg or -8 deg
- 6 to 10 seeds per wind speed
- Wind-wave misalignment with maximum loads from DLC 6.1a
- Support structure orientation with maximum loads from DLC 6.1a

DLC 6.2a considers a turbine idling in 50-year storm conditions during grid loss, meaning the yaw system is inactive, resulting in significant yaw misalignments. Thus, wind direction shall be considered misaligned to the rotor axis between 30 deg and 180 deg (in 30 deg steps). The remaining load case setup equals DLC 6.1a despite for the support structure orientation and the wind-wave misalignment. The support orientation shall be determined by the support orientation for DLC 6.1a that resulted in maximum loads. Accordingly, wind-wave misalignment shall account for those site-specific values that resulted in maximum loads for DLC 6.1a.

Again, during load case computation, the influence of the aerodynamic wake model should be taken care of.

DLC 2.2: Safety system fault

- $V_{in} < V < V_{out}$; $H_s(V)$; $T_p(V)$
- NTM model for turbulent wind
- Wind bin width 2m/s
- One H_s , T_p -combination per wind bin
- Wind misalignment +8 deg or -8 deg
- 6 to 10 seeds per wind bin
- Wind and waves in line
- Two support structure orientations (0°; 45°)

The setup is comparable to DLC 1.2 in the step one fatigue analysis. For reason of preliminary jacket design, safety system fault computations may be limited to one significant pitch fault at high wind speeds (near cut-out). It is conservatively proposed to assume all blades turn to fine (with a reasonable average pitch rate such as 5 deg/s) until the safety system is activated again by reaching the safety system over-speed limit.

DLC 1.6: Power production in 50-year sea state

- 0.8 V_r ; V_r ; 1.2 V_r ; V_{out}
- NTM model for turbulent wind
- 50 year sea state with embedded $H_{max,50}$ wave
- Wind misalignment +8 deg or -8 deg
- 6 to 10 seeds per wind speed
- Wind and waves in line
- Two support structure orientations (0°; 45°)

DLC 1.6 represents power production in turbulent wind conditions and a 50-year sea state. For conservative reason of preliminary jacket design, an embedded wave with a maximum 1-year wave height ($H_{max,1}$) may be assumed. Furthermore, a minimum of 6 wind seeds shall be computed in combination with wind misalignment and seeds for sea states as described for DLC 1.2.

DLC 2.3 (DLC 1.5 in GL standard [31]): Generator cut-out

- $V_r \pm 2m/s$ and V_{out} ; $H_s(V)$; $T_p(V)$
- EOG1
- Rotor start position 0 – 90 deg (30 deg steps)
- Generator cut-out at 3 time instants
- Wind misalignment +8 deg or -8 deg
- Wind and waves in line
- Two support structure orientations (0°; 45°)

DLC 2.3 represents a load situation of a turbine in power production during a one-year gust (EOG₁) that loses the generator torque due to a generator cut-out from the grid. The grid loss shall be considered at the three time instants, lowest wind speed, highest gust acceleration, maximum wind speed (see GL 2005

Guideline, DLC 1.5). Furthermore, the rotor start positions shall vary from 0 deg to 90 deg (in 30 deg steps).

Fatigue Load cases

An extreme load analysis shall be carried out for the fatigue load cases.

5.4 Design load case parameter analysis for jacket structure

The design of offshore wind turbine support structures is strongly driven by parameters relating to the external conditions at the site at which the turbine is to be located, as well as the properties of the structure and turbine itself. For the purposes of offshore wind turbine support structure design it is important to understand the relative importance of the various external conditions applied to the structure in the design process. These external conditions include the following:

- Wind speed
- Wind direction
- Wave height
- Wave period
- Wave direction
- Tidal levels
- Current velocity and profile
- Current direction
- Turbulence intensity

If all possible combinations of these factors were accounted for in the design of the structure, the number of simulations required would be huge and exceed practical limits for the designer. In order to achieve an economic design it is therefore important to know which of these factors are the most significant in determining the loading on the structure, so that the amount of computational time and effort can be minimised whilst maintaining accuracy of results.

The effects of changing the above parameters on monopile support structures are reasonably well known. However, as suitable shallow water sites in European waters become more limited jacket support structures are increasingly being used as a preferred solution for offshore wind turbines. Therefore, this section uses the UpWind reference jacket support structure [54] to test the relative influence of a number of key design load case parameters affecting offshore wind turbine jacket support structure design.

General considerations

In order to account fully for the dynamics of an offshore wind turbine the combined wind and wave loading on the whole structure must be modelled in a non-linear time-domain simulation. This ensures that the aerodynamic damping of wave-induced motion is properly captured, which can be an important effect. The importance of integrated analysis for jacket structures has also been shown in [52], in which a significant interaction between rotor rotation and local jacket brace vibration was demonstrated.

The GH Bladed software tool [9] is used to perform integrated load calculations and analysis. The UpWind 5MW reference wind turbine [52] is used for the analysis, mounted on the UpWind reference jacket support structure [54] shown in Figure 5.5. This structure was optimized using the UpWind 50m design basis [55], so the external conditions from this document are used as a baseline. Local joint flexibilities are not included in the model, as it has been shown that for jacket structures modelling flexibility in the joints does not typically affect the magnitude of forces and moments [66]. A full description of the geometry, mass and stiffness of the jacket support structure can be found in [54].

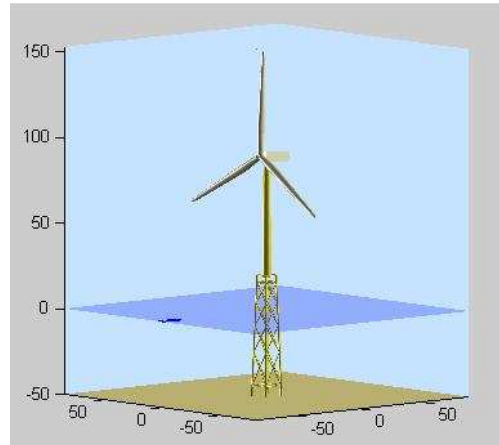


Figure 5.5: Jacket support structure implemented in GH Bladed

5.4.1 Fatigue load case parameter study

The fatigue load cases investigated are DLC 1.2 and DLC 6.4, which cover the full range of normal operation and idling conditions experienced by the wind turbine over its lifetime. DLC 7.2 is also considered for the availability study. The wind speeds and sea state parameters used for the simulations can be found in [55]. Irregular waves are modelled using a Jonswap spectrum with a peakedness parameter (γ) equal to 1.

Firstly a baseline fatigue load set was performed. Subsequent load sets were run with the following parameters varied individually, to determine the effect on the fatigue loading:

- Wind/wave misalignment
- Availability
- Wind class
- Structural natural frequency
- Tide height

In this section results are presented in terms of damage equivalent loads (DELs), with a specified S-N slope and frequency. Usually for welded steel details a bi-linear S-N curve is used with inverse slopes $m_1=3$ and $m_2=5$. If the fatigue load is wind dominated (i.e. more stress ranges with high frequency and low amplitude) then $m_2=5$ is most relevant. If wave load is dominating (i.e. more stress ranges with low frequency and high amplitude) then $m_1=3$ is most relevant. In the case of jacket structures the wind load is normally dominating; however for the purposes of this study it is important that the wave loads are still properly represented. A single m value is required for the below comparisons, so $m=4$ is used for all DELs as a compromise. A reference frequency of 0.0158Hz is used, equivalent to $1e7$ cycles in 20 years. Lifetime-weighted DELs are derived using a rainflow cycle counting algorithm with application of Miner's rule, based on the appropriate annual wind speed distribution.

For jacket structures joints are generally the weakest point in structure due to concentration of stresses at the welds. During the optimization of the structure the lowest fatigue lives were found to be in the upper joint at the top level of bracing [54]. Other loads on the jacket which give a significant contribution to the fatigue damage are the tower base overturning moment and the pile head axial forces. For the purposes of this section, therefore, damage equivalent loads are reported at the pile head, the upper joint and the tower base. A list of output locations and load components is given in Table 5.28. The output locations on the Bladed model are shown in Figure 5.6.

Table 5.28: Output locations for damage equivalent loads

Jacket location	Bladed identifier	Load component
Pile head	Mbr 1 End 1	Axial force Fx
	Mbr 2 End 1	Axial force Fx
	Mbr 3 End 1	Axial force Fx
	Mbr 4 End 1	Axial force Fx
Upper joint	Mbr 109 End 1	Axial force Fx
	Mbr 110 End 1	Axial force Fx
	Mbr 111 End 1	Axial force Fx
	Mbr 112 End 1	Axial force Fx
Tower base	Mbr 134 End 1	Overturning bending moment Mz

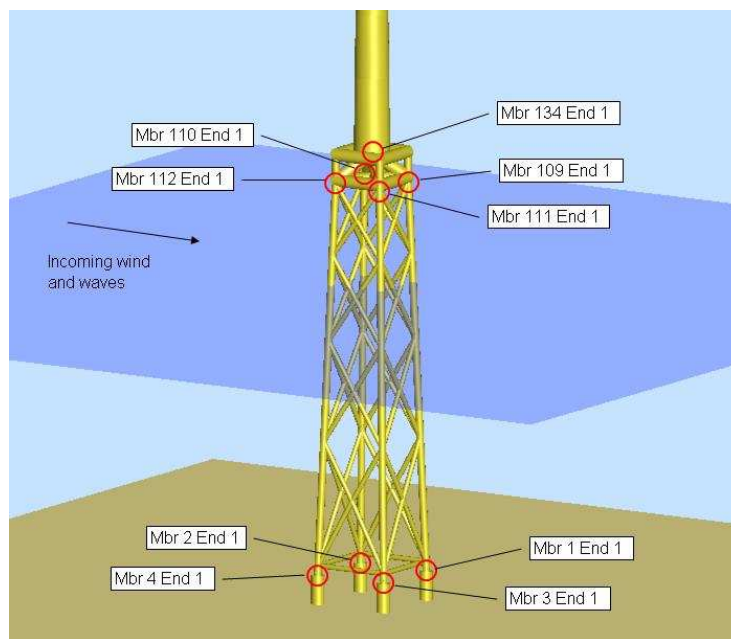


Figure 5.6: Output locations for damage equivalent loads

Sources of loading

For jacket structures it is generally assumed that wind loads dominate over hydrodynamic loads, due to the relative hydrodynamic transparency of jackets. In order to confirm this assumption, two additional fatigue load sets were performed, one with wind only and one with waves only, in order to investigate the relative influence of the different sources of loading.

Figure 5.7 shows a sample time history of the axial force at one of the pile heads, during normal power production. Figure 5.8 presents normalized DELs at the chosen output locations on the jacket for the three different cases.

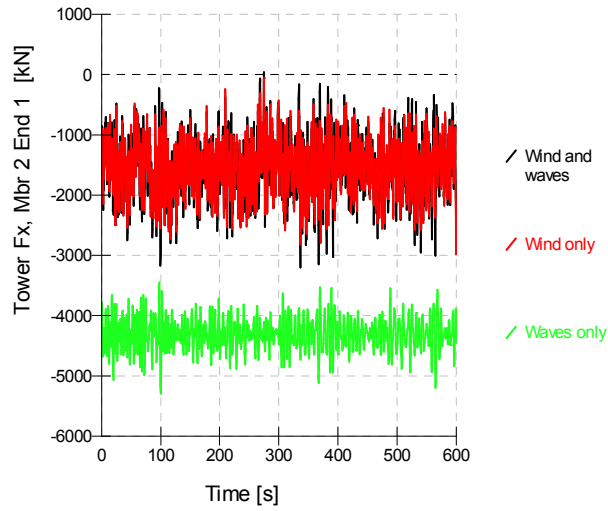


Figure 5.7: Sample time history of axial force at pile head

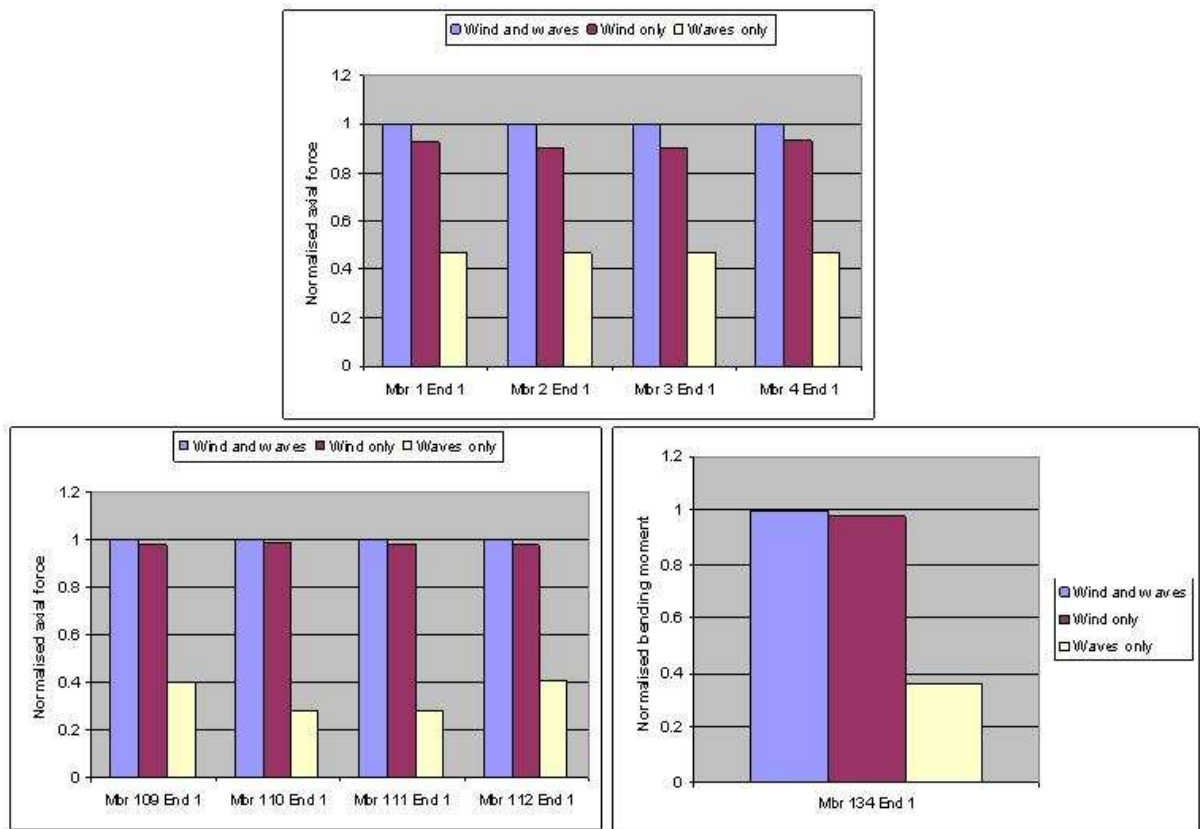


Figure 5.8: Normalised DELs with variation in sources of loading

From these results it can be clearly seen that the loads on the jacket are dominated by the wind. This is due to the small member diameters in the jacket at the water level, which results in a relatively low contribution from the hydrodynamics. At the pile head the contribution from the waves is proportionally greater, as expected, but even at this depth the relative contribution from the waves is still small.

The DEL histograms also show the effect of aerodynamic damping. The damage equivalent loading from combined wind and waves is lower than the sum of the damage calculated from the wind and waves separately. This is due to the damping of the wave-induced motion resulting from the rotor thrust.

Wind-wave misalignment

The baseline fatigue loads were calculated with codirectional wind and waves. In order to test the influence of wind-wave misalignment on jacket structures, three additional cases were considered with the wind-wave misalignment varied. The waves were considered to approach the structure at six different angles from the wind, from -30° to 120° in 30° intervals. A different proportion of time was then assigned to each wind-wave misalignment angle for the three cases. Case 3 models a uniform distribution between all six misalignment angles, and Cases 1 and 2 are intermediate weightings. A graphical display of the cases considered is shown in Figure 5.9.

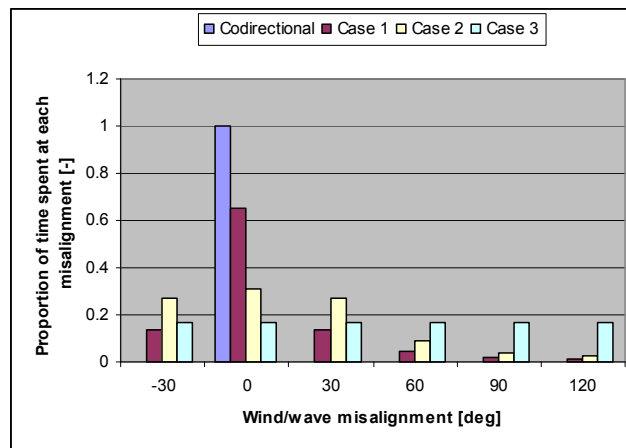


Figure 5.9: Misalignment cases considered

Figure 5.10 presents normalized DELs at the chosen output locations on the jacket for the four different cases. At the pile head the damage equivalent load increases by up to 2.5% when misalignment is taken into account. This is due to the additional forcing from the waves approaching from a different angle. However the DEL also increases by nearly 2% at the upper joint, which is located 15m above the water level. This may be due to the fact that jackets are relatively soft in the torsional mode, which can be excited by large misalignments. The reduced aerodynamic damping may also have an effect.

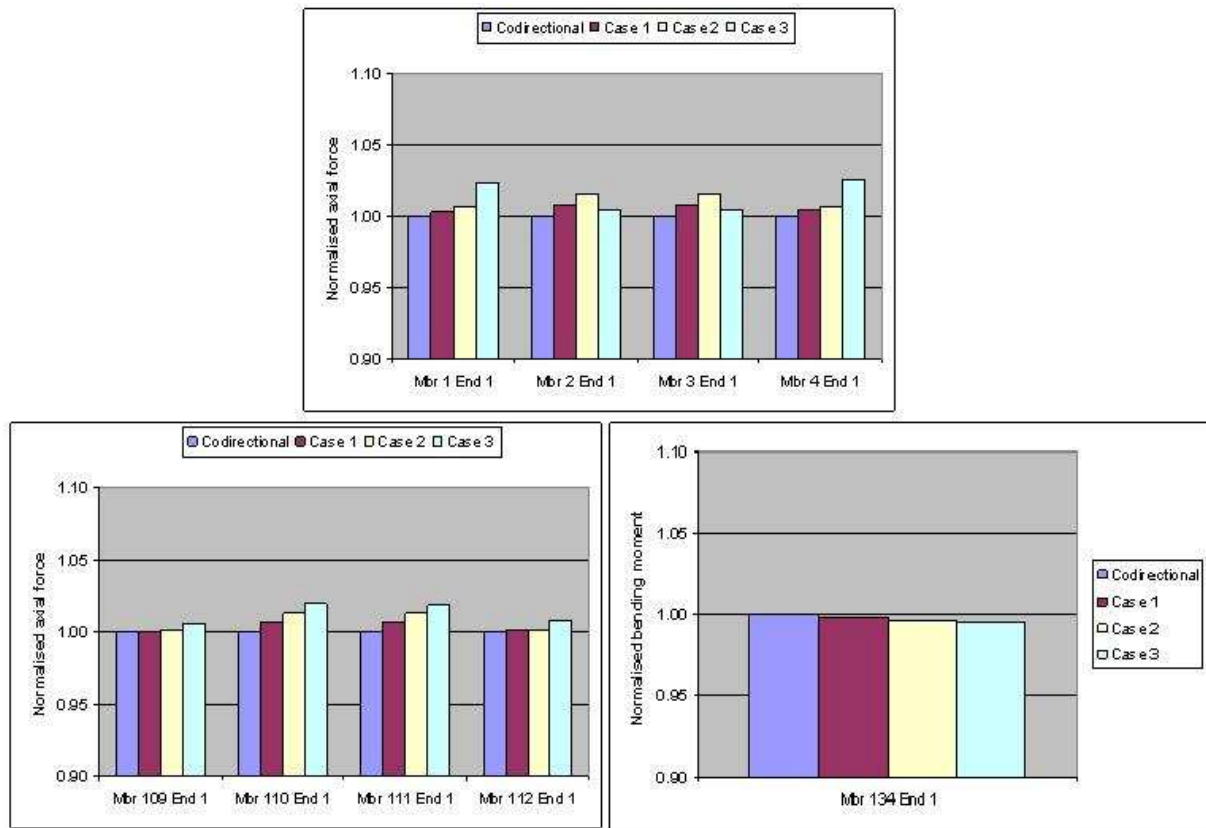


Figure 5.10: Normalised DELs with variation in wind-wave misalignment

Availability

The baseline fatigue loads were calculated assuming 100% availability. For monopile support structures it has been shown that in some cases, depending on site conditions and structure diameter, a lower availability can lead to design driving loads due to the loss of aerodynamic damping [67]. In order to test the influence of availability on jacket structures, four additional cases were considered with availability varied from 95% to 80% in 5% intervals. The reduction in availability was calculated by replacing a proportion of the DLC 1.2 simulations (power production) with DLC 7.2 simulations (idling with fault).

Figure 5.11 presents normalized DELs at the chosen output locations on the jacket for the five different cases. It can clearly be seen that a reduction in availability leads to a reduction in fatigue loading across the whole structure. This is because the largest loading contribution comes from the wind, so it is more damaging for the machine to be operating.

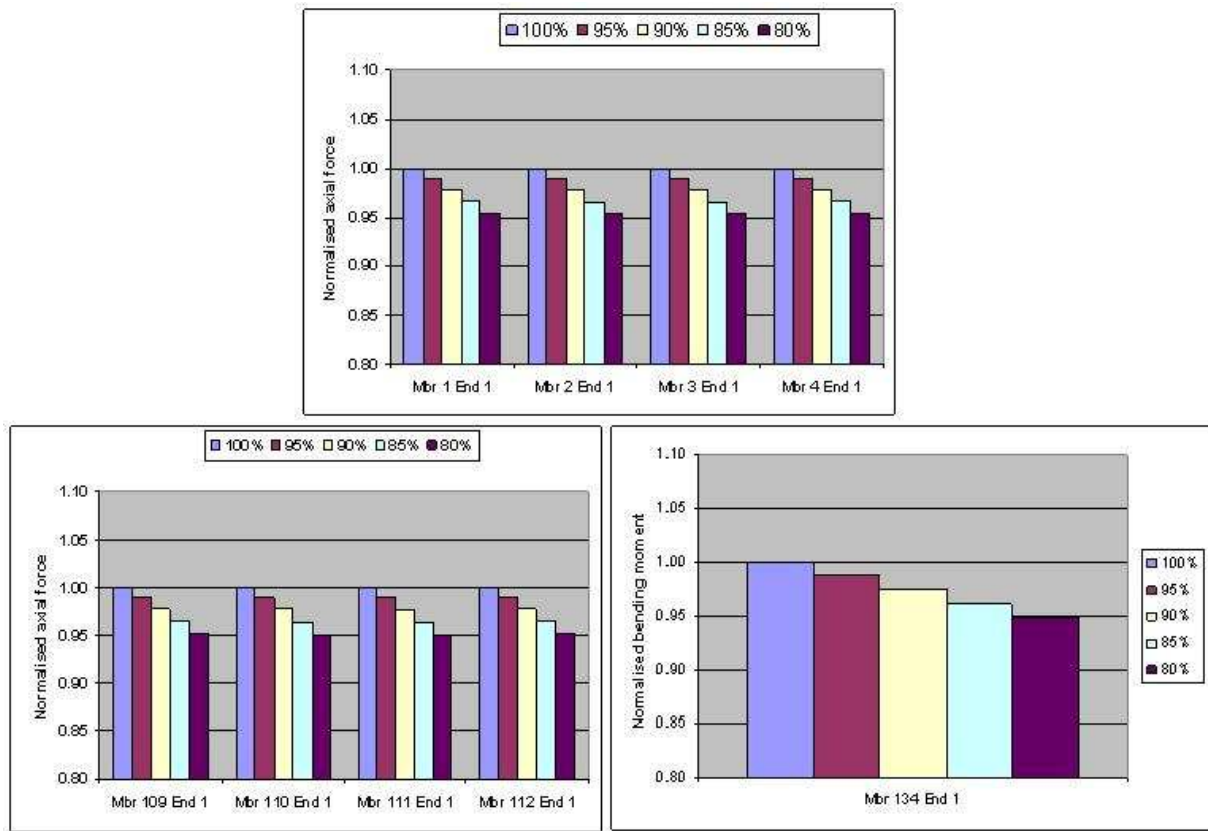


Figure 5.11: Normalised DELs with variation in availability

Wind class

The baseline fatigue loads were calculated using site-specific data for the annual wind speed distribution, as presented in Figure 5.12 using the blue line. In order to test the influence of wind class on jacket structures, three additional cases were considered using the wind speed distributions from IEC wind classes I to III (shown in Figure 5.12).

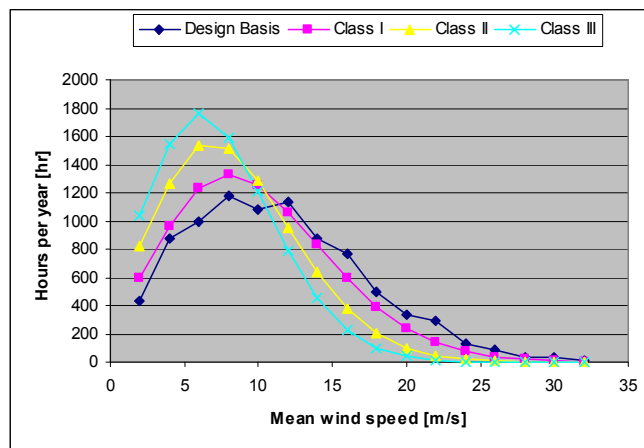


Figure 5.12: Wind speed distributions considered

Figure 5.13 presents normalized DELs at the chosen output locations on the jacket for the four different cases. The results show that the fatigue loads decrease by up to 20% when the wind speed distribution is reduced to Class III. This scale of reduction is seen across the whole structure. These results demonstrate that one of the main drivers for jacket fatigue loads is the wind loading, and that the local wind speed distribution is an important factor in jacket support structure design.

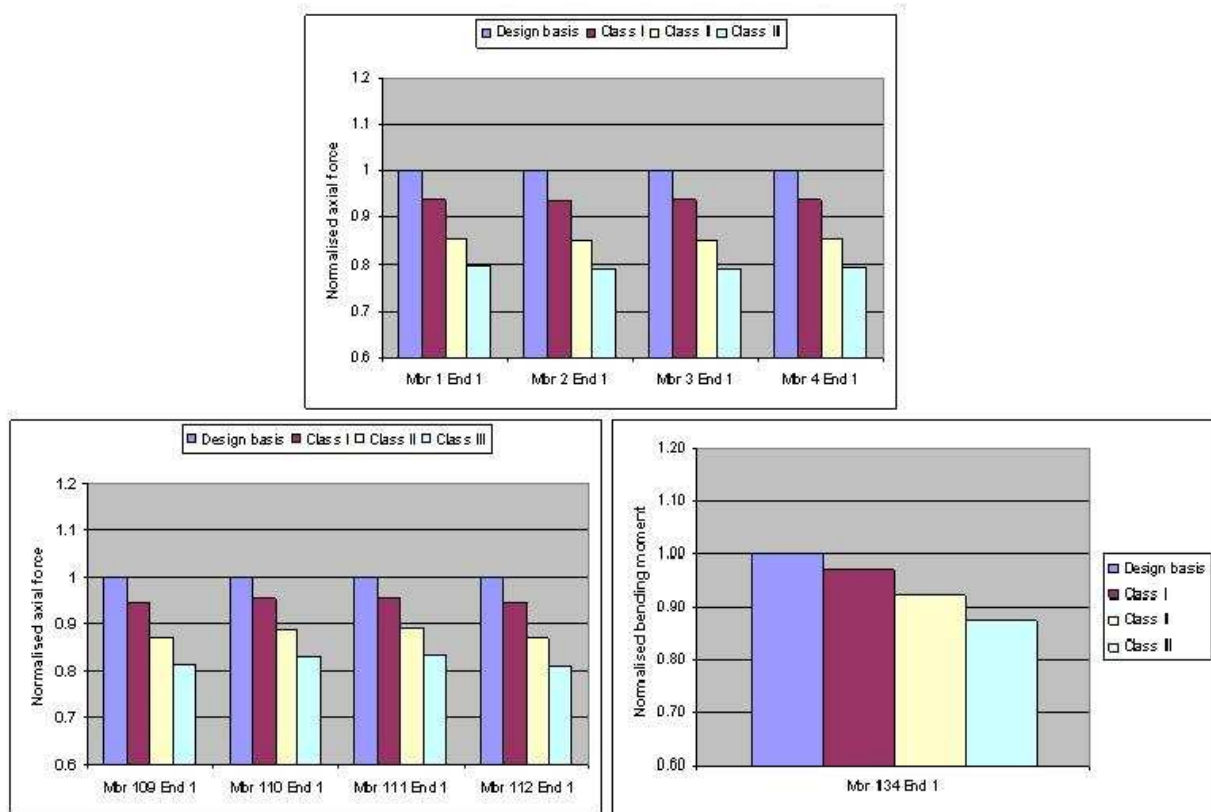


Figure 5.13: Normalised DELs at pile head, with variation in wind class

Structural natural frequency

The baseline fatigue loads were calculated with a structural natural frequency for the first tower mode equal to 0.29Hz. This is equivalent to 1.44P, where 1P is the rotational frequency at rated speed (12.1rpm). In order to test the influence of natural frequency on jacket structures, the stiffness of the support structure was artificially forced by changing the Young's modulus of steel. Five cases were considered in addition to the baseline case, shown in Table 5.29.

Table 5.29: Structural natural frequencies considered

Frequency (multiple of 1P)	Frequency (Hz)	E_steel (N/m ²)
1.09	0.219	1.1E+11
1.18	0.237	1.3E+11
1.26	0.254	1.5E+11
1.35	0.273	1.8E+11
1.44	0.291	2.1E+11
1.53	0.309	2.4E+11

Figure 5.14 presents normalized DELs at the chosen output locations on the jacket for the six different cases. The results show a significant variation in DEL when natural frequency is varied, in some cases up to 65%. The loads tend to increase when the natural frequency is either lower or higher than the original value, and the scale of the increase is much larger than for other parameters. These results show the importance of designing a support structure with a fundamental natural frequency in the right range. If the frequency is too low then the structure may experience resonance with the rotational frequency of the rotor. If the frequency is too high then the structure will be overdesigned and the high stiffnesses will lead to increases in member loading.

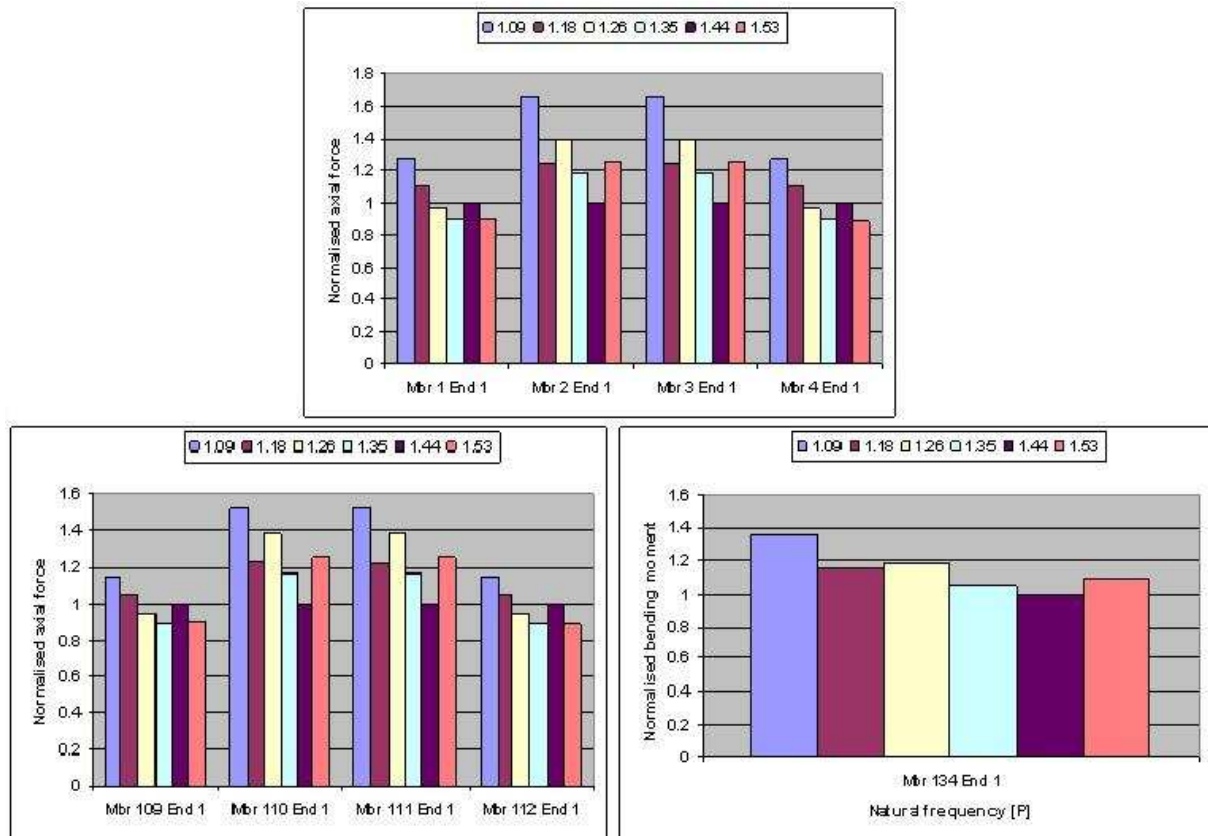


Figure 5.14: Normalised DELs at pile head, with variation in natural frequency

Tide height

The baseline fatigue loads were calculated with the water level at mean sea level (MSL) of 50m. In order to test the influence of tide height on jacket structure loads, four additional cases were considered with water levels at LSWL, LAT, HAT and HSWL (values taken from [55]). The total water level variation between LSWL and HSWL is 5.66m.

Figure 5.15 presents normalized DELs at the chosen output locations on the jacket for the five different cases. The results show that tide height has only a minimal effect on fatigue loading, with a maximum of 1% difference from the baseline. A study into tidal effects on monopile support structure fatigue loading [68] has shown that for fatigue load calculations using a water level of MSL + 10% of tidal range gives accurate damage equivalent loads. The mean difference from the baseline results across the calculated DELs is small but positive, which indicates that the above conclusion derived for monopiles is also appropriate for jacket structures.

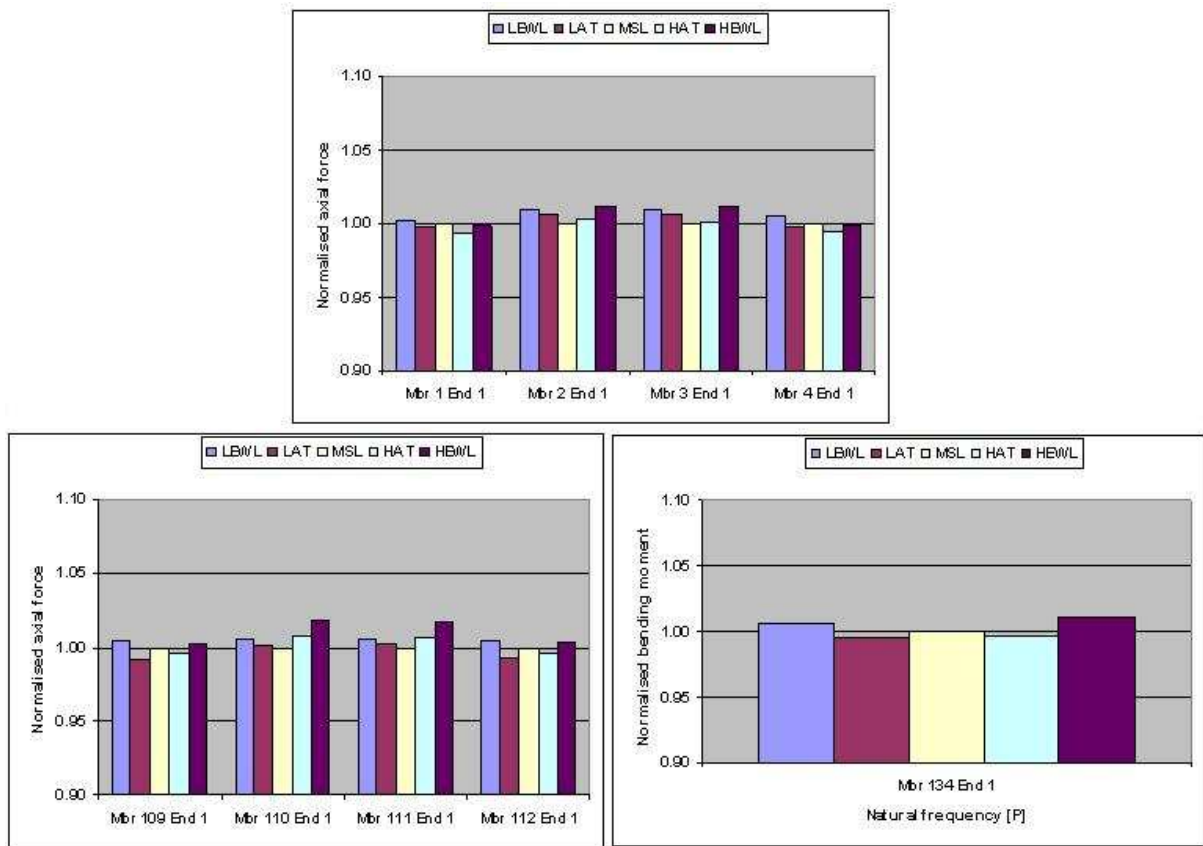


Figure 5.15: Normalised DELs at pile head, with variation in tide height

5.4.2 Extreme load case parameter study

For the design of the UpWind reference jacket support structure, a comprehensive set of extreme load cases was simulated to calculate the driving loads on the structure [54]. The worst case wind and wave combination was found to come from DLC 6.1 (idling during 50 year storm). Therefore DLC 6.1 is investigated in this analysis. The 50 year wind speeds and wave conditions used for this load case can be found in [55]. Irregular waves are modelled using a Jonswap spectrum with a peakedness parameter (γ) equal to 3.3. A constrained wave is used in GH Bladed to model the 50 year individual wave height. This approach ensures that the irregularity of the background sea state and the nonlinearity of the extreme wave are both modelled in the simulation.

First, a baseline extreme load set was performed with parameters as described above, with multiple wind seeds and wind-wave misalignment as required by the IEC 61400-3 offshore standard [69]. The driving load combinations were identified, and subsequent load sets performed with these load combinations. The IEC standard states that for storm load cases a range of wave periods and water levels must be considered [69]. This can lead to a huge number of simulations. The constrained wave period and tide height parameters are varied individually, to determine the effect on the extreme loading:

Results in this section are presented in terms of the absolute maximum load from the Bladed simulation. The results are normalized so safety factors are not required. The extreme loading on a jacket structure is generally driven by the axial forces in the pile heads, so for the purposes of this section extreme loads are reported at the pile head only. The output locations on the Bladed model are shown in Figure 5.16.

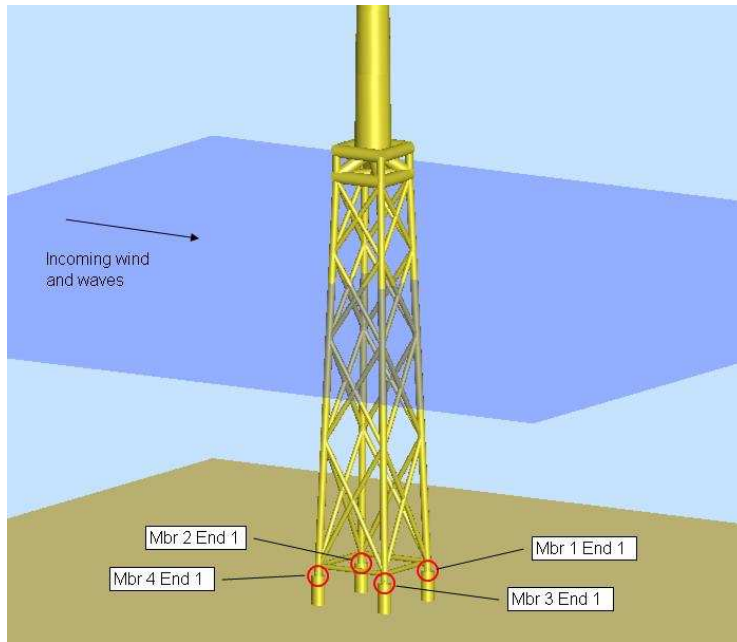


Figure 5.16: Output locations for extreme loads

Constrained wave period

The baseline extreme loads were calculated with a constrained wave period of 10.87s. This is the lower bound of the range specified by the IEC standard [69], which is generally considered to be conservative. In order to test the influence of the wave period on the extreme jacket loading, three additional cases were considered in addition to the baseline case with wave periods varying from 9.3s to 14.0s.

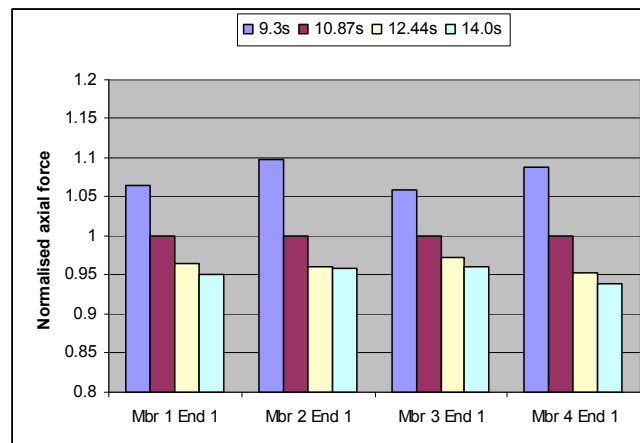


Figure 5.17: Normalised extreme loads at pile head, with variation in constrained wave period

Figure 5.17 presents normalized extreme loads at the pile heads for the four different cases. The results confirm that shorter wave periods result in higher extreme loads, with load increases of up to 10% resulting from a reduction in wave period to 9.3s. This is an important result, because it enables designers to perform preliminary extreme load calculations at a single wave period with greater confidence that they

are capturing the worst case loading. This significantly reduces the number of simulations required in the preliminary extreme load analysis.

It is important to note, however, that for detailed design using the most conservative load will not necessarily result in the most cost effective support structures. Rather, the load with a return period of 50 years should be used. This implies that a statistical approach should be used as a basis for the rules in the standard.

Tide height

The baseline extreme loads were calculated with the tide height at HSWL, equal to +3.29m. This is the upper bound of the range specified by the IEC standard [69], which is generally considered to be conservative. In order to test the influence of the tide height on the extreme jacket loading, three additional cases were considered in addition to the baseline case with tide heights varying from LSWL to HSWL+2.13m.

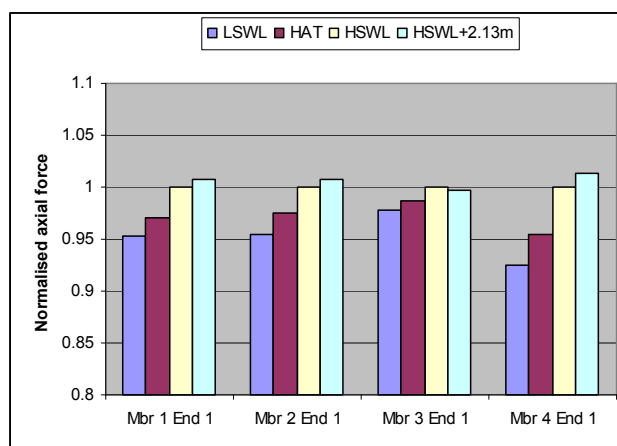


Figure 5.18: Normalised extreme loads at pile head, with variation in tide height

Figure 5.18 presents normalized extreme loads at the pile head for the four different cases. The results confirm that higher water levels result in higher extreme loads, although the load increases are smaller in magnitude than when the wave period is varied. Again, this is an important result because it enables designers to perform extreme load calculations at a single water level with greater confidence that they are capturing the worst case loading.

5.4.3 Summary and key findings

The fatigue loading on the structure is found to be dominated by the wind, with a relatively low contribution from the hydrodynamics. This is reflected in the small changes in DEL when marine parameters are varied (tide height, wind-wave misalignment) compared to the large changes in DEL when wind parameters are varied (wind class). The small hydrodynamic influence is also shown in the fact that a decrease in availability leads to a reduction in loading. The parameter which has the most effect on fatigue loading is the structural natural frequency. This demonstrates the importance of placing the natural frequency in the right range when designing a jacket support structure.

The parameter which has the most effect on the extreme loading on the structure is the wave period of the 50 year maximum wave. Conservative load results are given when this parameter is set to the lower bound of the range given in the standard.

PART II: Design Methods for Floating Support Structures

A large part of the global offshore wind resource is in locations where the water is much deeper than that currently experienced in offshore wind farm design, for instance off the coasts of the United States, China, Japan, Spain and Norway. In these locations fixed-bottom support structures are not feasible. Therefore the possibility of mounting wind turbines on floating support structures opens up the potential to utilise this deepwater resource. The economic potential of floating offshore wind turbines (FOWT) is demonstrated in [70]. In order to realise this potential, cost-effective floating wind turbine designs are needed which can compete with other energy sources. This requires appropriate and targeted development of the design tools, methods and standards used in the industry. In view of this, Part II of this report has its focus on design methods for floating support structures.

In order for an offshore wind turbine to be certified, the IEC 61400-3 standard [69] requires that an integrated loads and response analysis be performed. This type of analysis is fundamental to the design process as it enables the structure to be optimised taking into account the fully coupled response of the whole system. Reliable and validated design tools and methods are therefore needed which can model the dynamics and response of floating wind turbine platforms in a comprehensive and fully integrated manner.

Chapter 6 presents a review of the current state-of-the-art in floating wind turbine design tools. An overview is given of modelling techniques for FOWTs and the advantages and disadvantages of the various approaches are discussed, together with recommendations for future development needs.

Chapter 7 presents a summary of the benchmarking activities performed for some of the available floating design tools. The comprehensive testing and validation of these design tools is important for designers to have confidence in their predictions.

Chapter 8 presents the development of advanced modelling approaches for selected aerodynamic, hydrodynamic and mooring line simulation techniques and their applicability for integrated floating wind turbine modelling. The combined aerodynamic, hydrodynamic and mooring line effects on floating wind turbines create unique operating and failure design conditions which have not yet been studied in detail.

Chapter 9 presents recommendations for possible extensions to the IEC 61400-3 standard to enable applicability to deep-water floating wind turbine designs, including the implementation of additional/different design load cases.

6. Integrated design tools

6.1 Modelling methods for floating offshore wind turbines

In this section an overview is presented of the methods used for the numerical modelling of floating offshore wind turbines. Different methods for the modelling of structural dynamics, aerodynamics, hydrodynamics and mooring lines are compared and comparative strengths and weaknesses presented. The detailed equations describing the various theories are not presented here for the sake of clarity and brevity.

6.1.1 Previous work

Frequency-domain methods are commonly used in the offshore oil and gas industries to analyse and design floating structures. These methods have also been employed in a number of instances for the preliminary design of floating wind turbines. Bulder et al. [71] used linear frequency-domain hydrodynamic techniques to find response amplitude operators (RAOs) to investigate a tri-floater concept. Lee [72] used a similar process to analyse a tension-leg platform (TLP) design. Vijfhuizen [73] used frequency domain analysis to design a barge for a 5MW turbine including a wave energy device. Wayman [74] also performed calculations in the frequency domain to model various TLP and barge designs.

There are a number of advantages to design calculations in the frequency domain: the above studies were useful in order to demonstrate the initial technical feasibility of floating wind turbines by showing that they could be designed so that the natural frequencies are placed away from the wave energy spectrum to minimise dynamic response. However, frequency domain calculations also have important limitations: they cannot capture non-linear dynamic characteristics or model transient loading events, both of which are important for wind turbines since the non-linear dynamics introduced through transient events and control system actions are a big factor in the loads analysis. Matha [75] performed a typical frequency domain analysis for a floating wind turbine and showed that some couplings between the platform motion and the flexible tower and blades were not accounted for, which could lead to natural frequencies being wrongly predicted and critical system resonances not being identified. This result underlines the importance of performing calculations for floating wind turbines in the time domain.

For the purposes of this section, therefore, frequency domain calculations are not considered and the design tools presented are all based on a time domain analysis.

6.1.2 Structural dynamics

Modal representation

The majority of the wind turbine simulation codes available for the onshore market utilise a modal approach for the calculation of structural dynamics. This approach can also be used for the modelling of floating offshore wind turbines. In this approach the fundamental mode shapes and frequencies of the structure are calculated, usually using a finite element pre-processor. These eigenmodes are then superimposed and coupled together to enable the calculation of the overall dynamic response of the total structure using the system equations of motion.

This method of structural analysis benefits from a low number of degrees of freedom: the exact number will depend on the structural properties of the turbine but is typically less than 30. Modal representation is therefore computationally very efficient and results in rapid simulation times. For this reason it remains the method of choice for many of the onshore wind turbine simulation codes currently used.

The flexibility of this method is limited somewhat by the restrictions on the number and type of degrees of freedom allowed in the structure. This is not so much of a problem when modelling conventional fixed-bottom wind turbines as it is possible to generate a reliable representation of the wind turbine dynamics using relatively few degrees of freedom. However when modelling floating wind turbines additional degrees of freedom are required which often are not available using simple modal representation. In addition to this the modal method does not allow the modelling of more complex floating wind turbine configurations e.g. multiple rotor concepts.

Another limitation of modal representation is that the method is inherently limited to linear responses, i.e. the deflected shape of the blades or tower at any instant must be a linear combination of the available mode shapes. This means that large deflections of flexible components may not be accurately predicted, for example in the case of lightweight rotor blades. This is of particular importance when it comes to modelling floating offshore wind turbines as they can experience significant translational and rotational displacements during normal operation, which may not be accurately predicted using modal representation.

Multibody systems

An alternative method for the calculation of wind turbine structural dynamics is the multibody system approach. In this method the structure is split up into a number of elements, which can be either rigid or flexible. These elements are interconnected by joints, each with the required constraints applied, and may undergo large translational and rotational displacements. The dynamics of the resulting system can then be analysed using equations of motion, usually derived from the Newton-Euler equations or Lagrange's equations.

The multibody method benefits from increased modelling flexibility due to the ability to create and couple together any number of separate bodies in any number of configurations. This enables an increased number of degrees of freedom to be modelled compared to modal representation, but still with a relatively small number of equations of motion compared to a full finite element analysis.

In addition to this, because the bodies are treated separately and without the assumption of linearity the multi-body method also enables accurate modelling of systems with large displacements and rotations. This is an important feature for the modelling of floating offshore wind turbines, and as a result the multibody system method is more common for floating wind turbine simulation codes.

Finite Element Modelling

Finite element modelling is the most detailed and also the most computationally expensive of the three methods described here. In this method the wind turbine structure is discretized into a mesh of finite elements interconnected at nodes, each of which has a number of degrees of freedom. The elements can be modelled as one-dimensional beams, two-dimensional plates or three-dimensional solids, and are given physical properties including mass and stiffness. In most cases the theory of linear elasticity but large deflection is applied. The dynamic behaviour of the system can then be analysed by finding numerical solutions to the ordinary and partial differential equations of motion for each element.

The main advantage of finite element modelling is that it allows complex structures to be modelled with a high level of detail and a very large number of degrees of freedom. This is useful for the modelling of more complicated floating platform geometries. Another important advantage of the finite element approach is that it allows for modelling of material non-linearities. This is important for fixed-bottom wind turbines when modelling pile-soil interaction, but also for the modelling of additional components found in floating wind turbines such as mooring lines.

However the level of detail in finite element analysis means that the computational effort required is very high, which results in slow simulations compared to the alternative methods described above. This is a major disadvantage for a commercial wind turbine modelling code where thousands of fully integrated time-domain simulations may be required in order to fulfil the design criteria specified by the international standards. Finite element modelling can also be less efficient than the multibody systems approach for modelling wind turbines, particularly in the way that large rotations, relative kinematics of system components and deformations of structural members are handled. The efficiency of the method depends on the numerical methods and algorithms employed. Standard finite element packages are generally used to model structures for which the motion occurs about a mean undisplaced position, and for this reason finite element codes used to model wind turbines must be specially developed to model large movements of one structural component with respect to another.

A number of wind turbine modelling codes use combinations of the above approaches; for instance some use a multibody representation with modal elements included, and others use a combined multibody and linear finite element approach.

6.1.3 Aerodynamics

Blade Element Momentum theory

The vast majority of commercial aeroelastic wind turbine simulation codes use combined blade element and momentum (BEM) theory to model the aerodynamic forces acting on a wind turbine rotor. This method was developed from helicopter aerodynamics and due to its convenience and reliability has remained the most widely-used method for calculating the aerodynamic forces on wind turbines. Floating wind turbine design codes are no exception and BEM theory is used in all the floating codes currently available.

In this method the rotor is modelled as an actuator disc assuming axi-symmetric, incompressible, steady flow in a stream tube. The power extracted by the rotor and the thrust force acting on the rotor can be derived using Bernoulli's theorem, which assumes that the balances between changes in momentum and energy flow rates are conserved. Momentum theory can then be applied on an annular level to match the results of momentum analysis with the blade element properties and geometry. Simple BEM theory is very rarely used in isolation, as it does not deal with the unsteady nature of the aerodynamics experienced by a wind turbine rotor. There are a number of corrections commonly applied in conjunction with the BEM model to account for this.

The first of these corrections is the inclusion of tip and hub loss factors in the BEM equations. The tip and hub loss factors account for the fact that the axial flow induction factor a is not uniform over the rotor area but fluctuates between the passing of each blade, with the overall effect of reducing the net power extracted. This fluctuation is due to the vorticity distribution in the wake arising from the finite number of blades. At the blade root and blade tip the bound circulation around the aerofoil must reduce to zero resulting in a vortex being trailed

into the rotor wake, which is what causes the losses. The most common implementation of the tip and hub loss factors is based on an analysis by Prandtl from propeller theory.

Another important correction is dynamic inflow theory. BEM theory in its most simple form assumes that the induced velocities along the blade can be calculated instantaneously for given flow conditions, i.e. that the wake reacts instantaneously to changes in blade forces. In practice, the vorticity distribution in the rotor wake is influenced by changes in blade loading, and the full effect of this change in the induced velocity flow field takes a finite time. Dynamic inflow theory enables this dependence of induced velocities on rotor loading to be modelled. This is done by rewriting the BEM equations for the calculation of axial inflow as dynamic differential equations, which can then be integrated to give time dependent values for inflow including a time delay. One advantage of this method is that it allows induced velocities to be determined non-iteratively, rather than going through loops to convergence as in the BEM equations. However the theory was developed for lightly loaded rotors which is questionable for wind turbines especially in situations with high thrust coefficients.

The occurrence of stall on a wind turbine blade in unsteady flow is a complex process, as the angle of incidence can change rapidly and with significant amplitude. As a result the onset of stall may be delayed beyond the static stall angle, and the corresponding aerodynamic forces can undergo large hysteresis. In order to represent this process dynamic stall models to calculate the unsteady lift coefficient have been implemented as an extension to BEM theory. These models also include a time lag in the calculation of trailing edge separation. The inclusion of these models is important as the quasi-steady approach, in which the flow field adjusts instantaneously to each change in the angle of incidence, can result in an under-prediction of the aeroelastic damping associated with stalled flow and hence an over-prediction of structural vibrations.

There are a number of advantages to the use of BEM theory for calculating aerodynamic forces on a wind turbine rotor. The main advantage of this method is its simplicity and consequently its speed. It has also been extensively validated against measured data and shown to be accurate and reliable. However BEM theory also has a number of limitations. It is really intended only for steady flow with wind directly approaching the rotor, and although the extensions described above can be applied to improve the accuracy of prediction in turbulent flow these extensions do not fully capture all the unsteady effects. In addition to this the theory is still not validated for rotors operating in large yaw angles or with significant upflow.

There are also research codes which use free wake lifting line methods, such as the free-vortex based AWSM code developed by ECN in the Netherlands [77]. This is based on Prandtl's lifting line theory taking into account non-linear contributions, and is able to more accurately describe the shape and strength of the time-dependent wake generated by the turbine blades. The use of this method leads to better predictions in situations where the aerodynamic characteristics vary significantly with time and where the dynamic wake effects are important, for instance in yawed flow. It also captures the effects of mutual blade interference which BEM theory does not do, and models the dynamics of tip vortexes more accurately. However it is significantly slower than the BEM method, and also numerically more unstable meaning that the iteration scheme may require relaxation of the tolerances in order to prevent divergence. The assumption of irrotational flow also means that effects such as wind shear cannot strictly be included.

The alternative to BEM theory and vortex-based methods is to use computational fluid dynamics codes, which use the Navier-Stokes equations. This approach is much more complex and has high computer processing requirements, which makes industry-scale analysis impractical.

6.1.4 Hydrodynamics

Wave particle kinematics

In order to calculate the hydrodynamic loading on a submerged structure in the time domain the wave particle kinematics must be determined. For linear sea states the wave particle velocity and acceleration vectors and dynamic pressure can be calculated using linear Airy wave theory. This theory represents the wave elevation as a sinusoid propagating with a constant amplitude and period. For fatigue load calculations in which irregular sea states are required, Airy wave theory can be combined with an appropriate wave energy spectrum in order to create an irregular sea state.

One limitation of Airy theory is that wave particle kinematics can only be defined up to the mean water surface (i.e. at $z = 0$). The theory can be extended up to the instantaneous free surface by using positive values of z ; however this approach tends to over-estimate particle kinematics at the wave crest and under-estimate particle kinematics in the trough. In order to take proper account of the forces acting between the mean water level and the instantaneous free surface, Wheeler stretching may be used. This is described in more detail in [78].

Airy wave theory is widely used due to the relative simplicity and speed with which it calculates wave particle velocities and accelerations. The main disadvantage of Airy wave theory is that it relies on the assumption of linearity, which means that the non-linear characteristics of real sea states, such as steep-sided waves and breaking waves, cannot be modelled. This rules out the possibility of calculating slap and slam loading which can result from non-linear waves.

The assumption of linearity is taken to be reasonable in deep water, where wave heights are much smaller than wavelengths. However for large waves or for waves in shallow water it may be required to account for non-linearities in the wave structure. In this case stream function wave theory may be used. This theory gives more accurate wave kinematics than linear Airy theory in shallow waters or when the wave height is large compared to the water depth. However the limitation of stream function theory is that it cannot be used to compute irregular sea states, which are required for fatigue load calculations according to [69].

Morison's equation

Once the wave particle kinematics have been derived, the hydrodynamic loads acting on the support structure may be calculated using Morison's equation. Morison's equation is valid for slender, vertical cylinders and is a function of the diameter of the cylinder, fluid particle velocity and acceleration, and the hydrodynamic drag and inertia coefficients C_D and C_M . The drag and inertia coefficients are functions of Reynold's number, Keulegan-Carpenter number and surface roughness as well as a number of other factors. In order to calculate the applied hydrodynamic loads acting over the length of the structure the cylinder can be divided into a number of elements, in a similar way to BEM theory, and the total applied load found by integrating the loads acting on each element. Morison's equation accounts for the relative motion between the platform and the fluid and includes added mass effects from the movement of the water.

One major advantage of Morison's equation is that the hydrodynamic loads are calculated in terms of wave particle velocities and accelerations rather than velocity potential. This enables Morison's equation to be used not only with linear Airy wave theory but also with non-linear wave kinematic models. This is the reason that Morison's equation is used in the majority of codes used to model fixed-bottom offshore wind turbines in relatively shallow water.

However when it comes to modelling floating support structures Morison's equation also has a number of disadvantages. For support structures with a small diameter relative to the wavelength of the incident waves, i.e. when the member diameter is less than 0.2 times the wavelength, diffraction effects may be neglected [32]. This comes from G.I. Taylor's long-wavelength approximation, which states that for surface-piercing bodies with a small diameter relative to the wavelength, the wave potential can be assumed to be constant across the body and therefore calculations can be performed at the centre of the body. Morison's equation uses this approximation to simplify the diffraction problem. However when the submerged body has a diameter large enough for the waves to be disturbed by the presence of the structure, wave diffraction effects must be accounted for in order to correctly determine the local pressure force and global wave loads. This is often the case for floating platforms, in particular for those stabilised by buoyancy, which means that Morison's equation cannot be used.

Morison's equation also assumes that viscous drag dominates the drag loading, and that wave radiation damping can therefore be ignored. This assumption is only valid if the motions of the support structure are very small, which is usually the case for fixed-bottom support structures with soft-stiff characteristics. However for floating platforms with low-frequency rigid modes the support structure may experience significant movement, which means that wave radiation forces should be accounted for.

Because Morison's equation is only used for axi-symmetric cylindrical structures it does not take account of any added mass-induced coupling between hydrodynamic force and support structure acceleration in different degrees of freedom. This is a reasonable assumption for cylindrical structures; however for an accurate modelling

of non-cylindrical floating platforms these coupling terms should be taken into account. Morison's equation also neglects hydrostatic restoring forces; however additional terms can be added to account for this.

Linear hydrodynamic equations

When dealing with slender structures it is considered to be a reasonable assumption that the submerged body does not exert any influence on the surrounding fluid either in terms of diffraction or radiation. However we have seen above that when the structures in question are larger in diameter and experience significant movement, as is often the case for floating platforms, then wave diffraction and radiation forces must be included in the analysis. In order to calculate these effects the additional boundary condition of zero flow velocity perpendicular to the surface of the structure must be followed. For most practical cases the resulting problem cannot be solved analytically, so numerical methods based on the assumptions of linear wave theory must be used. Assuming that the hydrodynamics of the sea state are linear, the sources of loading can be sub-divided into three separate problems: radiation, diffraction and hydrostatic restoring. These problems can then be solved individually and the resulting loads summed together. This approach is described in more detail in [82].

Wave radiation loading describes the loads which arise from the influence of a moving body on the surrounding fluid when no incident waves are present. In this case it can be assumed that loads due to wave radiation are independent of incident waves since the radiation problem is being treated separately from the diffraction problem. The loading on the body arises as the body radiates waves away from itself, and includes contributions from both added mass and damping. The added mass contribution, defined in the added mass matrix A_{ij} , comes from the hydrodynamic forces resulting from the outgoing wave pressure field induced by the acceleration of the support structure. The damping contribution comes from free surface memory effects; because the pressure field induced by outgoing waves continues for as long as the waves radiate away, radiation loading depends on the history of motion of the submerged body. The free surface memory effect can be accounted for using a radiation kernel, K_{ij} , to represent the hydrodynamic forces at any given moment in time due to a change in support structure velocity. Both the added mass matrix A_{ij} and the radiation kernel K_{ij} depend on the geometry of the floating platform and must be computed in the frequency domain using potential flow theory.

Wave diffraction loading describes the loads which arise from the influence of the surrounding fluid on a stationary body when incident waves are present. In this case it can be assumed that loads due to wave diffraction are independent of the motion of the body, i.e. the loads are calculated for the body fixed at its mean position, since the diffraction problem is being treated separately from the radiation problem. As the waves pass the stationary body the wave pattern is modified due to the presence of the body and loading on the body arises as a result of the modified pressure field. The wave excitation force is closely related to the wave elevation, which can be computed using linear Airy wave theory, and also depends on the geometry of the floating platform, the frequency and the direction of the waves. A normalised complex transfer function to represent this force can be computed in the frequency domain using potential flow theory.

Hydrostatic loading describes the static loads on the body arising from the pressure in the surrounding fluid. It is normally calculated by computing the surface pressure applied by the fluid on the submerged part of the structure, including the restoring forces due to water plane area arising from the displacement of the support platform. The magnitude of the net upward force is equal to the weight of the fluid displaced by the body, in accordance with Archimede's Principle. The hydrostatic load contribution is relatively simple to compute.

The advantage of this method for calculating hydrodynamic loads is that it takes proper account of the influence of the body on the fluid. This is particularly important for floating bodies which often have large diameters and experience significant motion. It is also possible that there may be additional dynamic effects which are only accounted for when diffraction and radiation are included in the analysis: for instance it has been shown that the presence of wave radiation damping can in some cases reduce instabilities in platform surge motion arising from controller actions [17]. This illustrates the importance of including these effects in the hydrodynamic loadings calculations for floating wind turbines.

The main limitation of this method is that it requires the assumption of linearity, which restricts its use to deep water sites where wave heights are much smaller than wavelengths. The use of linear Airy wave theory means that the steep-sided or breaking waves often found in shallow water cannot be modelled, together with the resulting slap and slam loading. However it should be said that this is not as much of a limitation for floating wind

turbines as it is for most of the fixed-bottom offshore wind turbines installed to date, since floating wind turbine sites will normally be in deep water. In addition to this the potential flow theories used in a number of floating wind turbine design tools to calculate hydrodynamic loads were developed for stationary bodies, and are only valid when the support structure motion is small relative to the length of the platform. However many floating configurations experience large translational displacements relative to the wavelengths or characteristic length of the platform, or large rotational displacements of the platform relative to the wave steepness (for instance catenary moored systems where there is low resistance to surge and sway). This means that the linearisation assumptions are invalidated.

6.1.5 Mooring lines

Mooring systems are necessary for floating bodies in order to restrain the global movement of the platform against the effects of wind, waves and currents. It is important to accurately model the effect of mooring lines on the response and dynamics of a floating system, particularly in the case of floating wind turbine configurations which use mooring lines to achieve stability. However mooring system dynamics are non-linear in nature, and often include hysteresis effects. An accurate modelling of mooring line dynamics is therefore a complex problem and is dealt with fully only by dedicated codes. However the interaction of the mooring lines with the floating platform can also be approximated in a number of ways as described below.

Force-displacement representation

A common method for modelling foundations for fixed-bottom offshore wind turbines is to use P-Y springs in the translational and rotational degrees of freedom to represent the relationship between force and displacement in the soil. This method can be extended to the modelling of mooring lines for floating wind turbines by applying non-linear spring stiffnesses for all six degrees of freedom at the fairlead position. A damping matrix may also be included as appropriate. The relevant force-displacement characteristics of the mooring system must be calculated separately and added as inputs into the model. This method can also be extended to include a force-velocity relationship to account for mooring line drag.

The force-displacement method enables the non-linear geometric restoring properties of the mooring system to be described in a single stiffness matrix, which has the advantage of simplicity and ease of implementation. However in most cases this method is limited due to the fact that the loads are generally not specified as functions of displacement in all six degrees of freedom (surge, sway, heave, roll, pitch, yaw). Often restoring forces are specified as independent functions of each platform displacement, in which case important couplings can be missed; although modelling a spring at each mooring line attachment can minimise this loss of accuracy. Because the load-displacement data is given in discrete form it must also be interpolated, which can lead to small losses in accuracy.

Quasi-static representation

An alternative method for representing the non-linear mooring line restoring forces is the quasi-static approach. In this method the tensions in the mooring lines are solved from the equations of static equilibrium for the suspended mooring line for a given platform displacement at any instant in time, not accounting for the drag and inertia of the lines. The elasticity of the mooring lines should be included in the analysis, otherwise the tensions in the lines can be significantly overestimated.

This approach enables the properties of the mooring lines (length, diameter, mass and extensional stiffness) to be provided as direct inputs to the system, thus cutting out the pre-processing requirement of the force-displacement method. The quasi-static approach also accounts for the non-linear geometric restoration of the complete mooring system, but with a full representation of restoring forces as a function of displacement in all degrees of freedom built in to the method. This is because the restoring forces on the support platform are calculated at each time step taking into account the contribution from the tension in each mooring line.

Both of the above approaches have the limitation that they do not account for the dynamics of mooring lines. The assumption that the mooring lines are in static equilibrium for each successive instant in time could be considered to be appropriate for slowly varying platform motion where frequencies are of the order of minutes rather than seconds. However the motion of the platform due to waves is typically at frequencies of the order of

0.1Hz, and at these frequencies the inertia and damping of the mooring lines means that they are unable to follow the platform motion instantaneously. Neglecting mooring line damping can lead to inaccuracies since the dynamics of mooring lines are significantly affected by the drag loading due to hydrodynamic damping [79]. Neglecting mooring line inertia is justified in [82] (for the system and water depth in question) since it represents such a small percentage of the overall inertia of the system (around 2%). The bending stiffness of the mooring lines is also neglected in both the force-displacement and quasi-static approaches: however this is rarely of any significance.

Full dynamic modelling

The governing equations for mooring line dynamics are rather complex and cannot be solved analytically, so advanced numerical techniques must be used. One approach is to discretise the line into point masses connected by weightless inextensible elements, and solve the resulting ordinary differential equations using the finite difference method. A more general solution can be found using the finite element method. A number of discrete finite elements are used to approximate a continuum, each with physical properties, and the differential equations for each element solved numerically to find the dynamics of the line. Both these methods are extremely computer intensive. There are a number of codes, mainly developed for the offshore oil and gas industries, which provide full models of the dynamics of mooring lines for floating offshore systems.

The full dynamic modelling approach gives an accurate representation of the drag and inertia of mooring lines and their effect on the floating platform. These effects can be significant, especially in very deep water where the mooring line is much less likely to take up its catenary shape instantly and a quasi-static analysis is unable to accurately predict the line tensions. Therefore for floating wind turbines with catenary mooring systems in deep water a full dynamic analysis of the mooring lines should be undertaken.

One of the limitations of this method is that it requires much more processing time than the alternatives, due to its complexity. This is a problem for offshore wind turbine design calculations, in which a large number of simulations is required to fulfil the design criteria. It can also be difficult to find an appropriate way to interface the mooring line analysis codes with conventional aeroelastic offshore wind turbine design tools.

6.2 Overview of available floating design tools

There are a number of design tools available to the offshore wind industry that have the capability to model floating offshore wind turbines in a fully coupled time-domain dynamic analysis. In this section the content and structure of these design tools is presented, in particular the methods employed by each design tool for the modelling of structural dynamics, aerodynamics, hydrodynamics and mooring lines. The summaries presented here apply to the design tool capabilities available at the time of writing; future development is planned for most codes to expand their capabilities

FAST by NREL

FAST is a publicly-available simulation tool for horizontal-axis wind turbines developed by the National Renewable Energy Laboratory (NREL) in North America. It has been largely developed by Jonkman [80]. The FAST code was developed for the dynamic analysis of conventional fixed-bottom wind turbines, but has been extended with additional modules and to enable fully coupled dynamic analysis of floating wind turbines.

Structural dynamics

The FAST code uses a combined modal and multibody dynamics representation. The wind turbine blades and tower are modelled using linear modal representation assuming small deflections, with two flapwise bending modes and one edgewise bending mode per blade and two fore-aft and two side-to-side bending modes in the tower. The drive train is modelled using an equivalent linear spring and damper. A finite element pre-processor (BModes) is used to calculate the mode shapes of the blades and tower.

Aerodynamics

The aerodynamic subroutine package AeroDyn is used to calculate aerodynamic forces in FAST. This model uses quasi-steady BEM theory or a generalized dynamic inflow model. Both of these models include the effects of axial and tangential induction. The aerodynamic calculations include tip and hub losses according to Prandtl, and dynamic stall corrections using the Beddoes-Leishman model. Further details can be found in [81].

Hydrodynamics

The hydrodynamic subroutine package HydroDyn is used to calculate applied hydrodynamic forces in FAST. Wave kinematics are calculated using Airy wave theory with free surface corrections. The hydrodynamic loading includes contributions from linear hydrostatic restoring, non-linear viscous drag contributions from Morison's equation, added mass and damping contributions from linear wave radiation (including free surface memory effects) and incident wave excitation from linear diffraction. Full details are given in [82]. The linearised radiation and diffraction problems are solved in the frequency domain for a platform of arbitrary shape using 3D panel-based program WAMIT (or an equivalent hydrodynamic pre-processor). The resulting hydrodynamic coefficients are used in HydroDyn.

Mooring lines

The FAST code uses a quasi-static mooring system module to represent the non-linear mooring line restoring forces. This module accounts for the apparent weight of the mooring line in fluid, the elastic stretching of the mooring line and the seabed friction of each line. For a given platform displacement the module solves for the tensions within each mooring line by assuming that each cable is in static equilibrium at that instant, and uses the resulting tensions to solve the dynamic equations of motion for rest of the system. Full details of the quasi-static mooring line module are given in [82].

FAST has been used in a number of research contexts to model coupled wind turbine and floating platform dynamics. The configuration described above is that used by Jonkman et al [82]. However the FAST code has also been coupled with a number of other dynamic analysis programs to model the dynamics and response of floating wind turbines. Two examples of this are presented below.

FAST with Charm3D coupling

The FAST code is coupled with floater-mooring dynamic analysis program Charm3D by Shim [84]. Charm3D is a finite element program jointly developed by Texas A&M University and Offshore Dynamics Inc. with partial funding from Charm3D JIP (Joint Industry Program) for the dynamic analysis of moored floating offshore structures. The coupling of this program with FAST enables the mooring line and rigid body dynamics of a floating wind turbine system to be integrated with the wind turbine dynamics in a fully coupled time-domain simulation. In Charm3D the hydrodynamic coefficients of the floating platform are calculated in the frequency domain using a panel-based 3D diffraction and radiation program (in this case WAMIT). In the time domain analysis various non-linearities are taken into account including the drag force on the mooring lines, the large (translational) motion of the platform, the free surface effects, and the geometric non-linearity of the mooring system. The mooring line dynamics are solved simultaneously at each time step by a coordinate-based FEM program. The floating body motions and velocities computed by Charm3D are provided as inputs to FAST, and the resulting dynamic loads from the wind turbine computed by FAST are returned as external forces.

FAST with TimeFloat coupling

The TimeFloat software has also been coupled with FAST in order to model the dynamic response of the WindFloat floating foundation concept for large offshore wind turbines [83]. TimeFloat is a time-domain software tool developed by Marine Innovation and Technology for the analysis of floating structures. The coupling of TimeFloat with FAST enables the aerodynamic, hydrodynamic and mooring system forces acting on the structure to be simultaneously computed, including non-linear quasi-static mooring forces and the non-linear viscous forces generated by the water-entrapment plates.

As above, the wave interaction effects are processed in the frequency-domain software WAMIT and the resulting added-mass, damping and mean drift coefficients and wave-exciting forces passed to the TimeFloat code. The hydrodynamic forces are then calculated by TimeFloat. These include memory effects, wave-excitation forces (using force components computed by WAMIT), viscous forces resulting from drag effects, drift forces, mooring line forces and wind forces. The hydrodynamic forces are provided as an input to FAST, which then solves the turbine and tower equations of motion and passes the platform motion back to TimeFloat.

ADAMS by MSC

ADAMS (Automatic Dynamic Analysis of Mechanical Systems) is a commercially available general purpose multibody dynamics code developed by MSC Software Corporation. The code is not wind turbine-specific and is

also used by the automotive, aerospace and robotics industries. ADAMS models of wind turbines can be generated by the FAST tool through its FAST-to-ADAMS pre-processor functionality.

Structural dynamics

The ADAMS code uses a multibody representation to allow a large number of structural configurations and degrees of freedom. The wind turbine blades and tower are modelled as flexible members consisting of a series of rigid bodies with lumped mass and inertia connected by flexible joints with linear stiffness and damping. The drive train may either be modelled similarly as a series of lumped masses or through a simple hinge/spring/damper element. ADAMS can also model a number of additional features including torsional degrees of freedom in the blades and tower, flap/twist coupling in the blades, mass offsets in the blades and tower, and pitch actuator dynamics.

Aerodynamics

The AeroDyn aerodynamic subroutine package [81] is used to calculate aerodynamic forces in ADAMS, as described above.

Hydrodynamics

The hydrodynamic forces may be calculated in ADAMS by interfacing with the hydrodynamic subroutine package HydroDyn [82]. Alternatively an equivalent subroutine may be used for calculating loads on the floating platform (see for instance Withee [85]).

Mooring lines

The ADAMS code can also be extended in a similar way to the FAST code to enable the modelling of mooring lines. This can be done either by solving the mooring line tensions quasi-statically in a separate module and interfacing with the main code at each time step, or using an equivalent force-displacement relationship defined at the mooring line interface point.

Bladed by Garrad Hassan

GH Bladed is an integrated software tool for calculating wind turbine performance and dynamic response [9], developed by Garrad Hassan in the UK. It was originally developed for the modelling of onshore fixed-bottom wind turbines, but has been extended to include hydrodynamic loading for the modelling of offshore wind turbines.

Structural dynamics

The Bladed code uses a combined modal and multi-body representation to model the structural dynamics of a wind turbine. The wind turbine structure can be made up of any number of separate bodies, with flexible components such as the blades and tower modelled using a modal representation. Individual modal properties for each component are computed independently using a finite element representation of the body. The mode shapes and frequencies are dependent on the mass and stiffness distribution and the position of the neutral axis of the body, as well as other parameters specific to the body in question. The modes are coupled together using the appropriate equations of motion in the dynamic response analysis. For modelling the tower a multi-member model may be used, consisting of an arbitrary space-frame structure of interconnecting beam elements with user-specified mass and stiffness properties. Craig-Bampton style modes are used for the support structure. The resulting mode shapes are three-dimensional with six degrees of freedom at each node.

Aerodynamics

The aerodynamic forces on the rotor are calculated in Bladed using combined Blade Element and Momentum theory, including tip and hub loss models based on Prandtl. A dynamic wake model is included to account for the effect of blade loading on wake vorticity. The model included in Bladed is based on Pitt and Peters and has received substantial validation in the helicopter field. Dynamic stall is also accounted for using the Beddoes-Leishman model.

Hydrodynamics

The applied hydrodynamic forces on the wind turbine support structure are calculated in Bladed using Morison's equation. For linear sea states the wave particle kinematics are calculated using Airy wave theory with free surface corrections using Wheeler stretching. If linear waves are used an irregular sea state may be defined using either a JONSWAP spectrum or a user-defined wave energy spectrum. For linear irregular sea states the effects of wave diffraction may be accounted for using a time-domain MacCamy-Fuchs approxima-

tion. In this approach the wave energy spectrum is altered to give the same resulting hydrodynamic load on the structure as the standard MacCamy-Fuchs method, in which the C_d and C_m coefficients are modified in the frequency domain. For non-linear waves the wave particle kinematics are calculated using stream function theory. The order of the solution is chosen based on the input values of wave height, wave period and water depth.

Mooring lines

The Bladed code uses a user-defined force-displacement relationship to model non-linear restoring forces from mooring lines. The relationship between the displacement of the platform and the applied force from the mooring line is calculated separately by the user and implemented via a stiffness matrix at the fairlead position.

SIMO/RIFLEX by MARINTEK

SIMO (Simulation of Marine Operations) is a general-purpose time-domain program developed by MARINTEK for the modelling and simulation of offshore structures. It is used extensively to model motions and station keeping of floating structures in the offshore industry. The code has been extended to enable modelling of floating wind turbines by the addition of an external module for the simulation of rotor aerodynamic forces [86]. SIMO has also been coupled with non-linear finite element code RIFLEX [87], also developed by MARINTEK, a tailor-made code for the static and dynamic analysis of slender marine bodies such as risers and mooring lines.

Structural dynamics

The SIMO code uses interconnected multibody systems to model structural dynamics. In order to model a floating offshore wind turbine multiple bodies may be defined and coupled together. In [86] the turbine and support structure are defined using a small number of rigid bodies (2-body and 4-body configurations are investigated). In this case the rotor loads are transferred to the support structure using three flexible coupling elements consisting of two radial bearings and one axial bearing. In [87] the coupling with RIFLEX enables a finite element formulation of the structure, allowing for unlimited displacements and rotations in 3D space. The rotor is still modelled as a rigid body but the tower is made up of flexible beam elements, each with 12 degrees of freedom, which means that the elastic behaviour of the tower can be investigated.

Aerodynamics

The aerodynamic forces are calculated in a separate module and implemented in SIMO as a user-specified external force. Blade Element Momentum theory is used to calculate the forces on the rotor blades, with dynamic inflow effects included. Individual blade element forces are then summed together and applied in SIMO as a six-component external load on a rotating body. The drag force on the tower and nacelle is also accounted for in the aerodynamic loading.

Hydrodynamics

The hydrodynamic forces are modelled within the standard SIMO code. Linear Airy wave theory is assumed for calculating wave kinematics. The calculation of hydrodynamic loads takes into account linear and quadratic potential forces including frequency-dependent excitation, added mass and damping contributions (calculated in the frequency domain using WAMIT) and slow drift. Viscous drag forces from Morison's equation, mooring line forces and body-to-body hydrodynamic coupling force models are also included.

Mooring lines

The mooring lines are modelled using the RIFLEX code. This enables the representation of mooring lines as flexible finite elements, incorporating non-linear material properties and dynamic properties. A separate mooring system module is not required as it is an integrated part of the RIFLEX code.

SIMO/RIFLEX with HAWC2 coupling

The SIMO/RIFLEX code has also been coupled with the HAWC2 code in [88] and [89]. HAWC2 is an aero-elastic simulation tool developed by Risø National Laboratory for the dynamic analysis of fixed-bottom wind turbines [90]. The coupling of these two codes enables detailed modelling of both the aerodynamic and hydrodynamic forces acting on a floating offshore wind turbine. The HAWC2 code has also been used to directly model a floating wind turbine in [91], with the mooring line analysis performed separately in SIMO/RIFLEX.

Structural dynamics

The HAWC2 code uses a combined linear finite element and nonlinear multibody representation to calculate the structural dynamics of a wind turbine. A number of separate bodies can be defined, consisting of an assembly of linear Timoshenko beam finite elements. The bodies are connected by algebraic constraint equa-

tions, which can take the form of flexible joints, bearings or rigid connections. Internal forces are calculated from these algebraic constraints. In order to couple the two codes together the position, velocity and acceleration vectors and rotation matrix at the interface point are passed to HAWC2 by SIMO/RIFLEX and the reaction force at the interface point is returned to SIMO/RIFLEX by HAWC2 at each time step.

Aerodynamics

The aerodynamic forces on the rotor are calculated in HAWC2 using Blade Element Momentum theory. The classic approach has been modified to include the effects of dynamic inflow, dynamic stall, skewed inflow, shear effects on induction and effects from large deflections. The aerodynamic calculation points are positioned independently of the structural nodes to provide an optimal distribution of these points.

Hydrodynamics and mooring lines

In [88] and [89] the modelling of hydrodynamics and mooring lines is performed in SIMO/RIFLEX, as described in Section 3.4 above. In [91] the hydrodynamics are calculated using Morison's equation based on the instantaneous position of the platform. The mooring lines are modelled in SIMO/RIFLEX using a finite element model and the resulting force-displacement relationship applied as an external force at the fairlead position.

3Dfloat by UMB

3Dfloat is a code developed by the Norwegian University of Life Sciences (UMB) for the modelling of floating offshore wind turbines with full coupling between structural dynamics, aerodynamics, hydrodynamics and control system actions. The code has been used to analyse floating offshore wind turbine models and compare conceptual designs [92].

Structural dynamics

3Dfloat uses a finite element method for modelling the structural dynamics of a floating wind turbine. Euler-Bernoulli beams with 12 degrees of freedom are used, and geometric non-linearities in the elements are taken into account by casting the model in a co-rotational framework. The rotor and drive train are modelled as rigid, with no interaction between the rotor and the tower. Flexibility is included in the tower. The global motion of the structure is taken into account using structural modes.

Aerodynamics

The rotor aerodynamics are calculated in 3Dfloat using Blade Element Momentum theory. Extensions for dynamic inflow and large yaw errors are also included.

Hydrodynamics

The hydrodynamic forces are calculated in 3Dfloat using Morison's equation, with wave particle kinematics derived using linear Airy wave theory. The hydrodynamic loads include terms for added mass of water from the acceleration of the structure, linear hydrostatic restoring and non-linear viscous drag.

Mooring lines

The mooring lines are modelled using finite elements in 3Dfloat with bending stiffness neglected. The mooring lines can also be replaced by linear stiffnesses at the fairlead positions for the purposes of eigen-frequency analysis.

SIMPACT by SIMPACK AG

SIMPACT is a commercially available general purpose multibody dynamics code developed by SIMPACK AG. The code is used by the automotive, railway, aerospace and robotics industries. A version of SIMPACK, SIMPACK Wind, offers extensions to the original code which allow integrated wind turbine simulation. Several wind turbine manufacturers and suppliers are using the code, primarily for drive train analysis, but also for integrated wind turbine load simulations.

Structural dynamics

The SIMPACK code uses a multibody representation to allow a large number of structural configurations and degrees of freedom. In SIMPACK the parts or bodies of the wind turbine structure are connected using complex joints with different types of force elements acting from the inertial system on the bodies (for example aerodynamics on the rotor, hydrodynamics on the support structure) and between bodies (for example spring-damper elements). Parts of the WT, where the relative deflection of the bodies is small in comparison to the

rigid body motion, are considered rigid. SIMPACK has the capability to include flexible FE bodies of arbitrary geometry with the Craig-Bampton (C-B) method into the MBS model to account for larger deflections. This option is used for modelling of the WT blades and tower. A FE blade model, consisting of Euler-Bernoulli or Timoshenko beam elements is reduced by the C-B method and is capable of considering bending in flap- and edgewise direction, torsional and tensional rigidity and the relevant coupling effects. The relevant geometric stiffening effects are included for the reduction, representing a non-linear model for medium displacements. The blade model can also be split into separate C-B reduced flexible bodies, which are connected with zero DOF, representing a non-linear blade model for large displacements. The flexible tower is modelled with the same approach. Single and multi-torsional drive train models can be implemented, accounting for flexibility of the bedplate and other components as well. Drive train models for specific analysis, mainly for frequency domain analysis, also can include models for tooth contacts.

Aerodynamics

The AeroDyn aerodynamic subroutine package [81] is used to calculate aerodynamic forces in SIMPACK, as described above.

Hydrodynamics

The hydrodynamic forces in SIMPACK are calculated by interfacing with the hydrodynamic subroutine package HydroDyn [82], as described above.

Mooring lines

SIMPACK can either model mooring lines by solving the mooring line tensions quasi-statically in a separate module and interfacing with the main code at each time step, or using an integrated non-linear MBS mooring line model, where each line is discretized into separate rigid or flexible bodies, connected by spring-damper elements.

7. Benchmarking of design tools

The development of design tools capable of modelling floating platforms is an important step forward for the offshore wind turbine industry, but in order to give security to the industry the results obtained from these codes must be shown to be accurate and reliable. Comprehensive testing and validation is therefore crucial for giving sufficient confidence to developers and investors. The best way to achieve this kind of confidence is to take measurements from a real machine and compare the measured data with the results from numerical simulations (code-to-measurement comparisons). In the case of floating wind turbines there is limited measurement data available with which to validate the codes, so a second method is also employed, that of comparing the results of different codes with each other (code-to-code comparisons).

7.1 Code-to-measurement comparisons

A number of studies have been performed by Hydro Oil & Energy for the development of the Hywind floating wind turbine concept [87]. The floating platform consists of a deep-water slender spar-buoy with three catenary mooring lines. The integrated SIMO/RIFLEX/HAWC2 design tool was used in [88] to model the structure, as described above. As part of the development of this concept model scale experiments were carried out at the Ocean Basin Laboratory at Marintek in Trondheim in order to validate the coupled wind and wave modelling of the Hywind concept. A variety of sea states, wind velocities and control algorithms were tested and a number of parameters measured for the purposes of comparison. The hub wind speed from the model scale experiments was measured and used as the basis for the turbulent wind field used in the simulations. The JONSWAP wave spectrum was applied for both simulations and model experiments. The results of these tests showed very good agreement between the responses of the scale model and the predictions from the simulation code. The results also showed a significant increase in the damping of the tower motion when active blade pitch damping was introduced.

Another floating wind turbine code which has been validated with the use of measurements is TimeFloat, a time-domain design tool for coupled analysis of floating structures described above. The hydrodynamic calcula-

tions within this code were validated using wave tank tests performed at the UC Berkeley ship model testing facility [83]. A scale model of the floating platform was fabricated at 1:105 scale, with a foam disk at the tower top to represent wind forces and an electrical motor to model the gyroscopic effect of the rotor. A 3-hour realization of the 100-year sea state was generated with and without steady wind, and the resulting platform motion measured using a digital video camera. The floating platform was also modelled in the TimeFloat software using a simplified model for aerodynamic forces acting on the rotor. The results from these numerical simulations were then compared with the measurements from the tank tests. The comparison between model test results and numerical simulations showed good agreement, with the TimeFloat software generally underpredicting platform motion slightly.

Further measurement campaigns are being planned. The University of Maine DeepCwind Consortium in the U.S. has been awarded a \$7.1m grant to develop floating offshore wind capacity [93]. One of the stated aims of this project is to validate the coupled aero-/hydro-elastic models developed by NREL, as part of a research program which will include tank testing, deployment of prototypes and field validation.

The EOLIA project, led by Acciona [94] has also included some code-to-measurement tests. The objective of the project is to develop solutions for the design and implementation of deep water offshore wind farms. As part of the project the capabilities of FAST with AeroDyn and HydroDyn have been extended and applied to the analysis of three floating concepts (spar buoy, TLP and semi-submersible), alongside comparisons with the Simo-Riflex code. Tank tests have also been performed for each of the concepts at 1:40 scale, in order to verify the models.

The HiPRwind project [95] also aims to develop and test new solutions for offshore wind farms at a large scale. One of the main aims of HiPRwind is to install a 1:10 scale model of a future commercial-size floating wind turbine installation. The model will be deployed in real sea conditions, and will be used to monitor and assess the important operational parameters. The resulting measurement data will be an important contribution to overcoming the gap between small scale tank testing and full scale offshore deployment.

7.2 Code-to-code comparisons

In addition to the validation of codes using measurements, an important way to verify the predictive accuracy of numerical simulation tools is through code-to-code comparisons. Most of the codes used for the analysis of floating wind turbines have been validated in this way. One example is the FAST code, the aero-elastic features of which have been verified through comparisons with ADAMS, described in [96]. Another example is the SIMO/RIFLEX code used to model the Hywind floating wind turbine concept, which was validated in part through comparisons with HywindSim, a relatively simple Matlab/Simulink code developed for the purposes of such comparison [87]. The methods used to validate the hydrodynamic calculation module HydroDyn used in the FAST code are described in [82]. These methods included comparisons between the output from WAMIT and results from a different numerical solver, comparisons between the WAMIT frequency to time conversion and HydroDyn calculations, using a benchmark problem to test the accuracy of the quasi-static mooring line calculations, comparing the mooring line force-displacement relationship calculated by the quasi-static method with that calculated by another code, and comparisons of time-domain results with frequency-domain results.

The most extensive code-to-code comparison work in the offshore wind industry has been performed as part of the Offshore Code Comparison Collaboration (OC3) project within IEA Wind Task 23 [15]. In this project a number of participants used different aero-elastic codes to model the coupled dynamic response of the same wind turbine and support structure, with the same environmental conditions. The results were then compared in order to verify the accuracy and correctness of the modelling capabilities of the participant codes, and to improve the predictions.

7.2.1 Offshore Code Comparison Collaboration Phase IV

In Phase IV of the OC3 project a floating offshore wind turbine was modelled [17]. The turbine model used was the publicly available 5MW baseline wind turbine developed by NREL, and the floating platform was a modification of the Hywind spar-buoy developed by Statoil of Norway. The turbulent wind fields and irregular wave

kinematics were generated independently and provided to all participants in order to ensure tight control of all the inputs. A stepwise verification procedure was then used with the complexity of the model and the test cases being increased with each step.

A number of floating design tools were involved in Phase IV of the project, including FAST, ADAMS, Bladed, HAWC2, 3Dfloat, SIMO, Sesam and DeepC. A variety of different load cases were performed, including a full system eigenanalysis; a static equilibrium test; free-decay tests for each of the six rigid-body degrees of freedom of the platform; time series response tests with regular waves and irregular waves modelled with a rigid rotor and no wind; time series response tests with regular waves and irregular waves modelled with a flexible rotor and steady and turbulent wind; and “effective RAOs” calculated with regular waves at varying frequencies. Not all of the codes were able to contribute results to every test case performed, due to various limitations on their modelling capabilities. The test cases showed up a number of interesting results, some of which are outlined below.

Structural dynamics

The participating codes all employ different methods for modelling structural dynamics, which was illustrated in a number of differences in the results. The rotor-nacelle assembly was modelled rigidly in 3Dfloat and both the rotor-nacelle assembly and tower were modelled rigidly in SIMO, Sesam and DeepC. This meant that these codes could not model structural deflections in these components. The FAST code predicted a higher natural frequency for the second blade asymmetric flapwise yaw frequency than the other codes; this is because FAST does not account for a torsional mode in the tower whereas the other codes that include tower flexibility do account for this mode. The ADAMS code predicted less energy from the irregular wave simulations in the power spectra for tower top shear and rotor torque at the second tower and blade bending natural frequencies than FAST and Bladed. This may be because of an effect typical of ADAMS simulations in which numerical damping increases with frequency. The free-decay tests showed a few differences between codes in their prediction of the amount of damping present in the various modes. HAWC2 predicted too much heave and pitch damping; and ADAMS predicted too little pitch damping.

Aerodynamics

Most of the participating codes use BEM theory for the calculation of aerodynamic loads, with the exception of Sesam and DeepC which did not model aerodynamics for the purposes of this project. The 3Dfloat, SIMO, Sesam and DeepC codes modelled the rotor as rigid, which meant that the aero-elastic response was not correctly modelled. One example of this was in the calculation of effective RAOs, for which the 3Dfloat code showed lower excitation in yaw, higher excitation in fairlead tensions and higher excitation at the first tower bending frequency for all parameters. This was thought to be due to differences in aerodynamic damping due to rigid rotor, although it may also have been related to the modelling of the rigid spar with artificially high stiffness. The 3Dfloat code also gave a higher mean thrust in the simulations with regular wind and waves, which corresponded with higher platform surge and pitch displacements.

Hydrodynamics

The main difference in terms of hydrodynamic analysis was between codes which used linear potential flow methods and those which used simple Morison’s equation. The most interesting difference was found from the effective RAO calculations. The FAST code used by POSTECH was missing one hydrodynamic damping term, which led to the surge displacement and fairlead tension having a negative effective RAO: the physical meaning of this being that there was more system motion in still water than there was with waves. This occurred because there was a controller-induced instability of the platform surge mode at the surge natural frequency, where there was negligible hydrodynamic damping in the model. With waves included the wave radiation damping at the wave excitation frequency damped out this instability, thus reducing platform motion considerably. This result indicates the importance of using potential flow based solutions which include wave radiation damping for the analysis of floating support structures.

Mooring lines

The methods used for modelling mooring lines varied quite a lot between the codes, from user-defined force-displacement relationships to full dynamic models. The Sesam and DeepC codes used finite element models for the mooring lines, and also predicted more energy content above 0.1Hz for fairlead tension in the power spectra from irregular wave simulations both with and without wind. This is probably due to undamped high-

frequency motions in the finite element representations of the mooring lines. Other results confirmed that the mooring line tensions were interacting with the floating platform as expected: for instance, in the simulations with regular wind and waves the upstream fairlead tension was higher than the downstream fairlead tension, which is what you would expect given that the mooring line tensions are counteracting the thrust from the rotor. The fairlead tensions were also higher overall in 3Dfloat, which had a higher mean thrust. The results from the effective RAO calculations showed that the behaviour of the fairlead tension was similar to that of the surge displacement, which confirms that platform surge is what most influences fairlead tensions.

One of the most significant outcomes of the project is that it has helped to identify deficiencies and areas in need of improvement in the participating codes, which has led to significant improvements in the accuracy of modelling and response prediction. This is extremely beneficial both for the developers of the floating design tools and for the industry in general. More details and full results from the project can be found in [17].

7.3 Case study: testing and validation of GH Bladed v4.0

The GH Bladed code has recently undergone development from a modal representation of structural dynamics to a multibody representation, renamed as Bladed v4.0 [10] and described in Part I Section 1 of this report. One of the benefits of re-structuring the code in this way is to better enable the modelling of floating wind turbine platforms. The floating capabilities of Bladed v4.0 are based on the capabilities which are already present in the code: the same aerodynamic and hydrodynamic models are used, and the same structural dynamics for the deflection of blades and support structure. The main difference lies in the turbine and support structure not being constrained by a direct connection to the ground. The structure is connected to a reference frame by a free joint and constrained by mooring line forces, which enables all six support structure degrees of freedom to be modelled with large rotations and displacements. Mooring line forces are applied using the foundation module which is flexible enough to incorporate non-linear mooring responses.

The testing and validation of the new code structure is important due to the fact that Bladed is used commercially by a large number of wind turbine manufacturers worldwide for design calculations. The testing and validation of the new Bladed v4.0 code is described fully in [98].

Several different types of testing and validation have been carried out. In the first level of testing each individual feature of the multibody code was checked against hand calculations and simulations using the previous version of Bladed. Cases were chosen which were simple enough for the results to be known, either in terms of the output values or the expected dynamic behaviour of the turbine. Results confirmed the new code structure to be performing as expected [98].

In the next level of testing code-to-code comparisons were performed against the general purpose FEM package ANSYS. The first test case was a simple beam modelled by separate beam elements, mainly in order to calibrate the methods. The following results were calculated and compared:

- The frequency of the ten (10) lowest natural vibration modes
- The displacement (translation and rotation) of two of the stations in global coordinates
- The section force and moment (stress resultants) at two of the nodes in element coordinates

This test case showed that the results were identical, which verified the method for defining the input parameters in ANSYS.

The second test case considered a separate blade, assuming the blade is fixed at the root and free at the tip. The lowest mode shapes were calculated and compared with respect to frequency and shape. The results from this test case showed the relative differences between the calculated frequencies of the lowest four modes to be smaller than 0.2%, which indicates a close agreement between the modes calculated by ANSYS and Bladed v4.0. For mode 7 (the torsional mode) the relative difference between the calculated frequencies was 0.5%, which still indicates a close agreement between the calculated modes. The relative differences between the calculated mode shapes were generally small for the most significant displacement components. An important exception is that a very large relative difference appears for the axial displacement (elongation) and the axial rotation (torsion). It is believed that this discrepancy is mainly caused by the fact that the axial displacement is not completely constrained in the ANSYS model.

The third test case considered a complete wind turbine structure consisting of a three blade rotor supported by a tubular steel tower. Again, the lowest mode shapes were calculated and compared with respect to frequency and shape. Full results are given in [98], and indicate an excellent agreement between the modes calculated by ANSYS and Bladed v4.0.

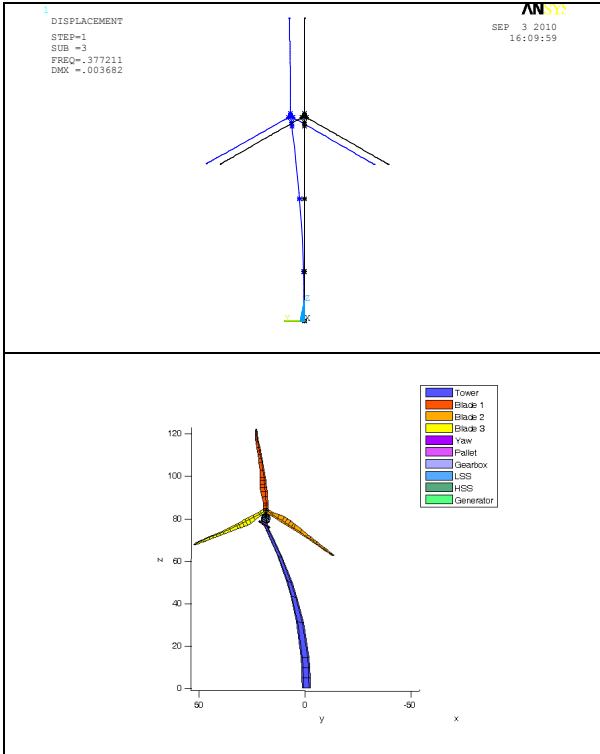


Figure 7.1: Mode shape 2 of the complete wind turbine structure calculated by ANSYS (above) and Bladed v4.0 (below)

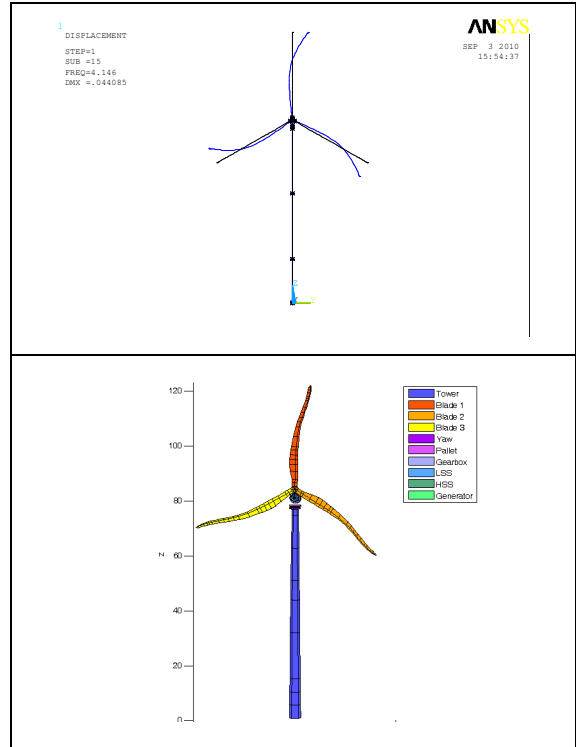


Figure 7.2: Mode shape 14 of the complete wind turbine structure calculated by Ansys (above) and Bladed v4.0 (below).

In the third level of testing a code-to-code comparison was performed using test cases from phase I of the OC3 project [15], modelling a 5MW offshore turbine mounted on a monopile support structure. Figure 7.3 presents the natural frequencies of the complete system calculated by GH Bladed Multibody, together with the average over all the participant codes. The error bars show the standard deviation in frequency between the different codes. Two series are shown for the natural frequencies because the results differ substantially depending on whether the yaw degree of freedom of the support structure has been included in the calculation, especially for the 2nd blade asymmetric flapwise yaw mode. Good agreement is seen for the both cases, with or without the tower torsion mode included. Figure 7.4 presents time histories of the tower base bending moment due to wave loads. Differences in higher frequency may be due to differences in damping of transient structural vibrations. Overall the results for the complete wind turbine show good agreement with other simulation codes, which include modal, multibody and finite element structural models.

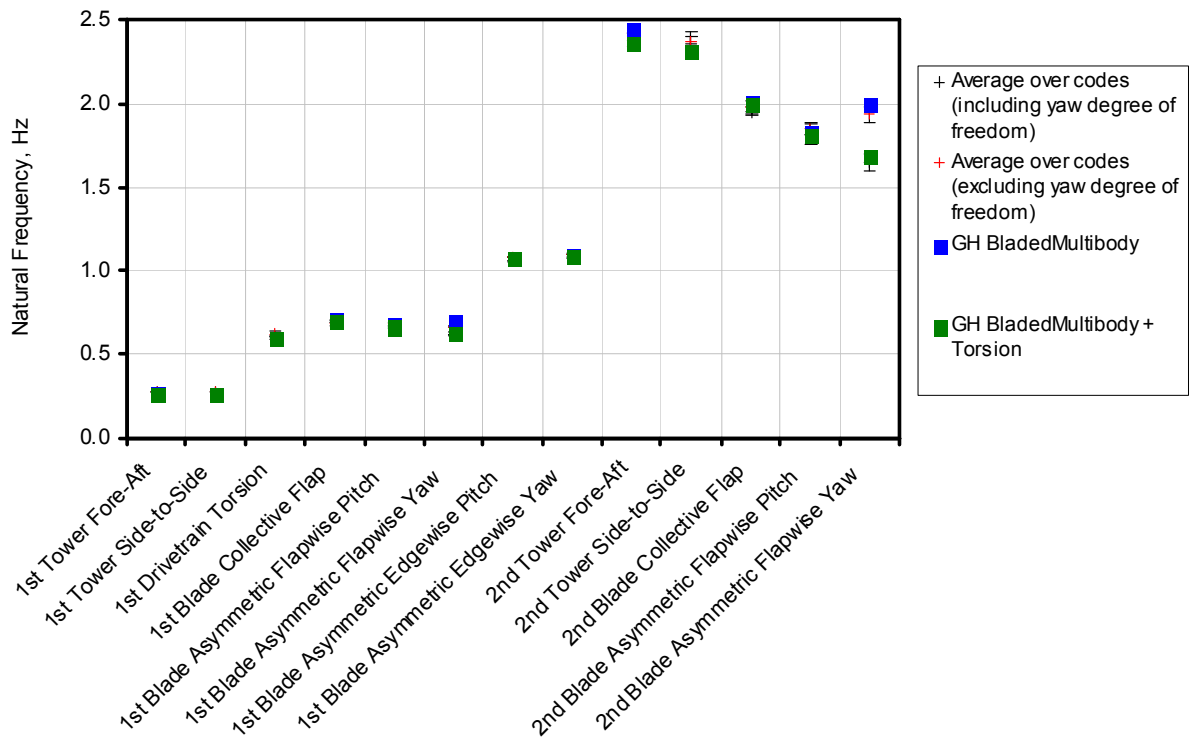


Figure 7.3: Comparison of natural frequencies [98]

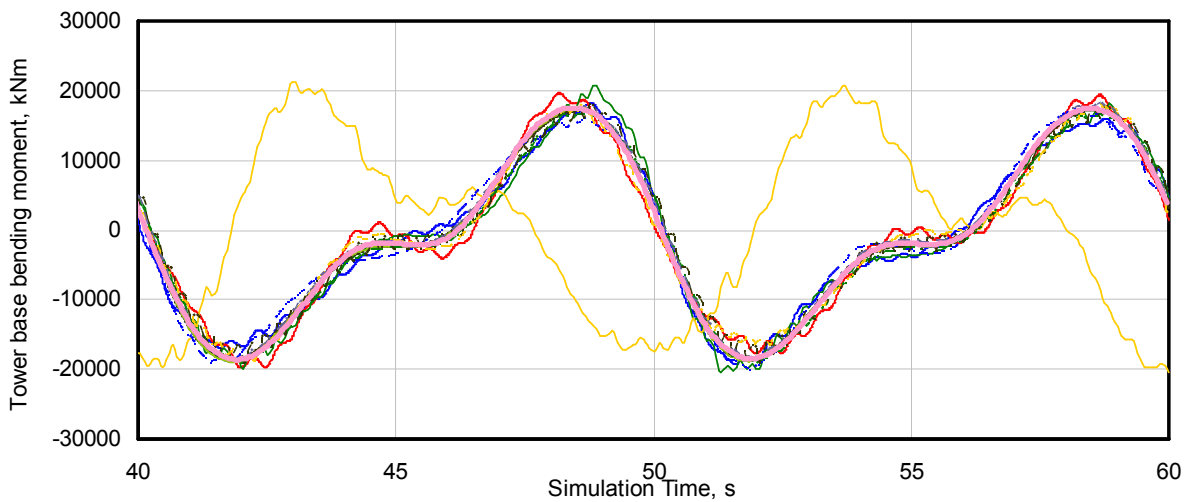


Figure 7.4: Comparison of tower base bending moment, regular waves [98]

In the fourth level of testing a number of complete fatigue and extreme load sets were performed using Bladed v4.0 and compared against equivalent load sets calculated using previous versions of Bladed. The previous GH Bladed code was extensively validated against measured data from a large number of turbines of different sizes and configurations [9], so these internal comparisons are an important check. In total, five complete load-sets were compared, covering a range of different turbine types and configurations:

- Multi-megawatt, offshore, 3-blade, multi-member support structure, upwind, variable speed, pitch regulated
- Multi-megawatt, onshore, 3-blade, monopile tower, upwind, variable speed, pitch regulated

- Multi-megawatt, offshore, 3-blade, monopile tower, downwind, variable speed, pitch regulated
- < 500kW, onshore, 3-blade, monopile tower, upwind, fixed speed, stall regulated
- ~1 Megawatt, onshore, 2-blade, tethered tower, upwind, variable speed, pitch regulated

Figure 7.5 and Figure 7.6 present comparisons of selected loads from one of the above load sets. In general good agreement was found between the previous versions of Bladed and Bladed v4.0. The main difference is in the edgewise fatigue loads, which have reduced a little. This is due to the use of individual blade modes rather than rotor modes, which tends to increase the damping in the edgewise direction due to the additional component of aerodynamic damping. The use of blade modes rather than rotor modes is one of the major advantages of the new structural model as it allows for the correct multidirectional mode shapes as well as the correct modelling of individual blade modes for transient load cases.

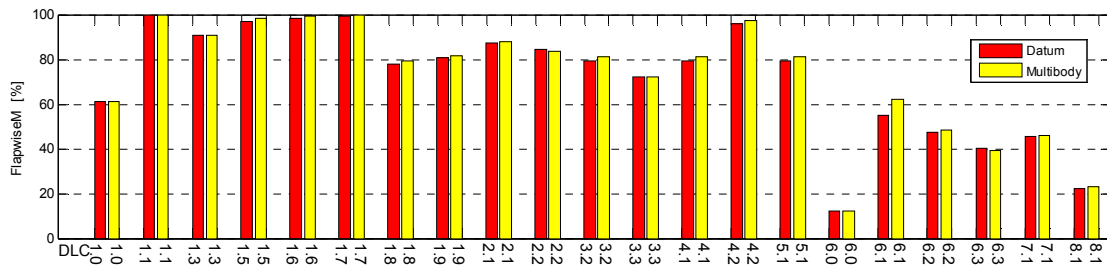


Figure 7.5: Blade root flapwise bending moment: extreme loads [98]

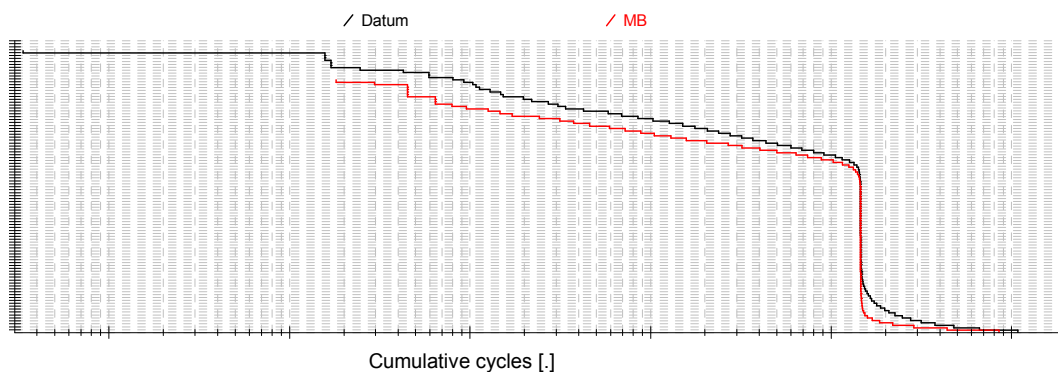


Figure 7.6: Blade root edgewise bending moment: cumulative cycles [98]

The final level of testing involved a code-to-measurement comparison. The CART2 research turbine at NREL in Colorado was used to obtain measurements, primarily for the purpose of testing advanced control features [99]. A Bladed model was set up based on data supplied by NREL, with a number of assumptions where data was not available (e.g. shaft torsional damping, teeter brake friction, pitch actuator model, rotor imbalance). Four measured datasets were used to compare against simulations. Initial simulations were carried out using the above-mentioned assumptions, as a result of which some adjustments were made to the assumptions before the final runs.

The measured and simulated results were compared by means of spectral analysis, and also using rainflow cycle counting to give an indication of fatigue loading. Figure 7.7 presents an example of tower top load spectra for the four datasets. In general a very good level of agreement is demonstrated, with the spectral peaks representing structural resonances corresponding very closely with the predicted frequencies of the coupled system modes. There are some discrepancies, but in most cases this is likely to be due to the uncertainties in modelling the wind field. The fatigue loading is sensitive to the turbulence model used in the simulations, and since the detailed structure and coherence of the actual wind field could not be known it was not possible to produce an exact fit. Differences are also present due to noise on the measured signals, and imbalances in the real turbine.

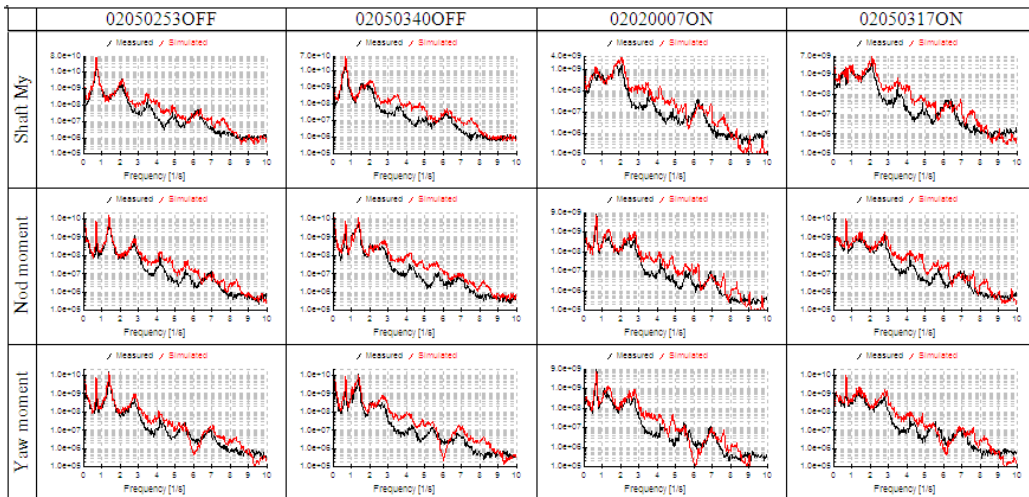


Figure 7.7: Example of Bladed v4.0 validation against measurements: spectra for tower top loads [98]

The floating capabilities of the Bladed code have also undergone testing. Prior to the incorporation of multibody dynamics into Bladed a version of the code, modified to include large rigid body motions and global rotations of the support structure, was used to carry out simulations for Phase IV of the IEA Offshore Code Comparison Collaboration [17]. Good agreement was found between Bladed and the other codes in the calculation of the surge, sway, heave, roll, pitch and yaw natural frequencies of the platform and turbine. The Bladed v4.0 code will also participate in the IEA Task 30 (Offshore Code Comparison Collaboration Continuation) phase 2 which will involve the modelling of a floating offshore wind turbine. The type of floating platform has yet to be finalised.

More recently, Bladed v4.0 was used to model a tension leg floating platform with the purpose of assessing the suitability of these structures for supporting wind turbines in the North Sea [97]. The natural periods and buoyancy of the structure calculated by Bladed were validated against analytical calculations based on the tension leg properties and platform mass and inertia.

8. Advanced modelling approaches

Current modelling techniques applied for fixed-bottom offshore wind turbines, for instance blade element momentum (BEM) method for rotor aerodynamics and Morison's equation for hydrodynamics, are insufficient to accurately describe the large rotor and platform motions and the usage of non-slender support-structures for FOWTs. Advanced modelling methods and techniques are therefore required in order to effectively design and analyse wind turbines on floating offshore platforms.

Regarding aerodynamics, the large low-frequency platform motions experienced by FOWTs, including significant pitch and surge motions, lead to a change in the interaction between the rotor and wake. Dynamic stall and yawed inflow models also have increased importance. Section 3.1 discusses the limitations of BEM and the capabilities of CFD and potential flow (PFM) methods for FOWT simulations.

Regarding hydrodynamics, for modelling of non-slender floating platforms potential theory is required in order to correctly determine the local pressure force and global wave loads due to diffraction and radiation. Section 3.2 presents the results of detailed comparisons between first and second-order hydrodynamic models for simple floating body configurations. The development of non-linear potential flow based methods is outlined, and the importance of vortex induced vibrations for FOWT simulations is discussed.

Regarding mooring line dynamics, different techniques for the representation of mooring lines, including quasi-static, look-up table, FEM and MBS methods, and their impact on global system loads are investigated in Section 3.3.

8.1 Aerodynamic theories

All of the design codes currently capable of performing integrated modelling of floating wind turbines use combined Blade Element Momentum theory to calculate aerodynamic forces on the wind turbine rotor. However the large low-frequency platform motions experienced by floating offshore wind turbines result in flow conditions which are considerably more complex than those experienced by conventional onshore or fixed-bottom offshore wind turbines. Extensive load-case simulations performed by Jonkman and Matha [107] have shown, particularly for catenary moored floating wind turbines, that significant rotational pitch motions occur at approximately the incident-wave frequency. For the investigated OC3 Hywind spar buoy featuring the NREL 5MW baseline turbine, pitch motions of up to 8° for production design load cases (DLCs) and 14° for extreme DLCs have been found. In addition to significant pitch motions, large lower frequency translational surge motions are also predicted. These rotational and translational motions cause the rotor to operate often in non-axial flow conditions and lead to a change in the interaction between the rotor and wake, with the rotor in some cases traversing back over its own wake. The transitions between windmill and propeller states where the rotor interacts with its own wake cannot be accurately modelled using traditional BEM theory with common corrections, as Sebastian and Lackner [100] have shown in a preliminary study. BEM cannot model the resulting development of a turbulent region behind the rotor leading to a toroidal recirculation normal to the rotor blade, most significantly expected at the blade tips, where the effect on loads is most significant. Sebastian and Lackner identify this transitional aerodynamic phenomenon as vortex ring state (VRS), and conclude that momentum equations used in typical BEM analysis methods break down and yield unrealistic results for the axial and the rotational motion of the rotor.

Since wind turbine airfoils in production up to rated power usually operate close to their maximum lift coefficient to generate maximum power, the described pitch motions also cause the airfoil to more often operate in stalled condition, increasing the importance of dynamic stall models. Common dynamic stall models such as Beddoes-Leishman are semi-empirical and their applicability for the dynamic stall effects occurring on floating wind turbines has yet to be investigated.

For floating support platform designs with relatively little yaw stiffness, yawed inflow conditions also occur more often. Yawed inflow is also likely to occur frequently for proposed downwind floating concepts without tower-top mounted yaw drive (such as Sway's concept). BEM theory originally assumes flow perpendicular to the rotor plane and the common skewed wake correction models introduced have been shown to give unreliable load predictions, with deviations increasing with higher yaw errors. The proposed downwind FOWT configurations, combined with the increased WT motions, also increase the importance of tower dam and shadow models as well as improved models for aerodynamic blade and tower interaction.

While beyond the scope of this section, the aero-elastic representation of the rotor blade is also important when investigating the aforementioned effects and has significant influence on the resulting loads and deflections

CFD

To model these aerodynamic effects, several possibilities exist. The computationally most demanding, but physically most accurate approach is to solve the Navier-Stokes Equations (NSE) with a CFD solver. In CFD, to model turbulent flows with their large range of length scales, three basic approaches exist. Direct Numerical Simulation (DNS), where the full Navier Stokes Equations are solved, needs all relevant length scales to be resolved by the computational grid, resulting in extremely large grids. With current available computational power, DNS is therefore not applicable to structures such as wind turbines with large Reynolds numbers. Large Eddy Simulation (LES), where larger turbulent structures are resolved, is well applicable for the turbine wake. To resolve the smaller turbulent structures in the boundary layer of the blades with LES is also currently very difficult to apply due to the very large number of necessary grid cells. The least computationally expensive method to model turbulent flows in CFD is the Unsteady Reynolds Averaged Navier Stokes (URANS) method. URANS uses a time-average formulation of the NSE. The occurring nonlinear Reynolds stress term requires the introduction of turbulence models (for example 2-equation models like $k-\omega$) to close the RANS equations. These turbulence models have large effects on the CFD solution and need to be selected carefully. A combination of URANS and LES, using URANS for the flow around the blades, and LES for the wake, is also possible and could provide a good solution for floating wind turbine modelling.

Regardless of the specific CFD method used, due to its very long resulting simulation times, CFD can only be applied to very specific load situations. The primary application of CFD is to investigate and analyse the aerodynamic flow phenomena occurring in the situations mentioned above and help quantify their influence on loads. With this knowledge it can be decided whether current models are still sufficient and, more importantly, how large their errors are and in what load situations these errors become most significant. Based on that knowledge, simpler aerodynamic codes suitable for integrated design codes, e.g. correction models for BEM, might be introduced, correction factors derived, or new additions to the IEC standard, including novel load case definitions unique for floating turbines, can be defined. CFD is already used in wind turbine blade design and can be applied to develop floating offshore specific blades as well.

The studies by Jonkman and Matha [107] also show that for extreme DLCs with occurrence of failures (e.g. in DLC6.2 where the rotor is idling, all blades are pitched to feather and large yaw errors occur) severe instabilities, only occurring for floating WT, can be identified. The particular DLC6.2 instability is caused by negatively damped modes due to the blade aerodynamics, which are for idling or stand-still conditions, calculated with no induction factor (airfoil data look-up table). That means the aerodynamic lift and drag forces on the blade segments are computed without taking into account the influence of the blade on the flow. To investigate this effect, as well as other observed instabilities for floating turbines more closely, CFD could also provide valuable insight.

Potential Flow Methods

For integrated load simulations, aerodynamic codes based on vortex theory are more suitable in terms of simulation time. The flow field around the airfoil is generally described through the distribution of discrete sources and vortices, with several possible implementations, e.g. lifting line, lifting surface or vortex lattice methods. In these time-accurate aerodynamic codes, the shape and strength of the wake of the blades will develop in time (e.g. free wake particle method). To reduce simulation time, the shape of the wake can also be prescribed. This approach, like BEM, is also based on measured profile data, i.e. the aerodynamic lift-, drag-, and pitching-moment characteristics of the blade cross-sections are assumed to be known and corrected for the effects of blade rotation. In comparison to the currently used BEM-based codes, more accurate predictions are expected in situations where local aerodynamic characteristics strongly vary with time and where dynamic wake effects play a significant role, effects which are increasingly important for floating wind turbines.

Related Studies

Aerodynamic and load analyses by Matha et. al. at University Stuttgart with ECN's non-linear lifting line free vortex wake code AWSM and a URANS (&LES) CFD code (FLOWer, developed by the German Aeronautical and Aerospace Centre DLR, capable of URANS/LES CFD simulation) and by Sebastian, Lackner et al. at UMASS with an in-house free-wake code are currently performed to address the above mentioned aerodynamic problems regarding floating wind turbines. First results of the former study are presented below.

Rotor-only CFD Study

To investigate the aerodynamic effects occurring on a rotor of a FOWT, a CFD model of a generic multi-megawatt rotor has been setup in the RANS code FLOWer. The spinning direction of this particular rotor is counter-clockwise. Figure 8.1 presents the used mesh and prescribed motion of the rotor. The prescribed motion was selected from the IEC load simulations of the OC3 Hywind FOWT conducted by Matha and Jonkman [75] in the design code FAST with HydroDyn. To select a representative extreme platform pitch motion occurring in WT production mode, DLC 1.6 was chosen. The selected specific DLC 1.6 simulation run featured 12.0 m/s hub-height wind speed (close to rated, i.e. maximum rotor thrust) and, using the extreme sea state (ESS) model, a significant wave height of 15.0 m and a peak spectral period of 19.2 s. From the platform pitch time-series, one pitch motion was selected, where the rotor is first pitching -11.5° in downwind direction and then $+4^\circ$ in upwind direction before reaching 0° again. This motion has been approximated by two appended sine functions, as presented in Figure 8.1. Following the work of Streiner [108], a sufficient timestep size corresponding to an azimuth movement of $\Delta\Psi = 5^\circ$ per timestep was chosen. Before starting the CFD calculation of the prescribed floating motion, 4 rotor rotations have been pre-calculated to ensure, that the wake behind the rotor is fully developed in the background grid when the motion starts. Due to good experiences in former studies [108], the k- ω SST turbulence model is used.

The computational grid used consists of the components blade, hub and background grid, leading to total number of about 10 million grid points. Refined grids around each blade (Figure 8.1, green grid) with a dimensionless grid distance y^+ -value between 0.1 and 2 are embedded in a cylindrical grid around the hub (Figure 8.1, red grid), which is rotating within a coarser background grid (Figure 8.1, blue grid). Overall, the grid has the in-plane dimension of 3 rotor diameters in each direction, centred at the hub, and an out of plane dimension of 3.5 diameters upwind and downwind respectively. FLOWer features the Chimera technique [109], allowing for arbitrary relative motion of aerodynamic bodies. Applying the Chimera technique, the previously described pitch motion was prescribed as a rigid body motion on the rotor and hub grids, which are moving within the background meshes. Chimera is also applied for modelling the rotor rotation. In this study, no elastic deformation of the blade is introduced, but fluid-structure coupled simulations are planned for next analyses. Further studies will also include the tower and nacelle, as already performed by Meister et. al. with FLOWer for a 5MW onshore turbine without prescribed floating motions [110].

The presented CFD results showed good numerical convergence, therefore it is assumed that the presented flowfield is realistically representing the actual aerodynamic conditions during such a motion. Nevertheless the presented results are only a preliminary study and need further validation from CFD and potential flow calculations, as well as, ultimately, experimental data.

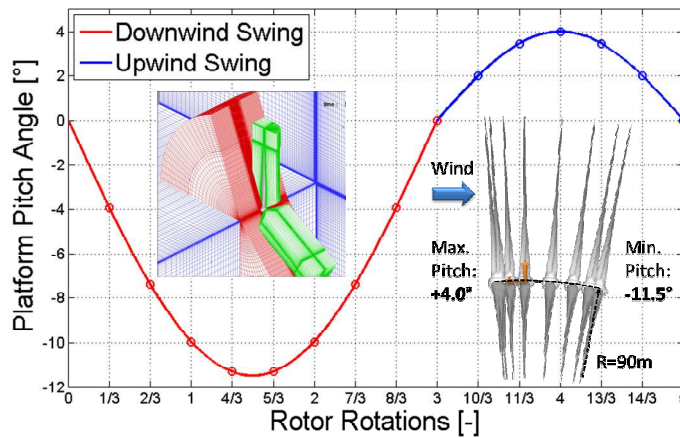


Figure 8.1: Prescribed rotor motion for CFD study and CFD mesh

The pressure distribution over the blades is presented in Figure 8.2. Motion (1) corresponds to the first half of the downwind swing (c.f. Figure 8.1), i.e. 4/3 rotor rotations, motion (2) corresponds to the 2nd half of the downwind swing and the first half of the upwind swing, i.e. from 5/3 to 4 rotor rotations, and motion (3) finally represents the last half of the upwind swing, i.e. 13/3 to 5 rotor rotations. During motion (1), the pressure is decreasing due to the backward motion and the increased turbulence in the wake. When the turbine is pitching upwind again (2), the pressure on the blades is increasing until the rotor is back in vertical position and then slightly decreasing until the end of move (2). The pressure increase is due to the increased inflow velocity, and possibly also due to rotor wake interactions. In the last part of the period (3), the pressure again is decreasing, but to a lesser extent than in the first downwind motion (1).

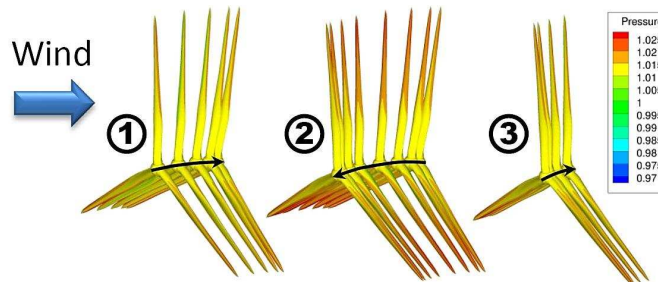


Figure 8.2: Pressure contours of rotor during prescribed motion

While no dedicated scientific research on FOWT-specific blade design has been published yet, the work package “Offshore Blades” of the European KIC (Knowledge & Innovation Community) InnoEnergy research project Offwindtech, led by University of Stuttgart and started beginning of 2011, will address this issue.

8.2 Hydrodynamic theories

In order to take proper account of the influence of a floating body on the surrounding fluid, potential flow theory must be used. This is particularly important for floating wind turbine support structure designs which have large diameters and experience significant motion. In potential flow theory the fluid is considered to be incompressible, inviscid and surface tension effects are neglected. The flow is irrotational and so the velocity of the fluid (\vec{v}) at a certain point $\vec{r} = (x_1, x_2, x_3)$ in a Cartesian coordinate system fixed in space and instant (t) is given by:

$$\vec{v}(\vec{r}, t) = \vec{\nabla}\phi \quad [8-1]$$

The total velocity potential (ϕ) satisfies the Laplace equation in all fluid domain:

$$\nabla^2\phi = 0 \quad [8-2]$$

and also at the boundary conditions at the air and solid interfaces that define the problem. The complete formulation of these boundary conditions is in general difficult to solve, and first or second-order approximations are typically used to define the respective hydrodynamic formulation. These are also referred to in the literature as the linear and weakly nonlinear formulations.

Linear potential flow theory is used in many different offshore engineering problems. This theory considers, in addition to the potential flow assumptions described above, that the amplitudes of both the incident waves and the motions of the floating structure are small when compared with the incident wavelength. Second-order, weakly nonlinear hydrodynamic theory assumes (as in the first-order case), small amplitudes for the incident waves and motions in comparison with the wavelength and characteristic body dimensions. However, this theory takes into account a more detailed representation of the velocity potential (ϕ) and all derived variables by considering a second-order approximation through a Taylor expansion series about the mean positions. A full description of the second-order approximation can be found in [111].

The second order approximation more properly accounts for hydrodynamic loading on the wetted surface of the body for platforms which are subject to steep-sided or very large waves. Second order hydrodynamic loads are proportional to the square of the wave amplitude, and have frequencies equal to both the sum and the difference of the multiple incident wave frequencies. This means that although the natural frequencies of the structure are designed to be outside the wave energy spectrum, the second order forces will excite these frequencies, so despite the forces being small in magnitude the resonant effect can be important. Three examples of second order hydrodynamic forces are given below.

- *Mean drift forces.* These forces result in a mean offset of the body relative to its undisplaced position, and are typically an order of magnitude lower than first order wave excitation forces. The mean drift force is a combination of second order hydrodynamic pressure due to first order waves and the interaction between first order motion and the first order wave field. The viscous drag contribution to this force is significantly increased when there is a current present. Since the mooring line tension is often related non-linearly to platform displacement, the mean drift forces can have an important effect.
- *Slowly varying drift forces.* These forces have much longer periods than the main wave energy spectrum but are still within the range of horizontal platform motion. They result from non-linear interactions between multiple waves with different frequencies. Again the forces resulting from slowly varying drift are generally small compared to forces at the wave frequency, but they can cause large displacements in moored floating wind turbines which can in turn lead to high loads in the mooring lines. In addition these forces can excite the large amplitude resonant translational motion of the floating platform.
- *High frequency forces.* These forces have a frequency which is higher than the wave frequency and are also generally small in amplitude. They arise from the same source as low frequency drift forces, i.e. interactions between multiple waves of varying frequency. The contribution from these forces can be particularly important when analysing ‘ringing’ behaviour for floating wind turbine configurations such as

as TLP concepts, which typically have high natural frequencies in heave, roll and pitch.

8.2.1 Comparison of first and second-order hydrodynamics

A detailed comparison has been performed between the solution of first (linear) and second-order potential flow hydrodynamic models with regard to the characterisation of the wave induced loading and motion response of typical floating offshore wind energy converters, under both regular and irregular waves [111].

Two floating offshore wind structures are considered. The first case study is a spar-buoy originally developed by StatoilHydro and later modified to accommodate a NREL-5MW offshore wind turbine. This concept is called “OC3-Hywind” and is described in detail in [112]. Figure 8.3(a) shows schematically this concept and Table 8.1 lists the main properties for this structure. The second case study is a semi-submersible platform with geometric dimensions similar to the WindFloat platform concept [83]. This structure is shown in Figure 8.3(b) and comprises three equidistant columns and a wind turbine centred in one of the columns. The stabilisation of the position of this structure is achieved through an active water ballast system which transfers water between columns to compensate for changes in the mean wind loading of the turbine. The hexagonal water-entrapment plates at the bottom of each column are designed to provide high heave added-mass and viscous damping to decrease the motions in this mode. Table 8.2 gives an overview of the main properties associated with this structure. The geometry for this structure is based on the dimensions reported in [83] and the mass is uniformly distributed.

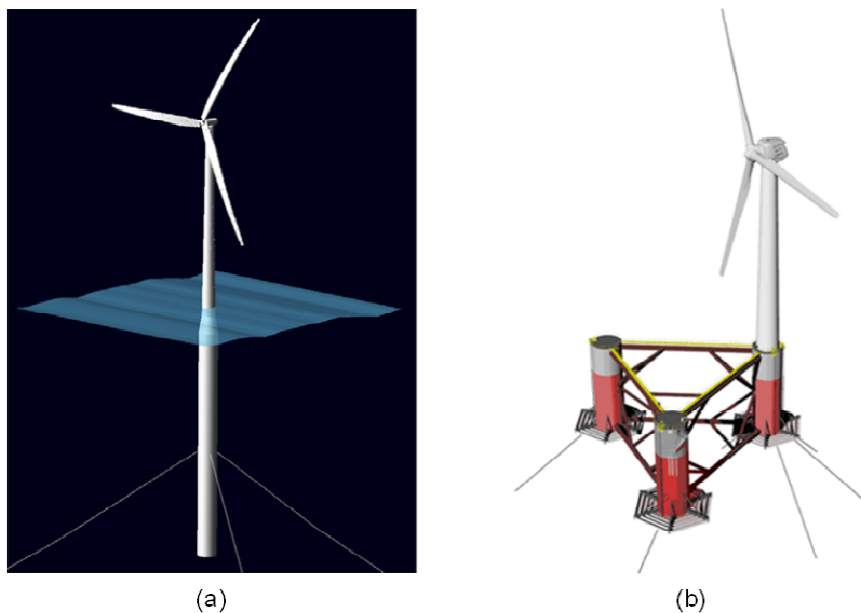


Figure 8.3: Offshore wind floating structures: (a) OC3-Hywind (b) WindFloat

Table 8.1: Main properties for the OC3-Hywind platform [112].

OC3-Hywind Platform			
Total draft (below SWL) [m]	120	Centre of mass below SWL [m]	89.9155
Tower base above SWL [m]	10	Mass including ballast [kg]	7 466 330
Platform diameter above taper [m]	6.5	Inertia (I11 = I22)	4 229 230 000
Platform diameter below taper [m]	9.4	Inertia (I33) [kg m ²]	164 230 000
Depth top to bottom taper below SWL [m]	4 - 12	Water depth (z0) [m]	320
Water density [kg m ³]	1025		

Table 8.2: Main properties for the semi-submersible platform (Geometry from [83] with mass uniformly distributed).

WindFloat Platform			
Total draft (below SWL) [m]	22.9	Total mass [kg]	6 523 059
Diameter of each column [m]	10.7	Centre of mass below SWL	11.70
Diameter of hexagonal plates [m]	27.4	$I_{11}=I_{22}$	4525602948.75
Volume bellow SWL [m3]	6363.96	I_{33}	6742642572.74
Water depth (z0) [m]	320		

The hydrodynamic quantities compared in this exercise are:

- The first and second-order excitation force.
- The first and second-order Response Amplitude Operator (RAO) for unconstrained motions.

The comparisons between linear and second-order quantities are performed for three distinct monochromatic waves and three unidirectional Pierson-Moskowitz spectra with parameters listed in Table 8.3. Both first and second-order hydrodynamic quantities were computed with the commercial software WAMIT (v6.1s).

Table 8.3: List of monochromatic incident waves and Pierson-Moskowitz spectra used for the comparisons between linear and second-order hydrodynamic quantities.

Monochromatic waves		
1	H = 1.0 m	T = 5.0 s
2	H = 2.0 m	T = 7.0 s
3	H = 4.0 m	T = 9.0 s
Pierson Moskowitz spectra		
1	Hs = 0.5 m	(Tp = 3.54 s)
2	Hs = 2.5 m	(Tp = 7.9057 s)
3	Hs = 5 m	(Tp = 11.1803 s)

Convergence tests

Prior to the evaluation of any hydrodynamic quantity it is necessary to assess the degree of accuracy of the numerical solution with regard to a certain discretisation of the geometry. Finer discretisations should represent more accurately the geometry and therefore evaluate more accurately the velocity potential. However the computational effort increases with finer discretisations and so this exercise is required to understand and find the right balance between the required accuracy and computational effort.

The methodology presented in this paragraph follows closely the methods presented by Cruz in [113] which applied standard convergence procedures based on Richard extrapolation method to the computations performed with WAMIT higher order method [114]. The exact value of a certain quantity (ϕ_0) is estimated by evaluating its value at three different discretisations of the geometry (ϕ_i). The error associated with the finer discretisations is given by:

$$E_1 = \phi_1 - \phi_0 = \frac{\phi_2 - \phi_1}{\left(\frac{h_2}{h_1}\right)^p - 1} \quad [8-3]$$

where (ϕ_i) are the values of the quantity being evaluated and h_i is the grid cell size associated with the discretisation i . The subscript 1 refers to a finer discretisation than 2 and 3 to a coarser discretisation than 2.

The order of convergence (p) is a quantity which depends on the implementation of the code itself and in general is not known. The value for this quantity is straightforward to compute for a constant refinement ratio, i.e. $h_3/h_2 = h_2/h_1 = r = \text{const}$. Assuming also that the asymptotic range has been reached, p is given by:

$$p = \frac{\ln\left(\frac{\phi_3 - \phi_2}{\phi_2 - \phi_1}\right)}{\ln(h_2/h_1)} \quad [8-4]$$

The results of the convergence in the present study are evaluated through the error norm defined by:

$$L_\infty = |\max(\phi_i - \phi_0)| \quad [8-5]$$

The grid converge ratio (R) is a useful quantity to identify the behaviour of the convergence. This quantity defined by:

$$R = \frac{\phi_2 - \phi_1}{\phi_3 - \phi_2} \quad [8-6]$$

And the solution is classified in terms of the value of R as:

- Oscillatory divergence, if $R < -1$
- Oscillatory convergence, if $-1 < R < 0$
- Monotonic convergence, if $0 < R < 1$
- Monotonic divergence, if $R > 1$.

The uncertainty (U_k) associated with the computations finer discretisation (ϕ_1) is given by:

$$U = (F_s - 1)|E_1| \quad [8-7]$$

where F_s is a safety factor which may vary between 1 and 3. The present study considers a very conservative approach and takes $F_s = 3$.

Convergence studies for the OC3-Hywind platform

The geometry of OC3-Hywind spar buoy was discretised for three grid sizes shown in Figure 8.4. Following Cruz in [113], the grid cell size (h_i) is related to the WAMIT higher order panel size parameter associated to an automatic discretisation of the geometry. Panel sizes equal to 10 m, 5.0 m and 2.5m were considered and the hydrodynamic quantities were evaluated for five wave periods selected randomly between 3 s to 16 s.

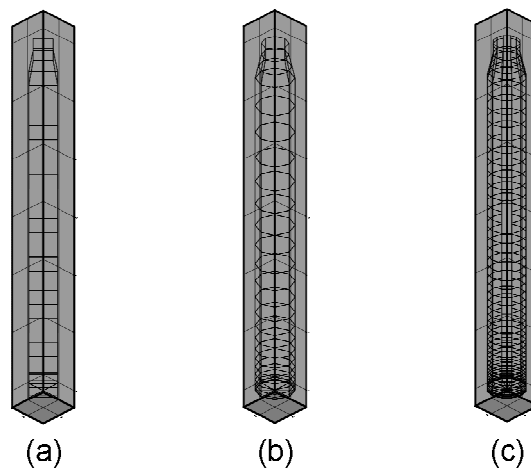


Figure 8.4: Three discretisations of the geometry of the OC3-Hywind used for the convergence tests. The panel size parameter equal to (a) 10.0 m, (b) 5.0 m and (c) 2.5m.

The convergence ratio (R) (Equation 3-6) associated with the discretisation triplet used in this study computed for the linear excitation forces is shown in Table 8.4. The values of (R) depend on the hydrodynamic quantity being evaluated and on the frequency. Most of the values are between -1 and 1 and the solution for the majority of evaluated cases can be classified as convergent.

Table 8.4: Convergence ratio (R) associated with the absolute value of the linear excitation force for a discretisation triplet with panel sizes equal to 10.0 m, 5.0 m and 2.5 m for the OC3-Hywind geometry.

T (s)	$ F_{X1} $	$ F_{X2} $	$ F_{X3} $	$ F_{X4} $	$ F_{X5} $	$ F_{X6} $
3.9	-1.86	0.25	0.48	0.25	-2.10	-0.12
7.1	0.07	0.03	0.33	-0.09	-0.05	0.09
7.9	0.1	0.13	0.33	0.06	-0.02	0.11
8.5	0.18	0.20	0.33	0.11	0.03	0.12
14.4	0.41	0.37	0.22	0.31	0.28	0.23

An estimation of the exact solution for the linear excitation force associated with the incident wave periods considered in this study is presented in Table 8.5. The uncertainty associated with the finer mesh (panel size equal to 2.5m) for the linear excitation forces is presented in Table 8.6. The evolution of the convergence for four different discretisations is presented in terms of the error norm L_∞ defined by Equation 3.5 for the linear excitation forces in Figure 8.5. WAMIT does not provide the solution on each panel, and it also does not output the total number of panels. Throughout the study the number of equations (N) in the linear system (which corresponds to the number of unknowns) is used as a measure of the total number of panels. The relationship between N and the panel size is presented in Table 8.7. Overall the uncertainty estimates are relatively small when compared to the absolute value of the excitation force for all tested wave frequencies.

A panel size equal to 2.5m was chosen for the computations of the hydrodynamic quantities associated with the OC3-Hywind.

Table 8.5: Estimations of the exact value associated with the linear excitation force for the incident wave periods considered in this study.

T (s)	$ F_{X1} $	$ F_{X2} $	$ F_{X3} $	$ F_{X4} $	$ F_{X5} $	$ F_{X6} $
3.9	5.80E+1	1.40E-6	3.60E+0	1.20E-4	4.90E+3	1.50E-13
7.1	1.10E+2	2.60E-6	1.80E+1	1.90E-4	7.90E+3	7.10E-14
7.9	1.10E+2	2.70E-6	2.10E+1	1.90E-4	7.90E+3	6.10E-14
8.5	1.10E+2	2.80E-6	2.30E+1	1.90E-4	7.90E+3	5.30E-14
14.4	1.10E+2	2.80E-6	2.50E+1	1.30E-4	5.50E+3	1.40E-14

Table 8.6: Uncertainty associated with the computations for the finer mesh (panel size 2.5) for the linear excitation force at the incident wave periods considered in this study.

T (s)	$ F_{X1} $	$ F_{X2} $	$ F_{X3} $	$ F_{X4} $	$ F_{X5} $	$ F_{X6} $
3.9	1.50E-2	3.30E-10	5.70E-3	1.50E-8	1.32E+0	2.49E-14
7.1	2.10E-4	9.30E-13	3.30E-3	1.89E-10	6.60E-3	1.08E-14
7.9	4.50E-4	7.80E-12	2.91E-3	1.20E-10	7.50E-4	1.29E-14
8.5	1.41E-3	2.55E-11	2.64E-3	6.00E-10	2.01E-3	1.44E-14
14.4	8.10E-3	1.59E-10	4.20E-4	5.40E-9	1.68E-1	2.25E-14

Table 8.7: Relation between panel size parameter and the number of unknowns in the equations in WAMIT for the OC3-Hywind discretisations of the geometry.

Panel Size (m)	2.5	5.0	7.5	10
Number of Unknowns	300	136	81	66

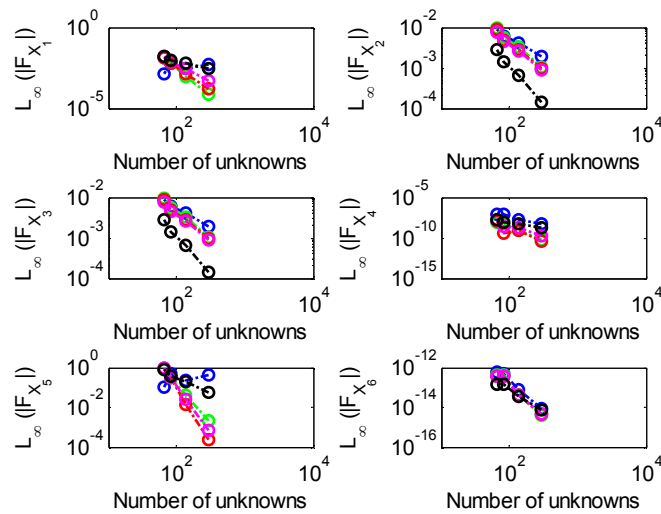


Figure 8.5: Evolution of the convergence in terms of the error norm L_∞ for the linear excitation force associated with the OC3-Hywind.

Convergence studies for the semi-submersible platform

To simplify the model used to compute the hydrodynamic loads of the semi-submersible platform it was assumed that the major contributions of the hydrodynamic interaction are due only to the three cylindrical columns and horizontal damping plates. The influence of the submerged braces which interconnect the three columns was considered negligible with regard to the hydrodynamic loads (see Figure 8.3 b).

The geometry of this structure was discretised for three grid sizes with the panel size parameter equal to 10.0 m, 5.0 m and 2.5 m. The hydrodynamic quantities were computed for five wave periods selected randomly between 5 s to 16 s. The three discretisations considered for the convergence analysis are shown in Figure 8.6.

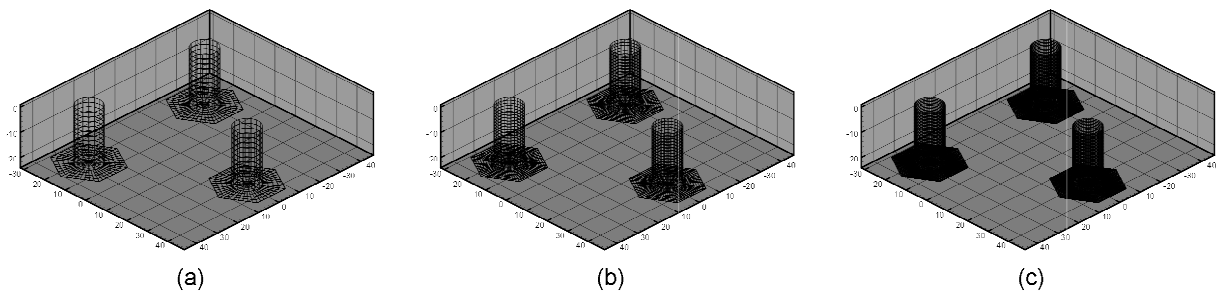


Figure 8.6: Three discretisations of the geometry of the semi-submersible platform used in the convergence tests. The panel size parameter equal to (a) 10.0 m (b) 5.0 m and (c) 2.5m.

The convergence ratio (R) associated with the excitation forces obtained for the discretisation triplet used in this study is shown in Table 8.8. As with the previous geometry, most of the values are between -1 and 1 and the solution for these quantities can be classified as convergent. The estimation of the exact solution for the linear excitation force at the incident wave periods considered in this study is presented in Table 8.9 and the uncertainty associated with the finer mesh is presented in Table 8.10. The evolution of the convergence for four different discretisations presented in terms of the error norm L_∞ for the linear excitation forces is presented in Figure 8.7. Once again the uncertainty estimates are several orders of magnitude smaller than the excitation force values, which is reassuring of the quality of the numerical solutions. The relation between the panel size parameter and the number of equations (N) in the linear system to be solved by WAMIT which is used as a measure of the total number of panels is shown in Table 8.11.

A panel size equal to 5.0 m was chosen for the computations of the hydrodynamic quantities associated with the semi-submersible structure.

Table 8.8: Convergence ratio (R) associated with the absolute value of the linear excitation force for a discretisation triplet with panel sizes equal to 10.0 m, 5.0 m and 2.5 m for the semi-submersible platform geometry.

T (s)	$ F_{X1} $	$ F_{X2} $	$ F_{X3} $	$ F_{X4} $	$ F_{X5} $	$ F_{X6} $
7.4	0.294	1.092	0.792	0.611	0.612	-0.675
8.4	-0.031	-0.532	0.601	0.613	0.616	-1.042
9.5	-0.212	-1.190	0.601	0.579	0.613	-1.864
10.3	-0.314	0.121	0.611	0.626	0.610	-1.512
11.7	-0.338	0.303	0.600	0.667	0.606	0.073

Table 8.9: Estimations of the exact value of the linear excitation force at five wave periods associated with the semi-submersible platform.

T (s)	$ F_{X1} $	$ F_{X2} $	$ F_{X3} $	$ F_{X4} $	$ F_{X5} $	$ F_{X6} $
7.4	1.80E+002	4.50E+001	1.80E+001	1.40E+003	5.90E+002	1.10E+004
8.4	1.70E+002	4.30E+001	1.80E+001	1.60E+003	1.10E+003	1.10E+004
9.5	1.60E+001	2.30E+001	5.40E+000	1.40E+003	1.50E+003	7.90E+003
10.3	1.30E+002	1.20E+001	2.60E+001	1.10E+003	1.60E+003	4.80E+003
11.7	1.90E+002	6.00E+000	4.90E+001	6.50E+002	1.40E+003	2.70E+003

Table 8.10: Uncertainty of the linear excitation force computations with the finer mesh (panel size 2.5 m) at five wave periods for the WindFloat platform.

T (s)	$ F_{X1} $	$ F_{X2} $	$ F_{X3} $	$ F_{X4} $	$ F_{X5} $	$ F_{X6} $
7.4	6.00E-3	1.77E-3	2.19E+0	2.46E+2	2.07E+1	9.30E-1
8.4	8.10E-1	4.80E-3	2.16E+0	1.98E+2	3.60E+1	2.55E+0
9.5	4.20E-2	1.14E+0	1.62E+0	1.68E+2	1.71E+2	3.30E+0
10.3	7.20E-4	1.89E-2	3.30E+0	1.44E+2	2.52E+2	2.49E+0
11.7	2.64E-2	1.17E-2	7.20E+0	9.00E+1	2.70E+2	1.59E+0

Table 8.11: Relation between the panel size parameter and the number of unknowns which is used as measure of the number of panels in WAMIT for the semi-submersible platform.

Panel Size (m)	2.5	5.0	7.5	10
Number of Unknowns	2976	1287	981	792

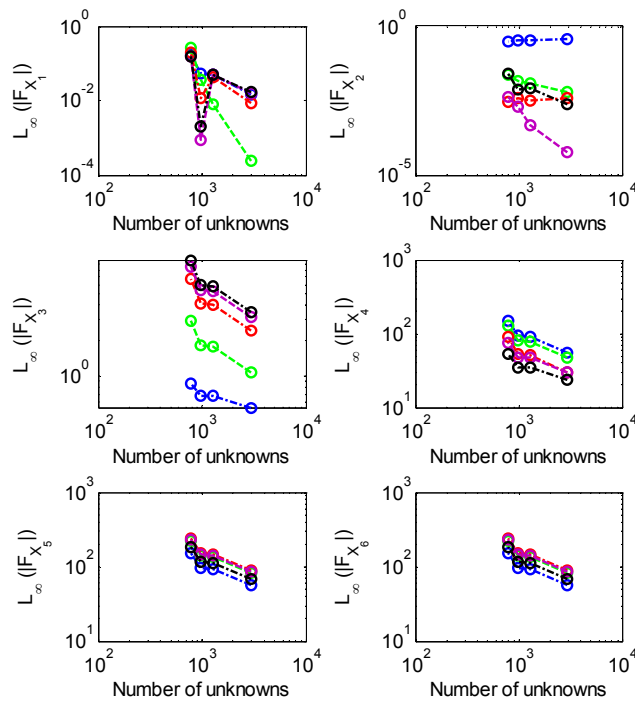


Figure 8.7: Evolution of the convergence in terms of the error norm L_∞ for the linear excitation force associated with the semi-submersible platform.

OC3-Hywind results

Linear hydrodynamic loads and unrestrained motions

This section presents the linear hydrodynamic loads computed for the spar buoy OC3-Hywind concept. The frequency dependence of the excitation forces and moments are shown in Figure 8.8 for incident waves with a head angle of zero degrees and periods up to 25s. The forces and moments are computed at the centre of mass of the structure and are given as non-dimensional quantities. The dimensional value of the excitation forces is obtained by multiplying the non-dimensional value of the force or moment by the density of the water (ρ), the gravitational constant (g) and the wave amplitude (a):

$$\widetilde{F}_X = \rho g a F_X \quad [8-8]$$

In what follows the modes of motion surge, sway, heave, roll, pitch and yaw are referred to by the subscript numbers 1,2,3,4,5,6 respectively.

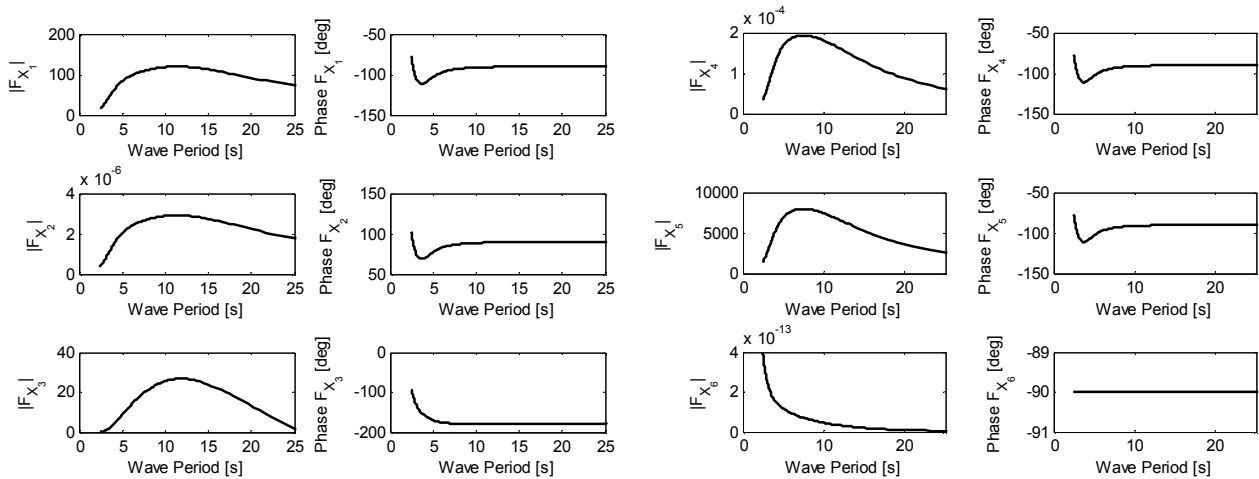


Figure 8.8: Excitation forces and moments in surge (1), sway (2), heave (3), roll (4), pitch (5) and yaw (6) for the OC3-Hywind for incident wave periods up to 25 s (head-on waves).

For a structure with axial symmetry and incident waves at a head angle of zero degrees the only excitation forces of importance are in the surge, heave and pitch modes. This is confirmed in Figure 8.8 as the sway, roll and yaw components are negligible. The frequency dependence of the added-mass and damping coefficients required to compute the radiation force is shown Figure 8.9. The symmetry of the added-mass matrix implies that all crossed terms are equal ($A_{kl} = A_{lk}$ for $k, l = 1, \dots, 6$) and the axi-symmetry of the structure implies that the terms in surge and sway are equal ($A_{11} = A_{22}$), as are the roll and pitch terms ($A_{44} = A_{55}$). The crossed terms are all null apart from $A_{15} = -A_{24}$. Note that the same relations apply to the hydrodynamic damping components. The hydrodynamic coefficients are given as non-dimensional quantities. To convert to dimensional quantities, both coefficients should be multiplied by the value of density of the fluid (ρ) and the hydrodynamic damping should be also multiplied by the angular frequency of the incident wave (ω):

$$\widetilde{A}_{kl} = \rho A_{kl}, \text{ and } \widetilde{B}_{kl} = \omega \rho B_{kl} \quad [8-9]$$

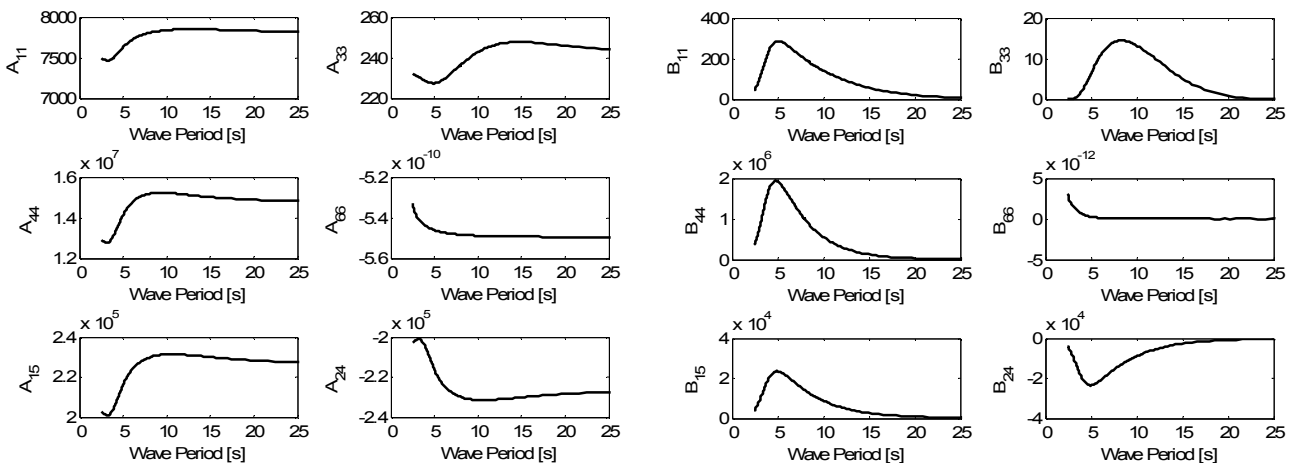


Figure 8.9: Added-mass and hydrodynamic damping coefficients for the OC3-Hywind for incident wave periods up to 25 s (head-on waves).

The linear hydrostatic force is proportional to the displacements of the structure. The non-dimensional hydrostatic coefficients computed for the OC3-Hywind are shown in

Table 8.12. These coefficients do not depend on the frequency of the incident wave and are computed relatively to the centre of mass of the structure. The axi-symmetry of the structure implies that the hydrostatic coefficient in roll (C_{44}) is the same as in pitch (C_{55}). The dimensional values of these coefficients can be obtained by multiplying the non-dimensional values by the density of water (ρ) and the gravitational constant (g):

$$\tilde{C}_{kl} = \rho g C_{kl} \quad [8-10]$$

Table 8.12: Non-dimensional hydrostatic coefficients associated with the OC3-Hywind.

Coefficient	Value
C_{33}	33.183
C_{44}, C_{55}	0.22370E+06

The frequency dependence of the response amplitude operator (RAO) for the unrestrained motions of the OC3-Hywind platform is shown in Figure 8.10 for incident waves with periods up to 25 s. The freely floating OC3-Hywind platform has a resonance period in surge and pitch close to 17 s. For this wave period, the unrestrained motion amplitude in surge is of about 7 times the wave amplitude and in pitch of about 0.5rad (~30deg.) per meter of wave amplitude. The unrestrained motions in heave have a maximum of about one third of the amplitude of the incident wave occurring at a wave period close to 20s.

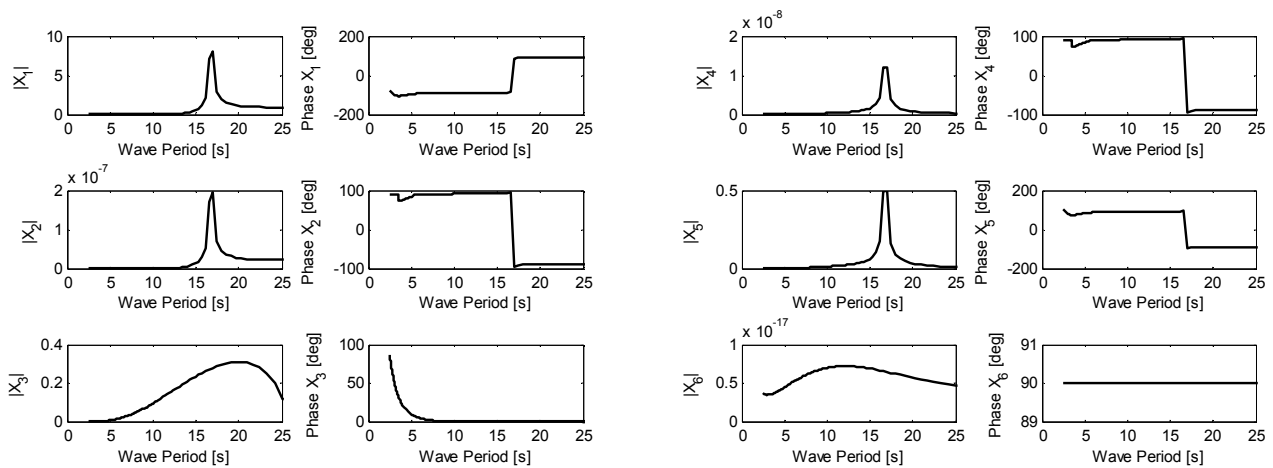


Figure 8.10: Frequency dependence of the response amplitude operator (RAO) for the linear unrestrained motions in surge (x1), sway (x2), heave (x3), roll (x4), pitch (x5) and yaw (x6) associated with the OC3-Hywind.

Second-order hydrodynamic loads and unrestrained motions for monochromatic waves

The second-order solution requires the free-surface to be discretised. An example of the mesh associated with the OC3-Hywind structure used in the present study is shown in Figure 8.11.

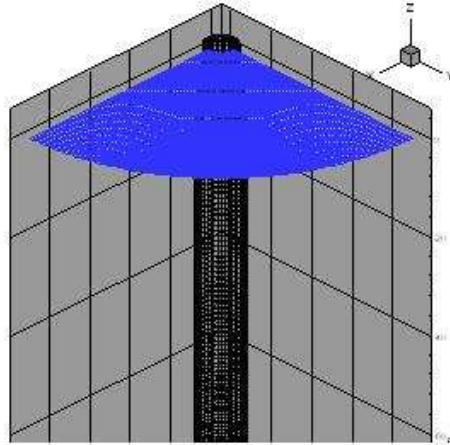


Figure 8.11: Mesh used to discretise the free-surface for the computation of the second-order hydrodynamic quantities for the OC3-Hywind platform.

The problem of monochromatic, head-on waves with periods and height defined in Table 8.13 is first studied.

Table 8.13: Wave periods of the monochromatic waves considered for the comparisons between linear and second-order hydrodynamic quantities.

Period (T) [s]	Height (H) [m]	Wavelength (λ) [m]	Steepness (H/ λ)
5.0	1.0	37.5	0.0267
7.0	2.0	73.5	0.0272
9.0	4.0	121.5	0.0329

For a monochromatic wave, the second-order excitation force is reduced to the computation of the sum- and difference-QTFs (f^{\pm}) at the double ($\omega^+ = \omega + \omega = 2\omega$) and zero frequency ($\omega^- = \omega - \omega = 0$). The second-order excitation force is thus given by:

$$F_X^{(2)}(t) = \text{Re}\{a^2 f^+ e^{-i2\omega t} + a^2 f^-\} \quad [8-11]$$

where a is the complex amplitude of the incident (monochromatic) wave which has a phase component (ϵ) uniformly distributed between $[0, 2\pi]$:

$$a = |a|e^{i\epsilon}$$

The non-dimensional values for the sum- and difference- QTFs are given in Table 8.14 for surge, heave and pitch modes and for the three monochromatic wave periods considered in the present study.

Table 8.14: Non-dimensional sum- and difference- quadratic transfer functions at double and zero frequency for surge (1), heave(3) and pitch (5) modes at three monochromatic wave periods for the OC3-Hywind.

Mode		T=5 s		T=7 s		T=9 s	
		Abs val.	Phase [deg]	Abs val.	Phase [deg]	Abs val.	Phase [deg]
1	f^+	4.67	138.8	4.86	-175.06	4.92	-146.34
	f^-	0.49	-180.0	0.01	180.00	0.01	-180.00
3	f^+	0.83	125.7	0.13	-26.90	0.35	-12.04
	f^-	0.18	0.0	0.04	0.00	0.13	180.00
5	f^+	354.6	146.2	422.4	-169.56	435.5	-141.68
	f^-	45.73	180.0	1.58	180.00	0.54	-180.00

The non-dimensional first-order excitation forces are given for the same modes and wave periods in Table 8.15. The sum- component is about twenty times smaller than the first-order excitation force and ten times larger than the difference component for surge and pitch modes. For heave the sum- component is ten times smaller than the first-order excitation force and about five times larger than the difference component.

Table 8.15: Non-dimensional linear excitation forces for surge (1), heave (3) and pitch (3) modes at three monochromatic wave periods for the OC3-Hywind.

Mode	T= 5s		T=7s		T=9s	
	Abs val	Phase(deg)	Abs val	Phase	Abs val	phase
1	84.3	-102.6	106.0	-94.30	116.0	-91.79
3	8.85	-170.8	18.02	-177.93	23.95	-179.44
5	6912.43	-102.6	7937.18	-94.30	7740.44	-91.79

An example time series comparison between first- and second-order excitation forces associated with the OC3-Hywind platform with monochromatic waves is shown in Figure 8.12. The Figure shows the excitation forces in the surge mode for the largest of the three monochromatic waves considered, with period T=9s. The results are similar for the pitch and heave modes and for the smaller wave periods. The first-order excitation forces are dominant relative to second-order and only small differences between the total excitation force and the first-order can be perceived for the steeper waves at the crests and troughs of the excitation force signals.

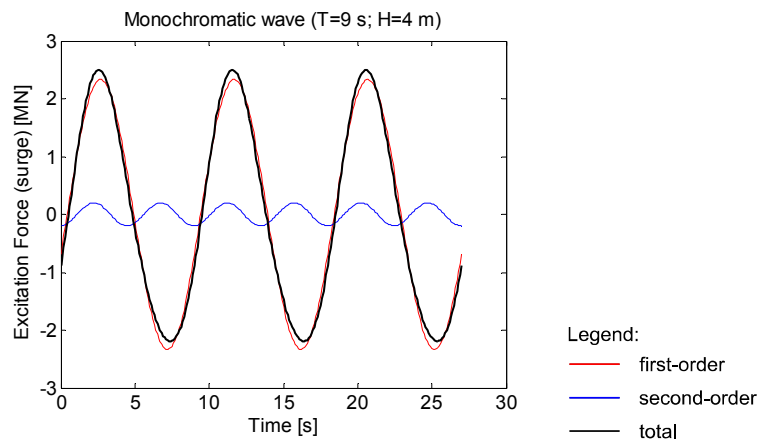


Figure 8.12: Comparison of first and second-order excitation forces in surge mode with monochromatic waves for the OC3-Hywind platform.

An example time series comparison between first- and second-order unrestrained motions associated with the OC3-Hywind platform with monochromatic waves is shown in Figure 8.13. The Figure shows the unrestrained motions in the surge mode for the largest of the three monochromatic waves considered, with period T=9s. The results are similar for the pitch and heave modes and for the smaller wave periods. The time histories show that for the three incident waves studied, the unrestrained motions are small and the second-order effects are in turn very small when compared with the first-order effects.

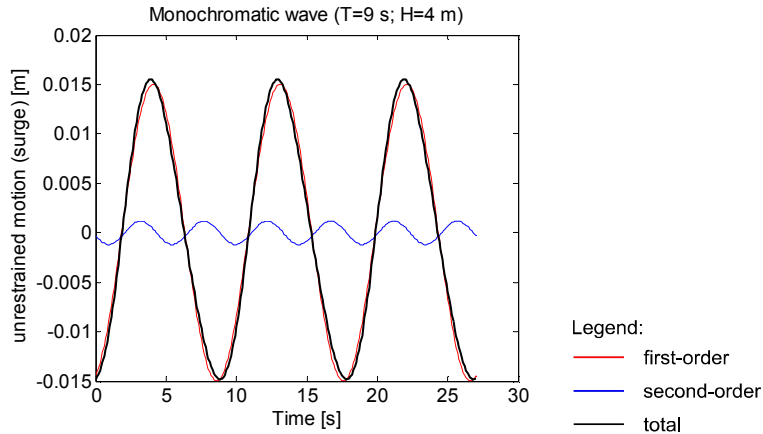


Figure 8.13: Comparison of first and second-order unrestrained surge motion of the OC3-Hywind for three monochromatic waves.

Second-order hydrodynamic loads and unrestrained motions for mixed seas

This section describes the comparisons between first and second-order excitation forces and unrestrained motions obtained for the OC3-Hywind floating structure associated with three sea states described by a Pierson-Moskowitz distribution. This distribution is used to describe fully developed seas for when wind blows steadily over a large area of the ocean for a long time. The three unidirectional Pierson-Moskowitz spectra considered in this study are described with sixteen components with the parameters listed in Table 8.16.

Given the input wave spectrum and the second-order sum- and difference-frequency force QTFs (f^+ , f^-), the time series of the second-order excitation force is directly calculated from:

$$F_X^{(2)}(t) = \text{Re}\left\{ \sum_{k=1}^{16} \sum_{l=1}^{16} [a_k a_l f_{kl}^+ e^{i(\omega_k + \omega_l)t} + a_k a_l^* f_{kl}^- e^{i(\omega_k - \omega_l)t}] \right\} \quad [8-12]$$

where the sum and difference-frequency force QTF satisfy the symmetry relations: $f_{kl}^+ = f_{lk}^+$ and $f_{kl}^- = f_{lk}^{-*}$.

Table 8.16: Parameters which define the three Pierson-Moskowitz spectra considered in this study.

Hs [m]	Tp [s]	fmin [Hz]	fmax [Hz]	df [Hz]	TR [s]
0.5	3.54	0.15	0.8	0.04	25
2.5	7.91	0.08	0.4	0.02	50
5.0	11.18	0.06	0.2	0.01	100

The number of components (N) for each spectrum is equal to sixteen. In the above table Hs is significant wave height; Tp is peak period; fmin and fmax are the minimum and maximum cutoff frequencies; df is equal to (fmax-fmin)/N; and TR is the repeat period. An example of the frequency components associated with the most severe of these spectra, with significant wave height equal to 5.0m, is shown in the top histogram of Figure 8.14. The bottom histogram shows the wave amplitude and periods associated with this spectrum.

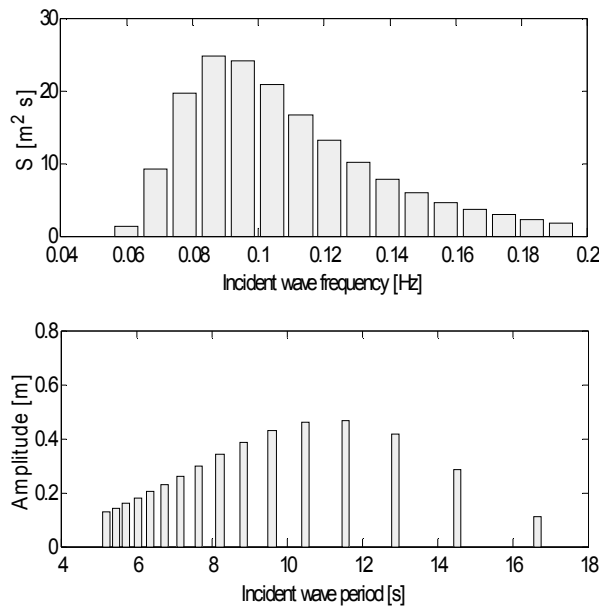


Figure 8.14: (Top) Pierson Moskowitz spectrum with $H_s = 5.0$ m ($T_p = 11.18$ s) described by sixteen components. (Bottom) Wave amplitude and period associated with the top spectrum.

The absolute value of the sum- and difference- frequency force QTFs (f^+ , f^-) computed for the OC3-Hywind platform in surge, heave and pitch modes for the sixteen frequency components associated with these Pierson-Moskowitz spectra is shown in Appendix A of [111]. As expected the sum-frequency components are symmetric satisfying the relation: $f_{kl}^+(\omega_k + \omega_l) = f_{lk}^+(\omega_l + \omega_k)$, whereas the difference-frequency components are complex conjugate symmetric satisfying the relation: $f_{kl}^-(\omega_k - \omega_l) = f_{lk}^{*-}(\omega_l - \omega_k)$.

Pierson-Moskowitz spectrum with $H_s=0.5$ m

The first and second-order excitation forces in surge, heave and pitch for the OC3-Hywind associated with a Pierson Moskowitz spectrum with $H_s=0.5$ m ($T_p=3.54$ s) are shown in Figure 8.15. For this spectrum the influence of the second-order components is more important in surge and pitch modes than in heave. The time series for surge and pitch show the presence of higher frequency components due to the predominance of the sum-frequency force QTFs.

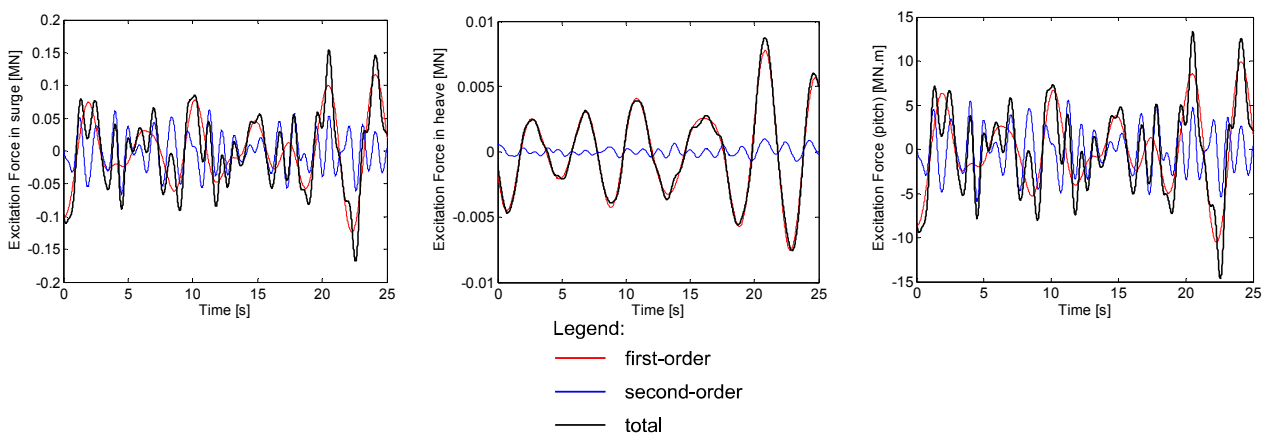


Figure 8.15: Comparisons between first and second-order excitation forces in surge, heave and pitch modes for a Pierson-Moskowitz spectrum with $H_s=0.5$ m ($T_p = 3.54$ s).

The comparisons of first and second-order unrestrained motions in surge, heave and pitch for the OC3-Hywind for a Pierson-Moskowitz spectrum with $H_s=0.5\text{m}$ are shown Figure 8.16. For this spectrum, the unrestrained motions are very small. However it should be pointed out the relative importance of the second-order components of the motion.

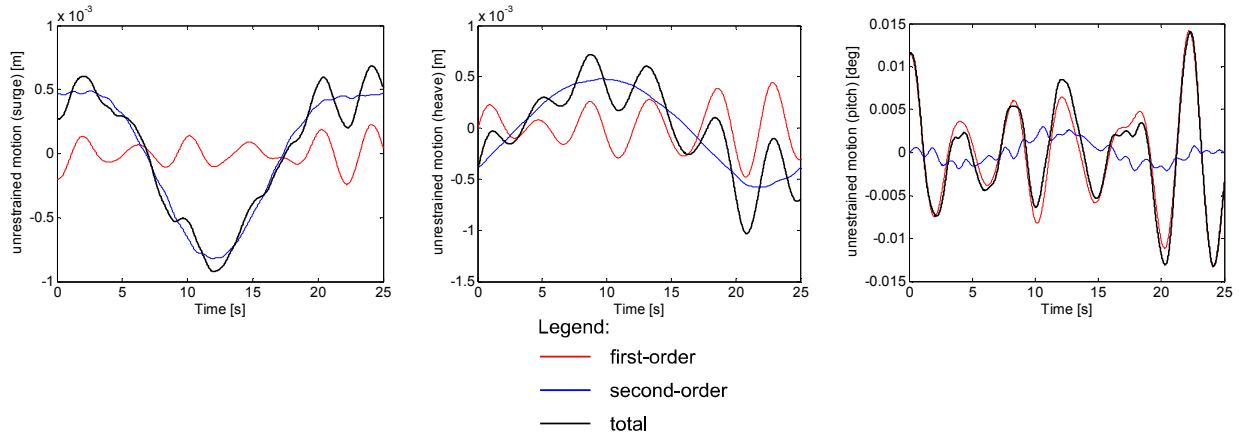


Figure 8.16: Comparisons between first and second-order unrestrained motions in surge, heave and pitch modes for the OC3-Hywind for a Pierson-Moskowitz spectrum with $H_s=0.5\text{ m}$ ($T_p=3.54\text{ s}$).

Pierson-Moskowitz spectrum with $H_s=2.5\text{ m}$

The first and second-order excitation forces in surge, heave and pitch modes for the OC3-Hywind associated with the Pierson-Moskowitz spectrum with $H_s=2.5\text{m}$ ($T_p=7.9\text{s}$) are shown in Figure 8.17. As in the previous case ($H_s=0.5\text{m}$) the influence of the second-order components is more important in surge and pitch modes. The presence of higher frequency components in surge and pitch are due to the predominance of the sum-frequency force QTFs for these modes.

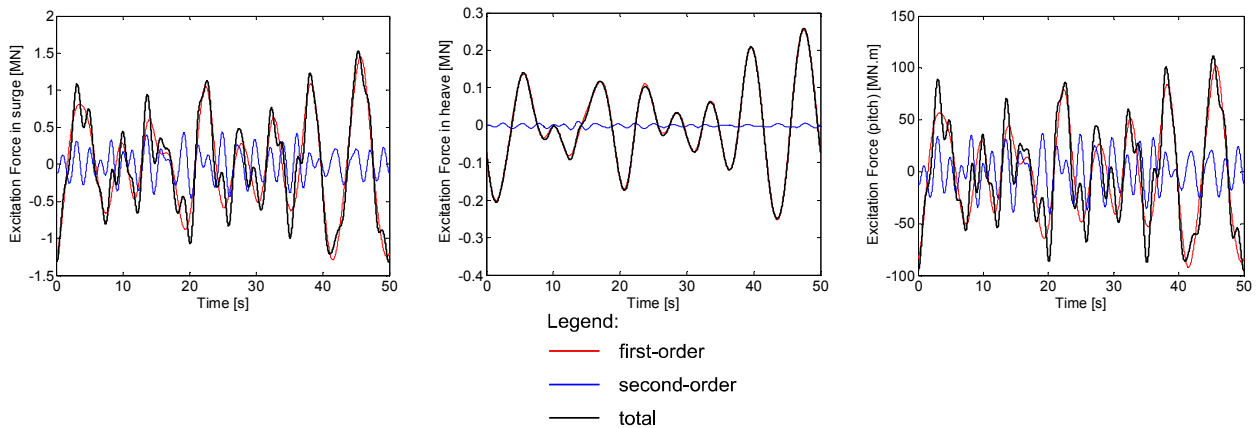


Figure 8.17: First and second-order excitation forces in surge, heave and pitch modes of the OC3-Hywind for a Pierson-Moskowitz spectrum with $H_s=2.5\text{ m}$ ($T_p = 7.9\text{ s}$).

The comparisons of first and second-order unrestrained motions in surge, heave and pitch for the OC3-Hywind for a Pierson Moskowitz spectrum with $H_s=2.5\text{ m}$ ($T_p=7.9\text{ s}$) are shown in Figure 8.18. The unrestrained motions of this structure are very small. The second-order component is dominant in surge, in heave has very little importance and in pitch is of the same importance as the first-order component.

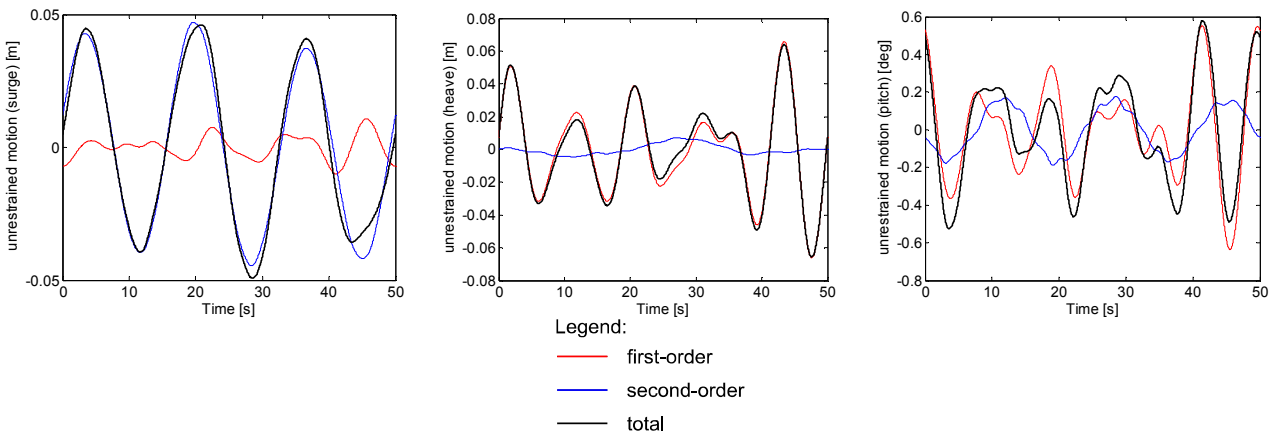


Figure 8.18: First and second-order unrestrained motions in surge, heave and pitch modes for the OC3-Hywind for a Pierson-Moskowitz spectrum with $H_s=2.5$ m ($T_p=7.9$ s).

Pierson-Moskowitz spectrum with $H_s=5.0$ m.

The comparisons of first and second-order excitation forces in surge, heave and pitch mode for the OC3-Hywind associated with this Pierson Moskowitz spectrum ($H_s=5.0$ m) are shown in Figure 8.19. For this spectrum the influence of the second-order components is of the same order of magnitude as the first-order for the three modes and due to the higher frequency components the second-order excitation force, the total force shows sharper peaks when compared to the first-order excitation force.

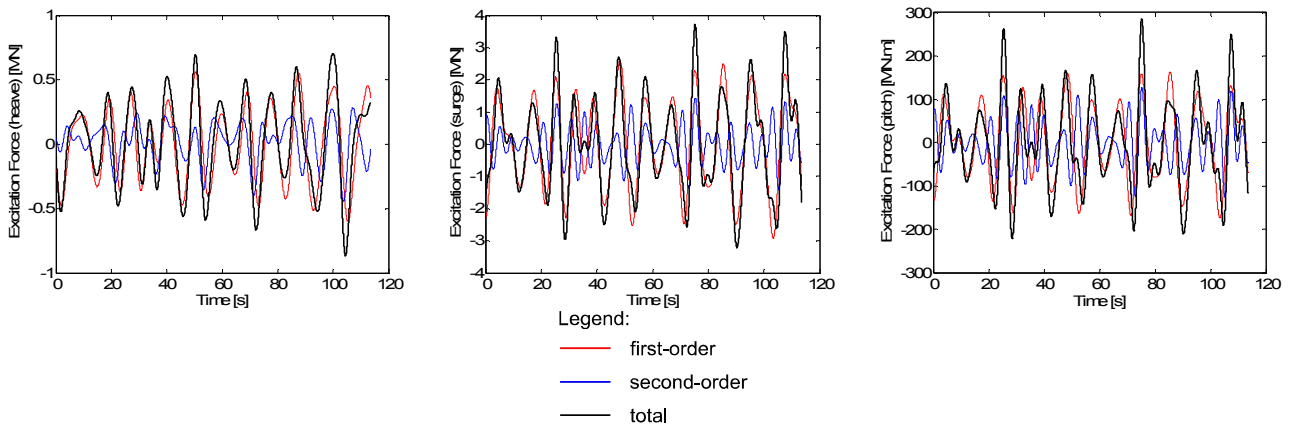


Figure 8.19: First and second-order excitation forces in surge, heave and pitch modes of the OC3-Hywind for a Pierson-Moskowitz spectrum with $H_s=5.0$ m ($T_p = 11.18$ s).

The comparisons of the first and second-order unrestrained motions of the OC3-Hywind in surge, heave and pitch associated with this spectrum are shown in Figure 8.20. The plots show a maximum amplitude value of about 3m in surge, 1m in heave and 13deg in pitch. The influence of second-order unrestrained motions in surge and pitch are small, but dominant in heave when compared to the first-order motions.

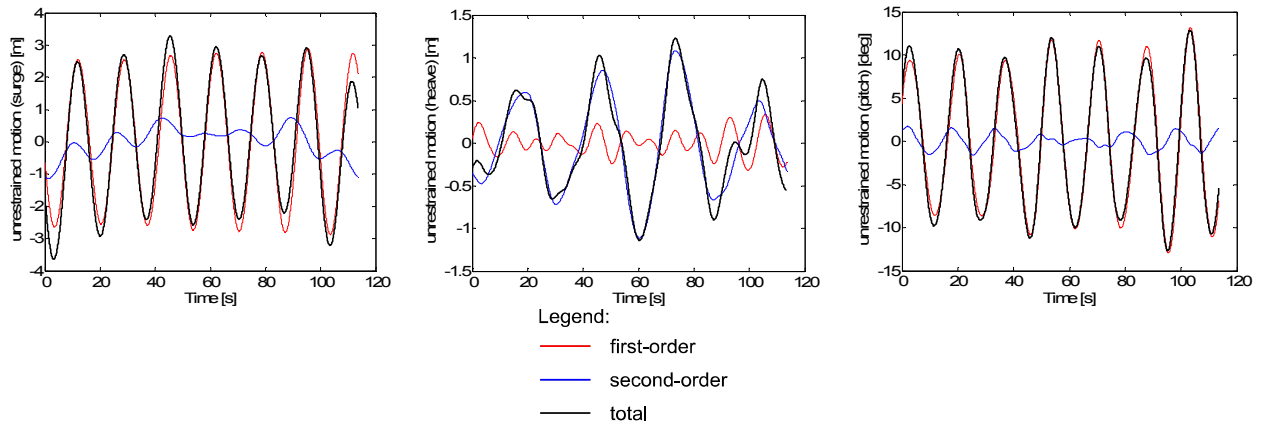


Figure 8.20: First and second-order unrestrained motions in surge, heave and pitch modes for the OC3-Hywind for a Pierson-Moskowitz spectrum with $H_s=5.0$ m ($T_p=11.18$ s).

Semi-submersible results

Linear hydrodynamic loads and unrestrained motions

The frequency dependence of the linear excitation forces and moments are shown in Figure 8.21 for incident wave periods up to 25s. These are computed at the centre of mass of the structure and given as non-dimensional.

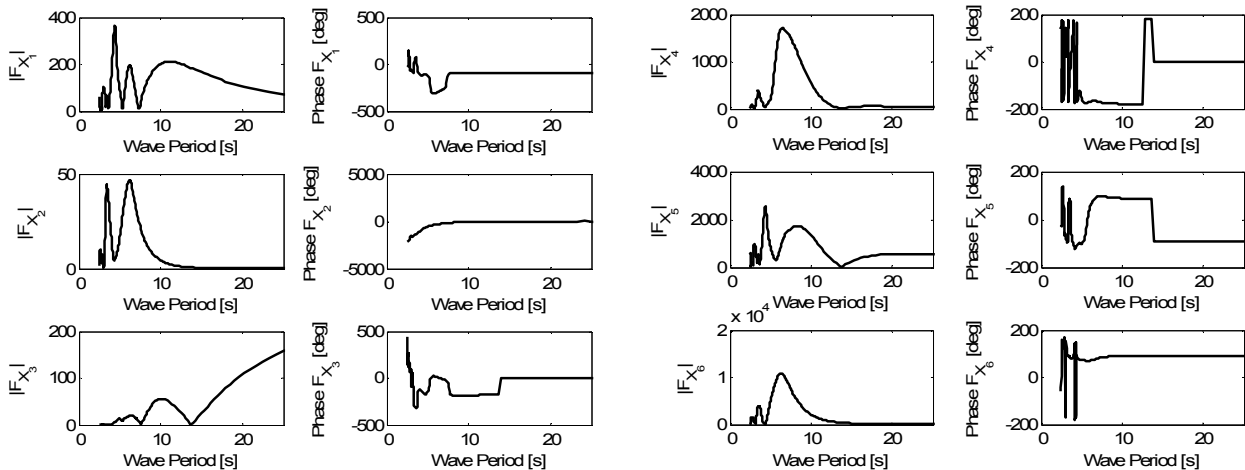


Figure 8.21: Excitation forces and moments in surge (1), sway (2), heave (3), roll (4), pitch (5) and yaw (6) for the semi-submersible platform for incident wave periods up to 25 s.

The frequency dependence of the non-dimensional added-mass and damping coefficients is shown in Figure 8.22. Taking into account the symmetry of the hydrodynamic coefficients and the geometry of the semi-submersible platform only six coefficients shown are of interest. The coefficients in surge and sway are equal and also in roll and pitch. All crossed terms are negligible except the surge-pitch and sway-roll. Finally, the non-dimensional hydrostatic coefficients computed for the semi-submersible platform are shown in Table 8.17.

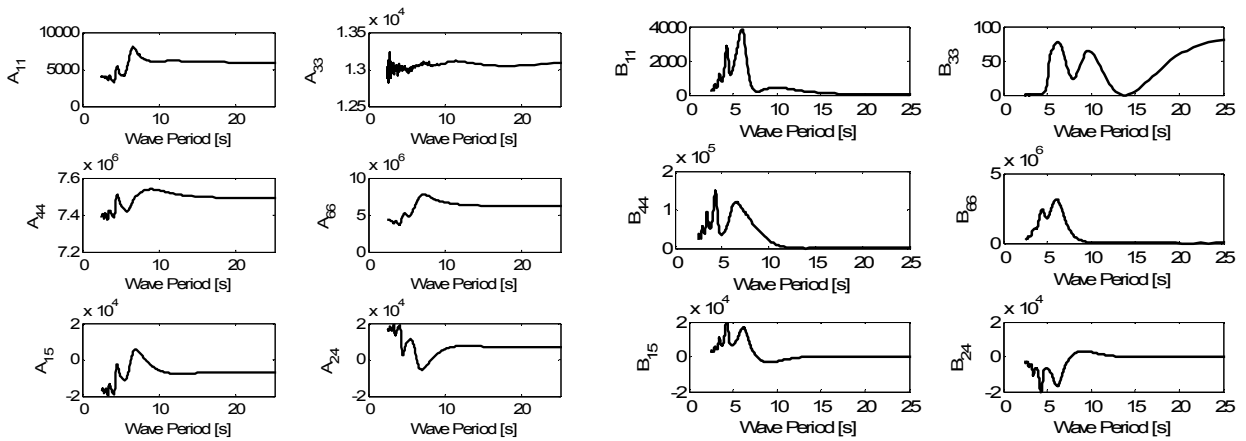


Figure 8.22: Added-mass and hydrodynamic damping coefficients for the semi-submersible platform for incident wave periods up to 25 s

Table 8.17: Non-dimensional hydrostatic coefficients for the semi-submersible platform.

Coefficient	Value	Coefficient	Value
C_{33}	269.76	C_{45}	0.13018E-01
C_{34}	-0.16089E-02	C_{46}	0.13611
C_{35}	-0.14339E-02	C_{55}	0.14636E+06
C_{44}	0.14636E+06	C_{56}	-0.70826E-01

The frequency dependence of the response amplitude operator (RAO) for the unrestrained motions of the semi-submersible platform is shown in Figure 8.23. For this structure, resonance occurs in heave for the unrestrained submerged motions at about 17 s. At this wave period the motions in surge, roll and pitch have also maximum amplitude.

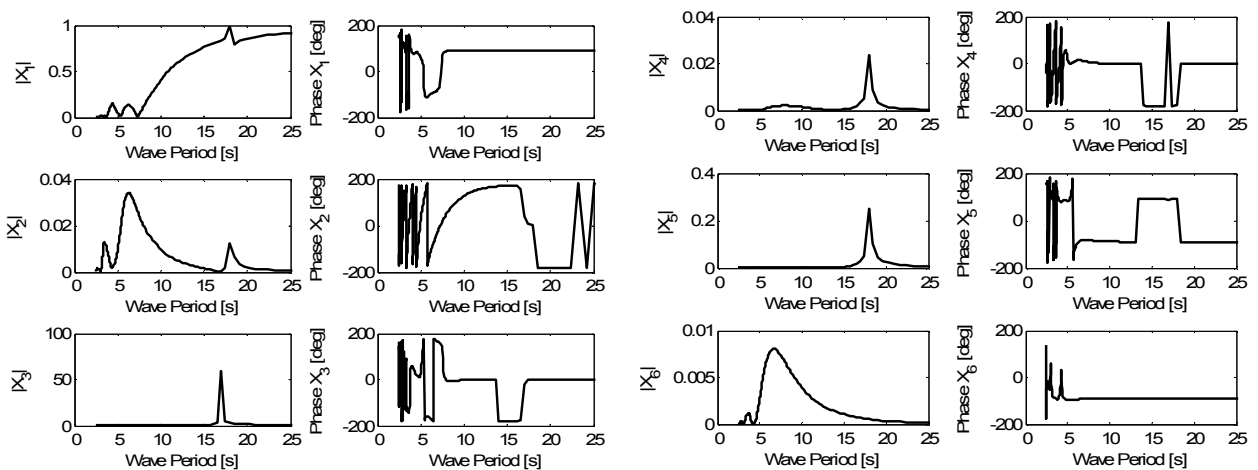


Figure 8.23: Frequency dependence of the response amplitude operator (RAO) for the linear unrestrained motions in surge (x1), sway (x2), heave (x3), roll (x4), pitch (x5) and yaw (x6) associated with the semi-submersible platform.

Second-order hydrodynamic loads and unrestrained motions for monochromatic waves

Given the input wave spectrum represented by N components, the time-series of the total excitation force is computed as for the OC3-Hywind platform. The second-order solution requires the additional discretisation of the free-surface. This mesh is shown in Figure 8.24 for the semi-submersible platform.

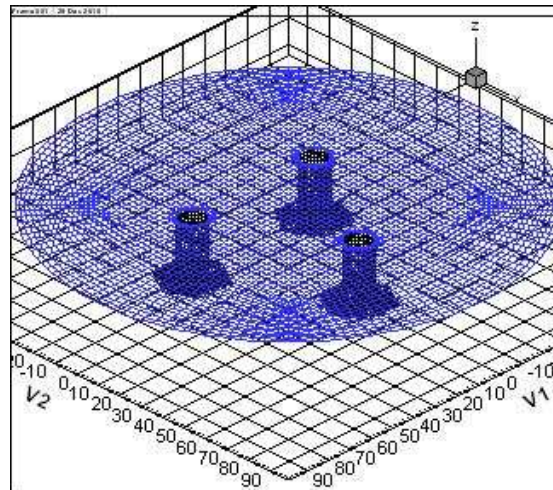


Figure 8.24: Mesh used to discretise the free-surface for the computation of the second-order hydrodynamic quantities for the semi-submersible platform.

This section presents the results for monochromatic, head-on waves for the same wave periods and heights listed in Table 8.13. For a monochromatic wave, the second-order excitation force is given by Equation 3-11.

The non-dimensional values of the sum- and difference- force QTFs for the three monochromatic wave periods considered in the present study are given in Table 8.18. The first-order excitation forces are also given for comparison in Table 8.19 for the same modes and wave periods. The sum- frequency components of the force QTFs (f^+) are higher than the difference- frequency components (f^-) for all modes and monochromatic waves.

Table 8.18: Non-dimensional sum- and difference- force QTFs at double and zero frequency for surge (1), sway (2), heave(3), roll (4), pitch (5) and yaw (6) modes at three monochromatic wave periods for the semi-submersible platform.

Mode		T=5 s		T=7 s		T=9 s	
		Abs. value	Phase (deg)	Abs. value	Phase (deg)	Abs. value	Phase (deg)
1	f^+	510.29	-66.07	39.16	-176.84	14.93	-51.10
	f^-	12.42	180.00	2.91	180.00	0.83	180.00
2	f^+	408.46	54.67	23.02	16.40	5.07	-118.96
	f^-	0.16	0.00	0.07	0.00	0.14	180.00
3	f^+	4.36	-103.79	1.22	-70.50	1.84	29.91
	f^-	0.01	0.00	0.44	0.00	0.55	0.00
4	f^+	3,966.57	-125.86	202.49	177.28	42.30	123.52
	f^-	6.20	180.00	8.37	0.00	6.58	0.00
5	f^+	4,968.51	-65.70	373.25	-163.92	81.98	-29.44
	f^-	164.03	-180.00	41.64	-180.00	9.52	-180.00
6	f^+	10,484.50	-164.69	3,946.98	-145.71	205.89	41.62
	f^-	2.87	0.00	20.27	0.00	10.19	-180.00

Table 8.19: Non-dimensional linear excitation forces for surge (1), sway (2), heave (3), roll (4), pitch (5) and yaw (6) modes at three monochromatic wave periods for the semi-submersible platform.

Mode	T=5 s		T=7 s		T=9 s	
	Abs. value	Phase (deg)	Abs. value	Phase (deg)	Abs. value	Phase (deg)
1	97.7	-131.6	65.5	99.0	169.2	-91.0
2	15.7	-162.0	31.5	157.6	8.2	-85.8
3	13.6	-148.7	14.6	-16.9	44.5	175.5

4	198.8	-154.6	1628.6	-169.3	901.0	-178.2
5	824.4	-101.9	1459.6	97.8	1650.5	90.8
6	4978.5	74.3	9370.9	81.4	3483.6	89.3

The plots in Figure 8.25 and Figure 8.26 show the comparisons between first and second-order excitation forces for surge and pitch modes respectively for three monochromatic waves considered in this study. For the shorter waves with period equal to 5s, the second-order component is dominant relative to the first-order. For the longer waves with periods equal to 7s and 9s, the second-order component is gradually smaller and less dominant. For the heave mode, results for which are not shown, the first-order component is dominant relative to the second-order for all three waves as for the OC3-Hywind platform.

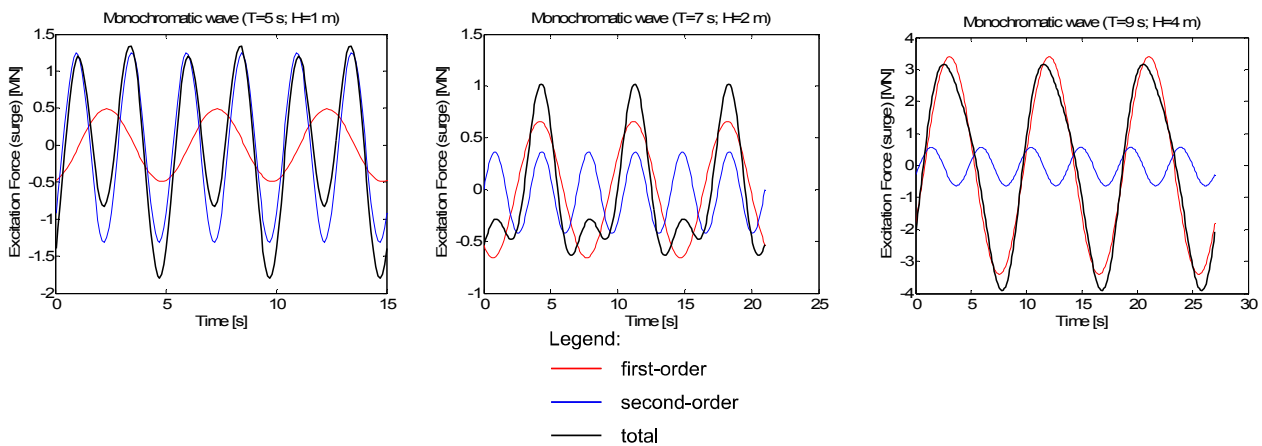


Figure 8.25: Comparison of first and second-order excitation forces in surge mode for three monochromatic waves for the semi-submersible platform.

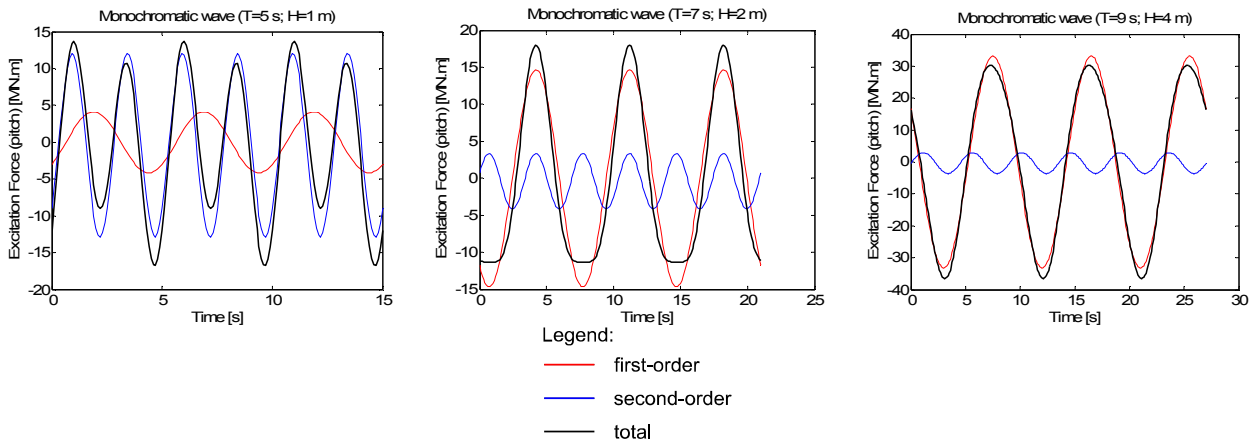


Figure 8.26: Comparison of first and second-order excitation forces in pitch mode for three monochromatic waves for the semi-submersible platform.

The plots in Figure 8.27 and Figure 8.28 show the comparisons between first and second-order unrestrained motions for surge and pitch modes respectively for the three monochromatic waves considered in this study. All motions are small, and as for the excitation forces the influence of the second-order unrestrained motions is more important for the shorter wave with period equal to 5s in surge and pitch modes. The first-order component is dominant for the longer waves with period equal to 7s and 9s. For the heave results, which are not shown, the first-order motions are dominant relative to the second-order for all three waves.

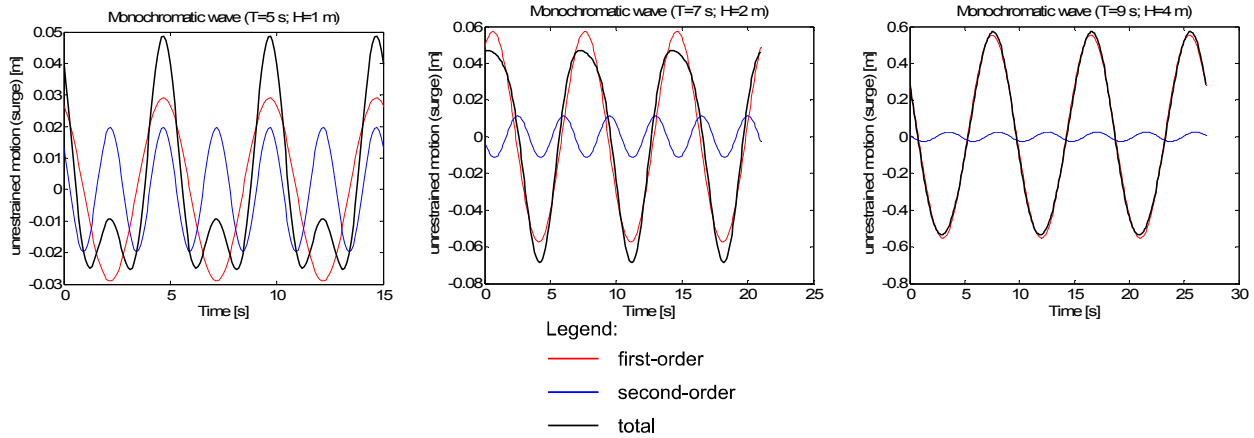


Figure 8.27: Comparison of first and second-order unrestrained surge motion for the semi-submersible platform for three monochromatic waves.

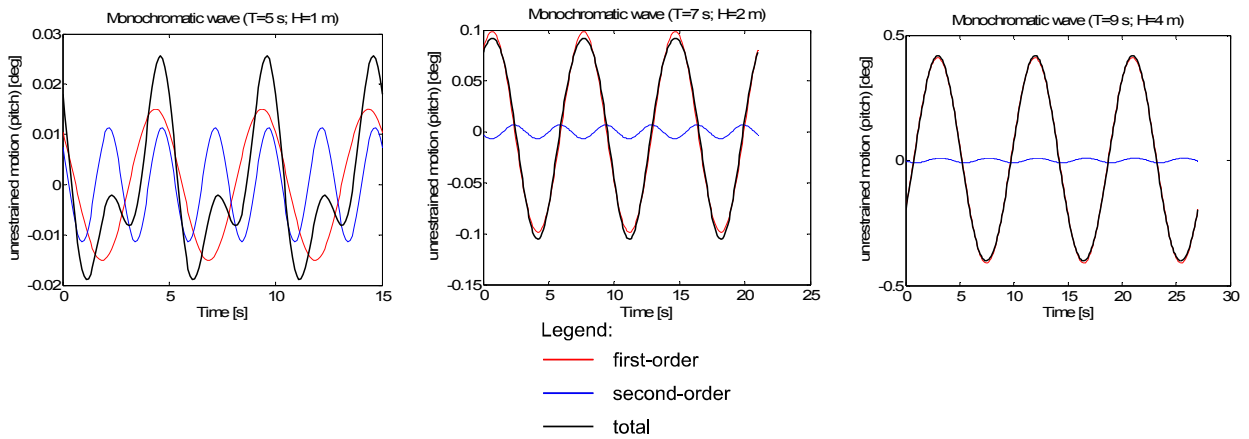


Figure 8.28: Comparison of first and second-order unrestrained pitch motion for the semi-submersible platform for three monochromatic waves.

Second-order hydrodynamic loads and unrestrained motions for mixed seas

This section presents comparisons between first and second-order excitation forces and unrestrained motions for the semi-submersible platform, for three sea states described by Pierson-Moskowitz distributions with the parameters listed in Table 8.16. The absolute values of the sum- and difference- frequency force QTFs (f^+ , f^-) for the semi-submersible platform in the six modes of motion can be found in Appendix B of [111].

Pierson-Moskowitz spectrum with $H_s=0.5$ m

The comparisons between first and second-order excitation forces in the six modes of motion (surge, sway, heave, roll, pitch and yaw) for the semi-submersible platform associated with this spectrum are presented in Figure 8.29. For this spectrum and for all modes, the second-order excitation forces are dominant relative to the first-order excitation forces.

The comparisons of the first and second-order unrestrained motions in the six modes for this spectrum are shown in Figure 8.30. The unrestrained motions are small in all modes. Slow drift motions can be identified in all modes except heave. For surge, pitch and yaw, the second-order component of the unrestrained motions is of the same order of importance as the first-order. For the other modes (sway, heave and roll) the second-order component is dominant over the first-order.

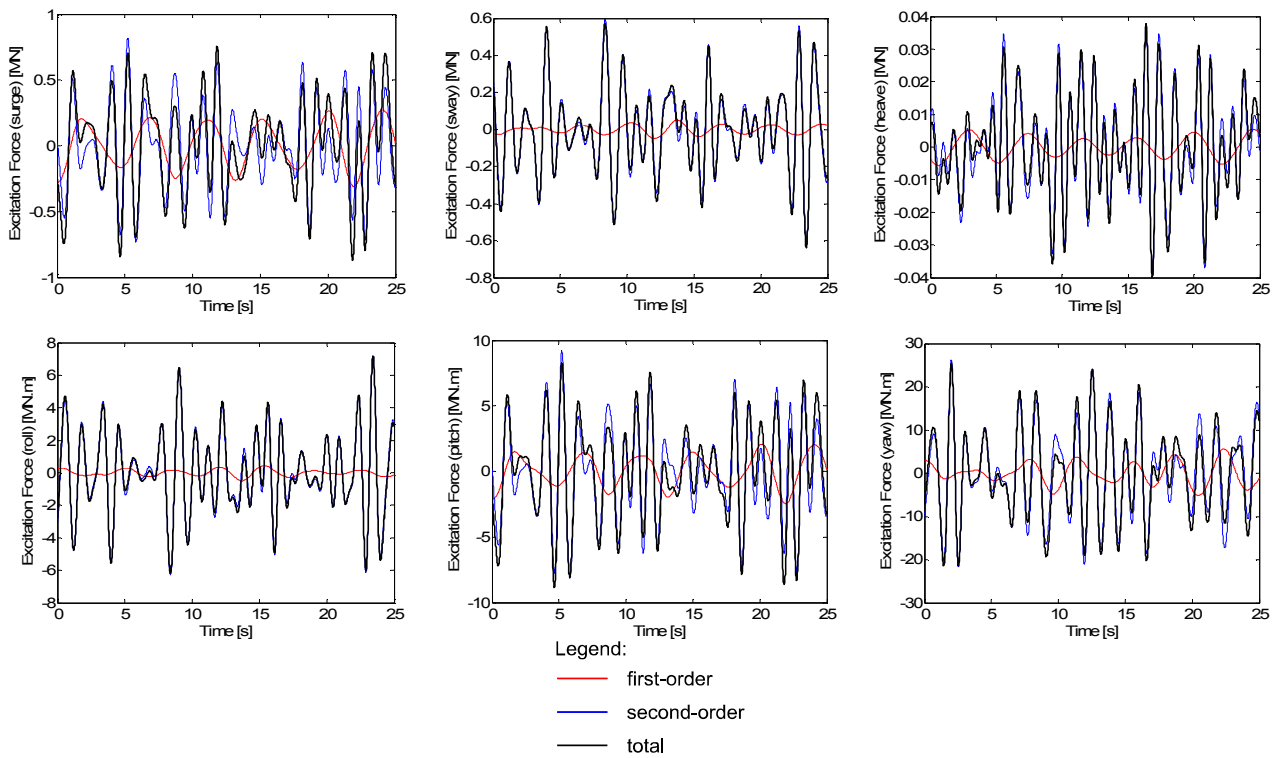


Figure 8.29: Comparisons between first and second-order excitation forces in surge, sway, heave, roll, pitch and yaw modes for a Pierson-Moskowitz spectrum with $H_s=0.5$ m ($T_p = 3.54$ s).

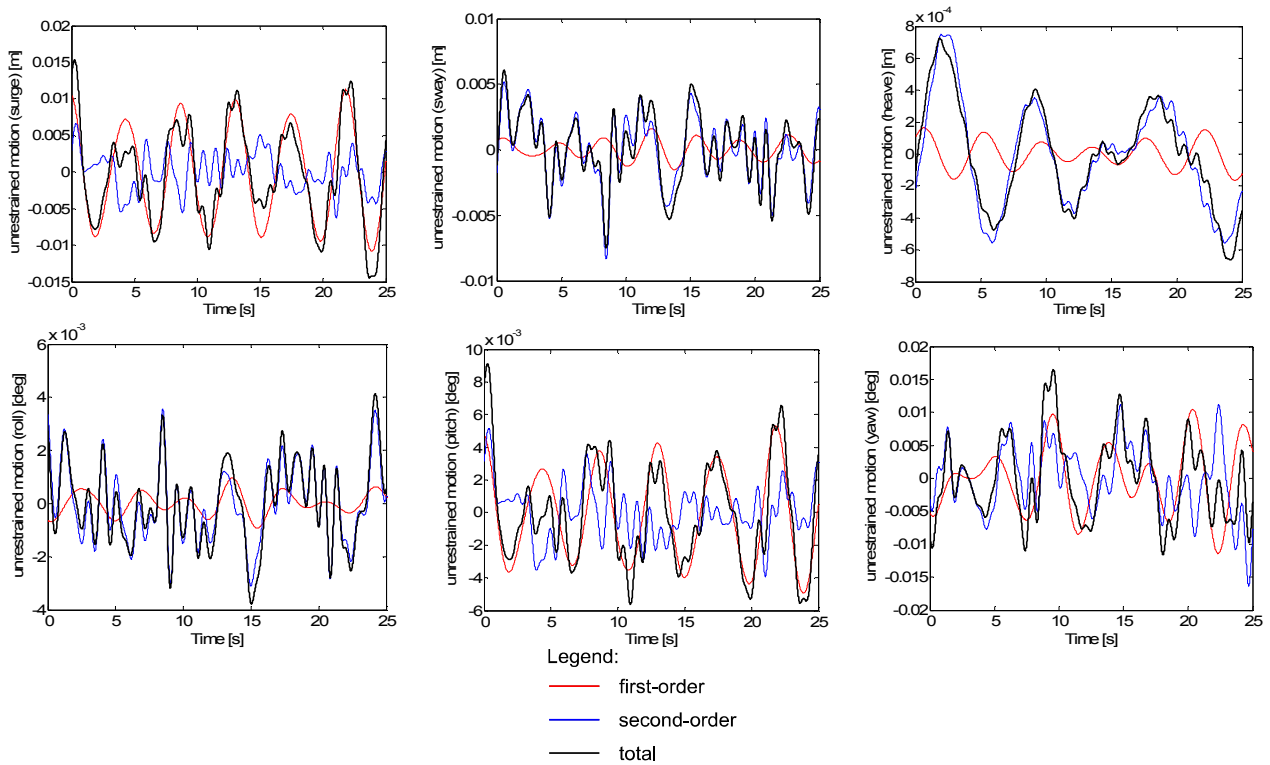


Figure 8.30: Comparisons between first and second-order unrestrained motions for the semi-submersible platform for a Pierson-Moskowitz spectrum with $H_s=0.5$ m ($T_p=3.54$ s).

Pierson-Moskowitz spectrum with $H_s=2.5$ m

The comparisons of the first and second-order excitation forces in the six modes of motion for the semi-submersible platform associated with this spectrum are presented in Figure 8.31. For this spectrum the second-order excitation forces are dominant relative to the first-order excitation forces for all modes except for heave, and the character of these forces is due to the dominance of the sum-frequency force QTFs.

The comparisons of the first and second-order unrestrained motions for this spectrum are shown in Figure 8.32. The unrestrained motions are small in all modes and slow drift motions can be identified in all modes except heave. For surge, roll, pitch and yaw, the second-order component of the unrestrained motions is smaller than the first-order which dominates the motions. For heave, the second-order component is of the same relative importance as the first-order component of the motions, and for sway, the second-order component of the unrestrained motions dominates over the first-order component.

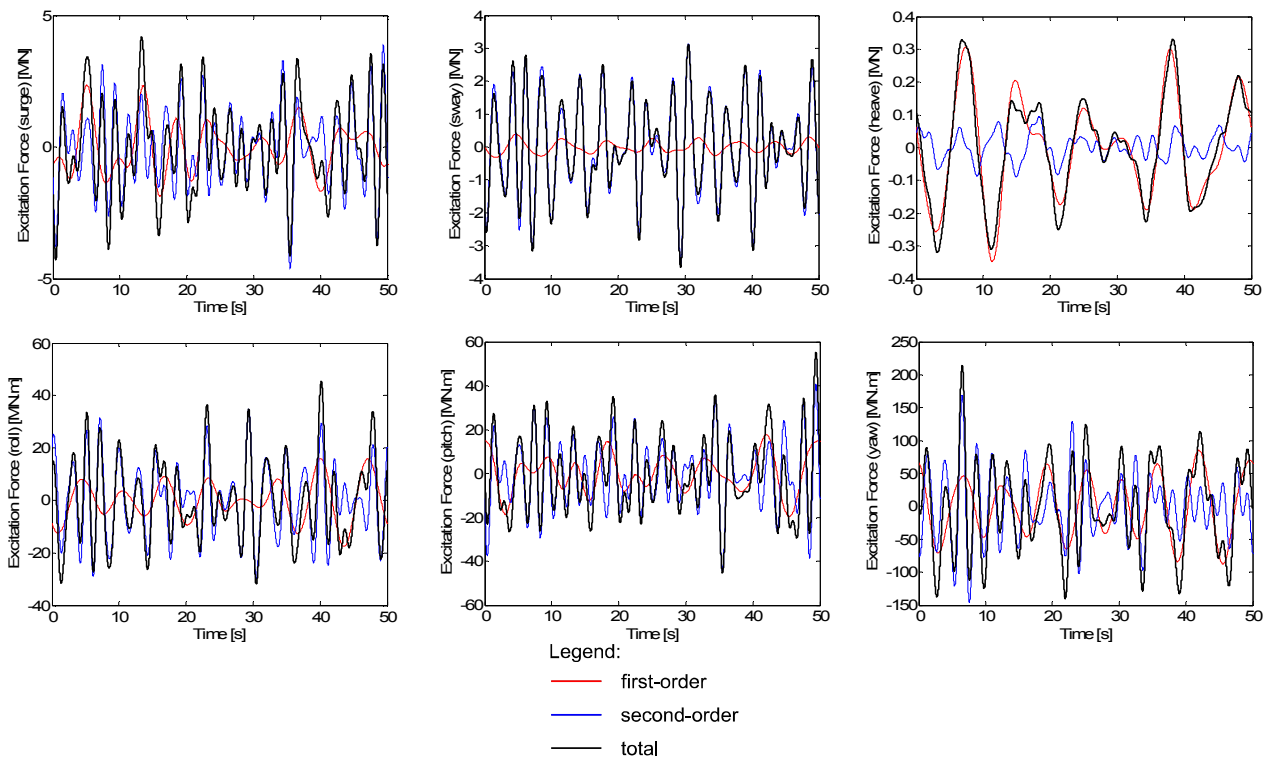


Figure 8.31: Comparisons between first and second-order excitation forces in surge, sway, heave, roll, pitch and yaw modes for a Pierson-Moskowitz spectrum with $H_s=2.5$ m ($T_p = 7.9$ s).

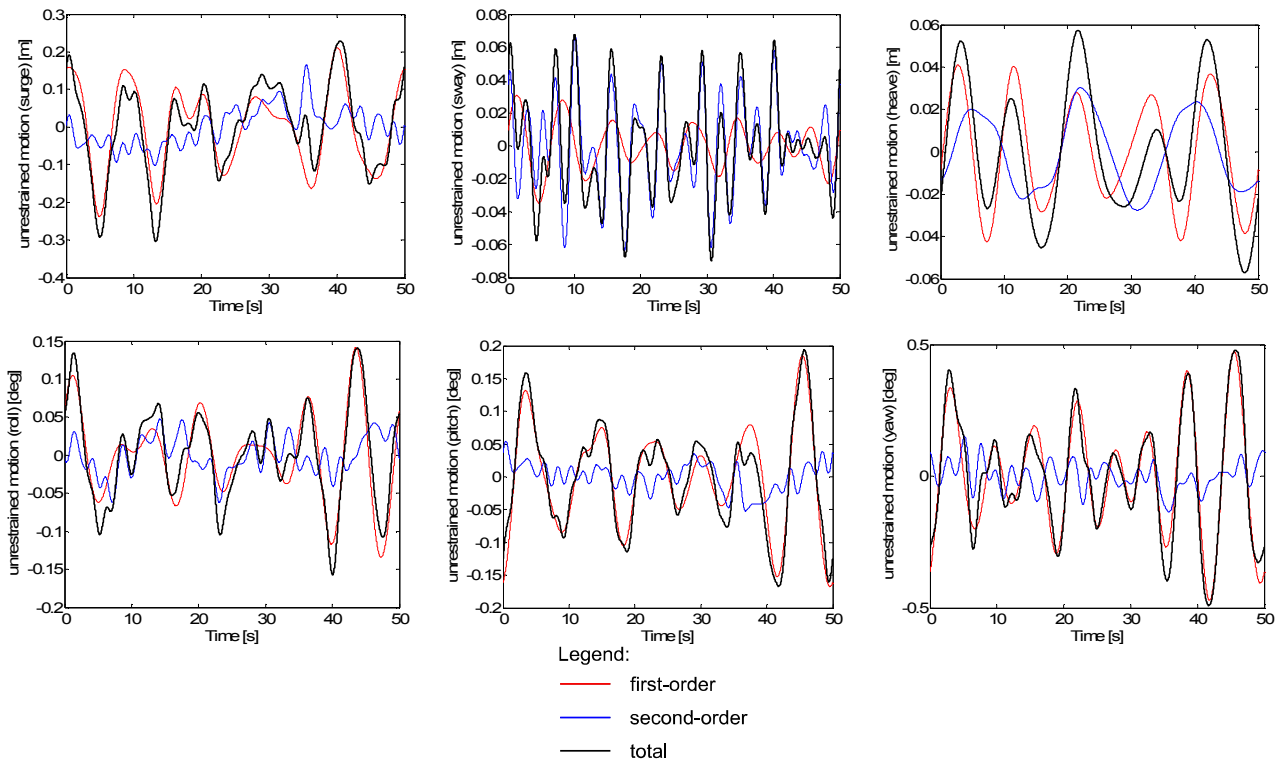
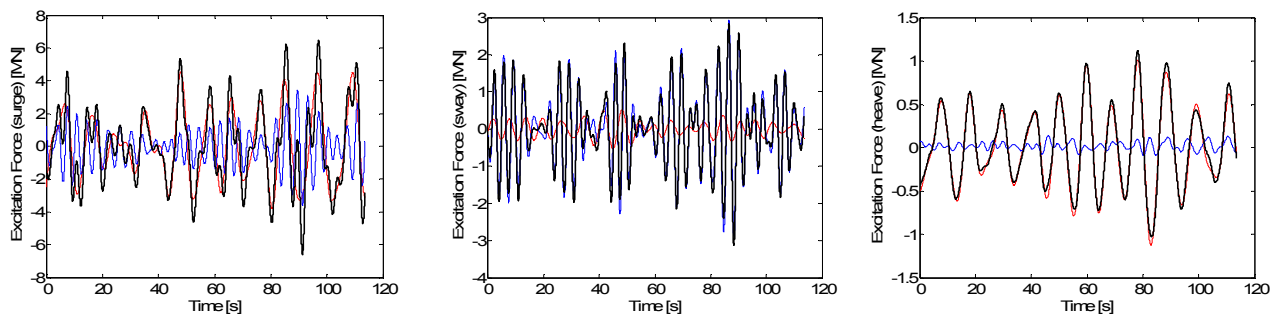


Figure 8.32: Comparisons between first and second-order unrestrained motions for the semi-submersible platform for a Pierson-Moskowitz spectrum with $H_s=2.5$ m ($T_p=7.9$ s).

Pierson-Moskowitz spectrum with $H_s=5.0$ m

The comparisons between first and second-order excitation forces in the six modes of motion (surge, sway, heave, roll, pitch and yaw) for the semi-submersible platform associated with this spectrum are presented in Figure 8.33. For surge, roll, pitch and yaw, the second-order effects are important when compared with first-order. In sway the second-order excitation force is dominant and in heave the contribution from the second-order excitation force is small.

The comparisons of first and second-order unrestrained motions in the six modes of motion for this spectrum are shown in Figure 8.34. The unrestrained motions are small in all modes. Slow drift motions can be observed in surge, sway and yaw. The second-order unrestrained motions are of the same importance as the first-order for roll and pitch motions and are dominant in sway. In heave the effects of second-order motions are small when compared to first-order.



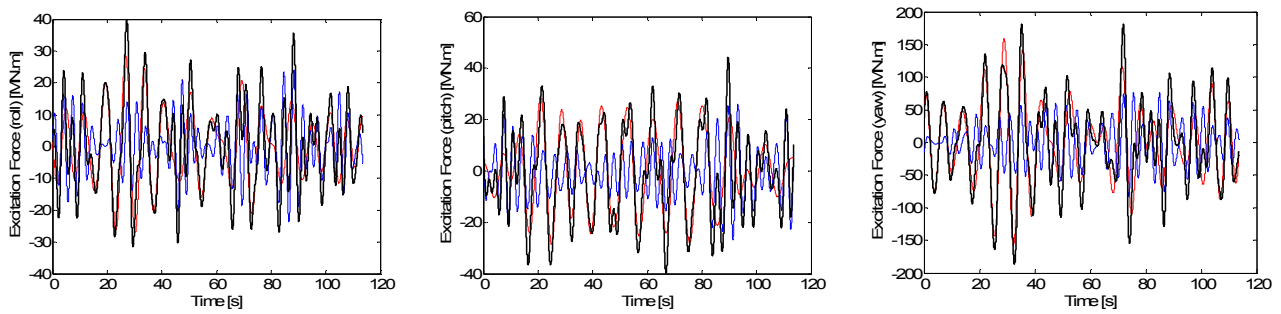


Figure 8.33: Comparisons between first and second-order excitation forces in surge, sway, heave, roll, pitch and yaw modes for a Pierson-Moskowitz spectrum with $H_s=5.0$ m ($T_p = 11.2$ s).

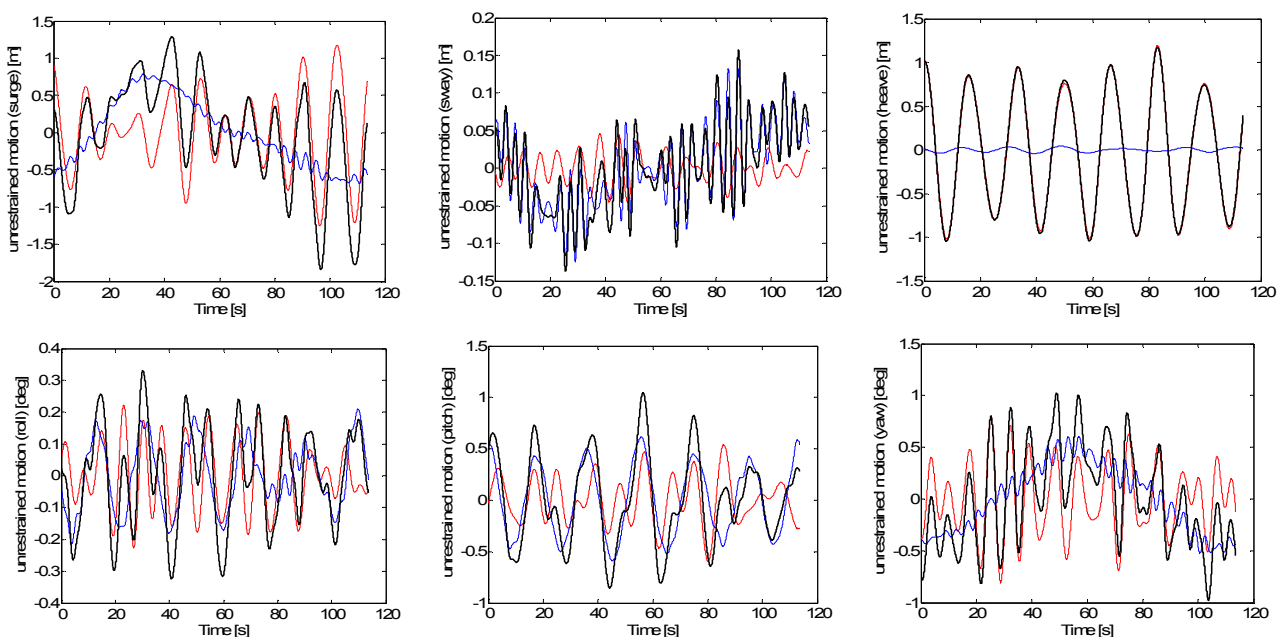


Figure 8.34: Comparisons between first and second-order unrestrained motions for the semi-submersible platform for a Pierson-Moskowitz spectrum with $H_s=5.0$ m ($T_p=11.2$ s).

Summary and Key Findings

A study is presented which compares the results obtained from linear and weakly nonlinear potential flow hydrodynamics models applied to two floating offshore wind structures: a spar-buoy adapted to accommodate a NREL 5MW offshore wind turbine called “OC3-Hywind” and semi-submersible platform with geometric dimensions similar to the WindFloat platform concept.

All potential flow hydrodynamic models assume that the fluid is incompressible and inviscid and the flow irrotational, allowing the fluid velocity to be described by a potential function required to satisfy the Laplace equation in all fluid domain and certain boundary conditions at the fluid, solid and air interfaces. The full expression of these boundary conditions is mathematically difficult to solve and computationally intensive as the numerical methods developed require the redefinition of the problem conditions at each time step to fully cover the changes of the free-surface of the fluid and describe fully the floating structure motions. It is usual however to approximate the hydrodynamic solution of the problem to first or second order by assuming that the wave amplitude of the incoming waves is small in relation to the wavelength. These approximations are computationally more efficient as they avoid a time stepping solution by computing the hydrodynamic forces and motions over the mean wet surface instead of the instantaneous wet surface of the floating structure.

The commercial software WAMIT (v6.1s) was used to compute both the linear and weakly nonlinear hydrodynamic loads and unrestrained motions for the two structures considered in this study. This software solves the hydrodynamic problem in the frequency domain. The generalisation of the second order theory to the case of wave-body interactions with irregular waves requires the definition of bi-chromatic wave components and the solution is obtained in terms of the sum- and difference- frequency components of the usual hydrodynamic quantities. The second order excitation forces are obtained as the sum of the force quadratic transfer functions (QTF) in the sum- and difference-frequency.

The linear and weakly nonlinear comparison exercise is focused on the excitation forces and unrestrained motions associated with regular waves and irregular waves which interact with the two offshore wind structures. For a monochromatic wave the second order excitation force can be expressed as the sum of only two components of the force QTF in the double and zero frequency. For the OC3-Hywind the second order excitation force associated with the three monochromatic waves studied is much smaller than the first order excitation force component in all modes of motion. For the semi-submersible platform the second order component of the excitation force is dominant over the first order component for the less steep wave (period 5s) for all modes except heave. The importance of the second order component decreases for the steeper waves being smaller than the first order for the steepest wave (with period equal to 9s).

The unrestrained motions of the two structures for the three monochromatic waves studied in this report are small. For the OC3-Hywind, the second-order component of the excitation force is negligible when compared with the first order for the three monochromatic waves studied and in all modes of motion. For the semi-submersible platform, the second order component of the unrestrained motions is higher than the first-order component for the less steep wave (period equal to 5s) in all modes except heave. For the steeper waves the importance of this component decreases with respect to the first order and is small for the steepest wave (of period equal to 9s).

The comparisons between first and second order quantities were also performed for three Pierson-Moskowitz spectra with sixteen components. For the OC3-Hywind the second-order components are important in surge and pitch modes. In heave these components are smaller for the spectra with lower significant wave height and of the same importance as first order for the spectra with higher significant wave height ($H_s=5\text{m}$). The second order component of the excitation forces and moments for the semi-submersible platform is higher than the first-order component for the spectra with lower significant wave heights (0.5m and 2.5m) for all modes except heave. For the spectra with $H_s=5.0\text{m}$, the second-order effects are of the same importance as the first-order for surge, roll, pitch and yaw and dominant sway. In heave mode the effect of the second order component of the excitation force is very small in relation to the first-order.

The unrestrained motions associated with the three spectra for both structures are very small. For the OC3-Hywind the second-order unrestrained motions are important for surge and pitch for the spectra with the lower significant wave heights (0.5m and 2.5m) and in heave for the spectra with significant wave height equal to 5.0m. For the semi-submersible platform slow drift motions are identified with the second order component being dominant or of the same order for most of the modes for the three spectra.

8.2.2 Nonlinear potential flow methods

The above study does not access any results associated with fully nonlinear potential flow hydrodynamic models. Ongoing research is being performed at the University of Hamburg into a nonlinear seakeeping simulation technique by using a Rankine-Airy panel method [115]. The base flows from which the flow around the moving body is superimposed are not only source (and possibly vortex) flows, but also Airy waves. Nonlinear boundary conditions at the free surface (constant pressure, no flux through the surface) are satisfied numerically in each time step by superimposing Airy waves of different wave numbers and propagation directions. The amplitudes and phase angles of the Airy waves are not constant over time, but have to be computed from evolution equations. These are derived from the kinematic and dynamic free-surface conditions. The method is suitable for arbitrary geometries and can deal with most of the before mentioned nonlinear effects in steep waves. This method can be effectively applied for the estimation of extreme behaviour of floating offshore wind turbines in survival conditions.

The major difficulty associated with a fully nonlinear potential flow formulation is related with the solution of the complicated nonlinear free surface boundary conditions which has to be satisfied over the instantaneous free surface which is not known a priori. Most of methods developed use a Mixed Eulerian-Lagrangian (MEL) time stepping technique for which the fully nonlinear boundary conditions are satisfied over the instantaneous free water and body surfaces. The unknowns of the linear equations which result from the discretisation of the geometry are distributed on the boundary of the whole computational domain and a new system of equations is generated and solved at each time step, since the free surface change and the body surface move to new positions. An advantage of second order methods when compared with fully nonlinear is that through the approximations involved the linear system of equations to solve are always the same and so are computationally more efficient.

Vortex induced vibrations

Another effect currently not accounted for in hydrodynamic analysis for floating wind turbines is vortex-induced vibrations. This effect is caused by steady currents or by velocities associated with long period waves, and refers to the dynamic loading which occurs as a result of fluctuations in pressure due to the motion of vortices in the wake of a body. If the frequency of excitation is near a natural frequency of the structure the interaction between the flow and the motion of the structure can cause the two frequencies to lock in to each other, which can result in large amplitudes of oscillation. The forces due to vortex shedding are complex and predictions of loading and response are not well understood; however the frequencies at which oscillations may occur can be predicted with more confidence. Vortex-induced vibrations are not generally seen in conventional fixed-bottom offshore support structures, but are more likely to be experienced in mooring lines and can be critical for the stability of some designs.

8.3 Mooring line dynamics

Floating offshore wind turbine structures are held in position by means of mooring systems, which have, depending on the type of the structure and the water depth, different levels of complexity. For floating WT applications a general distinction must be made between slack catenary, taut catenary and taut tension leg mooring systems. In slack catenary designs, often the lower part of the line is resting on the seabed, adding more complexity to the system. In the oil and gas industry, large floating drilling platforms are restored by up to 20 mooring lines with different geometrical and material properties, consisting of a combination of chains and cables made of natural or synthetic fibres (e.g. polyester, aramid, polyamide or polypropylene fibres). Submerged buoyancy tanks along the mooring lines are also common. Such complex mooring solutions will likely be implemented and specially adapted for future floating WTs as well, requiring the codes to have adequate capabilities.

In addition to station-keeping, the mooring system also provides stability; for some platform designs such as the tension leg platform (TLP), the mooring system is the main contributor to the system's stability, meaning a failure in this component would cause the likely destruction of the complete system. The mooring system of floating WT platforms is therefore one of the most important components regarding the stability and the dynamic behaviour of floating offshore wind turbines, making appropriate modelling of the mooring system highly critical during the design process.

The central issue with regard to mooring line dynamics is whether or not it is acceptable to neglect the dynamic effects of mooring lines for floating wind turbines. For shallow mooring systems the total mass of the lines is negligible and the motion is small, so even though the drag force of the lines through the fluid may still be significant it is generally accepted that dynamics may be neglected. However for deeper water configurations mooring line dynamics become increasingly important. A number of studies have been performed in the context of oil platforms, ships and semi-submersible vessels in order to determine the depth at which mooring line dynamics become significant. Polderdijk [101] proposed approximate analytical solutions to the line dynamic problem which can be used to give preliminary checks as to whether line dynamic effects are likely to be significant. Kwan and Bruen [102] analysed line dynamic tensions due to platform wave frequency motion for a range of conditions using both dynamic and quasi-static methods, and showed that the ratio of maximum dynamic to quasi-static tension varied between 1.2 and 19.5 across the cases investigated. Their results can be used to help determine whether or not dynamic analysis is necessary for a given configuration. A Joint Industry Project managed by the Noble Denton Group on the dynamics of catenary mooring [103] studied a number of vessel types, mooring systems and water depths from both a theoretical and practical point of view. The conclusion

clusion from these studies was that line dynamic analysis should be conducted when the wave frequency response of the vessel is large, when the water depth exceeds 150m, or when the mooring line includes large drag elements such as chain moorings [79].

In order to make the design of floating offshore wind turbine platforms as efficient and commercially viable as possible, it would be useful to derive equivalent results for FOWTs. In order to do this, the existing floating wind turbine design tools must be extended to include accurate modelling techniques for mooring lines, including dynamic effects. Further research into mooring systems specific to floating wind turbines could then be performed, incorporating the following elements:

- Quantitative comparison between the different methods for calculating mooring line tension forces for FOWTs
- Analysis of which aspects of mooring line behaviour are important specifically for FOWTs
- Analysis of which mooring system types and configurations have the most dynamic effect on FOWTs and therefore need to be designed using a full dynamic analysis
- Investigation into the transition depth at which dynamic mooring line effects become non-negligible for FOWTs.

There are two main approaches to modelling mooring lines for floating offshore wind turbines. The first option is to couple a dedicated mooring line code with a wind turbine analysis code. The advantage of this approach is that it enables mooring line dynamic effects such as line inertia, drag of the line through fluid and vortex shedding to be fully accounted for. An attempt has been made by Jonkman et al. to couple the dynamic mooring line system LINES of SML with the aero-elastic wind turbine codes FAST and ADAMS. However, this attempt was abandoned after it was found that LINES encountered numerical instabilities when modelling the slack catenary mooring lines of interest [82]. The most fruitful attempt to date is the coupling between offshore floating structures code SIMO/RIFLEX and the multi-body wind turbine code HAWC2, described in [88]. However this approach is still limited in that the floating wind turbine cannot be modelled as a single integrated dynamic structure, since the two problems must be solved in separate programs and information exchanged between the programs at a single interface point. This interface was also known to be quite numerically unstable.

The alternative approach is to extend the capabilities of existing wind turbine design tools to incorporate mooring line modelling techniques. The force-displacement and quasi-static representations discussed in Section 6.1.5 fit into this category. This integrated approach is more common than the coupled approach because it is simpler to implement and generally gives greater numerical stability. The remainder of this section therefore deals with this second approach.

In order to enhance existing FOWT design tools it is useful to incorporate methodologies and techniques currently available from other industries e.g. oil and gas. A number of software tools exist which can model the behaviour of mooring configurations for floating platforms. Section 8.3.1 presents a review of the available mooring line codes, with the aim of better understanding the commercial options available for incorporation into FOWT design tools. Section 8.3.2 presents initial results from simulations performed with the multi-body system approach. It is hoped in the future to be able to make comparisons with results from full dynamic mooring line codes, in order to analyse the relative strengths and limitations of the different modelling methods.

8.3.1 Review of mooring codes and approaches

A list of candidate mooring codes is drawn up and the most suitable options for FOWTs are assessed, taking into account the associated computational effort, flexibility and ease of adoption. As well as comparing tools, the several types of modelling approaches are also compared. The aim of this exercise is to obtain a clear view of the modelling approaches that are applied in commercial packages and their accuracy, in order to decide which is the most appropriate package and modelling approach for incorporation into FOWT design tools.

Table 8.20 shows a list of various candidate tools/packages which currently exist, along with a brief account of their properties. The tools shown in bold are those which have been investigated in detail. These four were chosen for detailed investigation mostly because:

- **ROMEO** was developed within the GL group, so GL Garrad Hassan has access to the source code.
- **MDD** is open-source so can be altered and used freely.
- **AQWA** and **OrcaFlex** are both widely used within the offshore engineering community.

This approach has enabled some key findings to be derived regarding the extension of wind turbine codes to include moorings modules. These key findings can be summarised as follows:

- The mooring line modelling approach currently used by a number of wind turbine codes involves using look-up tables to represent the damping/inertia/stiffness properties of the mooring configuration. This is an established approach which is also used in ROMEO and AQWA.
- A useful exercise would be to perform a study comparing the look-up-table approach with an alternative modelling approach that involves a more complex hydrodynamic and structural model of the mooring lines. Such a study is currently being undertaken by GL Garrad Hassan.
- Having investigated MDD, ROMEO, AQWA, and OrcaFlex, it is concluded that of these four only OrcaFlex (and AQWA in certain configurations) are suitable candidates for such a comparison, given that:
 - MDD has no wave-loading or dynamic load capability.
 - ROMEO is suitable only for frequency-domain modelling. This study is mainly concerned with time-domain modelling.

Table 8.20: Overview of selected moorings modelling packages

Tool / package / code	Main characteristics
ANSYS AQWA	Consists of several sub-components. AQWA-NAUT, AQWA-DRIFT, AQWA-FER, ..., each with specific properties (e.g. time-domain analysis, frequency-domain analysis)
Martec WaveLoad	Intended for ships. Frequency- or time-domain. Mooring line analysis available in FD only.
Flexcom	Strong focus on riser analysis; limited range of mooring options
Ariane-3Dynamic	Specialised mooring tool. Restricted water depth.
Optimoor	Ship-shaped bodies only; limited types of analysis possible. (Focussed on extreme-load analysis for mooring lines).
MDD	Open-source, static solutions only, no wave loads.
ROMEO	GL Noble Denton mooring and riser package. Frequency-domain only.
GMoor32	Catenary mooring and riser analysis
BMT SPM	Quasi-static analysis (plus transient analysis for line breaks only).
SEAMOOR 2000	Operational tool for station-keeping / line-break analysis. Limited modelling options.
TERMSIM	Tanker mooring simulation. Limited modelling options.
MOSES	A modelling language for marine dynamic simulations and stress analysis.
OrcaFlex	Marine dynamics tool, widely used by the offshore engineering community.

Mooring design and Dynamics (MDD)

Mooring Design and Dynamics (MDD) is an open-source MATLAB package produced by Richard Dewey at the University of Victoria, British Columbia. It was written with oceanographic research applications in mind. Specifically, it helps with the design of anchor and mooring systems for stationary oceanographic instruments, and can also perform calculations for moving (i.e. towed) instruments. MDD takes current and wind profiles into account, but does not deal with wave forces. Immediately this indicates that a considerable development effort would be necessary to adapt MDD; the main attraction to such a tool is therefore the fact that it is open-source.

MDD consists of a package of MATLAB files and is run from the MATLAB command-line. It allows the user to create / modify mooring or tow-line configurations. User interaction is done via a simple GUI (see Figure 8.35). Designs can be saved and loaded as .MAT files, and displayed as MATLAB 3-D or 2-D graphics. The package

also allows the creation of movie sequences so that the dynamic behaviour of a mooring can be visualised. Mooring configurations can be plotted, as shown in Figure 8.36, and the components are also listed in detail in the MATLAB console window.

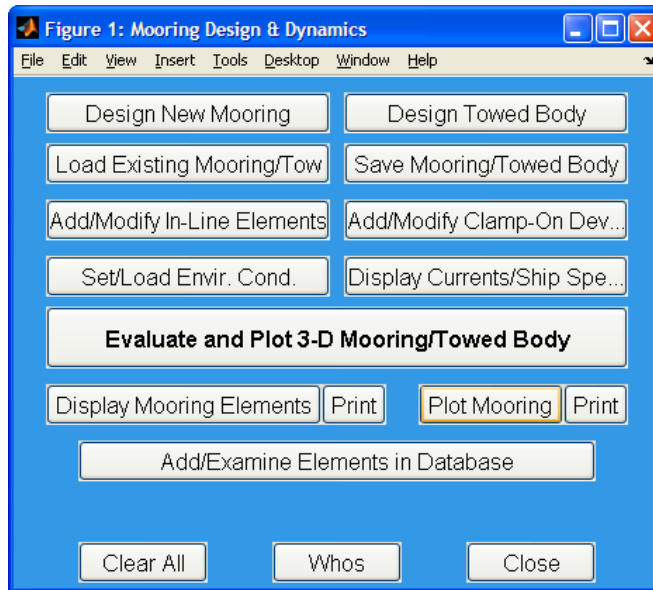


Figure 8.35: MDD's main GUI form.

The user can also enter current-depth profiles (i.e. a set of depth/speed/direction values), and wind profiles (speed and direction). The software uses this information to calculate the drag forces on the various elements of the mooring, in order to derive a steady-state solution for the mooring shape.

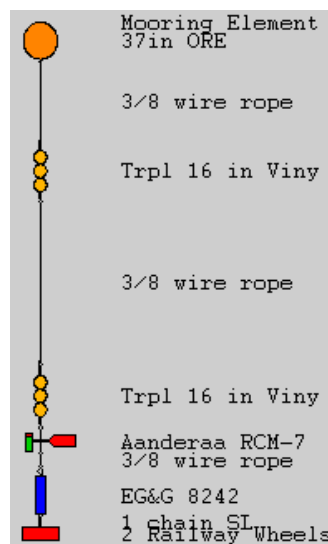


Figure 8.36: Typical mooring configuration (design view) in MDD.

MDD takes an iterative approach; it starts from a vertical configuration for the mooring and iteratively “moves” the mooring horizontally until a steady-state solution is reached. It can deal with time-varying inputs, i.e. a time-series of current-depth profiles can be provided as an input. When handling these time-series, it is assumed that the mooring has time to reach an equilibrium state between time-steps. In other words, the variation in the current is slow compared to the response time of the mooring. There are currently no detailed plans to extend MDD to include the action of wave forces.

MDD can produce any of the following outputs:

- Graphical plots of the steady-state shape of the mooring;
- Movie sequences showing the changing shape of the mooring in response to a time-varying current;
- Tension in each segment of the mooring;
- Final steady-state position of each component (horizontal and vertical);
- Final angle of each component to the vertical;
- Anchor mass required;
- Adequacy of buoyancy elements in maintaining vertical position of the mooring.

Key findings - MDD

MDD is designed as a stand-alone, self-contained mooring design package. It is not designed to interact dynamically with other software. In principle, as the MDD m-files are freely available, it would be possible to modify it so that it could be used as a mooring-force calculation module for a wind turbine package, but this would not be straightforward. Also it only produces what are effectively steady-state solutions, which are suitable for slowly-varying forces like those from wind or currents, but would not be appropriate for wave-induced forces.

MDD as it currently exists is not suitable as a mooring analysis module for interfacing with wind turbine codes. Its most serious drawback is its inability to carry out a true dynamic analysis of moorings subjected to rapidly-varying (wave-induced) loads, which would require a considerable extension. The principles of the approach are similar and some components (e.g. drag force calculation algorithms) and some of the post-processing capabilities may be useful (in both the frequency and time-domain).

ROMEO

ROMEO is a mooring and riser analysis package produced by GL Noble Denton. It can perform both static and dynamic (frequency-domain) analysis in response to wind, wave and current loadings. Systems of up to 16 mooring lines are supported. Riser calculations are ignored here.

ROMEO carries out three types of analysis on a mooring system: static analysis, dynamic analysis (both wave-frequency and low-frequency) and then a quasi-static analysis which is a combination of the first two. The inputs for all analyses include the details of the moored device or ship, “no-load” mooring geometry, and environmental conditions.

Static analysis

The environmental inputs for static analysis are steady wind and current forces. It is possible to enter current as a depth-dependent velocity profile. The algorithm uses Morison’s equation to calculate the drag on the mooring lines. This equation gives the inline force (i.e. force in the direction of the flow) on the mooring line element as

$$F = \rho V \dot{u} + \rho C_a V (\dot{u} - \dot{v}) + \frac{1}{2} \rho C_d (u - v) |u - v| \quad [8-13]$$

(i.e. the sum of Froude-Krylov force, hydrodynamic mass force, and drag force). It also calculates wind and current forces on the ship (or the WEC) using a simple drag equation as a function of cross-flow area, height coefficients and shape coefficients for the body in question. The coefficients are loaded in as part of the vessel definition file, so they have to be obtained externally. They are typically obtained either by manual estimation or, if higher accuracy is needed and there is no published data available for similar-shaped objects, they would be scaled-up from model tests.

The static analysis outputs consist of:

- steady-state shapes of mooring catenaries.
- steady-state (mean) position of the moored device.

Dynamic and quasi-static analysis

Dynamic analysis is carried out in the frequency-domain only. The following parameters are used to characterise the wave environment:

- significant wave height.
- zero up-crossing period.
- spectral shape factor (peak enhancement factor, γ).

- incident wave direction.

The user manual draws a distinction between wave-frequency and low-frequency analysis. The low-frequency effects are driven by both time-varying wind and longer-period wave activity

The outputs from dynamic analysis are:

- amplitude of the wave-induced motion of the moored vessel/device.
- maximum dynamically-induced tensions in the mooring lines.

Dynamic analysis is run after static analysis – the static phase gives the steady-state positions of all components, and these positions are then used as a starting-point for the dynamic analysis. Combining the static and dynamic results produces what is effectively a “quasi-static” analysis, i.e. a worst-case scenario in which the maximum dynamic displacement is added to the static displacement. This is primarily intended as a safety calculation to determine the minimum required breaking strain for mooring lines.

Key findings - ROMEO

The most serious limitation of ROMEO is the lack of any capability to conduct a time-domain dynamic analysis. This means that only frequency-domain simulations could be conducted. It may, however, be shown that a full time-domain solver is not necessary if the moorings package is to be used merely to establish the mooring configuration properties. As a frequency-domain tool ROMEO offers all the suitable functionalities.

AQWA

The ANSYS AQWA brand name covers an entire suite of tools:

- The AQWA Graphical Supervisor – this is the GUI which is used to control operations and allow the user to interact with other tools in the suite. It includes graphical renderings of the system being modelled, plotting facilities for output data, export to spreadsheets, etc.
- AQWA-LIBRIUM – for steady-state equilibrium load calculations.
- AQWA-LINE – for wave loading calculations (regular waves only).
- AQWA-FER – wave loading in irregular waves (frequency-domain only).
- AQWA-NAUT – time-domain analysis of floating body (or several bodies) in either regular or irregular waves. Includes several different types of basic mooring-line model and a cable dynamics module as an optional add-on.
- AQWA-DRIFT – time-domain modelling of long-period loads under irregular wave conditions. Complementary to AQWA-NAUT which deals with the wave-frequency loads.
- AQWA-WAVE – A link between AQWA-LINE and external FEA packages.

AQWA-LINE

AQWA-LINE can be used as a stand-alone tool for some types of wave-loading calculations, or as a pre-processor which calculates hydrodynamic coefficients for use by other products in the AQWA suite. The main analysis technique used in this code is Radiation/Diffraction theory. It can calculate both wave-frequency forces and second-order drift forces in regular waves. The Quadratic Transfer Function (QTF) matrix for second-order drift forces can also be passed on to AQWA-DRIFT for a full time-domain analysis in irregular waves.

AQWA-LINE only handles regular waves, but can take account of current and wind forces as well. It calculates the wave response of the structure in the frequency-domain and stores them as a set of RAOs for a range of different frequencies. These can be subsequently used by other tools such as AQWA-NAUT.

AQWA-NAUT

AQWA-NAUT is a time-domain analysis program for modelling the motion of large floating bodies in ocean waves. It deals with both regular and irregular waves, and can also include the effects of current and wind in the model. AQWA-NAUT does not calculate the effects of wave drift forces – AQWA-DRIFT is required for that. It can be used as a stand-alone tool or with AQWA-LINE as a pre-processor. It solves the second-order differential equations of motion and uses a “two-stage predictor-corrector” integration scheme to derive a time-history from the solutions.

AQWA-NAUT uses linear hydrodynamic coefficients for the various degrees of freedom at different frequencies, supplied by AQWA-LINE or an equivalent code, along with other hydrostatic and hydrodynamic information. In regular waves, RAOs are used to calculate the time-domain response of the device in waves of a given

frequency. The hydrostatic and Froude-Krylov forces are normally calculated by AQWA-NAUT itself, and used in conjunction with the linear coefficients to build up a complete envelope of the loadings and motions of the body. As part of the process, AQWA-NAUT requires a mesh of the body's surface to be built. Four different wave models are available for calculating the Froude-Krylov forces:

1. Linear wave theory – deep-water
2. Linear wave theory – finite depth
3. Second-order wave theory – deep-water
4. Second-order wave theory – finite depth

The Froude-Krylov force on a submerged body (e.g. an element of mooring line) is due to the unsteady pressure field $p(x,y,z,t)$ produced by undisturbed waves, which is calculated in different ways according to the type of wave model used.

AQWA-NAUT can model the interactions between floating bodies in an array (including radiation-coupling and shielding effects), for up to 20 bodies. This is a total number of bodies, thus if a FOWT platform has e.g. 3 bodies, arrays of up to six FOWTs can be modelled.

Moorings

In the core code of AQWA-NAUT, moorings are modelled as either linear or nonlinear cables. Five linear cable models are available:

- Linear elastic cables.
- Winch cables.
- Constant force cables.
- Pulleys.
- Drum winch cables.

Of these five, the one which may be of most interest for modelling FOWT platforms is the linear elastic cable, assuming that winches, pulleys etc will not be used as frequently. The linear elastic cable is basically modelled as a linear spring. Constant-force cables may also be useful for highly simplified mooring models where cable details are not available.

The following nonlinear cable models are also available:

- Nonlinear steel wire: allows modelling of the nonlinear properties of steel wire.
- Nonlinear elastic hawsers: These are treated as nonlinear springs, whose force-extension curve is represented by a polynomial (up to 5th order).
- Composite catenary lines: the lines themselves can be elastic, and the loading effects due to the catenary shape are also modelled.
- Clump weights and buoys: these can be added to the line model.

Wave and current forces on mooring lines are ignored in all the above types of mooring model, unless the "Coupled Cable Dynamics" module is used. This module has a dedicated user-interface window (see Figure 8.37), and allows the code to model mooring cables more realistically by calculating the drag and inertia (including added-mass) forces on the cable. In the absence of the Cable Dynamics module, it is still possible to model the effects of wave and current drag on mooring cables in AQWA-NAUT, using the "Slender Tube" (STUB) Morison element. For both of these latter approaches, the cable is divided into a number of rod-type elements and the force on each element worked out separately. The hydrodynamic force on an element of cable, in the direction perpendicular to the element's axis, is given by

$$dF = \frac{1}{2} \rho D C_d (u_f - u_s) |u_f - u_s| + \rho A C_m \dot{u}_f - \rho A (C_m - 1) \dot{u}_s \quad [8-14]$$

(drag force) (wave force) (inertia force)

(The "inertia force" is effectively an added-mass term.)

where

C_d = drag coefficient

D = effective cable diameter for drag purposes

- U_f = fluid velocity perpendicular to element axis
- U_s = cable element's own velocity perpendicular to element axis
- C_m = inertia coefficient
- A = effective cross-section area (for a chain which does not have a uniform cross-section, this is actually the volume of a unit length of cable)
- ρ = water density

These hydrodynamic forces are combined with the other loads on the cable (inertial / gravitational / tension loading) and then forces on all the elements are used to model the overall dynamic behaviour of the cable.

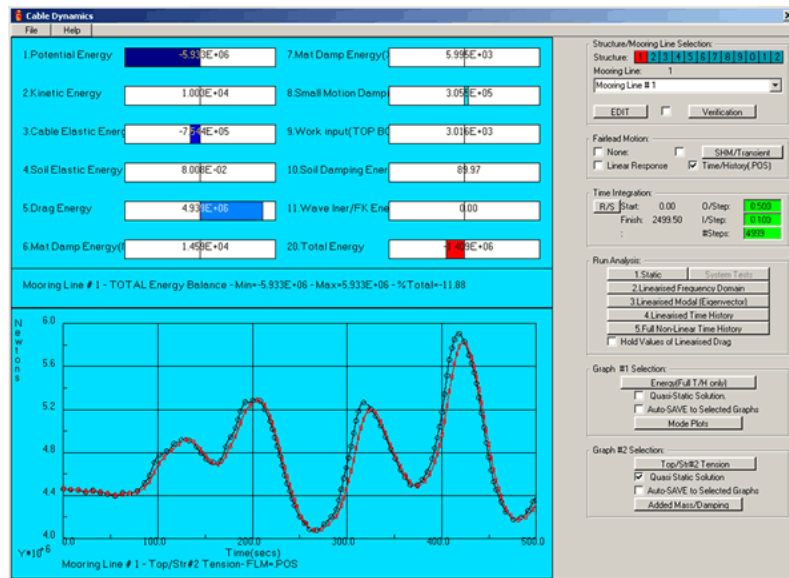


Figure 8.37 User interface window for the optional Coupled Cable Dynamics module in AQWA-NAUT.

Key findings - AQWA

The conclusion drawn from the above is that AQWA-NAUT, in combination with WAMIT or AQWA-LINE, would be a suitable tool for a comparison exercise with the look-up table or quasi-static approach. It can model mooring lines using Morison elements, which means a useful comparison can be made.

OrcaFlex

OrcaFlex is a dedicated “marine dynamics” analysis package produced by Orcina Software. It covers moorings and risers, as well as towing systems. OrcaFlex can carry out full modal, static and dynamic analysis in the time-domain. It supports a wide range of wave models as well as drift forces, wind drag, currents etc. The software has a Windows UI which includes animated or static 3-D graphical displays, including some quite realistic rendering. OrcaFlex can also be run in non-interactive (batch) mode.

There is an interactive click-and-drag type UI which allows the user to build up a model in a fairly intuitive way. Objects such as vessels, buoys, mooring lines etc. can be added from a library of predefined objects or custom-defined by the user. Environmental conditions (wind, waves, currents) can be similarly defined and added to the model. When a model has been completed a simulation is started. The behaviour of the model during the simulation can be visualised on the animated 3-D view window. Output quantities (load, motions, etc) can be sampled at user-defined intervals during the simulation and output to a file. Outputs can be easily imported to Excel, etc. for further processing. OrcaFlex also has its own graphical display function.

Theoretical aspects

The code supports a wide range of different wave models, including regular and irregular waves (four standard wave spectra are supported), and both linear and nonlinear waves. Wave drift forces are also available (in contrast to AQWA). Hydrodynamic forces on the mooring lines and the moored device are derived using an extended form of Morison’s equation. Mooring lines are modelled on a finite-element basis; each line is divided

into a number of straight-line elements each with a clump weight, buoyancy and drag. Figure 8.38 shows the coordinate frame of a line element. Each element is treated as a stiff massless rod with a telescopic sliding joint in the centre, so that it can change in length (and can also twist around its own axis). The user is given the option of specifying both stiffness and damping coefficients for the following degrees of freedom:

- Axial deflections (changes in the length of the rod element).
- Torsional deflections about the rod element's central axis. This means one end of the element twisting relative to the other end.
- Bending deflections (changes in the relative angle between the rod element and its immediate neighbouring elements).

N.B. The damping discussed above is only for the cable itself; external (hydrodynamic) damping is treated separately and is discussed below.

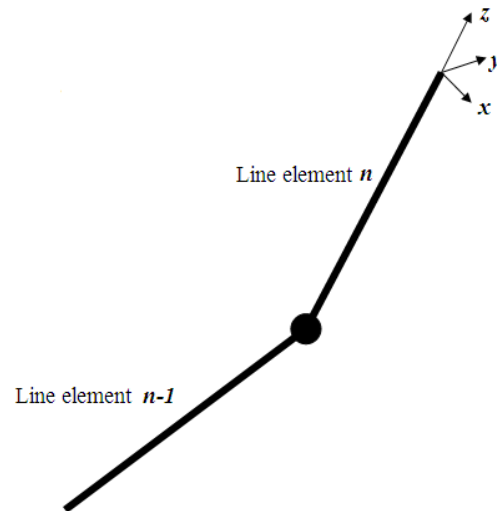


Figure 8.38: Line element representation in Orcaflex, showing the element's frame of reference.

The tension in each element of the line is given by the relation

$$T_e = EA\varepsilon + EAe \frac{(dL/dt)}{L_0} \quad [8-15]$$

where:

T_e = effective tension.

EA = axial stiffness of line (i.e. Young's modulus x effective cross-section area).

ε = mean axial strain = $(L - \lambda L_0) / (\lambda L_0)$.

L = instantaneous length of segment.

λ = expansion factor of segment.

L_0 = unstretched length of segment.

e = numerical damping of the line, in seconds.

Hydrodynamic drag forces on the line are found using a choice of three different relations, all based on Morison's equation. Drag forces are applied both in water and optionally also in air (wind forces). The same relations are used for both water and air, with appropriate values for fluid density. The three available relations are as follows:

- Standard formulation – the most commonly used; suited to general flow conditions.
- Pote formulation – preferred by some modellers for situations where flow is nearly tangential to the line.
- Eames formulation – sometimes preferred for bare (unsheathed) mooring cables.

As far as the wave-induced forces on the floating bodies are concerned, OrcaFlex relies on an external code (AQWA and WAMIT are the ones it explicitly supports) to provide the hydrodynamic coefficients. The following data can be imported from an external hydrodynamic solver:

- Displacement RAOs (amplitude and phase).
- Load RAOs.
- Quadratic transfer functions (QTFs) for wave drift calculations.
- Added-mass and damping coefficients.
- Hydrostatic stiffness.

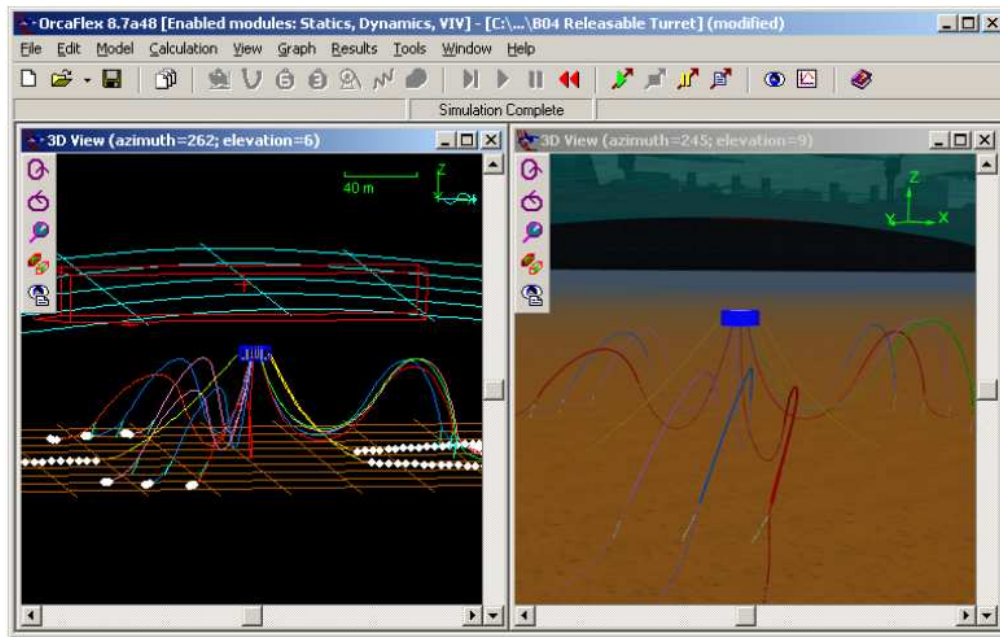


Figure 8.39: OrcaFlex screenshot showing both wire-frame and shaded 3-D views.

Key findings - Orcaflex

OrcaFlex is suitable for comparison with the look-up table approach because of the contrasting modelling method (mooring lines are modelled by means of Morison elements). It has all the necessary functionality to produce a sufficiently detailed simulation of the floating platforms and their moorings.

8.3.2 Simulation results: MBS approach

An approach for modelling mooring lines originally described by Kreuzer and Wilke for oil platforms [116], is to divide the mooring line into rigid (or flexible, modal reduced) multi-body elements connected by spring-damper elements. The line seabed interaction is modelled with a coulombic friction element including spring and hysteresis characteristics as a function of the translational forces. This MBS approach is currently investigated by Matha et al and Azcona. A multi-purpose commercial Multi Body code (Simpack) has been extended to model offshore floating wind turbines. An originally implemented quasi-static mooring line model (NREL's HydroDyn) has been replaced by a MBS based model. With this approach, no interface between separate programs is necessary since the turbine's structure and mooring lines are modelled within one code using the same mathematical MBS formulation. This MBS formulation is numerically stable and also allows for a simple implementation of line-seabed interaction, required for catenary systems. First results for the OC3-Hywind spar buoy in 320m water depth show significant differences in the floating WT system's response between both modelling approaches.

The MBS-model is built up of three mooring lines which are discretized into separate rigid bodies. Every single body is modelled as a cylindrical structure and has the gross properties of the particular part of the mooring line it represents. They are connected by spring-damper-elements to simulate the extensional stiffness and the ac-

cordant damping by using the linear beam theory. Although this is a significant simplification of the structural arrangement of the line's fibers, it is necessary to reduce the model's complexity and thereby simulation time. Using chain mooring lines, this stiffness and damping could be neglected.

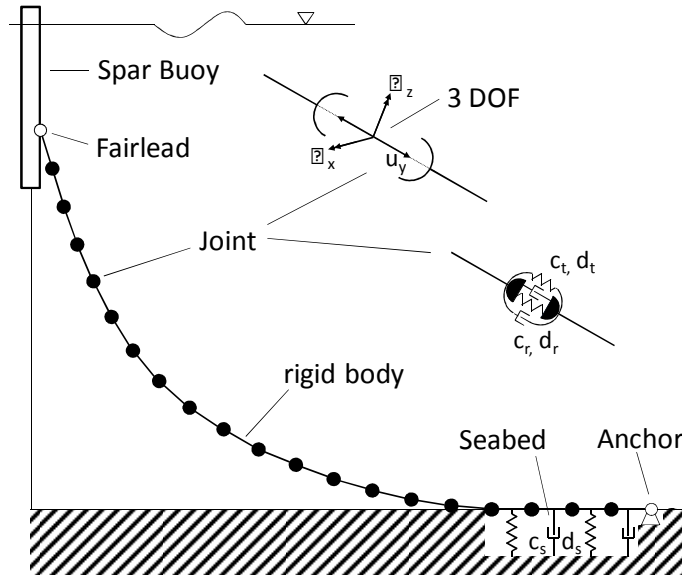


Figure 8.40: MBS mooring line configuration

The degrees of freedom (DOF) are reduced to a minimum of one translational and two rotational directions. To enable the simulation of the line's elongation the DOF in cylinder's longitudinal direction has to be maintained. Also the transverse rotational movements have to be enabled. The line's twist DOF could be eliminated because there is no significant effect on the hydrodynamic behaviour due to the use of symmetric cylinders for discretization.

The very complex behaviour of the seabed is reduced to a unilateral spring-damper-model with high stiffness and damping to represent a rigid floor. The lateral friction is modelled by a simple coulombic element with an empiric friction coefficient.

The hydrodynamic effects to the mooring line are represented by a variation of the Morison-Equation. Østergaard and Schellin describe this variation for slender hydrodynamic transparent cylindrical structures with arbitrary orientation to the current of the surrounding fluid.

$$F = \int_{-l_s/2}^{l_s/2} \left(\rho \frac{\pi D^2}{4} \frac{\partial v_n}{\partial t} + c_d \rho \frac{\pi D^2}{4} \frac{\partial u_{rn}}{\partial t} + c_m \rho \frac{D}{2} |u_{rn}| u_{rn} \right) ds$$

Where v is the fluid's velocity, u_r the relative velocity between structure and fluid and index n the normal direction to the segment. The drag and inertia coefficients c_d and c_m are chosen empirically which could lead to further uncertainties. By using the potential theory the Morison-Equation considers hydrodynamic drag and inertia but neglects effects based on dissipative flow, like vortex induced vibrations.

Investigations of the discretization show only small effects on the results when increasing the number of elements beyond a certain number of discretized elements. This number has to be identified by a sensitivity analysis. Following this procedure enables to come up with a moderate discretization and limit simulation time while keeping accuracy of the results.

Comparisons in Figure 8.41 of the platform's surge motion to quasi-static models show significant differences caused by the non-linear additional hydrodynamic damping of the MBS model. Accordingly, similar differences in the fore-aft bending moment at the tower base can be identified in Figure 8.42.

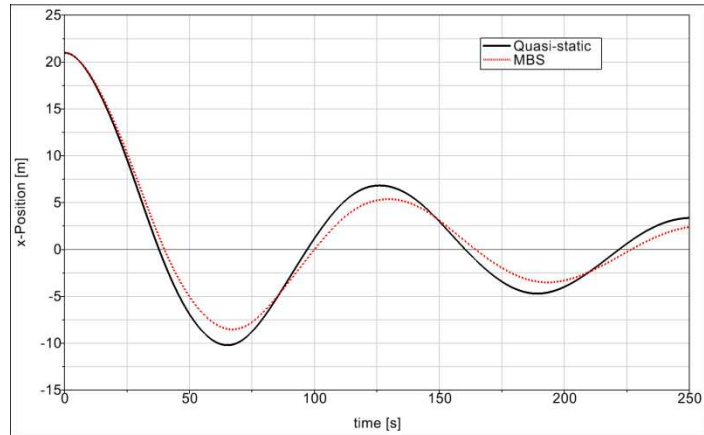


Figure 8.41: Time series of OC3-Hywind platform translation in surge direction with MBS and quasi-static mooring system

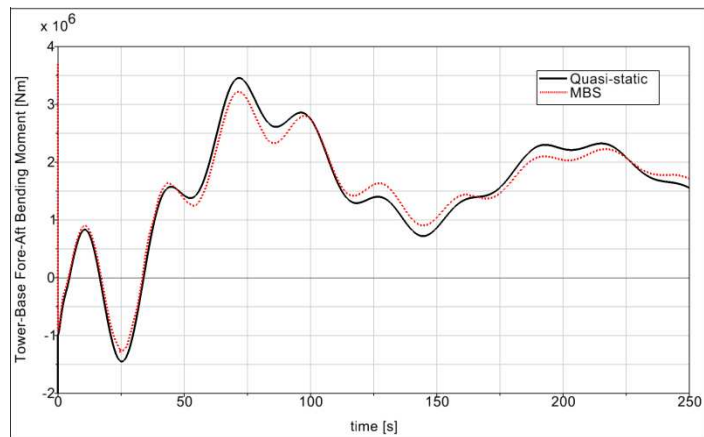


Figure 8.42: Time series of OC3-Hywind Tower Base My with MBS and quasi-static mooring system

9. Development of design requirements

9.1 Literature review of floating offshore standards

A literature review of current design standards relevant to offshore floating structures has been performed, together with comments on applicability to floating offshore wind turbines (FOWT), in order to provide input for the standardization of floating wind turbines.

GL Guidelines 2005 – Guideline for the Certification of Offshore Wind Turbines

Scope:

- Guideline applies to the design assessment and certification of offshore wind turbines and offshore wind farms.

Applicability for FOWT:

- Detailed requirements for design calculations. Description of load cases which cover design situations and external conditions. Is applicable for FOWT too. Extension to further specific requirements is under development with focus on stability requirements and mooring applications.
- Restrictions: specific requirements for FOWT (e.g. floating units, mooring) mainly as reference to GL Rules (cited below).

GL Rules for Classification and Construction 2007 - Part 6 Offshore Technology – Chapter 2 Mobile Offshore Units

Scope: Requirements for the different types of mobile offshore units as:

- Units connected to the sea bed by anchoring (mooring)
- Units kept on position by dynamic positioning/propelling system
- Units connected by legs in jacked up condition

Applicability for FOWT:

- Requirements for floating and anchored units. Contains mooring requirements
- Restrictions: No wind turbine specific design load case requirements

IEC 61400-3 - Guideline for Offshore Wind Turbines, Edition 1.0 International Electrotechnical Commission (IEC), Wind Turbines – Part 3: Design requirements of offshore wind turbines, 2009

Scope:

- Guideline for fixed offshore wind turbines

Applicability for FOWT:

- Detailed requirements for design calculations. Description of load cases which cover design situations and external conditions.
- Restrictions: No specific requirements for FOWT (e.g. floating units, mooring).
- Two extensions have been proposed: DNV - Commentary and amendments to IEC 61400-3 concerning offshore floating turbines ([117], also included in WP 1A1 as an Annex), and IEC TC88 proposal for new work item from Korean NC – Standard for floating offshore wind turbines [118].

DNV Energy Report: Guideline for offshore floating wind turbine structures, 2009

Scope:

- This provides requirements and recommendations for design floating support structures for offshore wind turbines.

Applicability for FOWT:

- Sections in the guideline made mostly reference to the DNV OS-J101, Design of Offshore Wind Turbine Structures, October 2007 and to other Rules for Offshore Structures
- Restrictions: Specific load cases for floating offshore wind turbines are still under development and some related aspects are briefly mentioned.

DNV OS-J101, Design of Offshore Wind Turbine Structures, October 2010

Scope:

- Guideline applies to the design assessment and certification of offshore wind turbines and offshore wind farms.

Applicability for FOWT:

- Detailed requirements for design calculations. Description of load cases which cover design situations and external conditions. Applicable for FOWT too. Extension to further specific requirements for FOWT is needed.
- Restrictions: specific requirements for FOWT (e.g. floating units, mooring) mainly as reference to Offshore Rules.

BV Guidance Note NI 572 DT R400 E, November 2010 – Classification and Certification of Floating Offshore Wind Turbines

Scope:

- This guidance notes gives requirements and recommendations for the classification of Floating Offshore Wind Turbines.

Applicability for FOWT:

- The load cases adopted for the design are defined on basis of the minimum load cases required by IEC 61400-3 or load combinations of Offshore Rules.

ISO 19904-1 - Petroleum and natural gas industries - Floating offshore structures - Part 1: Monohulls, semi submersibles and spars

Scope:

- Requirements and guidance for the structural design and/or assessment of floating offshore platforms used by the petroleum and natural gas industries. Reference to DNV-OS-C101.

Applicability for FOWT:

- General requirements for floating offshore platforms
- Restrictions: No specific wind turbine design load case requirements

ISO 19901-7 – Petroleum and natural gas Industries – Specific requirements for offshore structures – Part 7: Stationkeeping systems for floating offshore structures and mobile offshore units, 2005

Scope:

- This part of ISO 19901 specifies methodologies for the design, analysis and evaluation of stationkeeping for floating structures used by the oil & gas industries

Applicability for FOWT:

- General requirements for floating offshore structures
- Restrictions: No specific wind turbines design load case requirements

DNV-OS-C101 - Design of Offshore Steel Structures, General (LRFD method)

Scope:

- Provides design principles, technical requirements and guidance for the structural design of offshore structures. DNV-OS-C101 is the general part of the DNV offshore rules for structures.

Applicability for FOWT:

- General requirements for all offshore structures
- Restrictions: No specific wind turbine design load case requirements

DNV-OS-E301 - Position Mooring

Scope:

- Applicable to all types of floating offshore units including buoys

Applicability for FOWT:

- Specific guideline for mooring systems, e.g. applicable for FOWT
- Restrictions: n/a

API RP 2SK - Design and Analysis of Station keeping Systems for Floating Structures

Scope:

- Purpose is to present a rational method for analyzing, designing or evaluating station-keeping systems used for floating units.

Applicability for FOWT:

- Recommended practice with detailed guidance for moorings systems including design, analysis and operation.
- Restrictions: n/a

Other standards

API RP 2A-LRFD - Recommended Practice for Planning, Designing and Constructing Fixed Offshore Platforms - Load and Resistance Factor Design

API RP 2A-WSD - Recommended Practice for Planning, Designing and Constructing Fixed Offshore Platforms - Working Stress Design

API RP 2T - Recommended Practice for Planning, Designing and Constructing for Tension Leg Platforms

DNV-OSS-312 - Certification of Tidal and Wave Energy Converters

DNV-OS-C201 - Structural Design of Offshore Units (WSD method)

DNV-OS-C401 - Fabrication and Testing of Offshore Structures

ISO 19900 - Petroleum and Natural Gas Industries – General Requirements for Offshore Structures

ISO 19900-1 - Petroleum and natural gas industries - Specific requirements for offshore structures - Part 1: Metocean design and operating considerations

ISO 19902 - Petroleum and Natural Gas Industries – Fixed Steel Offshore Structures

9.2 Extensions to IEC 61400-3 standard for floating structures

The IEC 61400-3 standard specifies essential design requirements to ensure the engineering integrity of offshore wind turbines, in order to provide an appropriate level of protection against damage during the planned lifetime. The current edition of the standard is applicable to bottom-mounted offshore wind turbines only, and it is stated explicitly in the standard that the design requirements specified are not sufficient to ensure the engineering integrity of floating offshore wind turbines.

There are a number of design advantages to floating support structures for offshore wind turbines. The principal advantage is that floating support structures enable the use of deep water sites, which hugely increases the number of potential locations for offshore wind farms. There is also a decrease in the dependence of support structure design on site conditions, and therefore more opportunity for production at large scales. As suitable shallow water sites are used up it is expected that designers will increasingly investigate deep water sites which would require floating support structures. The projected increase in demand for floating wind turbines requires a corresponding development of the design standards and requirements, in order to ensure the engineering integrity of floating wind turbines.

Recommendations are presented for possible extensions to the IEC 61400-3 standard to enable applicability to deep-water floating wind turbine designs, including the implementation of additional/different design load cases.

Issues that need to be considered when defining DLCs for FOWTs include the following:

1. Potential large motions of the rotor-nacelle assembly. Influence of heave motion on air gap and rotor clearance needs to be revised.
For the majority of offshore wind turbines installed to date, the wind conditions have been the primary external consideration in the assessment of the structural integrity of the rotor-nacelle assembly (RNA) and marine conditions have been of much less importance. However, for floating wind turbines the dynamic properties of the support structure mean that the marine conditions will have a much greater influence on the RNA loads. The IEC 61400-3 standard currently states that the RNA may be designed to generic wind conditions, but that structural integrity of the RNA must be demonstrated by taking proper account of the marine conditions at each specific site where the offshore wind turbine will be subse-

subsequently installed. However, for wind turbines to be installed on floating platforms the marine conditions have a non-negligible influence on the structural integrity of the RNA. This means that the marine conditions need to be accounted for in the initial design of the wind turbine.

Preliminary results show that for spars or trifoat structures e.g. heel angles of up to 10° can occur. Due to this, relative motion has to be analyzed and mechanical parts have to be reviewed. The analysis requirements do not differ to those of floating structures of the oil & gas industry.

2. Inclusion of low-frequency components in wind and wave conditions shall be considered. These can be important in evaluating the sway motion of the mooring system.
3. The influence of the water depth on the heave eigenperiod is a crucial issue for platforms with compliant heave, roll and pitch modes. Increasing the water depth, the heave eigenperiod increases. The choice of the design water depth will be directly related to the environmental conditions, with the aim to avoid heave, roll or pitch resonance.
4. The relation between the heave and the roll/pitch eigenperiods shall be checked in order to avoid or at least to estimate the consequences of parametric excitations. For new concepts of floating wind turbines it must be ensured that the susceptibility of the structure to those parametric excitations and Vortex Induced Motions are unlikely to occur or can be avoided due to proper choice of operational conditions. Platforms with abrupt changes in the waterplane area and in metacentric height should be especially investigated.
5. Influence of wave drift forces on mean response e.g. for catenary moored systems shall be considered.
6. Influence of low frequency motions on the control system shall be analysed. The slow drift motions of the floating structure may interfere with the control system since their periods are in the typical range of coherent gust rising time.
7. Extension of the frequency range for wind/wave conditions to higher levels shall be taken into account. High frequency excitation forces, generally of small amplitude, may be of importance for floating platforms kept in place by tethers. The restrained modes (heave, roll and pitch) have eigenperiods below the typical wave periods between 5s and 15s. Those platforms can experience high order effects like springing (fatigue) and ringing. Ringing is understood as a natural frequency response of the structure due to the weak impact, caused by steep asymmetric waves. This shall be considered for the design assessment of TLPs.
8. Gust periods larger than 12 seconds shall be included in the analysis to cover the frequencies found from the dynamic analysis of floating offshore wind turbines.
9. Inclusion of two-peaked spectrum formulations that properly reflect the influence of swells is essential for the assessment of the mooring forces and the large period motion behaviour.
10. As mentioned in previous chapters the hydrodynamic and aerodynamic aspects of a FOWT are much more complex than fixed offshore wind turbines. Minimum requirements on simulation tools for the simulation of the coupled aero- and hydrodynamics of moored floating structures shall cover properly the different issues related to this. The main issues for the aerodynamics are the large amplitudes of low frequency motions combined with high heel angles. The wake formulation may have to be adapted for these high angles.
11. The complexity of the system may even require model tests in the basin to analyse the relative motion and impact load on deck structures. Until now no standard method to scale model tests for offshore wind turbines has been developed.
12. Simultaneous time simulations of wind, wave and current shall be necessary for proper fatigue analysis.

13. Longer simulation requirements and how this relates to wind/wave stationarity has to be discussed. Wind and sea spectra shall be extended to cover the requirements of simulations with proper time length. It is proposed to extend the minimum simulation time of every single time series from 10 to 20 minutes to capture slow drift motions. The total required simulation time at every wind speed bin, for e.g. DLC 1.1 to reach statistical convergence should not be less than 3 hours.
14. Importance of radiation and diffraction effects as well as wind/wave misalignment is to be considered on the hydrodynamic model. For some types of structures the radiation and diffraction forces have the same order of magnitude. As a result the Morison's equation neglecting the diffraction components is not applicable anymore. Enhanced panel methods may be applied. Hybrid formulations applying the drag forces according to the Morison's equation but including diffraction and radiation terms as analysed by classic methods may be a convenient solution for part of the hydrodynamic analysis.
15. Mooring and riser systems shall be considered as a new component with associated failure modes in the wave turbine concept design. Failure modes shall be considered in the turbine safety system with a following safety chain release (safety system activation) if threshold values are reached:
 - a. e.g. extreme heel angle during operation
 - b. vertical motion
 - c. extreme yaw of the floater
 - d. station keeping (deviation from reference point)
16. Condition monitoring systems may have to be extended to cover mooring specific issues (e.g. pre-tension control for taut moorings).
17. Ice loads can be important for the mooring systems and shall be further analyzed. The presence of ice will change the dynamics of a floating wind turbine considerably, as the significant horizontal displacement experienced by the structure under normal conditions will be impeded. This effect shall be considered for the design of floating wind turbines to be installed at sites where sea ice is expected to occur. This shall include guidance on modelling ice loads for floating turbines and possible extension of the ice design load cases.
18. Inclining, stability and watertight integrity requirements shall be considered **according to** the IMO intact stability code IS-Code 2008, unless other national regulations are mandatory on where the device will be installed. The unmanned platform should be treated as a pontoon. Damage instability is to be considered according to Offshore Rules and approved by National Authorities.
19. For transport ships that brings personnel to the site, the SPS-Code is to be applied, if no national regulations are mandatory. The IS-and the SPS-codes refer to the SOLAS document (definitions, etc...)
 - a. IS-Code 2008 International Code on Intact Stability, Res. MSC.267(85) adopted 2008
 - b. SPS-Code Code - Code of Safety for Special Purpose Ships, Res. MSC.266(84) adopted 2008
 - c. SOLAS Consolidated Edition, 2010 Consolidated text of the International Convention for the Safety of Life at Sea, 1974, and its Protocol of 1988: articles, annexes and certificates
20. Safety system, sensors for water in tanks, draft control, deck clearance shall be included. Alarm operator or activation of the safety system if threshold values are reached should be specified.
21. Safety factors (including non-redundant mooring systems) shall be considered for moorings. Guidance is given in ISO 19901-7.
22. For station keeping systems where no redundancy is available higher safety factors should be applied and need further consideration.
23. Assessment of seismicity may be of significant importance for design of tension leg platforms.
24. Ship impact loads due to normal operations should be revised, since more severe consequences are expected as for fixed offshore structures and due to the fact that two bodies are moving. Another issue

is related to the size of the service vessel that should be considered for load case definitions. It is expected that the vessels are larger than the ones used for fixed offshore wind farms.

Load Cases and Design Conditions

The load cases and design conditions can follow the structure of the GL Guidelines for Offshore Wind Turbines (shown below) or the IEC 61400-3 standard. Additional considerations from particular aspects of floating and moored structures, as listed on the previous paragraph, shall be considered in the specification of the design and operative conditions.

- Normal operation (DLC 1.x)
- Operation plus occurrence of faults (DLC 2.x)
- Start-Up, Stop (DLC 3.x, 4.x, 5.x)
- Parked / Standstill / Ready for operation (DLC 6.x)
- Parked / Standstill after occurrence of fault (DLC 7.x)
- Maintenance / Transportation / Repair (DLC 8.x)

Limit States: Examples

Possible resulting limit states for FOWTs from the above Guidelines are listed below and in Table 9.1. Especially the accidental and the serviceability limit states with requirements for the stability of the motions and cares about floatability and leakage shall be considered.

Ultimate limit state:

- Normal operation plus occurrence of fault
- Emergency stop procedures
- Extreme environmental conditions (current, wind, wave, sea ice, temperatures)
- Parked / standstill after occurrence of fault
- Line tension limit

Fatigue limit state:

- Normal operation
- Start / Normal stop procedures
- Parked / standstill due to non-availability reasons

Accidental limit state:

- Loss of station keeping e.g. anchor or mooring line (free drifting)
- Collision, ship impact

Serviceability limit state:

- Floating structure offset
- Hydrodynamic stability
- Motions
- Floatability
- Leakage
- Clearance requirements for mooring of different structures

Table 9.1: Possible Resulting Limit States

Limit State	Design Condition	DLC
ULS	Normal operation, operation plus occurrence of fault	DLC 1.x, 2.x, 3.x
	Normal and emergency stop procedures	DLC 4.x, 5.x
	Extreme environmental conditions (current, wind, wave, sea ice, temperatures)	DLC 1.5, 1.6, 1.8, 6.x
	Parked / standstill	DLC 6.x
	Hydrodynamic stability	all DLCs
	Transport, erection, maintenance and repair	DLC 8.x
FLS	Normal operation	DLC 1.2
	Start / normal stop procedures	DLC 2.3, 3.1, 4.1

	Parked / standstill due to availability reasons	DLC 6.4, 7.2
SLS	Hydrodynamic stability	all DLCs
	Motions	all DLCs
	Floatability	all DLCs
	Leakage, water on deck, openings	
	Limitation of the movement (blade deflection)	
ALS	Loss of station keeping (free drifting)	
	Ship impact	

Safety Factors

Table 9.2 gives a comparison of the current safety factors adopted in the existing standards GL Guidelines for Offshore Wind Turbines [31] and IEC 61400-3 [69]. Table 9.3 summarises the limit states and safety factors of different standards, together with the associated return periods. Table 9.4 gives assumptions for environmental conditions (return periods) associated with different design conditions.

Table 9.2: Safety Factors: Guidelines GL Offshore Wind Turbines 2005 and IEC 61400-3

Limit State	Design Condition	GL 2005 Offshore Wind Turbines	IEC 61400-3 Offshore Wind Turbines, Edition 1
ULS	Normal operation plus occurrence of fault	1,10 / 1,20	1,10 / 1,35
	Emergency stop procedures	1,20	1,35
	Extreme environmental conditions (wind, wave, sea ice, temperatures)	1,35	1,35
	Parked / standstill	1,35	1,35
	Parked / standstill after occurrence of fault	1,10	1,10
FLS	Normal operation	1,00	1,00
	Start / Normal stop procedures	1,00	1,00
	Parked / standstill due to availability reasons	1,00	1,00
SLS	Elastic deflections	1,00	n/a
ALS	n/a	n/a	n/a

It should be emphasized that safety factors for floating wind turbines should be assessed based on existing experience from various offshore standards, combined with consideration of:

- Reliability level required
- Uncertainties in loads, resistances and models used to calculate characteristic load effects and load bearing capacities
- Computational models required / recommended for calculation of loads and load bearing capacities

Table 9.3: Guidelines: Safety Factors vs. Limit States

Guideline	Limit State				Return period	Remarks
	ULS	FLS	SLS	ALS		
GL 2005 - Offshore Wind	1.1 to 1.35	1,00	1,00	n/a	50 years	Load safety factors Metallic materials - ULS: $\gamma_M = 1,1$; FLS: 1,0 to 1,25, depending on position and importance FRP materials – ULS: 2,3 to 2,65 FLS: 1,485 to 2,35, depending on manufacture and type
GL 2007 - Part 6 Offshore Technology – Chapter 2 Mobile Offshore Units	1,1 to 1,67	1,0 to 1,35	1,00	1,05 to 1.15	100 years	Global safety factors for working stress design
GL 2007 - Part 6 Offshore Technology – Chapter 2 Mobile Offshore Units Position Mooring	1.8 to 2.7	n/a	n/a	1.25 to 1.8	100 years	
IEC 61400-3 - Guideline for Offshore Wind Turbines, Edition 1	1,1 to 1,35	1,0	n/a	n/a	50 years	
ISO 19904 - Petroleum and natural gas industries - Floating offshore structures - Part 1: Monohulls, semi submersibles and spars	Refers to DNV-OS-C101					
DNV-OS-C101 - Design of Offshore Steel Structures, General (LRFD method)	1.0 to 1.3	1,00	1,00	1,00	100 years	Load safety factors for LRFD
DNV-OS-E301 - Position Mooring	1.1 to 2.5	n/a	n/a	1.0 to 1.35	100 years	VIM* ¹ may be neglected
ISO 19901-7 – Petroleum and natural gas industries Part 7: Stationkeeping systems for floating offshore structures and mobile offshore units.	1.2 to 2.0	3.0	n/a	1.0		

¹ VIM = vortex induced motions

Table 9.4: Load Groups for Design

Load Group	Design Condition	Environmental Conditions	Recurrence Period	Limit State
I	Normal operation, parked	Extreme	≤ 50 years	ULS, SLS
II	Operation, emergency stop, fault occurrence, parked after fault	Normal	≤ 1 year	ULS, FLS, SLS
III	Installation, maintenance and recovery	To be defined by the designer	-	ULS
IV	Secured/Parked during installation	Normal	≤ 1 year	ULS, FLS

10. Conclusions

The enhancement of design tools and methods and the development of dedicated international standards are essential for the progression of the offshore wind industry. As water depths increase and support structure solutions become more complex, it is important that the design methods and standards are improved and updated to reflect this. Enhancing design tools and methods enables a more accurate and detailed prediction of loads and dynamic response, which in turn leads to more optimised structures and therefore cost savings. Improved efficiency in the design process of complex support structures facilitates upscaling as it assists with the large-scale implementation of big offshore wind farms in deep water. Reviewing and updating the international design standards to ensure they are in line with industry best practice improves the reliability of offshore support structure design.

The development of integrated design tools for both bottom-mounted and floating structures is presented. Benchmarking activities are also presented for these design tools. For the benchmarking of the bottom-mounted design tools Flex5-Poseidon, GH Bladed and AdCOS-Offshore, the mass and frequency comparisons and overall trends of time series show good agreement. Small shifts are found in phase and magnitude, which can be explained through differences in operating conditions and wave modelling. For the benchmarking of floating design tools the results from Phase IV of the OC3 project are reviewed. Differences are found between some of the codes in their prediction of structural and aerodynamic damping, which can be explained through differences in modelling techniques. In one code a controller-induced instability in the surge mode was discovered at the surge natural frequency with no waves. With waves present this instability is damped out by wave radiation, indicating the importance of using potential flow based solutions for the analysis of floating support structures.

An advanced technique for modelling joints in braced support structures, the super-element technique, is presented. A study is performed using a wind turbine mounted on a tripod support structure, with comparisons drawn between a basic beam model of the tripod support structure and a model of the tripod including beams and super-elements. Results from a full system modal analysis show some of the important natural frequencies shifting towards the excitation ranges when super-elements are included. Results from time domain simulations show some increases and some decreases in DEL with super-elements included. However, the largest changes of DEL with significant values show a clear tendency of decreased moments using the super-element model.

The development of advanced modelling techniques for the numerical simulation of aerodynamic, hydrodynamic and mooring line effects for floating wind turbines are presented.

Regarding aerodynamics, improvements are required for simulation tools to capture all the possible relevant effects. BEM is used in the majority of floating simulation tools, but is insufficient since in theory BEM does not model aerodynamic effects such as wake interaction; yawed inflow; dynamic stall; and other aeroelastic effects such as flutter which are more important for floating wind turbines. Potential flow methods, CFD and improved BEM correction models tuned for floating wind turbines are investigated.

Regarding hydrodynamics, potential flow theory must be used to take proper account of the influence of the floating body on the surrounding fluid. Second-order effects such as mean drift, slow drift and sum frequency forces may also be more important. A comparison is performed between first and second-order hydrodynamic excitation forces for two floating wind turbine concepts, a spar-buoy and a semi-submersible. The results show that second-order effects are more important for the semi-submersible, as the structure is less hydrodynamically transparent. For this structure second order effects are dominant over first-order effects for all modes except heave, and are more important when waves are smaller and less steep.

Regarding mooring line dynamics, a number of modelling methods are available including the look-up table approach, the quasi-static approach and the full dynamic approach. The central issue is whether or not it is acceptable to neglect the dynamic effects of mooring lines for floating wind turbines. Simulations are performed comparing the quasi-static approach with a multi-body approach for a wind turbine mounted on a spar-buoy floating platform. Results show significant differences between the two methods due to additional non-linear hydrodynamic damping in the MBS approach.

Recommendations are presented for the implementation of a reduced set of design load cases for the preliminary design of jacket support structures. Two methods are presented for the fatigue load analysis: a simplified

method assuming wind and waves aligned which is fast but conservative; and a more precise method accounting for full directionality of wind and waves which is less conservative but requires more effort. A reduced set of extreme load cases assumed to drive support structure design is also presented.

A design load case parameter analysis for jacket support structures is performed, to test the relative influence of a number of key design load case parameters affecting offshore wind turbine jacket support structure design. The results show that the fatigue loading of the jacket is dominated by wind loads, with a relatively low contribution from hydrodynamics. This is shown by small changes in DEL when marine parameters are varied, compared to large changes in DEL when wind parameters are varied. The parameter which has the most effect on fatigue loading is the natural frequency of the structure, which demonstrates the importance of placing the natural frequency in the right range when designing a jacket support structure. The parameter which has the most effect on the extreme loading on the structure is the wave period of the 50 year maximum wave. Conservative load results are given when this parameter is set to the lower bound of the range given in the standard.

A review of the IEC 61400-3 standard is presented, including contributions from researchers, consultants, manufacturers and developers. Recommendations for the development of future editions include a review and simplification of the design load case table, and more detailed guidance regarding site-specific requirements to allow for site variability, for example the assessment of soil conditions.

A reliability-based calibration of safety factors for the fatigue design of offshore wind turbine support structures is presented. The study shows that for fatigue critical details where fatigue load is dominated by wind, FDF values of 2.5 are required. Slightly higher values are required if the wave load is dominating. A significant reduction in the required FDF values can be obtained if good inspection quality is used and e.g. 3 inspections are performed during the design lifetime.

A literature review of current design standards relevant to floating offshore wind turbines is performed, and recommendations are presented for possible extensions to the IEC 61400-3 standard to enable applicability to floating wind turbines. These include considerations for defining additional design load cases, as well as limit states and safety factors.

References

- [1] Fischer, T. – *Final report Task 4.1: Integration of support structure and wind turbine design*, UpWind deliverable D4.1.5, 2011
- [2] De Vries, W. et al. – *Final report Task 4.2: Support structure concepts for deep water sites*, Upwind deliverable D4.2.8, 2011
- [3] Fischer, T., De Vries, W. and Cordle, A – *Executive Summary, WP4: Offshore Foundations and Support Structures*, UpWind project 2011
- [4] Hald, T., Hogedal, M. - *Implementation of a finite element foundation module in Flex5 using Craig-Bampton substructuring*, Offshore Wind Conference, Copenhagen, 2005
- [5] Seidel, M., Mutius, M. von, Rix, P., Steudel, D. - *Integrated analysis of wind and wave loading for complex support structures of offshore wind turbines*, Offshore Wind Conference, Copenhagen, 2005
- [6] Passon, P. - *Aero-elastic design tool for bottom-mounted offshore wind turbines*, Deliverable D4.3.2, Upwind work package 4, 2008
- [7] Kaufer, D., Cosack, N., Böker, C., Seidel, M., Kühn, M. - *Integrated analysis of the dynamics of offshore wind turbines with arbitrary support structures*, European Wind Energy Conference, Marseille, 2009
- [8] Kühn, M. et al. - *Joint technology development for offshore wind turbines – the OWEA project at “alpha ventus”*, Conference paper, DEWEK, Bremen, 2008
- [9] Bossanyi, E.A. - *GH Bladed Theory Manual*, 2009
- [10] Bossanyi, E.A. - *Bladed Theory Manual Version 4.0*, October 2010
- [11] Kleinhansl, S.; Mayer, M. and Mangold, A. - *ADCoS - A Nonlinear Aeroelastic Code for the Complete Dynamic Simulation of Offshore- Structures and Lattice-Towers*, DEWEK 2004
- [12] Reese, L. C.; Cox, W. R. and Koop, F. D. - *Analysis of laterally Loaded Piles in Sand*, Offshore Technology Conference, 1974
- [13] API RP 2A-LRFD - *Planning, Designing and Constructing Fixed Offshore Platforms - Load and Resistance Factor Design*, American Petroleum Institute (API), 1993
- [14] Vorpahl, F. R.; Huhn, H.; Busmann, H. and Kleinhansl, S. - *A Flexible Aero-elastic Simulation Approach for Offshore Wind Turbines*, European Offshore Wind Conference (EOW), 2007
- [15] Passon, P., Kühn, M., Butterfield, S., Jonkman, J., Camp, T., Larsen, T.J. - *OC3 – Benchmark Exercise of Aero-Elastic Offshore Wind Turbine Codes*, 1995
- [16] Nichols, J. et al. - *Offshore Code Comparison Collaboration within IEA Wind Annex XXIII: Phase III Results Regarding Tripod Support Structure Modeling*, 47th AIAA Aerospace Sciences Meeting, 2009
- [17] Jonkman, J. et al. - *Offshore Code Comparison Collaboration within IEA Wind Task 23: Phase IV Results Regarding Floating Wind Turbine Modelling*, EWEC 2010
- [18] Jonkman, J., Musial, W. et al. - *IEA Wind Task 23 Offshore Wind Technology and Deployment, Subtask 2: The Offshore Code Comparison Collaboration (OC3)*, March 2010
- [19] Vorpahl, F. R. et al. - *Validation of a Finite Element Based Simulation Approach for Offshore Wind Turbines within IEA Wind Annex XXIII - Simulation Challenges and Results for a 5-MW Turbine on a Tripod Substructure*, Proceedings of the Nineteenth International Offshore and Polar Engineering Conference, 2009
- [20] Vorpahl, F. R., Strobel, M., Busmann, H. and Kleinhansl, S. - *Superelement approach in fully coupled offshore wind turbine simulation: Influence of the detailed support structure modelling on simulation results for a 5-MW turbine on a tripod substructure*, Proceedings of the Twentieth International Offshore and Polar Engineering Conference, 2010
- [21] Tarp-Johansen, T.-J., Agyriadis, K., Carstens, H., v.d. Tempel, J., Camp, T., Cheng, P.W. and Passon, P. - *Irregular, non-linear wave loading of offshore wind turbines: Review of modelling approaches and their relevance for future designs*, UpWind deliverable D4.3.1, 2008
- [22] Cordle, A. – *Interim review of IEC 61400-3 edition 1*, UpWind deliverable D4.3.3, May 2009
- [23] Tarp-Johansen, N.J. - *Clarification of Design Load Case Table*, January 2008.
- [24] Gjerding, Jens B. - *IEC 61400-3 SLS-load for Offshore Wind Turbine Support Structure*, December 2007.
- [25] API Recommended Practice 2A-WSD (RP 2A-WSD) Twentieth Edition, July 1, 1993 - *Recommended Practice for Planning, Designing and Constructing Fixed Offshore Platforms – Working Stress Design*.
- [26] Det Norske Veritas, CN 30.5 - *Environmental Conditions and Environmental Loads*, Classification Notes No. 30.5, March 2000.
- [27] Dong Energy - *Appendix A: Dong Energy method for estimating hydrodynamic coefficients accounting for appurtenances and marine growth on an offshore monopile foundation*.
- [28] ISO 19902:2007, *Petroleum and Natural Gas Industries – Fixed Steel Offshore Structures*

- [29] Sørensen, J.D. - *Reliability-based calibration of fatigue safety factors for offshore wind turbines*, Proc. ISOPE-2011, Maui, Hawaii, 2011
- [30] IEC 61400-1 ed. 3 - *Wind turbine generator systems – Part 1: Safety requirements*, 2005
- [31] Germanischer Lloyd, *Guideline for the certification of offshore wind turbines*, 2005
- [32] DNV OS-J-101, *Design of offshore wind turbine structures*, 2007
- [33] EN 1993-1-9, Eurocode 3: *Design of steel structures - Part 1-9: Fatigue*, 2005
- [34] Sørensen, J.D., S. Frandsen and N.J. Tarp-Johansen: *Effective Turbulence Models and Fatigue Reliability in Wind Farms. Probabilistic Engineering Mechanics*, Vol. 23, pp. 531-538, 2008
- [35] Faber, M.H., Sørensen, J.D., Tychsen, J. & Straub, D.: *Field Implementation of RBI for Jacket Structures. Journal of Offshore Mechanics and Arctic Engineering*, Vol. 127, pp. 220-226, 2005.
- [36] JCSS PMC: *JCSS Probabilistic Model Code. Resistance models: Fatigue models for metallic structures.* [www: http://www.jcss.ethz.ch/](http://www.jcss.ethz.ch/), 2006
- [37] Straub D.: *Generic Approaches to Risk Based Inspection Planning for Steel Structures. PhD thesis, Swiss Federal Institute of Technology, Zurich*, 2004
- [38] MOG (Mærsk Oil & Gas): *General Jacket Design and Reassessment Conditions – Inspection Planning*, 2003
- [39] Veldkamp, D.: *Chances in Wind Energy - A Probabilistic Approach to Wind Turbine Fatigue Design.* PhD thesis, DUWIND Delft University, Wind Energy Research Institute, Delft, 2006.
- [40] Sørensen, J. D. and Tarp-Johansen, N. J.: *Reliability-based optimization and optimal reliability level of offshore wind turbines*, International Journal of Offshore and Polar Engineering (IJOPE), Vol. 15 (2), 1-6, 2005.
- [41] Tarp-Johansen, N. J., Madsen, P. H., and Frandsen, S. T.: *Calibration of Partial Safety Factors for Extreme Loads on Wind Turbines*, Proc CD-ROM. CD 2. European wind energy conference and exhibition (EWEC 2003), Madrid (ES), 16-19 June 2003
- [42] Madsen, H.O. & Sørensen, J.D.: *Probability-Based Optimization of Fatigue Design Inspection and Maintenance*, Proc. Int. Symp. on Offshore Structures, July 1990, Glasgow, 1990.
- [43] Skjong, R.: *Reliability based optimization of inspection strategies*, Proc. ICOSSAR 85 Vol. III, Kobe, Japan, pp. 614-618, 1985.
- [44] Moan, T.: *Reliability-based management of inspection, maintenance and repair of offshore structures*, Structure and Infrastructure Engineering, Vol. 1, No. 1, pp. 33-62, 2005.
- [45] Sørensen, J.D.: *Framework for risk-based planning of operation and maintenance for offshore wind turbines*, Wind Energy, Vol. 12, pp. 493-506, 2009.
- [46] Dong, W.B., Z. Gao and T. Moan: *Fatigue reliability analysis of jacket-type offshore wind turbine considering inspection and repair*, Proc EWEC 2010, EWEA Brussels, 2010.
- [47] Rangel-Ramírez, J.G. and J.D. Sørensen: *RBI optimization of offshore wind turbines*, Journal of Structure and Infrastructure Engineering, (accepted for publication), 2011
- [48] NORSOK N-004: *Design of Steel Structures N-004*, Rev. 1, 1998
- [49] Newmann, J. and Raju, I.: *An empirical stress-intensity factor for the surface crack*, Engineering Fracture Mechanics, Vol. 22, No. 6, pp. 185-192, 1981.
- [50] Smith, I.J. and Hurworth, S.J.: *The effect of geometry changes upon the predicted fatigue strength of welded joints*, Welding Institute Report # 244, Cambridge, UK, 1984
- [51] Lassen, T.: *Experimental investigation and stochastic modelling of the fatigue behaviour of welded steel joints*, PhD thesis, Structural reliability theory, paper No. 182, Aalborg University, 1997
- [52] Seidel, M., Foss, G., - *Impact of different substructures on turbine loading and dynamic behaviour for the DOWNVInD project in 45m water depth*, Conference proceedings EWEC 2006
- [53] Jonkman, J., Butterfield, S., Musial, W. and Scott, G. - *Definition of a 5MW Reference Wind Turbine for Offshore System Development*, Technical Report NREL/TP-500-38060, NREL 2009
- [54] Vemula, K., De Vries, W., Fischer, T., Cordle, A. and Schmidt, B. - *Design solution for the UpWind reference offshore support structure*, UpWind deliverable D4.2.6, 2010
- [55] Fischer, T., De Vries, W. and Schmidt, B. - *Design Basis – UpWind Deep Water Site*, 2009.
- [56] De Vries, W. - *Soft-Stiff Bottom Mounted Support Structures - Analysis of monopile and multi-member support structures for offshore wind turbines*, UpWind deliverable D4.2.2, 2008
- [57] HSE - *The effects of local joint flexibility on the reliability of fatigue life estimates and inspection planning*, Health and Safety Executive (HSE), 2002
- [58] Buitrago, J. & Healy, B. E. - *Local joint flexibility of tubular joints*, Offshore Technology Conference, ASME, 1993
- [59] ANSYS - *Release 10 Documentation for ANSYS*, 2007
- [60] NASTRAN - *MSC.NASTRAN. Advanced Dynamics Analysis User's Guide*, 2004
- [61] Guyan, R. J. - *Reduction of Stiffness and Mass Matrices*, AIAA Journal, 1965, 3.

- [62] Craig, R.R. and Bampton, M.C.C. - *Coupling of Substructures for Dynamic Analysis*, AIAA Journal, 1968, 6
- [63] Vorpahl, F.R. - *Substructuring in aero-elastic design tool – verification of superelement feature and influence of detailed modeling on results for a wind turbine model with tripod substructure*, UpWind deliverable D4.2.7, 2010
- [64] Vorpahl, F. R.; Blunk, M.; Wingerde, A. V.; Busmann, H. and Kleinhansl, S. - *Implementation of a superelement approach in a design tool for offshore wind turbines with arbitrary support structures*, European Offshore Wind Conference (EOW), 2009
- [65] T. Fischer and M. Kuehn - *Site sensitive support structure and machine design for offshore wind farms*, European Wind Energy Conference (EWEC) 2009.
- [66] Dalhoff, P., Argyriadis, K. and Klose, M., - *Integrated Load and Strength Analysis for Offshore Wind Turbines with Jacket Structures*, Conference Proceeding European Offshore Wind 2007
- [67] Fischer, T., Kühn, M. - *Importance and Mitigation of Loading on Offshore Wind Turbines on Monopile Support Structures in Cases of Non-Availability*, 2010.
- [68] Recoff project - *Tidal Level Effects on Support Structure Loading*, 2002
- [69] IEC 61400-3 Ed. 1, *Wind Turbines – Part 3: Design requirements for offshore wind turbines*, 2009
- [70] Musial, W., Butterfield, S., Boone, A. – *Feasibility of Floating Platform Systems for Wind Turbines*, January 2004
- [71] Bulder, B.H. et al – *Study to Feasibility of and Boundary Conditions for Floating Offshore Wind Turbines*, November 2002
- [72] Lee, K. H. – *Responses of Floating Wind Turbines to Wind and Wave Excitation*, January 2005
- [73] Vijfhuizen, W.J.M.J. – *Design of a Wind and Wave Power Barge*, Sept 2006
- [74] Wayman, E. – *Coupled Dynamics and Economic Analysis of Floating Wind Turbine Systems*, 2006
- [75] Matha, D. - *Model Development and Loads Analysis of an Offshore Wind Turbine on a Tension Leg Platform, with a Comparison to Other Floating Turbine Concepts*, NREL Report, NREL/SR-500-45891, 2009
- [76] Butterfield, S., Musial, W., Jonkman, J. - *Engineering Challenges for Floating Wind Turbines*, October 2005
- [77] Schepers, G., Van Garrel, A. - *AWSM: Free Wake Lifting Line Model for Wind Turbine Aerodynamics*, 2006
- [78] Wheeler, J.D., - *Method for Calculating Forces Produced by Irregular Waves*, J. Petr. Techn., March 1970
- [79] Ed. Barltrop, N.D.P. – *Floating Structures: a guide for design and analysis*, CMPT, 1998
- [80] Jonkman, J.M. - *Dynamics Modeling and Loads Analysis of an Offshore Floating Wind Turbine*, November 2007
- [81] Laino, D.J., Hansen, A.C. - *User's Guide to the Wind Turbine Aerodynamics Computer Software AeroDyn*, 2002
- [82] Jonkman, J.M. - *Dynamics of Offshore Floating Wind Turbines—Model Development and Verification*, Wind Energy. Vol. 12, No. 5, July 2009
- [83] Roddier, D., Cermelli, C., Aubault, A. – *WindFloat: A Floating Foundation for Offshore Wind Turbines Part II Hydrodynamics Analysis*, June 2009
- [84] Shim, S., Kim, M.H. - *Rotor-Floater-Tether Coupled Dynamic Analysis Of Offshore Floating Wind Turbines*, ISOPE 2008
- [85] Withee, J. - *Fully Coupled Dynamic Analysis of a Floating Wind Turbine System*
- [86] Fylling, I., Mo, K., Merz, K, Luxcey, N. - *Floating wind turbine - Response analysis with rigid-body model*
- [87] Nielsen, F.G., Hanson, T.D., Skaare, B. - *Integrated Dynamic Analysis of Floating Offshore Wind Turbines*, 2006
- [88] Skaare, B., Hanson, T.D., Nielsen, F.G., Yttervik, R., Hansen, A.M., Thomsen, K., Larsen, T.J. - *Integrated Dynamic Analysis of Floating Offshore Wind Turbines*, 2007
- [89] Larsen, T.J., Hanson, T.D. - *A method to avoid negative damped low frequent tower vibrations for a floating, pitch controlled wind turbine*
- [90] Larsen, T.J., Hansen, A.M. - *How 2 HAWC2, The User's Manual*, December 2007
- [91] Karimirad, M., Gao, Z., Moan, T. - *Dynamic Motion Analysis of Catenary Moored Spar Wind Turbine in Extreme Environmental Condition*
- [92] Nygaard, T.A., Myhr, A., Maus, K. - *A comparison of two conceptual designs for floating wind turbines*
- [93] <http://www.deepcwind.org/about-the-consortium>
- [94] <http://www.accion-energy.com/innovation/eolica/eolia-project.aspx?pag=&desde=1983>
- [95] <http://www.hyperwind.eu/>
- [96] Buhl, M.L., Wright, A.D., Pierce, K.G - *FAST_AD Code Verification - A Comparison to ADAMS*
- [97] Henderson, A. et al. - *Offshore Wind Turbines on TLPs – Assessment of Floating Support Structures for Offshore Wind Farms in German Waters*, DEWEK 2010
- [98] Witcher, D. et al. – *Bladed Multibody Validation*, GL Garrad Hassan report 1042/BR/01/A, October 2010
- [99] Bossanyi, E., Wright, A. and Fleming, P. - *Progress with field testing of individual pitch control*, Proc. Conference on the Science of Making Torque from Wind, The European Academy of Wind Energy, June 2010

- [100] Sebastian, T., Lackner, M.A. - *A Comparison of First-Order Aerodynamic Analysis Methods for Floating Wind Turbines*, 48th AIAA Aerospace Sciences Meeting, Orlando, Florida, AIAA-2010-9982010
- [101] Polderdijk, J. - *Response of anchor lines to excitation at the top*, 1985
- [102] Kwan, C.T., Bruen, F.J. - *Mooring Line Dynamics: Comparison of Time Domain, Frequency Domain, and Quasi-Static Analyses*, May 1991
- [103] Noble Denton, Joint Industry Project - *Dynamics of Catenary Moorings*, 1991
- [104] Cordle, A. et al. - *State-of-the-art in design tools for floating offshore wind turbines*, UpWind Deliverable D4.3.5, 2010
- [105] Borgen, E. - *Floating Wind Power in Deep Water – Competitive with Shallow-water Wind Farms?*, Modern energy review volume 2 issue 1
- [106] Jonkman, JM (2007). "Dynamics Modeling and Loads Analysis of an Offshore Floating Wind Turbine," NREL Technical Report, NREL/TP-500-41958 (ref 47)
- [107] Jonkman, J. and Matha, D. - EOW paper or Wind Energy article, 2009 (ref 49?)
- [108] Streiner, S., Hauptmann, S. , Kühn, M. , and Krämer, E. - *Coupled Fluid-Structure Simulations of a Wind Turbine Rotor*, University Stuttgart, DEWEK2008, 2008
- [109] DLR Braunschweig - *FLOWer: Installation and User Manual of FLOWer MAIN version FLOWer 1-2007.1*, 2007
- [110] Meister, K., Lutz, T. and Krämer, E. – *Consideration of Unsteady Inflow conditions in Wind Turbine CFD Simulations*, University Stuttgart, DEWEK2010 Bremen, 2010
- [111] Lucas, J. - *Comparison of First and Second-Order Hydrodynamic Results for Floating Offshore Wind Structures*, GL Garrad Hassan report 11594/BR/02/A, January 2011
- [112] Jonkman, J. - *Definition of the Floating System for Phase IV of OC3*, NREL, 2009
- [113] Cruz., J. - *Numerical and Experimental Modelling of Offshore Wave Energy Converters*, PhD thesis, Instituto Superior Técnico, 2009
- [114] Roache, P. J. - *Quantification of uncertainty in computational fluid dynamics*, Annual Review of Fluid Mechanics, 29(1):123–160, 1997
- [115] Söding, H. - *Boundary Element Methods for Seakeeping*, Contribution to the Lectures on Seakeeping and Sea Loads, Duisburg, October 2010
- [116] Kreuzer, E. and Wilke, U - *Mooring Systems – A Multibody Dynamic Approach*, Multibody System Dynamics 8, p279–297, 2002
- [117] DNV – *Commentary and amendments to IEC 61400-3 concerning offshore floating turbines*, 2010
- [118] IEC TC88 – *New Work Item Proposal 88-379/TS Standard for Floating Offshore Wind Turbines*, October 2010